Del Campo Huertas, P.; Martínez, C.; Corma Canós, A. (2021). Activation and conversion of alkanes in the confined space of zeolite-type materials. Chemical Society Reviews. 50(15):8511-8595. https://doi.org/10.1039/d0cs01459a

Activation and conversion of alkanes in the confined space of zeolite-type materials

Pablo del Campo, Cristina Martínez*, Avelino Corma*

Instituto de Tecnología Química, Universitat Politècnica de València-Consejo Superior de Investigaciones Científicas, Avenida de los Naranjos s/n, 46022 Valencia, Spain

Abstract

Microporous zeolite-type materials, with crystalline porous structures formed by well-defined channels and cages of molecular dimensions, have been widely employed as heterogeneous catalysts since the early 1960's, due to their wide variety of framework topologies, compositional flexibility and hydrothermal stability. The possible selection of the microporous structure and of the elements located in framework and extraframework positions enables the design of highly selective catalysts with well-defined active sites of acidic, basic or redox character, opening the path to their application in a wide range of catalytic processes. This versatility and high catalytic efficiency is the key factor enabling their use in the activation and conversion of different alkanes, ranging from methane to long chain n-paraffins. Alkanes are highly stable molecules, but their abundance and low cost have been two main driving forces for the development of processes directed to their upgrading along the last 50 years. However, the availability of advanced characterization tools combined with molecular modelling has enabled a more fundamental approach to the activation and conversion of alkanes, with most of the recent research being focused on the functionalization of methane and light alkanes, where their selective transformation at reasonable conversions remains,

even nowadays, an important challenge. In this review we will cover the use of microporous zeolite-type materials as components of mono- and bifunctional catalysts in the catalytic activation and conversion of C_1^+ alkanes under non-oxidative or oxidative conditions. In each case, the alkane activation will be approached from a fundamental perspective, with the aim of understanding, at the molecular level, the role of the active sites involved in the activation and transformation of the different molecules and the contribution of shape-selective or confinement effects imposed by the microporous structure.

Keywords: zeolite, zeotypes, alkane C-C scission, alkane isomerization, alkane dehydrogenation, alkane dehydrocyclization, selective oxidation.

Graphical abstract

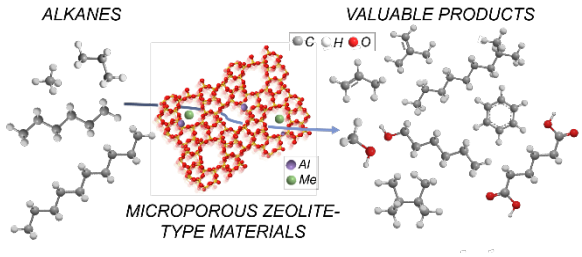

1. INTRODUCTION

Environmental and sustainability concern are being the driving forces for the progressive implementation of alternative energy sources , such as solar and eolic, in substitution of traditional fossil raw materials such as oil, coal or natural gas.[1] However, their contribution to the total energy demand is still small and they are considered as longer term solutions. In the meantime, it is necessary to develop strategies for making a better use of existing fossil resources, minimizing their CO_2 impact and improving existing processes in the chemical industry. Among the different possibilities, cost-effective processes for natural gas and oil upgrading to chemicals are gaining attention, due to the huge increase of proven natural gas reserves in the last decades,[2,3] the decrease in the demand of fuels and the need to face the fast growth of the chemicals market.[4,5] Some traditional conversion processes, such as catalytic cracking, have already been adapted for the latter purpose[4] and, in the same line, an important effort is directed towards the conversion of low value fractions, most of them rich in alkanes, into building blocks for the petrochemical industry such as light olefins and aromatics.[6]

From the sustainability perspective, the final goal in the chemical industry is a process involving maximum conversion and selectivity to the desired product that can be performed under environmentally friendly and energetically viable conditions, being catalysis a key tool for approaching this ambitious objective. Indeed, catalysis has been playing a major role in the chemical industry since the 1960's, and more than 90% of the nowadays processes producing commercial chemicals, including fuels, involve at least one catalytic step.[7] Catalysts can be homogenous and heterogeneous, and although the former present full accessibility to the active sites dissolved in the reaction media and

are highly selective,[8,9] their separation from the products is a serious drawback. Ease of separation, reutilization and high thermal stability are the main advantages of most heterogeneous catalysts, and among them, microporous crystalline materials, such as zeolites and zeotypes, may present high selectivity when the appropriate combination of topology and active sites is selected for a specific reaction.[10–13] Indeed, the great advantage of these microporous crystalline materials lies on their structure, formed by channels and cavities of molecular dimensions, on their compositional flexibility that enables the creation of different type of active sites, and on their thermal and hydrothermal stability.[14–18] This is the reason for their wide application as catalysts in a large variety of processes, including catalytic upgrading of alkanes.[19–25]

Along the last decades, an important effort is being made by the catalysis research community into a better understanding of the catalytic processes at the molecular level. Identification of the active sites and a thorough comprehension of the reaction mechanisms will allow the "ab-initio" design of more efficient catalysts for particular processes,[10,26] enabling the conversion of chemically more stable raw materials, such as methane or higher alkanes. Computational studies are being extraordinarily helpful when combined with experimental work,[27,28] and the development of increasingly complex characterization tools for in-situ and operando study of the catalytic reactions has also contributed to a deeper knowledge, not only of the catalysts, but also of the individual reaction steps and intermediates involved.[29,30] The fundamental knowledge acquired for a specific catalytic system may be then extrapolated to other reactions.

The aim of this review is to cover the use of microporous zeolite-type materials for the catalytic conversion of alkanes, ranging from methane to long-chain n-paraffins. Thus,

before moving into Sections 3 to 5, where the different catalytic processes will be discussed, we will summarize in Section 2 the main properties and main synthesis routes of zeolite-related materials, highlighting some of the new trends in this area. In Sections 3 to 5, we will revise the State of Art on the use of these microporous crystalline materials as catalysts for the conversion of alkanes. The most recent advances achieved in this field will be discussed, not only because of their industrial interest, but we will look at them from a fundamental point of view, directed to understand, at the molecular level, the role of the structure and the active sites of zeolite-type materials in the activation and transformation of alkanes to higher value products.

2. ZEOLITES AND ZEOTYPES

2.1. Definition, properties and preparation

Zeolites and zeotypes are crystalline oxides characterized by their microporous structure formed by well-defined pores, channels and cages with free diameters of less than 2 nm.[31–33] They differ in their chemical composition, with zeolites being limited to pure silica and silicoaluminate materials, whereas zeotypes incorporate other heteroatoms such as P resulting in families of aluminophosphates (AlPOs) or silicoaluminophosphates (SAPOs),[15,17,18,34] and/or metals, such as Ti, Sn, Ga, Fe, Zn, V or Co.[18,23] Some of these zeotypes are isostructural to specific zeolite topologies, others present unique structures. The framework elements are in tetrahedral coordination, reason why they are also known as T-atoms, and linked by oxygen bridges. Zeolite-type materials can be classified according to the number of T-atoms forming the largest opening giving access to the channels or cages of their structure as small, medium, large and extra-large pore when these windows are defined by 8, 10, 12 and more than 12 T-atoms, respectively. On the other hand, depending on their interconnection and spatial disposition, these channel systems may run along one, two, or three directions, leading to one-, two-, or three-dimensional pore structures, respectively. A particular type of zeolites are those presenting interconnected channels of different dimensions.[35]

Regarding zeolites, when the framework is formed by T^{IV} atoms, the structure is electrically neutral, and the incorporation of trivalent aluminum (T^{III}) in these framework positions generates a negative charge in the lattice that has to be compensated by an extra-framework cation. When this counter ion is a proton, the zeolite presents

Brønsted acidity, while when the counter ion is an alkaline cation the neighboring oxygen presents a basic character. In the case of zeotypes, AlPOs present a neutral framework, but the incorporation of Si^{4+} generates Brønsted acidity whereas the introduction of transition metals will generate redox activity. These acidic, basic and redox properties have allowed the application of zeolites and zeolite-related materials as catalysts in a large variety of processes, as will be shown in Sections 2.2 and 2.3. The need for compensating the negative lattice charge by extra-framework cations and the high cation exchange capacity of zeolites is the basis for their main application in terms of production volume. Thus, Linde Type A (LTA) and gismondine (Zeolite P, MAP), used as water softeners in detergents, are the synthetic zeolites produced in larger amounts, accounting for over 70% of the total production in 2013.[21] The rest is directed to their use as adsorbents and heterogeneous catalysts, as will be detailed later.

Zeolites can be found in nature, and their formation has been related to volcanic activity. Over 90 different minerals with varying composition and belonging to 44 different framework types have been identified as natural zeolites.[36,37] Although more than 60% of natural zeolites are used as cement additive,[21] the interested reader can find several reviews on their use in environmentally related applications, such as waste water treatment or soil pollution control.[38,39] Despite the availability and low-cost of some of these natural zeolites, the need for tailored compositions, specific topologies and high phase purity has directed many efforts into the preparation of synthetic zeolites. Nowadays the International Zeolite Association recognizes around 250 different zeolite and zeolite-type structures.[37] Among those, only a reduced number have been applied in commercial processes,[21,40,41] and only a relatively small selection of zeolites are produced in large scale for catalytic purposes, chabazite and its iso-structural SAPO-34

[CHA], ferrierite [FER], ZSM-5 [MFI], MCM-22 [MWW], zeolite L [LTL], mordenite [MOR], beta [BEA] and Y zeolite [FAU] (see Figure 1).[19] These zeolites are also the basis for many of the catalysts employed for alkane conversion, as will be shown along the following sections.

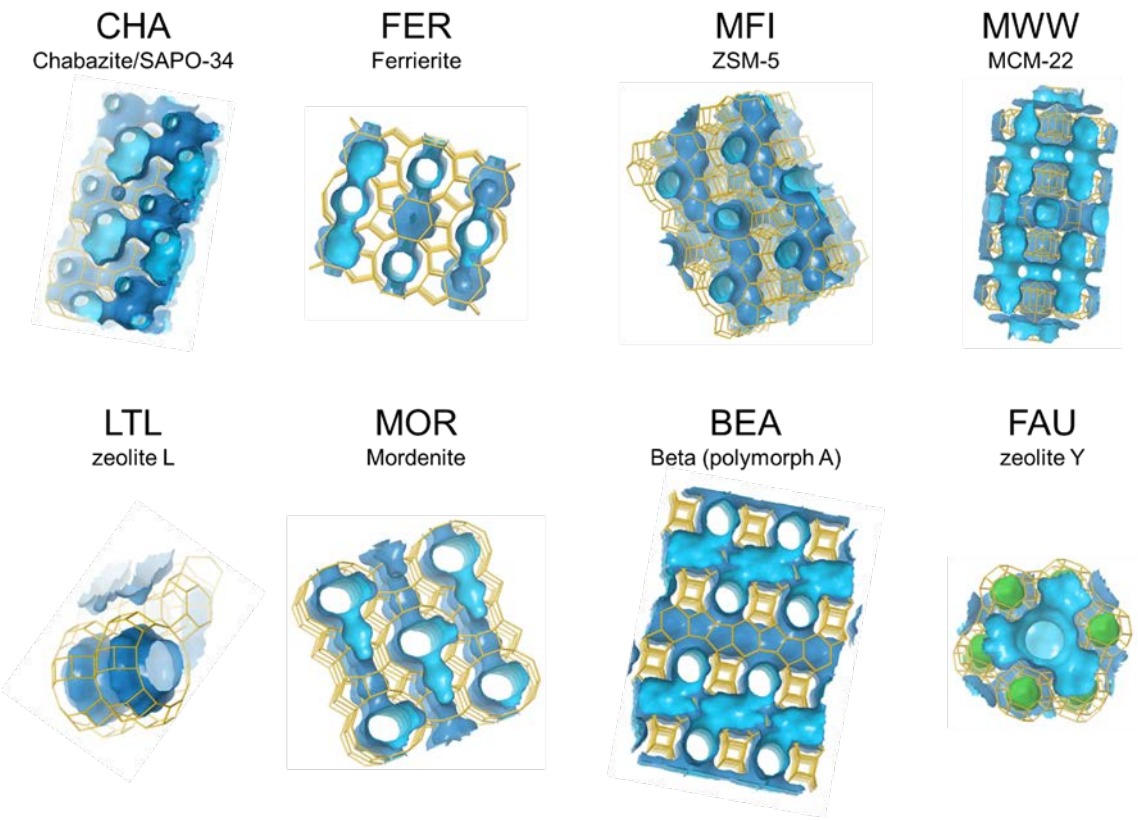

Figure 1. Microporous crystalline materials applied as catalysts in commercial catalytic processes. Structures taken from IZA webpage.[37]

Synthesis of zeolites and zeolite-related materials is usually performed under hydrothermal conditions in a temperature range of 100-200ºC.[34,42,43] The precursors of the different elements are mixed in an aqueous solution with organic and/or inorganic cations and a mobilizing or mineralizing agent. The role of the latter, generally hydroxide but also fluoride anions, is to increase the solubility of the different species in the

synthesis gel. F^- ions have an additional structure directing effect, as they stabilize small cage units such as double four rings (D4R), favoring the crystallization of zeolite topologies presenting these D4R. Alkali cations direct the synthesis towards formation of low Si/Al ratio materials. Not only extraframework elements but also framework cations, such as Ge, B, Zn or Ga can be considered as inorganic structure directing agents, as they are able to favor the crystallization of certain topologies not so stable in their silicoaluminate form. Moreover, the introduction of these elements has allowed the discovery of a large number of new low framework-density microporous structures.[44–48] The introduction of organic molecules in the early 1960's by Barrer and Denny[49] enabled, not only the synthesis of known materials with higher Si/Al ratios, but also the discovery of new high silica zeolites such as beta, ZSM-5 and ZSM-11, which were synthesized in the presence of tetraethylammonium (TEA), tetrapropylamonium (TPA) and tetrabutylammonium (TBA) ions, respectively.[34] A large effort has been done since then to understand the role of these organic compounds as structure directing agents.[45,50,51] Initially they were thought to play a true templating effect, as their confinement within the microporous structure leads to a thermodynamic stabilization of the organic-inorganic system by means of weak interaction such as van der Waals forces, and their size and shape seemed to have some control on the final pore architecture. Although OSDAs are not as specific as could be expected and different zeolite structures can be obtained with the same organic molecule, important advances have been made in the last decade by rational design of specific OSDAs. Simple quaternary tetraalkylammonium cations used in the early years such as TEA or TPA have evolved towards new, more complex quaternary and diquaternary SDAs.[52–55] The substitution of alkylammonium cations by tetralakylphosphonium cations, more stable

towards degradation, allowed zeolite synthesis under more severe conditions,[56] and the use of superbasic phosphazenes was seen to favor the crystallization of multipore zeolites with interconnected large and medium pores.[57] The use of self-assembled aromatic OSDAs forming a supramolecular complex by π-π interactions allowed the synthesis of the LTA material in its pure silica form, ITQ-29,[58] and as silicoaluminophosphate SAPO-42 with isolated Si sites in the framework.[59] Bulky aromatic diamines, also known as proton sponges, were successfully employed as OSDAs for the synthesis of extra-large-pore zeolites.[60] The use of ionic liquids such as imidazolium salts, not only as OSDAs but also as solvents, allowed the synthesis of microporous materials at atmospheric pressure,[61,62] and the design of OSDAs mimicking the transition state of selected reactions led to the synthesis of highly active and selective zeolites for that particular process (see Figure 2).[10,63]

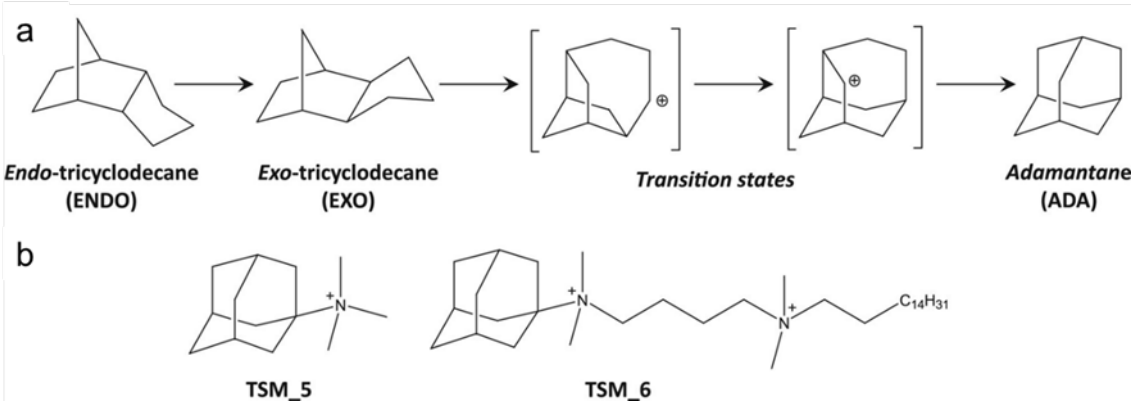

Figure 2. Adamantane synthesis. (a) Reaction mechanism for the endo-tricyclodecane isomerization; (b) Proposed transition state mimics (TSM) as OSDAs for the endo-tricyclodecane isomerization. Figure reproduced from ref.[10] *with permission from the American Association for the Advancement of Science, copyright 2017.*

Despite the advantages described before regarding the use of complex specifically designed OSDAs for the synthesis of highly efficient zeolite based catalysts, the addition of these organic molecules may involve a direct impact on the zeolite costs, which is not

always affordable. Different approaches have been proposed to overcome this issue, not only from an economic but also from an environmental perspective, such as using low-cost,[53] low-toxicity[64] organic molecules, including OSDA recycling steps[65] or performing the synthesis in the absence of organic molecules.[66–69] Two excellent reviews on greener routes for synthesizing zeolites were recently published by Meng and Xiao[70] and Liu and Yu.[71]

Besides hydrothermal and ionothermal synthesis routes, a third approach is synthesizing the microporous materials by means of solvent-free procedures, as first presented by the group of Xiao.[72] Both, the ionothermal and the solvent-less routes present the advantages of avoiding the generation of aqueous wastes and the need for high-pressure conditions.[73]

Microporous crystalline materials are successfully applied to different fields, such as ion exchange, gas separation and catalysis. In the particular case of catalysis, this has been the driving force for a rational approach to their synthesis, focusing on the discovery of new structures, on the discovery of alternative, more sustainable synthesis routes as described above, or on the synthesis of zeolites with optimized morphologies, such as 2D zeolites[74–78] or nanocrystalline materials.[79–81] Besides the rational design of OSDAs, other synthesis strategies have been proposed in the last two decades. Some of them are the combination of different treatments (dehydration, condensation, intercalation, dation or disassembly-reassembly) for the topotactic transformation of a precursor zeolite topology into another structure, employed, for instance, in the ADOR methodology,[82] or the 3D-3D topotactic transformation described recently for aluminophosphates by the group of Hong.[83] These methodologies have provided

alternative synthesis routes of targeted molecular sieves, whose crystallization was not feasible by conventional methods. Other approaches involve the heteroatom substitution in aluminosilicates, phosphates and germanates,[45,84] or the use of precrystallized units for building new zeolites.[85] Several recent reviews cover in more detail the most important advances in the synthesis of zeolite and zeolite-related materials.[16,45,51,70,80,86–90]

Despite the advances made in rationalizing the synthesis of microporous crystalline materials, the crystallization of a specific structure will be governed by a large number of interconnected variables and their influence on the complex nucleation and crystal growth mechanisms is still not fully understood. This makes zeolite synthesis a perfect field for application of Machine Learning methodologies.[91,92] The integration of theoretical modelling approaches has also been very useful for the discovery of new zeolites, enlightening the crystallization mechanism at the molecular level, selecting stable hypothetical structures, or predicting the most suitable framework elements or OSDAs for designing topologies with specific features.[27,45]

2.2. Microporous crystalline materials as heterogeneous catalysts

Zeolites and zeolite-related materials have been widely employed as catalysts since the first application of Y zeolites as acid catalysts for catalytic cracking in the early 1960's. Since then, the fields of application have been diversified and nowadays they range from classical refinery and petrochemical processes to fine chemicals or biomass conversion.[15,17,19,93] In addition to their environmentally benign nature and their high hydrothermal stability, their flexibility regarding topology and chemical composition allows tailoring these microporous crystalline materials towards optimum performance in specific

processes and in a wide range of experimental conditions. Traditionally, their application has taken advantage of the shape selectivity imposed by their microporous channel systems in order to maximize the production of the desired products,[14,94,95] and classical examples are the selective production of p-xylene by isomerization of a C_8 aromatic fraction catalyzed by ZSM-5, or the isomerization of a mixture of linear butenes to iso-butene in the presence of ferrierite. Besides the contribution of molecular sieve and shape-selective properties of the zeolite's structure to the chemical process, the dimension and shape of pores and cavities play an additional role, contributing by means of confinement effects.[15,96–100] In fact, the effect of confinement on the kinetics and the thermodynamics of a catalytic reaction and, therefore, on the diffusion and adsorption of the molecules involved was assessed by Smit and Maesen by means of the free-energy landscape approach. [95] This thermodynamic analysis quantifies the influence of the zeolite topology, independently of its chemical composition, on the free energies of formation of the reactants, intermediates and products participating in the process. This enables the identification of the main processes and interactions controlling the shape selectivity of a specific reaction, e.g., a molecular understanding of the reactions' shape selectivity.

Despite the benefits of the microporous crystalline structure of zeolite-related materials, the small dimensions of the channels may impose diffusional limitations to reactants and/or products leading to inefficient use of zeolite micropore volume and fast catalyst deactivation by pore blocking. This is particularly critical for small pore zeolites with cages and zeolites with one-dimensional channel systems, such as ZSM-22 or ZSM-23, or with topologies that can be considered one-dimensional regarding the diffusion of the molecules in most processes, such as mordenite or ferrierite, which

suffer from larger pore diffusion constraints and higher crystallite length/width ratio. The high interest in expanding the application of zeolites as catalysts in processes involving bulkier molecules has been the driving force for developing new strategies for increasing zeolite accessibility. Different approaches have been proposed to reduce diffusional path lengths within the microporous structure. Accessibility can be increased by means of direct synthesis strategies, such as the synthesis of zeolites with extra-large pores,[45] bi-dimensional or layered (2D) zeolites,[74–78,89,101–104] or nano-crystalline zeolites.[80] The use of hard or soft templates added to the synthesis gel will result, after removal of these templates, in hierarchical zeolites combining their characteristic microporous structure with additional mesoporosity. On the other hand, post-synthesis strategies such as delamination or pillarization of layered zeolite precursors or demetallation (dealumination or desilication) of microporous zeolites, or the preparation of composite materials with inter-component mesoporosity may also improve the textural properties from the accessibility point of view.[105] Several reviews concerning hierarchization and mesopore generation in microporous zeolites are available [106–109] and the synthetic and post-synthetic methods aimed to improve the alkane transport within the zeolite crystals have been widely revised. [110–112]. The importance of hierarchical structures in zeolite-catalyzed industrial processes has been reviewed recently by researchers from Sinopec.[41]

Although the application of large and medium pore zeolites based catalysts started in the early 1960's, the use of small pore zeolites or zeotypes in catalysis is significantly more recent.[113] Especially those presenting structures with large cavities have received increasing attention because of their outstanding properties as catalysts for the selective catalytic reduction of NOx or the methanol-to-olefins (MTO), particularly, the

methanol-to-propene (MTP) reaction. The use of metals, stabilized by the zeolite framework or confined in the zeolite structure, is also a hot topic, as they have shown excellent catalytic behavior in processes such as selective oxidation of methane to methanol, selective catalytic reduction of NO_x, or direct dehydrogenation of light paraffins. Some of these topics, related to the conversion of alkanes, will be covered in this review, but for a more detailed view on the range of application of zeolites as heterogeneous catalysts, the interested reader has available several reviews.[17–20,23,35,113,114]

2.3. Microporous crystalline materials as catalysts for alkane conversion

Alkanes are highly stable, low reactive molecules, difficult to activate, and this chemical stability increases when decreasing the length of the hydrocarbon chain. Although they may be converted even under mild conditions, as we will show in the following sections, the main problem for their upgrading derives from the higher reactivity of the products formed, especially in the case of methane and C_2-C_4 paraffins, which will have a direct impact on the selectivity of the overall process. Thus, alkane conversion is feasible, but the main challenge is to convert them selectively to the desired products with good yields, and this is where zeolites are playing a leading role. Independently of the activation route, e.g., by the zeolite Brønsted acid sites or by means of metals in framework or extra-framework positions, under oxidative or non-oxidative conditions, when microporous zeolite-type materials are used to catalyze the conversion of alkanes to higher value products, the materials' topology will have a major influence on the reaction mechanism. Indeed, confinement will affect not only the adsorption and the diffusion of the hydrocarbons, but it will also influence the stability of certain reaction

intermediates and the nature of active sites formed when it comes to extraframework species, such as metal atoms, clusters or particles.

Alkanes can be activated by zeolites in their acid form or by metallozeolites, with the metals either in framework or in extraframework positions. In the case of activation on Brønsted acid sites (BAS), the alkane will be protonated forming a high-energy penta-coordinated carbonium ion that will react following a protolytic Haag-Dessau mechanism.[115,116] The acid attack can be at the C-H bond, leading to H_2 and a carbenium ion with the same size as the original alkane, susceptible to further reaction (route *a* in Scheme 1), or at the C-C bond, leading to a shorter carbenium ion and alkane (route *b* in Scheme 1).

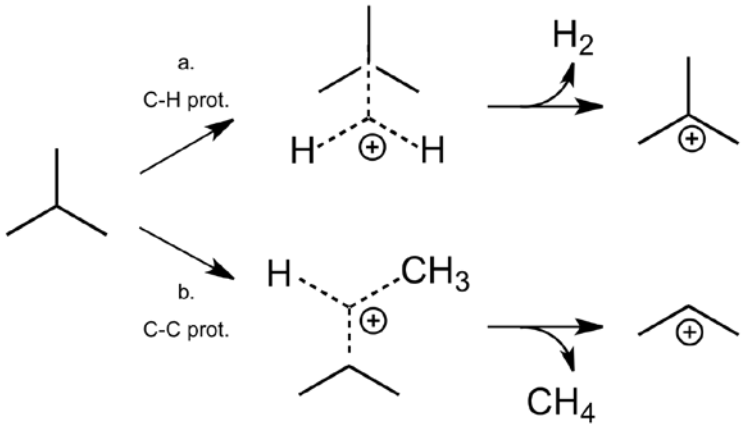

Scheme 1. Catalytic activation of alkanes over acid zeolites.

Protonation of methane and ethane involves the formation of primary carbocations, highly disfavored. In fact, methane is not converted on H-ZSM-5 even at temperatures as high as 700ºC [117] and catalytic steam cracking of ethane requires severe conditions to occur, with temperatures around 900ºC.[118] As we will detail in Section 3, methane can be converted on bifunctional zeolite-based catalysts under oxidative and non-oxidative conditions, with partial oxidation to methanol on Cu- or Fe- exchanged zeolites and

aromatization on Mo loaded H-ZSM-5, respectively, being the most representative processes. In both cases the nature of the active sites and the activation mechanisms are still under debate, and will be analyzed thoroughly in the corresponding sections.

Main zeolite-based process for converting ethane is aromatization, which also proceeds through a bifunctional mechanism on Ga or Zn-zeolites [119,120]. Ethane is activated on the metal species, dehydrogenated to ethylene, and the olefin is then oligomerized and cycled on the BAS of the zeolite. Propane and n-butane are also converted into aromatics following a similar bifunctional mechanism on metal-doped acid zeolites but at lower temperatures than in the case of ethane.[120]

Light alkanes with chains formed by 3 or more carbon atoms may form secondary carbocations by protonation and their activation mechanism by acid zeolites has been studied thoroughly in order to understand the contribution of protolytic cracking to the overall cracking process. Iglesia studied the influence of acid strength and confinement on the cracking rates of light alkanes on isolated BAS located within different void spaces in different zeolite frameworks. They observed that the rates were only weakly affected by changes in acid strength but highly affected by solvation or interaction effects.[97,121] Comparable activation barriers for different alkanes in different environments point out to differences in the entropies of the transition states as responsible for the differences observed for dehydrogenation and cracking turnover rates.[121,122] The zeolite topology will also affect the sorption of alkanes within their microporous structure. Lercher showed that, besides the higher heat of adsorption when increasing the size of the alkane or decreasing the size of the pore, the ordering of the sorbate molecules within the pores and the intermolecular interactions play an important role in the alkane-

zeolite interactions.[123] They also found a linear correlation between the sorption enthalpies and entropies, and this led to conclude that the interaction was similar in nature for the different alkanes, but characteristic for a specific zeolite.[124]

As mentioned earlier, metal-doped zeolites are used in order to overcome the high activation energies of alkane activation by BAS. Thus, direct dehydrogenation of propane is catalyzed by noble metals loaded zeolites. Under the severe process conditions, metal sintering is a major problem that can be solved by encapsulation of the metal function in specific locations, such as cavities, of the zeolite structure.[125–129]

Bifunctional metal-loaded zeolites are also employed for hydroconversion of C_{5+} alkanes. In these cases, the overall process involves a first activation and dehydrogenation of the n-paraffin on the metal side and further conversion by isomerization and/or cracking of the resulting alkene on the zeolite BAS, and the challenge for improved catalytic performance is to achieve an optimum metal-acid balance.[111]

Alkanes can also be converted by selective oxidation in the presence of multifunctional catalysts. Kinetic control of the selective oxidation process is critical, as thermodynamics will tend to total combustion of the hydrocarbon into CO_2 and water.[130]

3. METHANE CONVERSION

Methane, the main component of natural gas, is attracting increasing attention as transition raw material for current energy demands and chemicals production while moving from traditional fossil fuels, such as oil, into renewable energy sources, still under development.[3,131–134] This interest is due to its smaller environmental footprint

and higher hydrogen/carbon ratio, but also because of its availability and low cost due to the recent discovery of large reserves of shale gas, coalbed methane and methane clathrates,[135–138] and its presence in biogas.[139] In all cases, the difficulties related to methane storage and transport make its on-site conversion to liquid hydrocarbons highly desirable. Moreover, the implementation of cost-effective processes for methane upgrading into higher-value chemicals liquid fuels would not only reduce oil dependence, but would also help lowering its shipping costs, higher than those of petroleum or coal on an energy-delivered basis.[2] An additional advantage of those upgrading processes would be the possible harness of gas that is flared or vented from fossil reservoirs.[2]

Methane is the most abundant paraffin, but also the less reactive.[136] The methane molecule presents low polarizability, high ionization potential and very stable C-H bonds, with a bond dissociation energy of 439,3 $kJ \cdot mol^{-1}$. Because of the great energy costs required to overcome its high chemical stability, around 90% of its total production is directed to combustion for energy generation purposes.[2,140,141] Still, methane is nowadays an important carbon source for the chemical industry through its conversion to synthesis gas ($CO+H_2$) via steam reforming, partial oxidation or autothermic reforming (See Scheme 2).[132,142–144] Syngas is then further converted into hydrocarbons by means of the Fischer–Tropsch synthesis (FTS) or by the methanol synthesis followed by methanol to hydrocarbons (olefins, gasoline or aromatics).

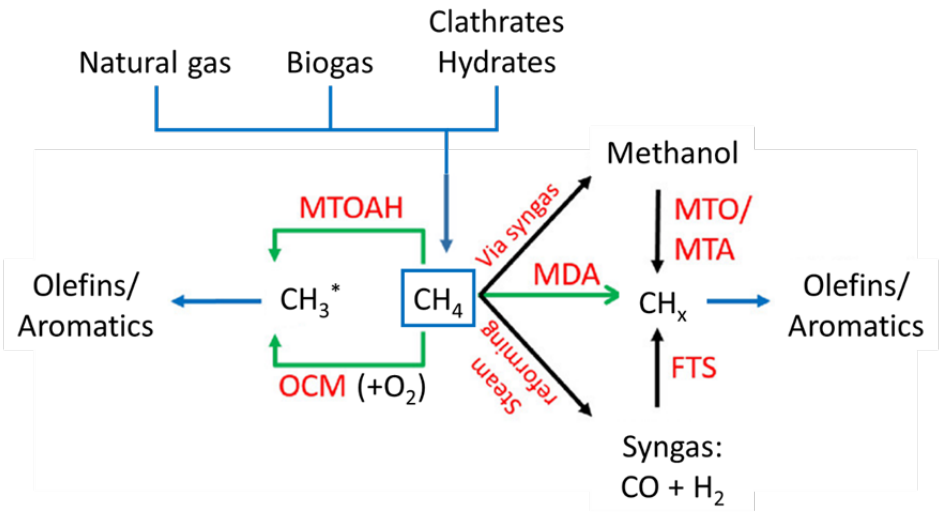

Scheme 2. Indirect and direct pathways for methane C−C Coupling to Olefins and Aromatics. Adapted from ref.[136] *with permission from the American Chemical Society, copyright 2017.*

The main inconvenience associated to this indirect route for methane upgrading is the high energy requirement due its strong endothermicity and, therefore, the inherent large CO_2 emissions. Thus, direct routes for selective methane conversion into C_{2+} products, although highly challenging, have been actively studied along the last decades, and different Gas-to-Liquid (GTL) approaches have been proposed and thoroughly analyzed in several reviews,[145–148] from an applied perspective[135,137] and from a more fundamental point of view.[136] Efficient methane upgrading by direct routes is a challenging task from the thermodynamic and from the kinetic point of view. Activation of the stable C-H bond requires high reaction temperature and leads to the formation of CH_x or CH_xO species, which have to be converted into the desired products in a single step process. The higher reactivity of the primary products formed, as compared to the starting methane, will result in their non-selective conversion unless they are selectively removed from the reaction media or kinetically protected.[149]

Direct conversion of methane can take place under oxidative or non-oxidative conditions.[146,149–151] The oxidative routes overcome the thermodynamic limitations by removing the hydrogen formed by reaction with an oxidant, usually oxygen, and the formation of water. Oxidative coupling of methane (OCM) and selective partial oxidation of methane to methanol or formaldehyde are the two main options. The former is a highly exothermic process and heat-managing issues have prevented its commercial application so far. On the other hand, the direct conversion of methane to methanol by partial oxidation has received increasing attention and significant advances have been made in the last years towards a deeper understanding of the active site and the reaction mechanism.[13,152,153]

Still, selective conversion of methane following direct oxidative routes is highly challenging, and the alternative non-oxidative conversion of methane to olefins or aromatics has gained importance in the last 25 years, despite the unfavorable thermodynamics of this endothermic equilibrium controlled reaction. Although the conversion levels achieved are low even at high temperatures, the process is highly selective to the desired hydrocarbons. However, the main problem is the rapid catalyst deactivation. This has opened a strong research line focused on the type of carbon species formed during the process and their more or less active participation in the methane activation step and in its further conversion into higher hydrocarbons.[154–157] An important effort has been directed towards productivity improvement by reactor and/or process design. Thus, membrane reactors for H_2 recovery and equilibrium shift, fluidized bed or CH_4-H_2 switch operation to deal with the fast catalyst deactivation, or combination with a second reaction such as oxidative dehydrogenation are some of the approaches proposed.[158–161]

Despite the significant advances achieved upon the fundamental understanding of the direct methane conversion processes, the critical analysis made by Lunsford 20 years ago is still valid nowadays. Each of the alternatives proposed has specific drawbacks that discard their industrial implementation, but they have in common the low yields to the desired products and, thus, the need for inexpensive separation steps, oxygen from air in the case of the oxidative conversion or hydrogen or hydrocarbons from diluted streams in the case of the non-oxidative dehydrogenation.[150]

The main advances in methane conversion processes catalyzed by microporous crystalline materials will be reviewed in the following section, emphasizing on the most recent and disruptive findings.

3.1. Methane conversion to syngas

Methane can be converted into syngas by means of steam reforming (SMR) (Eq. 1), dry reforming in the presence of CO_2 (DMR) (Eq. 2) and by partial oxidation (Eq. 3), with the former being the only one which is commercially applied.[162–167] For increasing H_2 production, the steam reforming reaction (Eq. 1) can be combined with the water gas shift (WGS) reaction (Eq. 4).[168]

$$CH_4 + H_2O \leftrightarrow 3H_2 + CO \qquad \Delta H_r^0(289\ K) = 206\ kJ\ mol^{-1} \qquad (1)$$

$$CH_4 + CO_2 \leftrightarrow 2H_2 + 2CO \qquad \Delta H_r^0(289\ K) = 247\ kJ\ mol^{-1} \qquad (2)$$

$$CH_4 + \frac{1}{2}O_2 \leftrightarrow 2H_2 + CO \qquad \Delta H_r^0(289\ K) = -36\ kJ\ mol^{-1} \qquad (3)$$

$$CO + H_2O \leftrightarrow H_2 + CO_2 \qquad \Delta H_r^0(298\ K) = -41\ kJ\ mol^{-1} \qquad (4)$$

High temperatures, above 750ºC, are necessary for overcoming thermodynamic limitations involving, therefore, high energy requirements, and the harsh process conditions lead to metal sintering, fast carbon deposition and, eventually, to catalyst deactivation. High steam to carbon ratios are employed, in order to reduce catalyst deactivation by coke and this leads to production of H_2-rich syngas, with H_2/CO ratios around 3. Moreover, large amounts of CO_2 are co-produced in the process, especially by the WGS reaction for increased H_2 make. Industrial SRM catalysts are non-microporous transition metal-based materials, usually Ni supported on inorganic oxides.[145,166,169,170] These have also been the most studied catalysts in the literature[171,172] and, as far as we know, only a few studies on zeolite-based SMR catalysts have been reported. An early work by Al-Ubaid and Wolf described the use of Ni/Na-Y for SMR and its deactivation due to surface oxidation of the active Ni species.[173] De Lasa compared α-alumina, NaY and USY as supports for Ni-based SMR catalysts and, although the zeolite based catalysts gave promising results for dry reforming, they presented limited application for SMR, below that of Ni/α-alumina.[174] An interesting approach is the use of core-shell type of composites, where zeolite membranes coat a steam reforming catalyst core. This is the case of silicalite-1 coated Ni/Al_2O_3[175] or NiO/M[176] or H-beta encapsulated Ce-Zr/Ni-Mg.[177] The core-shell catalysts showed in both cases improved catalytic activity as compared to the SMR catalyst alone. According to Cimenler et al.,[177] a possible reason for this increase in methane conversion could be the increased residence time within the catalyst's pores due to confined reaction effects. Al^{3+} promotion of the active sites was also suggested. Core/yolk shell catalysts have also been described as more resistant to metal sintering and coking.[176,178]

Dry (CO_2) methane reforming shares some of the main disadvantages of SMR, such as the high endothermicity of the reaction and the severe deactivation by coke formation.[167] However, it converts two abundant greenhouse gases, methane and CO_2, it produces less CO_2 as compared to SMR, and the syngas obtained has a H_2/CO ratio ≤1, more suitable for the synthesis of methanol, and even for the Fischer-Tropsch synthesis of long chain hydrocarbons. Supported noble metals (Rh, Pt, Pd or Ru) and transitions metals are commonly used as catalysts for DMR. The former are less sensitive to coke formation but more expensive, whereas metals such as Ni present the advantage of high turnover rates at lower cost, but suffer fast deactivation due to coke formation via the Boudouart reaction (Eq. 5) or methane decomposition (Eq.6).

$$2CO \leftrightarrow C + CO_2 \qquad \Delta H_r^0(298\ K) = -172\ kJ\ mol^{-1} \qquad (5)$$

$$CH_4 \leftrightarrow C + 2H_2 \qquad \Delta H_r^0(298\ K) = 75\ kJ\ mol^{-1} \qquad (6)$$

When the support is inert, such as SiO_2, the mechanism is mono-functional and both, methane and CO_2 are activated on the metal. However when the support is mildly acidic (Al_2O_3) or basic (La_2O_3, CeO_2), the reaction mechanism is accepted to be bifunctional, with methane being activated on the metal, and CO_2 on the support.[167] As in the case of SMR, important efforts have been made in order to improve catalyst deactivation, which has been attributed to metal sintering and metal coking. One of the strategies proposed in the literature is the confinement or stabilization of the active metal-species within porous structures such as carbon nanotubes,[179] silica nanotubes,[180] ordered mesoporous materials,[181] [182] or zeolites [183,184], limiting in this way the growth of the metal nanoparticles.

Thus, Ni-loaded zeolites, Ni-ZSM-5 or Ni-Y among others, have been described for dry steam reforming of methane (see Table 1). One of their advantages as compared to other supports such as mesoporous MCM-41 or SBA-15, in addition to their higher thermal and hydrothermal stability, is their high CO_2 adsorption capacity, which allows reducing reaction temperature while maintaining acceptable activity. However, the higher the activity of Ni-zeolites, the higher the coke selectivity.[185] Fast deactivation of zeolite-based catalyst is the main drawback of these type of catalysts.

Table 1. Catalytic performance of Ni Catalysts supported on different zeolites for the methane conversion (GHSV given for CH_4+CO_2 with 1:1 molar ratio). Adapted from [185]

Metal loading	**Support**	**GHSV ($mlg^{-1}h^{-1}$)**	**Temperature (ºC)**	**TOS (h)**	**CH_4 conv.(%)**	**Carbon (mg/mg)**
Ni	MCM-41	6000	600	–	42	–
Ni/7	Zeolite A	30000	700	5	12.3	0.25
Ni/7	Zeolite X	30000	700	5	71.5	0.24
Ni/7	Zeolite Y	30000	700	5	91.6	6.83
Ni/7	ZSM-5	30000	700	5	57.8	2.16
Ni/8.7	USY	12000	650	6	78	–
Ni/20	SBA-15	–	700	600	72	–

A different application of zeolites for the methane reforming processes is as coatings of Ni/Al_2O_3 catalysts, where the microporous material acts as a membrane layer in core-shell nanocomposite catalysts.[178] The presence of the zeolite shell improves the product selectivity and enhances the stability towards sintering.[177,186,187] Moreover, the

microporous coating acts, additionally, as a diffusion barrier against poisons such as alkali species.[188]

3.2. Methane partial oxidation to methanol

Methanol is one of the most interesting chemicals nowadays. Besides its high octane number and the possibility of its direct blending with conventional gasoline without modification of the vehicle fleet, it is an important C_1 building block in the chemical industry and a convenient liquid energy carrier for hydrogen storage and transportation.[189–191] In the late 1990's Olah already introduced the concept of Methanol Economy, proposing methanol as the alternative energy source to oil and gas (see [192] and references therein). At present, around 90% of its overall production follows the indirect route comprising the conversion of methane to syngas in a first step and production of methanol from the $CO+H_2$ mixture in a second step, a low-efficiency energy-intensive process. The high capital investment required for methanol production through the syngas route limits its economic viability to large-scale operations and makes it unsuitable for low capacity stranded natural gas exploitations. Thus, possible syngas-free alternatives have been intensively researched.

In nature, iron and copper methane monooxygenase are able to selectively hydroxylate methane to methanol under physiological ambient conditions using atmospheric oxygen.[193] The metal active sites are isolated and well defined, and the enzyme provides the appropriate structural and electronic stabilization. Following an enzyme-mimicking approach, copper and iron metallozeolites have been widely studied as catalysts for partial oxidation of methane to methanol, and the similarities between the structure of

the active sites and the hydroxylation mechanisms in enzymes and zeolite based materials have been thoroughly analyzed in several reviews published recently.[13,152,153]

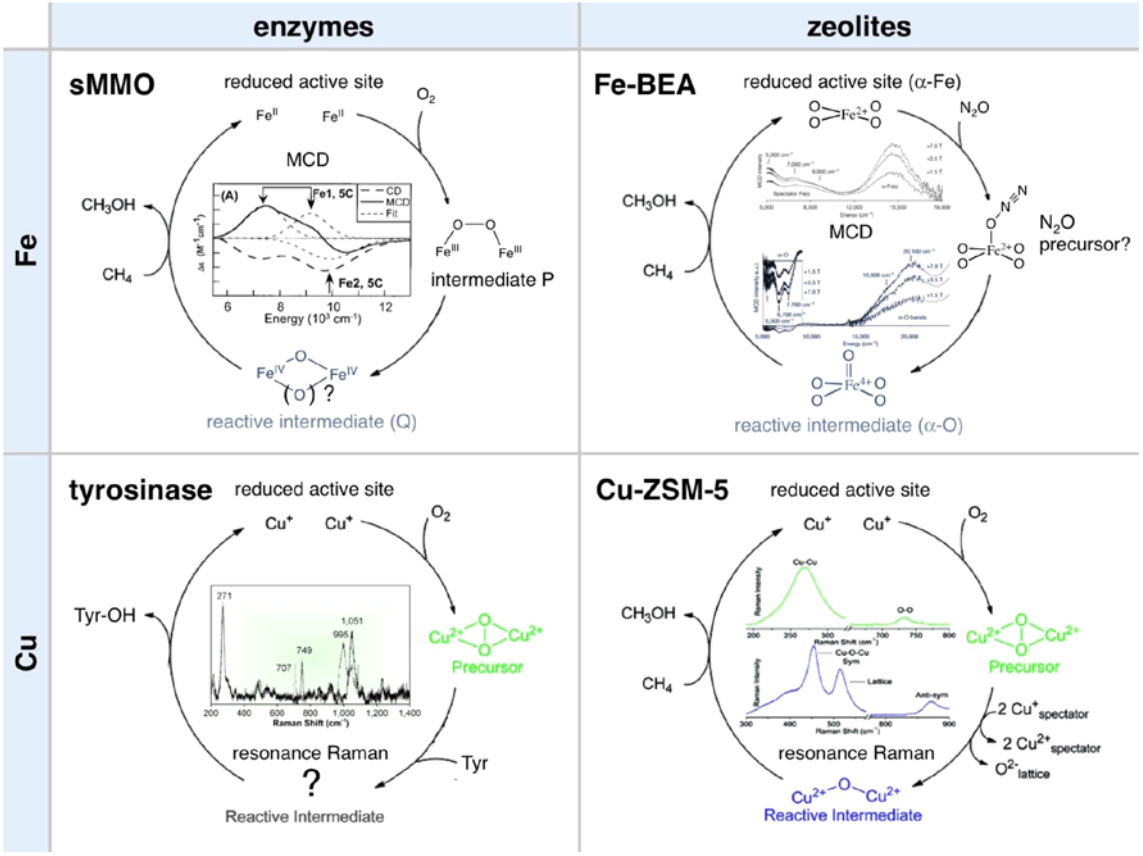

Figure 3. Comparison of Fe and Cu enzymes and zeolites that hydroxylate strong C–H bonds at low temperature, including their active site structures and catalytic intermediates defined from spectroscopy. Reprinted from ref.[13] *with permission from American Chemical Society, Copyright 2018.*

As described in detail by Snyder et al., despite the differences when comparing enzymatic and zeolite-based catalysis, there are also important resemblances, such as the high covalence of the metal–oxygen bond, the influence of second-sphere atoms on the reactivity of the metal site, and entatic effects associated to constrains imposed by the protein or the zeolite structure forcing an otherwise unstable, but highly active intermediate geometry (see Figure 3).[13] Still, the performance of transition metal

exchanged zeolites is far below that of enzymes in terms of reaction rates and process conditions.[194]

The use of metallozeolite based systems for selective oxidation of methane to methanol is a very active research field, and the number of publications on this subject is huge. The interested reader is directed to several comprehensive reviews, some of them more general describing the active sites and reactivity of different transition metal-exchanged zeolites,[13,152,153,195–197] others presenting a theoretical approach to the selective oxidation process,[153,198] or specifically focused on iron[199] or copper-zeolites.[200–204] An historical perspective on the evolution of methane selective oxidation from the point of view of the catalysts employed has been published by Ravi et al.,[205] and the need for methanol protection to avoid its over-oxidation is concluded to be critical. Improving the low methanol selectivity and other challenges related to the zeolite-mediated methane oxidation to methanol are addressed in several critical perspectives recently published by Román-Leshkov[152] and van Bokhoven.[194,204] They assess on the viability of Cu- and Fe-, and of Cu- exchanged zeolites, respectively, as catalysts for performing the methane to methanol partial oxidation. After an in-depth analysis of the benefits and drawbacks of the process, in both cases it is concluded that despite the interest awaken by this topic in the research community and the advances made in the fundamental understanding of the active sites and reaction mechanism, the results obtained up to now are far from industrial implementation (see Table 2). Both, continuous and step-wise stoichiometric operation lead to unrealistic low methanol productivity, and the main challenges remain the design of improved catalysts able to activate the stable C-H bond, perhaps not limited to zeolite based candidates, together with the design of novel methanol protection strategies.

Table 2. Status of zeolite-based gas-solid MTM concepts noting challenges to be addressed by further work and projected likelihood for success. Adapted from [204]

		Conversion and Selectivity	**Methanol concentration in the product stream**	**Methanol productivity ($mmol g^{-1} h^{-1}$)**	**Challenges/Needs**	**Likelihood for success**
Continuous operation	catalytic aerobic	Unfavorable	Unfavorable	Unfavorable	Novel methanol-protection strategies & Fast kinetics	Unknown
	catalytic aerobic	Unfavorable	Unfavorable	Unfavorable	All of the above & Removal of H_2 from reaction site	None to low
Stepwise operation	stoichiometric	Not applicable	Favorable	Unfavorable	Stable zeolites with Si/Al<2 Alternative Cu-loading methods leading to increased no. of active sites Cycle time<15′	Low to medium
	quasicatalytic aerobic	Not applicable	Unknown	Unknown	Collectors that capture several mmol of methanol per gr. High rates despite low methanol partial pressures, high T and presence of water	Low to none

Pioneering work on the use of metallozeolites for selective oxidation of methane was published by the group of Panov in the 1990's. They reported the formation of a highly active oxygen intermediate by decomposition of N_2O on Fe-ZSM-5 at temperatures below 300ºC. These active oxygen species, named as α-O, were capable of O_2 isotopic exchange and irreversibly binding of CO and CH_4.[206–208] The same group elucidated the methane and benzene selective oxidation mechanism on these type of materials by kinetic isotope effect (KIE) measurements.[208] Methane hydroxylation on Fe-ZSM-5,

using N_2O as oxygen source, could be stoichiometric, quasi-catalytic or catalytic depending on the reaction temperature. Thus, single-turnover cycles of methane oxidation took place at room temperature, and the reaction products, methanol and DME, had to be extracted in a second step.[209] At higher temperatures, up to 200ºC, the methanol formed was able to migrate from the α-sites, liberating them for starting new reaction cycles, and at 160 and 200ºC the turnover numbers were 3 and 7, respectively.[210,211] However, the methanol formed remained on the catalyst surface, and temperatures above 200ºC were needed for the reaction to proceed following a true catalytic mode, with product desorption into the gas phase. Still, water was seen to significantly increase the selectivity to methanol, which reached values of 62% at 275°C.[211]

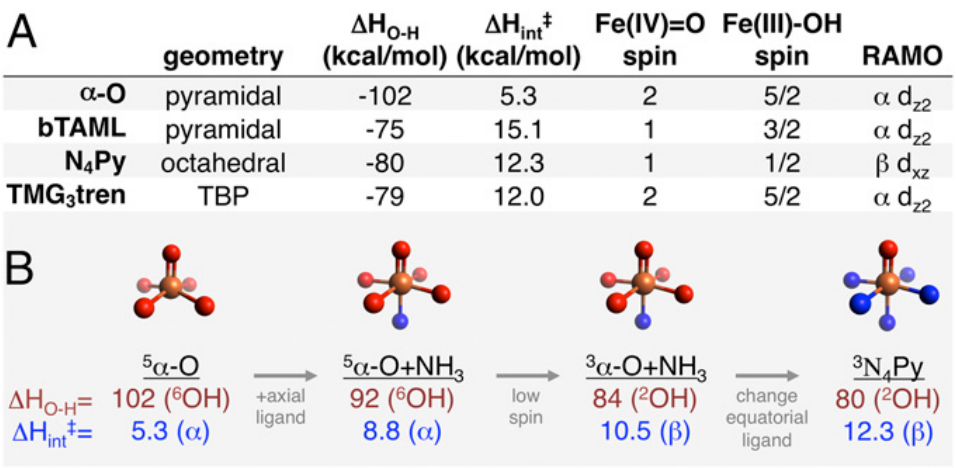

Figure 4. (A) Comparative reactivity of mononuclear Fe(IV)=O intermediates from DFT, including driving forces for O–H bond formation (ΔH_{O-H}), estimated intrinsic barriers for H-atom abstraction from CH_4 (ΔH_{int} ‡), spin states of the Fe(IV)=O reactants and Fe(III)-OH products, as well as the redox-active molecular orbital (RAMO) that ultimately accepts the electron following H-atom transfer; (B) Correlation of α-O to N4Py, with intermediate steps illustrating the effects of adding a trans axial ligand and then moving to an S = 1 ground state. Reproduced from ref. [212] *with permission from the National Academie of Science, copyright 2018.*

However, it was not until 2016 that the nature of the active site in Fe-exchanged zeolites was elucidated by Snyder et al.,[213] using magnetic circular dichroism, a novel site-selective spectroscopic methodology. Their studies on Fe(II)-BEA showed that the active α-Fe(II) site was a mononuclear, high-spin, square planar Fe(II) site and the α-O intermediate was a mononuclear, high spin Fe(IV)=O specie. Moreover, they confirmed the entatic effect produced by the topology of the host zeolite, evidencing that the high reactivity of this α-O site was directly related to the coordination geometry constrains imposed by the zeolite framework (see Figure 4).[13,212,213]

Hutchings' group has reported the hydroxylation of methane on Fe-ZSM-5 using N_2O as the oxidant under continuous operation in a fixed bed continuous flow reactor. A thorough kinetic study led them to a tentative reaction mechanism (see Scheme 3) where H_2O was shown to play a fundamental role in the product distribution, increasing the selectivity to methanol from 1 to 16% and reducing the formation of coke and, therefore, catalyst deactivation.[214] Comparing Fe-MFI catalysts showing different acidic properties (Fe–ZSM-5, Fe–silicalite-1 and Fe–TS-1) and Fe-loaded H-ZSM-5 with different Si/Al ratios but constant Fe/Al ratio and, therefore, different Fe loadings, indicated that Brønsted acidity was necessary in order to form the α-oxygen active site required for the initial hydrogen abstraction step. However, the presence of Brønsted acid sites reduced the rate of methanol and DME desorption and favored their conversion into secondary products such as ethene or aromatics and, ultimately, coke.[215]

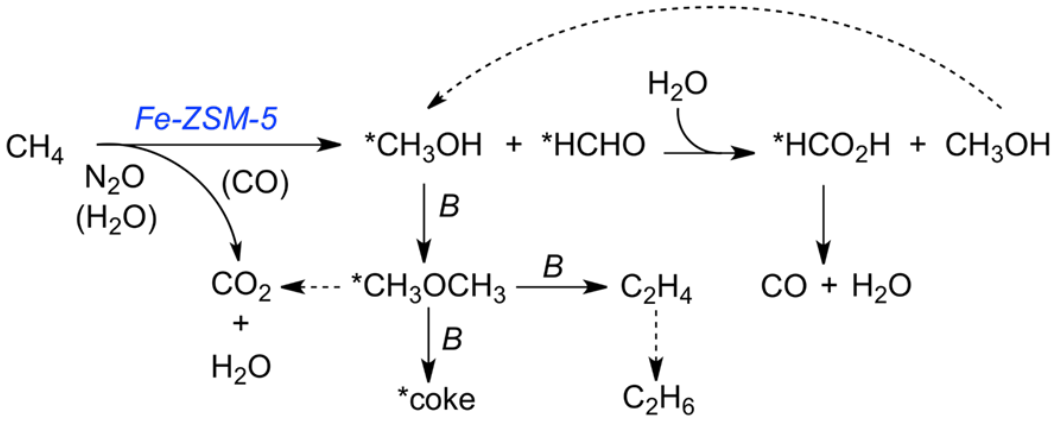

*Scheme 3. Proposed reaction network for CH_4 oxidation with N_2O over Fe-ZSM-5 catalysts according to delplot analysis. B is BAS and *indicates adsorbed or intermediate species not detected in the reactor effluent. Adapted from ref.*[214] *with permission from Wiley-VCH, copyright 2018.*

Most of the studies on Fe-exchanged zeolites as methane hydroxylation catalysts are focused on medium pore zeolites, mainly ZSM-5, but other medium pore or large pore zeolites such as ferrierite or beta have also been reported. Regarding small pore zeolites, they have generated great interest in the last years due to their exceptional efficiency in industrially relevant applications such as methanol-to-olefins and selective catalytic reduction of nitrogen oxides in exhaust gases.[51,113] The first application of small pore metallozeolites and zeotypes for selective oxidation of methane to methanol was reported by Lobo in 2015,[216] and the microporous materials considered in the study were SSZ-13, SSZ-16, SSZ-39, and SAPO-34, although exchanged with copper and not iron. Some years later, Fe-exchanged SSZ-13 zeolites were also evaluated as catalysts for methane hydroxylation, and their capacity for low temperature activation of methane was confirmed.[217,218] In these cases, the α-Fe/α-O active site was identified as a mononuclear isolated extraframework Fe^{II} species, which was stabilized by a six-membered ring (6-ring) containing two Al atoms in opposite tetrahedral locations. The CHA topology of SSZ-13 was seen to influence the properties of the active site due to

differences in the geometry of the double 6-ring (d6r) containing the α-Fe site as compared to Fe-beta (see Figure 5). Moreover, conversely to other medium and large pore zeolite host, the small pore structure favored the formation of the α-Fe site over other iron species and at low Fe loadings this α-Fe site was the only one observed. By directing the synthesis of SSZ-13 towards a material with higher proportion of Al pairs and, therefore, higher capacity for divalent cations exchange, the methane conversion activity and the methanol production were substantially increased.[218]

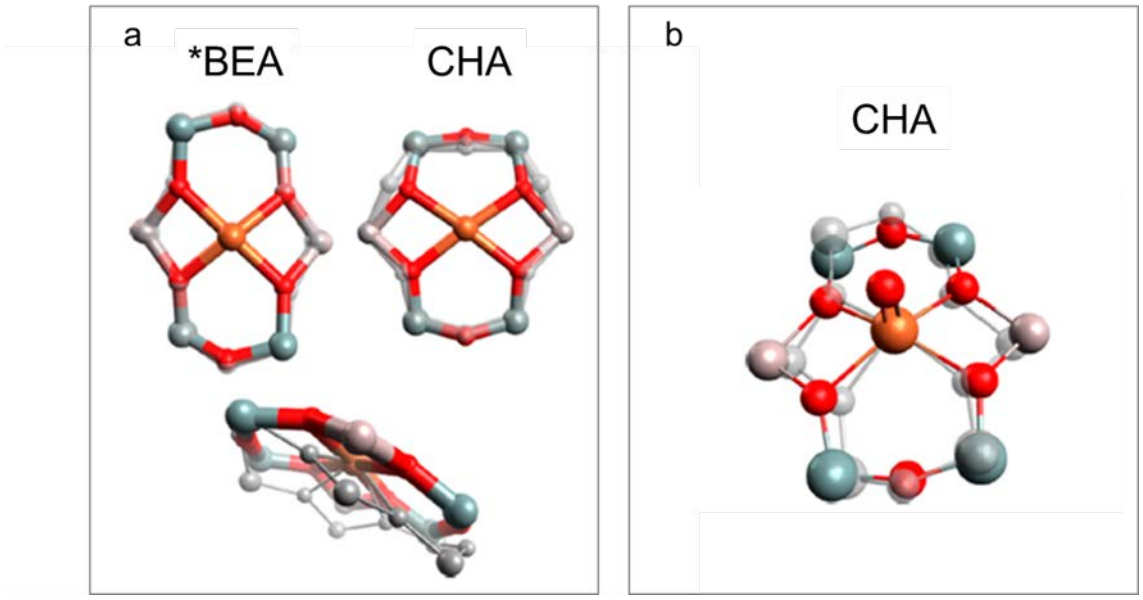

*Figure 5. (a) Above: overlays of the B3LYP-DFT optimized α-Fe models in *BEA (d6MR) (left) and CHA ($1R_{OPPOSITE}$) (right) and the corresponding B3LYP-DFT optimized models of the Al substituted 6MRs before Fe coordination. The empty 6MR models are shown in gray. Below: overlay of the Fe-CHA $1R_{OPPOSITE}$ model (colored) and the Fe-*BEA α(T6T6) model (gray) overlapped at the α-Fe atom; (b) Overlays of the B3LYP-DFT optimized α-O-CHA (colored) and α-O-BEA (gray) models. The models are positioned to overlap on the Fe atom and the F=O_{ax} bonds of the models are aligned. Reprinted from ref.[217] with permission from the American Chemical Society, copyright 2018.*

N_2O is not the only oxidant described for activation of Fe-zeolites. Thus, in 2012 Hutchings described the use of hydrogen peroxide as oxidant for the direct conversion of methane to methanol in aqueous media catalyzed by Fe-ZSM-5.[219] Under the

appropriate reaction conditions, methane conversion of 10% and selectivity of 96% to partial oxidation products (CH_3OH, CH_3OOH, HCOOH) were obtained, but selectivity to methanol was only 8%. Addition of copper to the Fe-ZSM-5 did not contribute to the methane activation step, but promoted the selective formation of methanol by inhibiting the formation of OH·radicals and the derived over-oxidation reactions, increasing its selectivity to 93% at comparable conversions of 10%. Additional studies performed by this group on this low-energy route for methane partial oxidation with H_2O_2 on Cu-promoted Fe-ZSM-5 catalysts resulted in the elucidation of a detailed reaction network for the activation of methane and for the formation of the intermediate hydroperoxy species and hydroxyl radicals,[220] and in the understanding of the specific roles of the Fe and Cu active sites (see Figure 6).[221,222]

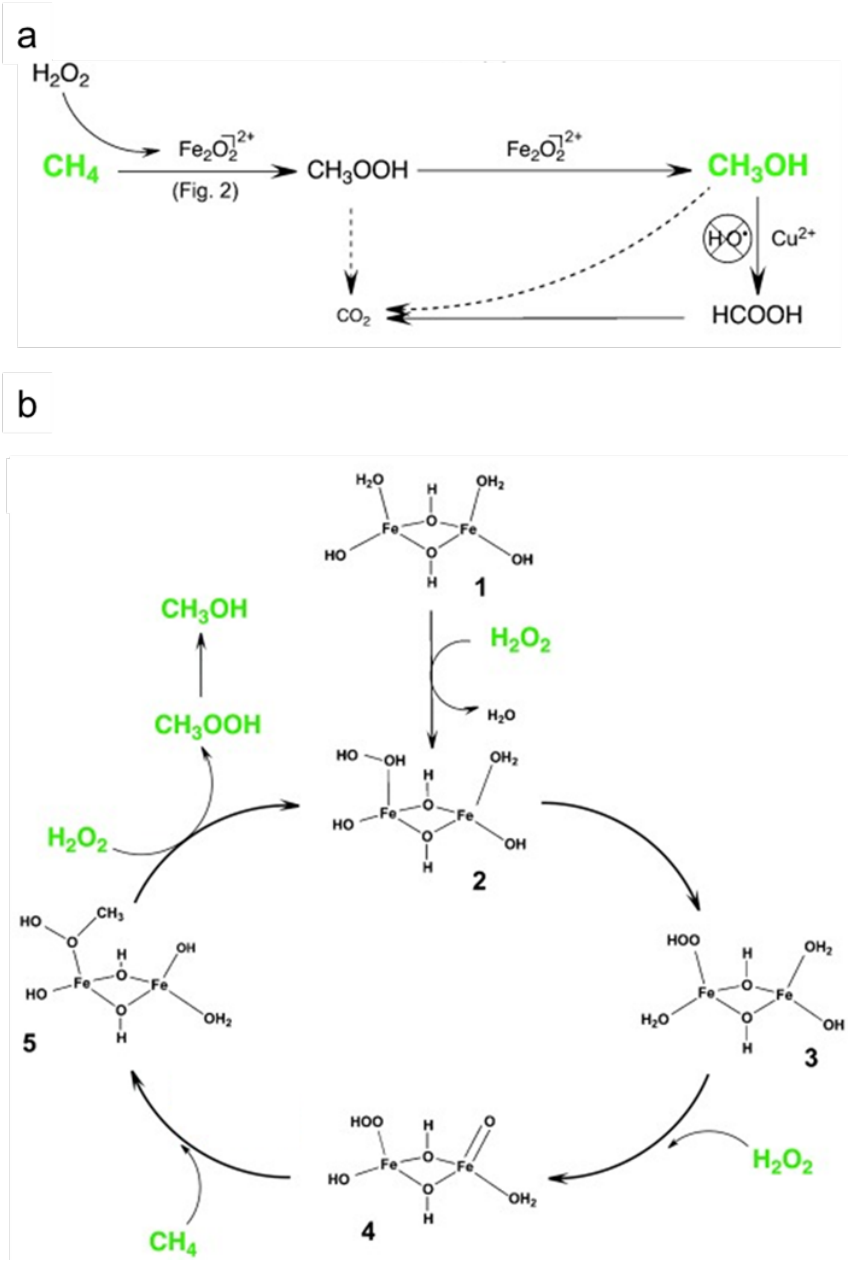

Figure 6. (a) Potential reaction scheme for the oxidation of methane based on the time-on-line profile. Methanol is formed through the conversion of the methyl hydroperoxide intermediate over the Fe sites present in the catalyst. COH radicals produced during the reaction are later responsible for the over-oxidation of methanol. The presence of Cu^{2+} inhibits undesired over-oxidation; (b) Catalytic cycle for the oxidation of methane to CH_3OOH using H_2O_2, catalyzed by a binuclear Fe species in ZSM-5. The overall charge in each case is formally +2 as the species acts as an extra-framework cation within the zeolite. Reproduced from ref.[219] *with permission from Wiley-VCH, copyright 2012.*

The active components for methane activation were found to be extra-framework Fe oligomers present in the micropores of the ZSM-5 zeolite. The role of the zeolite

structure was the stabilization, by confinement, of the high-energy, high-spin [Fe(IV)=O^{+2}] species, responsible of the C-H activation. The aqueous phase oxidation of methane to methanol was recently reviewed by Hutchings,[199] who, in a recent publication, describes the selective oxidation of methane to methanol on AuPd loaded ZSM-5 by in-situ generated H_2O_2 from molecular H_2 and O_2.[223]

Different drawback are associated to the methane to methanol process catalyzed by Fe-exchanged zeolites, such as the cost of the oxidant in the case of N_2O or the separation of low amounts of methanol from the aqueous media when employing H_2O_2. Although the use of inexpensive oxidants such as O_2 would very convenient, the activation of Fe under mild temperature conditions using molecular oxygen has not been reported so far.[13,152,204] This is not the case of copper, the active component of particulate methane monooxygenase enzyme. When exchanged in zeolite hosts, it is able to perform the selective oxidation of methane using N_2O, as Fe-zeolites do, but also using molecular O_2. This transition metal is well known for its redox properties and widely applied as catalyst in a large number of processes and has been thoroughly studied for selective methane hydroxylation.[200–204]

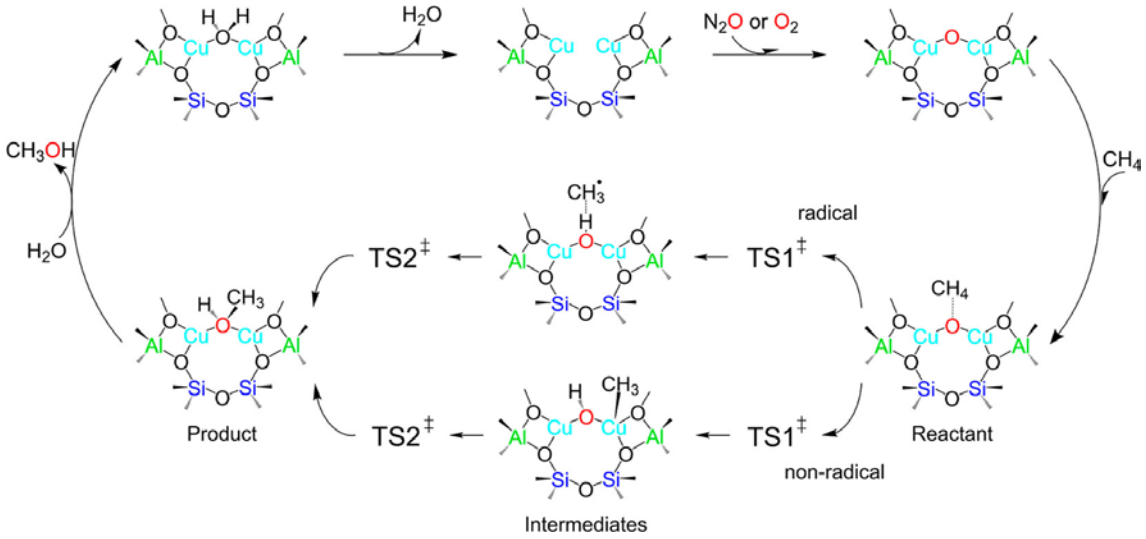

Scheme 4. Possible catalytic cycle of methane hydroxylation by $[Cu_2(\mu\text{-}O)]^{2+}$-exchanged zeolites. Reprinted from ref. [153] *with permission from the American Chemical Society, copyright 2018.*

Most studies for the methane to methanol oxidation process catalyzed by Cu-zeolites have been performed using a stepwise stoichiometric process (see Scheme 4). This chemical-looping system involves three steps, a first activation of the Cu-zeolite by an oxidant, usually N_2O or O_2 at high temperature (~450ºC), reaction of methane with the activated copper-site at lower temperature (125-200ºC), and a final extraction of the methanol formed using steam at temperatures around 200ºC. The reaction step can proceed following a radical or a non-radical mechanism.[153]

In order to avoid the final extraction step, Van Bokhoven proposed a cyclic batch-wise operation to recover methanol at the outlet of the reactor by on-stream water-assisted desorption of the product.[224] Later, the same group demonstrated that the selective methane oxidation process could be performed in an isothermal cyclic mode.[225,226] Thus, activation in O_2 flow, reaction with CH_4 and on-line methanol extraction with water enabled a continuous cyclic methanol production process.

Besides O_2 and N_2O, H_2O has been proposed as oxidant for the selective methane oxidation to methanol.[227] Methanol was produced under anaerobic conditions using water as the extraction agent which, at the same time, would regenerate the active site without the need for an additional oxidative treatment with O_2 or N_2O (see Figure 7). Moreover, the soft redox nature of H_2O when used as an oxidant prevented undesired over-oxidation reactions leading to methanol selectivities as high as 97%. In line with this study, in a recent publication, Koishybay and Shantz demonstrate that H_2O, and not dioxygen, is the main source of the oxygen present in the final methanol, by performing experiments in the absence of molecular oxygen and with the use of ^{18}O-labeled water.[228]

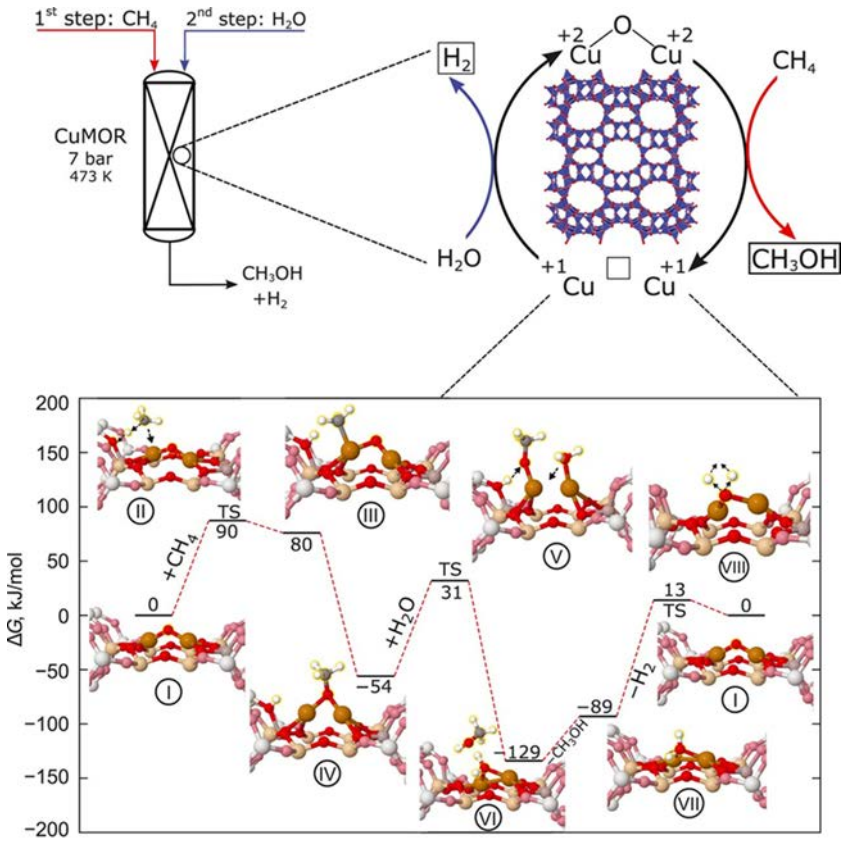

Figure 7. The mechanism of partial oxidation of methane using water as oxidant. (Top) Schematic representation of the reaction conditions. (Bottom) The DFT simulated pathway. Reprinted from ref.[227] with permission from the American Association for the Advancement of Science, copyright 2017.

The first experimental evidence for the activation of methane by a Cu-ZSM-5 after O_2 or N_2O activation at temperatures above 623K was reported by Groothaert in 2005.[229] The combination of different characterization techniques such as UV-vis, EXAFS, TEM and EPR allowed them to suggest the formation of a bis(μ-oxo)dicopper core, $[Cu_2\text{-}(\mu\text{-}O)_2]^{2+}$, in activated Cu-exchanged ZSM-5 and mordenite zeolites, species that were stabilized by the microporous structure. The active site strongly interacted with methane when the Cu-zeolite was exposed to the hydrocarbon at 398K, and further extraction of the used material with a 1:1 water/acetonitrile mixture led to the identification of methanol as the only reaction product. This work also demonstrated the influence of the zeolite topology on the methanol production capacity. Thus, zeolite Cu-Y presented low methanol yields whereas Cu-mordenite produced more methanol than Cu-ZSM-5. The poor behavior of the Cu-Y zeolite, comparable to that of a Cu-loaded amorphous silica, was related to the non-stabilization of the di-copper sites by these particular hosts.

Unlike in Fe-zeolites, the active site in Cu-exchanged microporous materials is still, nowadays, a matter of controversy. Since the first paper on Cu-zeolites by Groothaert, different structures have been proposed for the active copper species, and an instructive chronological evolution was shown by Newton et al, in a recent review (see Figure 8).[203] Elucidation of the nature of these active sites has only been possible thanks to the combined application of sophisticated characterization techniques, mainly spectroscopic,[201,203] and computation methodologies.[153,198]

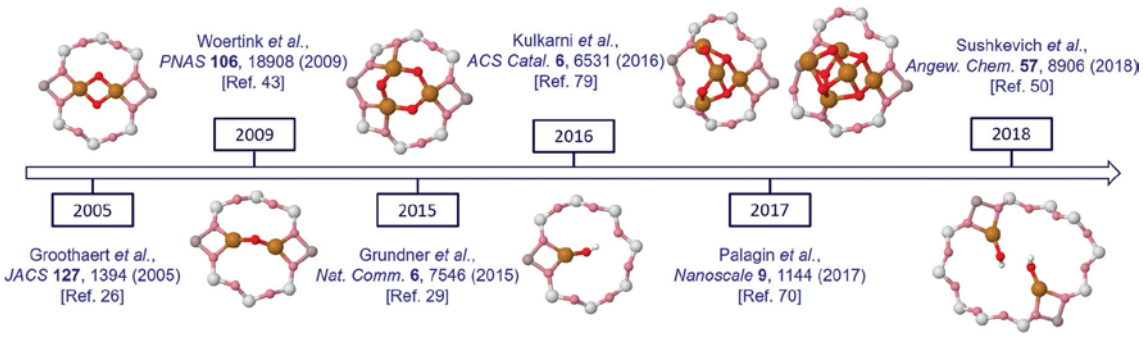

Figure 8. Timeline of various suggested configurations of the Cu oxide active species in Cu-MOR. Reproduced from ref.[203] *with permission from the Royal Society of Chemistry, copyright 2020.*

Thus, the combination of isotopic studies and theoretical calculations led Sels and Solomon, some years later, to discard the a bis(μ-oxo)dicopper core proposed in 2005,[229] and to define a bent mono-(μ-oxo)dicupric species as the activated copper active site in Cu-ZSM-5 (see Figure 9a,b).[230] The bridging oxygen was found to be highly reactive for low temperature cleavage of the stable C-H methane bond. The same group proposed a peroxo dicopper(II) species as the oxygen precursor to the mono-oxygen $[Cu_2O]^{2+}$ reactive site when the Cu-ZSM-5 was activated in O_2 (see Figure 9c),[231] a precursor that was not observed when N_2O was used as the oxidant. When methane was oxidized in the presence of N_2O, the latter was bridged between two Cu^I centers coordinated to framework Al bonded O atoms. It was shown that the two Cu^I centers had to be close enough to allow the formation of stable N_2O bridging structures.[232]

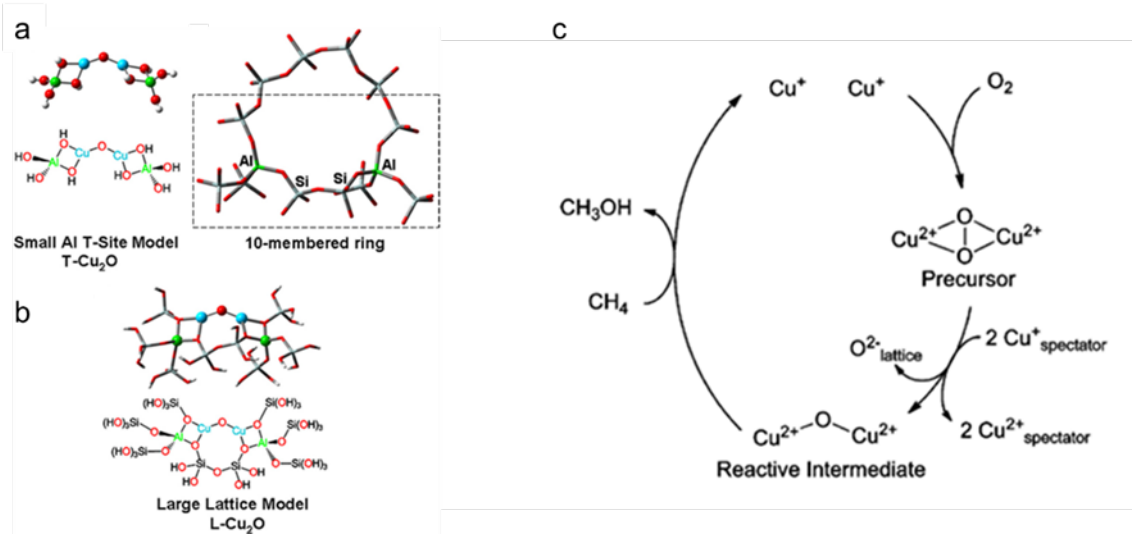

Figure 9. Bent $[Cu_2O]^{2+}$ active site (a) and oxygen precursor (b) in Cu-ZSM-5; proposed process for the selective oxidation of methane to methanol in oxygen activated Cu-ZSM-5. Reprinted from ref.[230] *and ref.*[231] *with permission from the American Chemical Society, Copyright 2010.*

The mono-(μ-oxo)dicupric site was also described to be present in activated Cu-mordenite, presenting similar spectral features assigned to this di-copper site and similar reactivities.[233] This zeolite structure [MOR] presents parallel 12-ring channels connected by 8-ring side pockets. The $(Cu_2O)^{2+}$ site was seen to be stabilized in the 8-ring windows of these pockets, and as they present two different 8-ring windows, facing the 12-ring and the 8-ring channels, two different sites were distinguished depending on the location of the Cu site.

Also in 2015, a single site tri-nuclear Cu-O cluster was proposed by Grundner et al.,[234] for Cu-exchanged mordenite (see Figure 10). Following a meticulous preparation procedure, they obtained a Cu-exchanged mordenite with a well-defined uniform single copper site located at the pore mouths of the 8-ring side pockets, compensating the charge of 2 paired Al located in this 8-ring. This Cu-mordenite was shown to be more active for methane conversion to methanol than analogous metallozeolites described

previously. DFT calculations showed that binuclear Cu species were more stable at 0K and under relatively low oxygen partial pressures,[235], but at 700K in a dry O_2 atmosphere the stability of the tri-copper $[Cu_3(\mu\text{-}O)_3]^{2+}$ was higher. Spectroscopic measurements confirmed the optimized structure proposed by DFT and demonstrated that the single sites formed in this particular Cu-mordenite were different from those observed in Cu-ZSM-5 prepared by means of conventional ion exchange procedure. The trinuclear Cu-oxo clusters were hydrolyzed during the methanol extraction step but the sites were fully recovered by treatment in O_2.

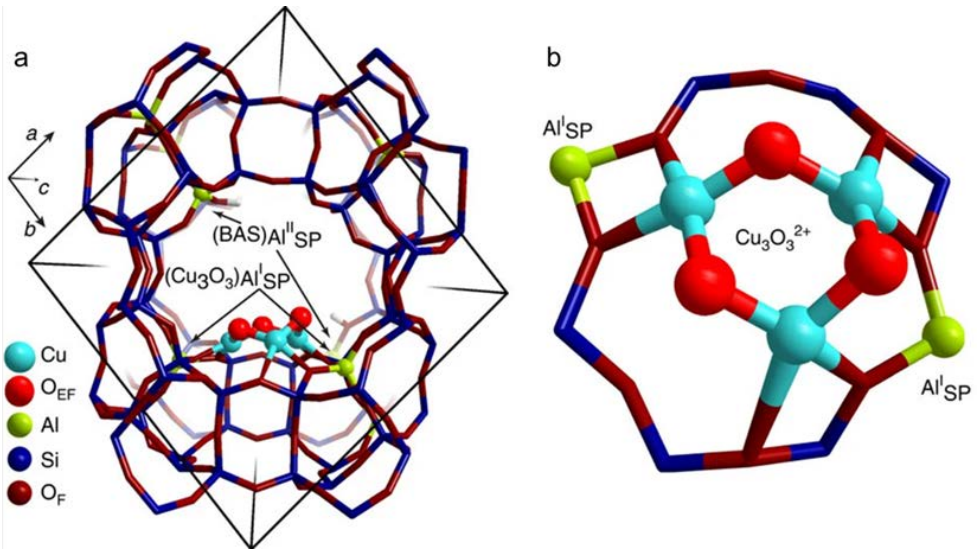

Figure 10. Structure and location of $[Cu_3(\mu\text{-}O)_3]^{2+}$ cluster in mordenite predicted by DFT. The zeolite model contained paired (type I) and isolated (type II) Al atoms located at the pore mouth of the side pocket. The cluster is stabilized by two anionic centres due to Al^{I}_{SP} lattice sites at the entrance of the MOR side pocket (b) so that the extra-framework oxygens responsible for the initial C–H activation are pointing towards the main channel of MOR (a). The charge due to the remaining Al^{II}_{SP} is compensated by acidic protons resulting in BAS formation. Reproduced from ref.[234] with permission from Springer Nature, copyright 2015

This work evidences, again, the similarities of Cu-exchanged zeolites with p-MMO enzymes in the selective methane oxidation to methanol, with the steric constrains imposed by the 8-ring side-pockets of the MOR structure enhancing the activity of the

active copper clusters located therein. Still, the application of multivariate curve resolution analysis of X-ray absorption spectroscopy data by Beato and Borfecchia identified the active copper site to be a di-nuclear species.[236]

Besides the di- and tricopper oxo species described so far, Palagin et al. showed that larger copper-oxide clusters, such as tetramers or pentamers, with $Cu_nO_n^{2+}$ and $Cu_nO_{n-1}^{2+}$ stoichiometries, were also stabilized in the 8-ring channels of Cu-mordenite. Increasing the size of the cluster from dimers to pentamers increased the overall stability of the system due to the effect of multiple Cu-O bonds, and this allowed a better stabilization of the OH and CH3 species during the methane activation step.[237]

For several years, the Cu-zeolites studied for methane hydroxylation were limited to microporous materials with medium and large pore structures. Besides ZSM-5 and mordenite, other topologies were also tested, such as ferrierite,[238,239] Y, EMT or beta zeolite.[238] Although ZSM-5 and mordenite were the only two structures able to stabilize the di-copper site and to hydroxylate methane to methanol at 150ºC, ferrierite and beta were capable of producing methanol at a higher temperature of 200ºC. This suggested the formation of a different type of Cu active site. Cu-exchanged EMT and Y zeolites, with structures presenting 3D 12-ring channel systems and large cages, were not active.

It was not until 2015 that Lobo proved Cu-exchanged small pore zeolites and zeotypes to be also active for the selective oxidation of methane to methanol[216], and the new materials studied, Cu-SSZ-13 [CHA], Cu-SSZ-16 [AFX], Cu-SSZ-39 [AEI] and Cu-SAPO-34 [CHA], were claimed to yield more methanol per copper atom than Cu-ZSM-5 or Cu-mordenite. Further studies from this group on Cu-SSZ-13 and Cu-SSZ-39 allowed them to identify di-copper species in both cases, although differing in their structure.[240] Thus,

trans-μ-1,2-peroxo dicopper(II) ($[Cu_2O_2]^{2+}$) and mono-(μ-oxo) dicopper(II) ($[Cu_2O]^{2+}$) were observed in Cu-SSZ-13 and Cu-SSZ-39, respectively, after O_2 or He activation at 450 °C. The concentration of Cu(II) located in the 8-ring windows was found to be related to the amount of $[CuOH]^+$, species that were suggested as intermediates in the formation of the active $[Cu_2Oy]^{2+}$ sites. On the other hand, Kulkarni et al., combining thermodynamic analysis of the oxygen activation process with periodic DFT calculations, identified a mono-copper species located in the 8-ring windows/channels of Cu-SSZ-13, as the active site responsible for methane activation,[241] and proposed the reaction mechanism presented in Scheme 5 that was consistent with previous experimental and spectroscopic data.

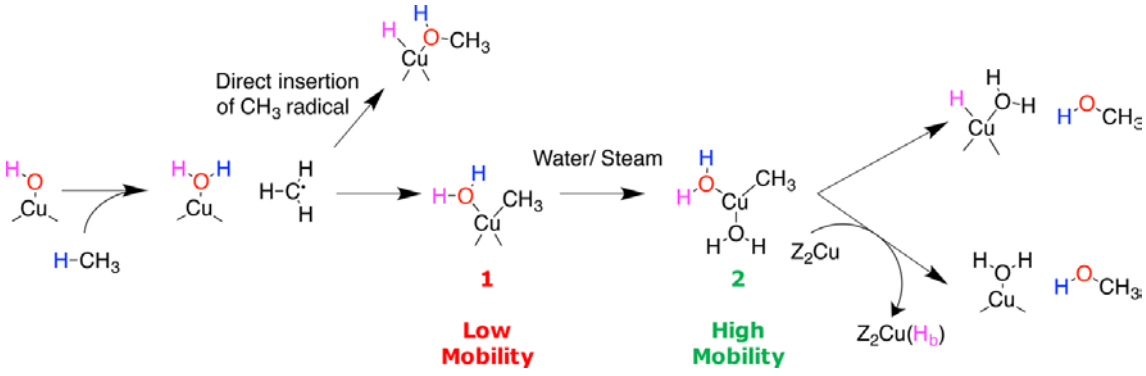

Scheme 5. Reaction scheme for partial methane oxidation to methanol for 8MR-$[CuOH]^+$ active site in Cu-exchanged CHA. Reprinted from ref.[241] with permission from the American Chemical Society, copyright 2016.

The composition of the Cu-SSZ-13 material (Si/Al ratio and Cu loading) will affect the redox properties of the copper species formed and their location within the host structure. In this line, Pappas et al. showed that low Si/Al ratios and low Cu-loadings favored the formation of copper species located in the 6-ring windows of the SSZ-13 structure, which are inactive for methane conversion due to their low reducibility. However, for intermediate Si/Al ratios, in the range of 12-15, and higher Cu loadings the

mono-Cu species were located in the 8-ring windows leading to optimal Cu reducibility and maximum methanol productivity (see Figure 11).[242]

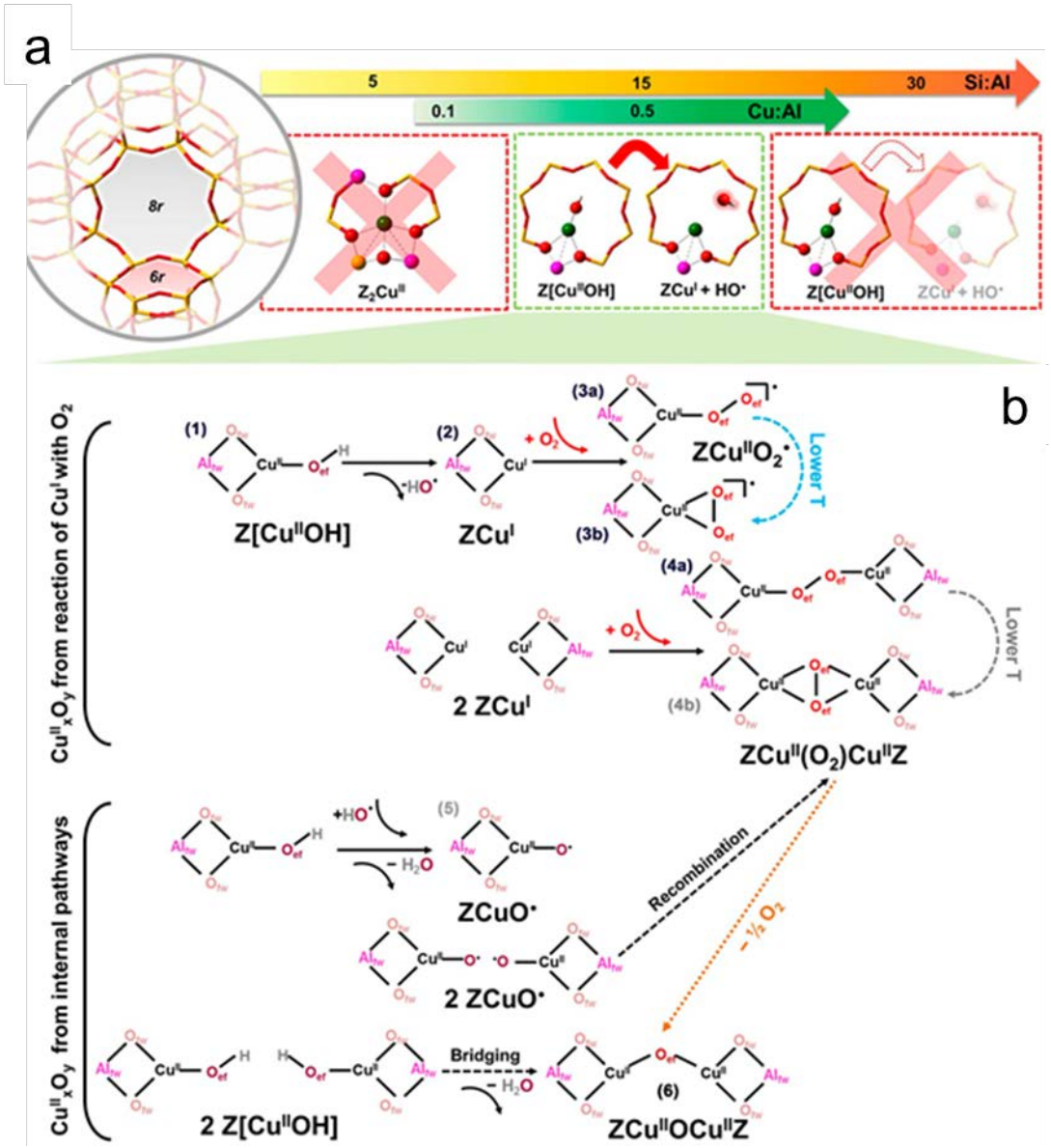

Figure 11. (a) Rationalization of the effect of composition (Cu/Al and Si/Al ratios) on the productivity for the methane-to-methanol conversion over Cu-SSZ-13,considering $Cu^{II}_xO_y$ formation from reaction of self-reduced ZCu^I sites with O_2 (b, top) and from internal pathways (b, bottom). Species indicated with grey labels have been previously detected in Cu-zeolites (4b) or proposed as intermediates (5) but are not directly observed here on Cu-SSZ-13 materials. Reprinted from ref.[242] with permission from the American Chemical Society, copyright 2017.

In a recent paper the performance of two Cu-exchanged small pore microporous materials with the same CHA topology but different chemical composition, silicoaluminate SSZ-13 and silicoaluminophosphate SAPO-34, were compared in the step-wise methane hydroxylation. According to spectroscopic results, the different framework polarities, and different amount and distribution of ion exchange sites in the two isostructural CHA materials were seen to affect the location and coordination of the copper species and, consequently, their activity towards methane conversion.[243]

The first evidences of a continuous, true catalytic process, carried out under mild conditions (atmospheric pressure and 483K) was reported in 2016 by Roman-Leshkov and his group.[244] Methane hydroxylation was catalyzed by different Cu-exchanged zeolites using O_2 as the oxidant, and although the reactions rates observed were low, isotopic studies demonstrated catalytic turnovers and, thus, catalytic oxidation of methane to methanol over copper sites stable in the presence of steam, sites that were also identified by Alayon et al. in Cu-exchanged mordenites.[245]

Independently of the zeolite structure hosting the copper active sites, the presence of Brønsted acidity was seen to have a beneficial effect on the performance of Cu-zeolites for methane hydroxylation following the step-wise and the continuous operating modes.[244,246–248] After activation and cleavage of the methane C-H bond on the active copper sites a surface methoxy species is formed, located at the zeolite BAS, surface methoxy groups that are key intermediates for the methane to methanol process.[247]. Regarding the influence of copper incorporation procedures or zeolite morphology, the interested reader can find additional studies, recently published.[248,249]

Besides iron and copper, other metals have been studied for the selective methane hydroxylation. Thus, Beznis et al. reported cobalt exchanged ZSM-5 for the selective conversion of methane to methanol,[250,251] Shan et al. converted methane to methanol in the presence of bent mono(m-oxo)dinickel species in ZSM-5,[252] and Huang et al. reported the low temperature selective oxidation of methane to methanol by H_2O_2 on Pd_1O_4 single-sites anchored to silicalite, the pure silica ZSM-5.[253]. In a very interesting approach, Xiao has recently presented a ZSM-5-based catalyst with AuPd alloy nanoparticles encapsulated inside of the zeolite micropores and a hydrophobic external surface achieved by anchoring of organosilanes.[254] The hydrophobic molecular fence avoids the diffusion of the H_2O_2, generated in situ on the AuPd nanoparticles from molecular H_2 and O_2, out of the crystals, while allowing methane to diffuse into the zeolite channels increasing, in this way, the efficient methanol production and preventing its over-oxidation. Isolated rhodium Rh^+ cations anchored on a ZMS-5 zeolite or titanium dioxide were used for methane conversion to methanol or acetic acid in the presence of O_2 or CO, respectively.[255] Acetic acid was also produced in an interesting approach by the group of Román-Leshkov, where the selective oxidation of methane to methanol was coupled with methanol carbonylation in Cu-exchanged mordenite.[256] The specificity of the copper and BAS within the 8-ring side pockets of the MOR structure, responsible for the high acetic acid yield, was demonstrated by means of coupled spectroscopic and reactivity measurements.

As mentioned at the beginning of this section, despite the huge amount of intense research performed in the methane to methanol conversion in the presence of metallo-zeolites and -zeotypes along the last two decades, the results are still far from

commercial implementation. Besides improving activity of the catalysts, it is crucial to implement protection strategies that allow increasing the selectivity to methanol.

3.3. Oxidative methane coupling

The first papers reporting on the oxidative conversion of methane to C_2 hydrocarbons date from the early 1980's and used alumina supported metal oxides.[257,258] However, since the pioneering work by Ito and Lunsford in 1985 on the use of lithium-doped magnesium oxide for catalyzing the oxidative methane coupling (OMC),[259] most of the research in this field has been focused on the use of basic oxides as catalysts for this process. When methane is contacted with these basic oxides in the presence of oxygen and at temperatures ranging from 650 to 950ºC, it is converted into ethane and water, and ethane reacts further to ethene and higher hydrocarbons by means of secondary-consecutive reactions.[260–262] Unfortunately, under these severe conditions close to those of catalytic combustion, the selectivity to the desired hydrocarbons is limited by their over-oxidation to CO and CO_2, thermodynamically favored, and is closely dependent on the oxygen availability.

Different approaches have been proposed in order to improve the hydrocarbon yield, such as the continuous removal of ethylene by operation in a recycle[263–265] or the integration of a second catalytic process where ethylene is further converted into aromatics or higher olefins on a zeolite based catalysts, following a single-pass[159,266] or a two-step strategy.[264,267–269] The catalysts described for the second step conversion of the C_2 hydrocarbons by aromatic alkylation are acid ZSM-5,[269] and those used for their aromatization are Ga- or Mo- doped H-ZSM-5,[159,264,267,268] or Mo/H-MCM-49.[266]

Aromatization reactions and the corresponding bifunctional catalysts will be covered in detail in Section 4.4.

Besides alkali, alkaline earth and rare-earth oxides, Mn–Na_2WO_4/SiO_2 was proposed as an active catalyst for OMC, with high selectivity to C_2 hydrocarbons and high stability under the high temperature reaction conditions.[270] An interesting approach in this line was that of Wang et al., where Ti-MWW and Ti-silicalite zeolites were employed not only as SiO_2-rich support but also as TiO source for a TiO doped MnO-NaWO/SiO OCM catalyst.[271] Under activation and testing conditions the microporous structures are lost, but the formation of a MnTiO mixed oxide favors the O activation on the Mn sites whereas NaWO activates methane at temperatures as low as 650ºC.

During the OCM process both surface catalyzed and gas-phase free-radical reactions take place. In a first step, CH_4 is activated on the catalyst and a surface CH_3·radical is formed by abstraction of a hydride. In a second step, these radicals are released to the gas phase where they will couple to form ethane or will participate in the formation of higher hydrocarbons by chain branching reactions.[150] For a critical analysis of the OCM process and the present drawbacks regarding its commercialization, the interested reader is referred to a recent viewpoint by Linic.[261]

Although traditionally non-microporous solids have been used for catalyzing this reaction, Ernst and Weitkamp described the ability of zeolite and zeotypes to catalyze the oxidative coupling of methane in the early 1990'.[272] Aluminophosphate $AlPO_4$-5 loaded with 10 wt.-% of a Na_2O/CaO-mixture (molar ratio Na_2O/CaO = 3.4 to 14) and Na-enriched zeolite NaY were the best performing catalysts, and maximum C_2 yields of 14% were claimed for the Na-rich large pore zeolite.

Kovacheva and Davidova also reported the use of basic AlPO-5 and zeolite X based catalysts for OCM. Basic sites were generated by impregnation with Pb[273] or Cs[274] or by ion exchange with Li^+ or Cs^+[275] and of medium pore ZSM-5 loaded with 1-10 wt% MgO.[276] Although stable with time on stream regarding activity and selectivity to C_2 hydrocarbons, the higher the basicity of the basic zeolites, the higher their activity but the lower the selectivity to the desired products. The same type of catalysts were also explored by the group of Kovacheva, with more success, for the oxidative cross-coupling of methane with ethylene or aromatics to produce propylene and higher value aromatic products. Cs-impregnated AlPO-5 presented higher selectivity and yield to ethylbenzene and styrene in the oxidative methylation of toluene than Cs-exchanged X, Y or ZSM-5 zeolites, where Cs was finely dispersed.[277] When comparing the catalytic behavior of X zeolite modified with alkali earth oxides, they found that BaO outperformed the others.[278] Regarding the effect of zeolite chemical composition and structure for BaO loaded zeolite catalysts, both were seen to affect their activity and selectivity in the oxidative methylation of toluene.[279] Thus, for large pore zeolites such as X or Y conversion was higher for higher framework Al contents, and BaO/NaX (Si/Al=1.2 was twice as active as BaO/NaY (Si/Al=2.5). However, BaO supported mordenite or ZSM-5 performed better than the large pore zeolites evidencing an important influence of the zeolite structures on the location of the basic oxide and on its accessibility to the reactants.

The methane cross-coupling reactions described so far were carried out in continuous flow reactors under high temperature and atmospheric pressure gas phase conditions, but the use of zeolite based catalysts for the direct methylation of aromatic compounds in batch reactors and under high methane pressures has also been studied. The earliest

publications confirmed by $^{13}CH_4$ isotopic tracing that the methyl groups of the alkylated products corresponded to methane molecules in the feed[280–282] and the reaction was thought to occur under non-oxidative conditions. However, later work by Adebajo[283,284] demonstrated that the presence of oxygen is essential for the methylation to occur (see Figure 12), and that the previous results reported by Long and Wilson were probably affected by the unintentional introduction of air during the reactor loading step. Thus, the overall process was shown to proceed via a two-step mechanism, with the formation of methanol by partial methane oxidation in a first step, and the alkylation of the aromatics with the methanol formed in a second step. This was seen to be the main benzene conversion route in the presence of ZSM-5 based catalysts or Cu-Beta, with reduced acidity. However, production of alkylaromatics was confirmed in the absence of oxygen when highly acidic H-Beta was the catalyst used for benzene methylation [285]. In this case, the alkylating agents were produced by catalytic cracking of the aromatic hydrocarbon. Oxidative methylation of toluene was complicated by the important contribution of toluene disproportionation to the overall process, yielding benzene, xylenes and heavier aromatics.[286] The extension of these side reactions could be reduced by decreasing the amount of BAS, either by increasing the zeolite Si/Al ratio or by neutralizing part of the sites by alkali cations.

A thorough overview of the high pressure oxidative methylation of aromatics and on the possible advantages as compared to direct alkylation of aromatics with methanol was given by Abadejo.[287] Unfortunately, and despite the exhaustive revision of the influence of experimental conditions and zeolite acidity on the aromatic conversion, taking place in the second alkylation step, no information is given regarding the nature of the active

sites for the non-trivial partial oxidation of methane to methanol occurring in the first step of the process.

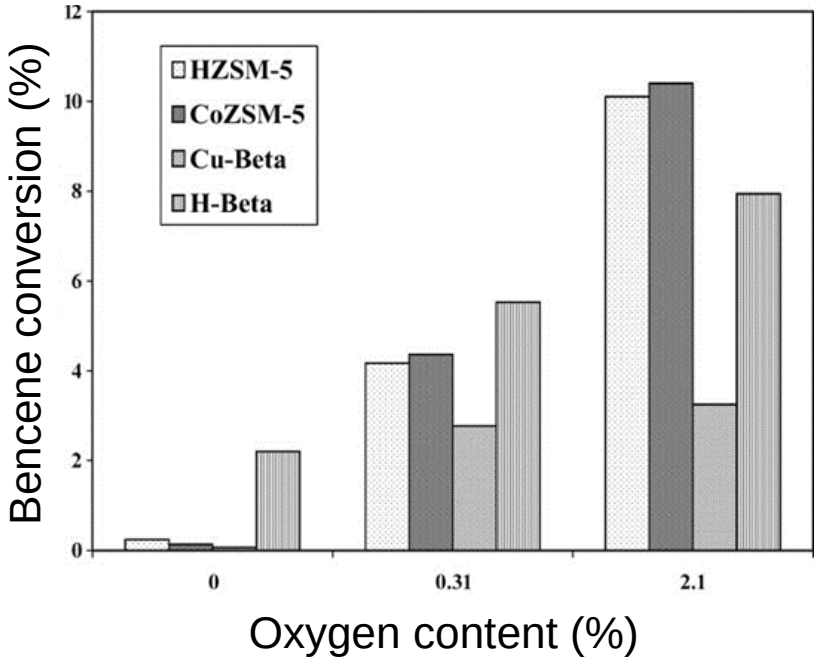

Figure 12.Variation of benzene conversion with oxygen content for the methylation of benzene with methane in a batch reactor at 400ºC and 6.9 MPa pressure for 4 h. Reprinted by from ref.[288] *with permission from Springer Nature Customer Service Centre GmbH: Springer Nature Research on Chemical Intermediates, copyright 2000.*

3.4. Non-oxidative methane coupling

The efficient direct conversion of methane to H_2, ethylene and aromatic hydrocarbons has been achieved by Bao under non-oxidative conditions and high temperatures (1363K) with a catalyst based on single Fe sites embedded in a SiO_2 matrix.[289] The absence of coke formation led to high hydrocarbon selectivity and stable performance during 60 h on stream, but the use of a non-shape selective catalyst resulted in a final product mixture formed by a wide range of products, including naphthalene in selectivities as high as 38.2%. An alternative route for converting methane to light

olefins or aromatics under non-oxidative conditions and lower temperatures is in the presence of bifunctional zeolite based catalysts. In this case the single-pass conversion is lower because of the lower reaction temperature and catalyst suffers fast deactivation by coking, but due to the high selectivity to C_{2+} hydrocarbons, mainly benzene, this direct zeolite-based route is still of high interest. Most of the effort has been directed to the conversion of methane to aromatics and, more specifically, to benzene.[136,290,291] However, some recent publications describe the selective formation of light olefins, which is possible by adjusting the acidity of the zeolitic support.[292,293]

The first publications on methane conversion into higher value hydrocarbons date from the late 1980's and early 1990's, where Cr, Ga, Zn or Pt-Cr loaded ZSM-5 were shown to catalyze its dehydroaromatization to aromatics. However, the results obtained by Wang et al. in 1993, using Mo-supported ZSM-5, were the starting point for the study of transition metal impregnated zeolites as catalysts for non-oxidative methane conversion, a research line that has remained active until today.

Several exhaustive reviews have been published in the last two decades on non-oxidative methane dehydroaromatization (MDA).[294–302] Here, we will summarize the main general aspects described there and we will focus on the most recent findings regarding the reaction mechanism and the nature of the active sites involved, as well as the nature of coke species formed and their contribution to the overall process.

Methane dehydroaromatization under non-oxidative conditions is a highly endothermic process and requires high temperatures in order to achieve reasonable conversions. Under those conditions, the thermodynamically favored product is coke (see Figure 13).

In fact, methane thermal or catalytic pyrolysis is an effective way for producing CO_x-free hydrogen for PEM fuel cells, oil refineries, and ammonia and methanol production.[294,303]

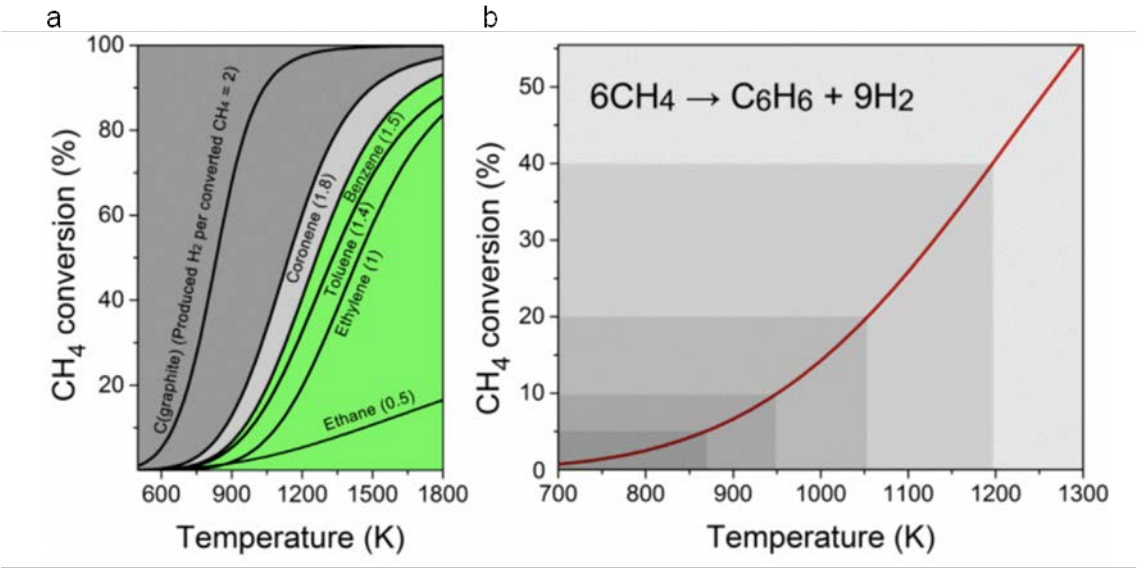

Figure 13. (a) Temperature dependence of equilibrium conversion of non oxidative methane conversion: $xCH_4 \rightarrow C_xH_y + (4x\text{-}y/2)H_2$; (b) equilibrium conversion for methane dehydroaromatization calculated by Aspen Hysys V.8.6 software. Adapted from ref.[298] *with permission from Wiley-VCH, copyright 2017.*

As mentioned before, multifunctional zeolite supported transition metal (TM) catalysts are able to convert methane into higher-value hydrocarbons under non-oxidative conditions. In the presence of these metal-loaded zeolite based catalysts, the MDA process usually occurs through three consecutive steps, an activation or induction period, an intermediate stage with quasi-steady-state benzene production and a final deactivation period (see Figure 14).

During the activation period, the starting Mo-oxo species are reduced to molybdenum carbide and oxo-carbide species, able to activate the methane C-H bonds, and the only products observed are CO, CO_2, H_2O and H_2.[304,305] Once the active species are formed benzene appears as the main product and CO is absent from the reaction product

stream. As catalyst deactivates with TOS, the yield to aromatics decreases and ethylene appears as the main hydrocarbon product.

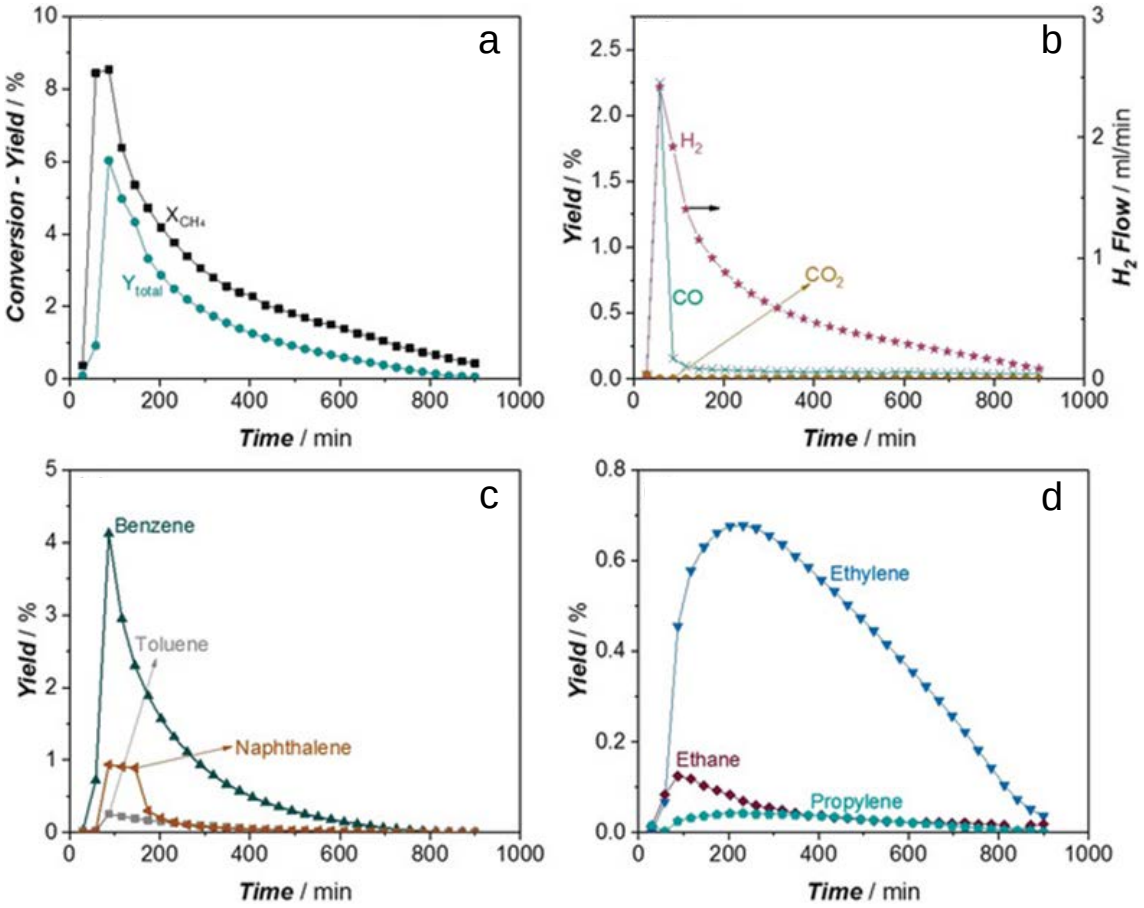

Figure 14. Catalytic activity of 2 wt.% Mo/H-ZSM-5 at 725ºC under non-oxidative conditions (11.765 mol% N_2 and 88.235 mol% CH_4 in the inlet, WHSV: 2.58 h^{-1}) (a) Conversion and total yield (without CO and CO_2); (b) Yields of CO, CO_2, and H_2 flow; (c) Yields of major aromatic products; (d) Yields of major aliphatic products.Reproduced from ref.[306] *with permission from Wiley-VCH, copyright 2020.*

ZSM-5 has been, by far, the most studied zeolite for MDA, but other zeolite structures have also been reported as the acid support component of the MDA catalysts.[297,302,307] As could be expected, the zeolite properties, such as its framework topology, its chemical composition, directly related to the Brønsted acid site density, or its crystal size and presence of additional secondary pore systems have an important effect on the catalyst's efficiency.[290] They will not only determine the final active species formed by

affecting the dispersion and location of the TM and, therefore, the catalyst activity, but will also influence the selectivity to the different products formed, including coke and, eventually, the catalyst deactivation rate. An early study by Zhang et al. compared a large number of zeolite and zeolite-related materials, including ZSM-5, ZSM-8, ZSM-11, Beta, mordenite, X, Y, MCM-41, SAPO-5, SAPO-11, and SAPO-34.[308] Among those, only the zeolites presenting two- or three-dimensional channel systems and pore sizes in the range of 5.5-6 Å, close to the kinetic diameter of benzene, such as H-ZSM-5, H-ZSM-8, H-ZSM-11 or beta, were able to catalyze the selective methane conversion to aromatics, as the formation of heavier aromatics was limited by shape selectivity. Large pore zeolites produced mainly coke, and small amounts of ethylene, whereas the SAPO-materials where much less active because of their lower acidity. Shu et al. showed that small pore zeolites were also active for methane conversion but, as in the case of large pore zeolites, main product was coke and none of them were able to give benzene as a product, even when prepared and tested in the same way as 10-ring ZSM-5.[309]

Other medium pore zeolites studied as acid supports for MDA catalysts have been those belonging to the MWW family, MCM-22, ITQ-2, and MCM-36. These zeolites can be prepared starting from the same layered precursor P-MCM-22, formed by microporous layers presenting a sinusoidal 10-ring channel and external hemicavities or cups. Topotactic condensation of these layers by calcination leads to the microporous 3D zeolite MCM-22, which presents a second, independent pore system formed by 12-ring cavities connected through 10-ring windows. Separation of the layers by swelling with $CTMA^+$ followed by delamination or pillarization leads to ITQ-2[74] and MCM-36 [310], respectively, with higher external surface area and mesoporosity as compared to MCM-22. In good agreement with the lower sterical restrictions, Mo/ITQ-2[311] and Mo/MCM-

36[312] were less selective to benzene than Mo/MCM-22 and produced more naphthalene. On the other hand, Mo/MCM-22 was described to be as active and selective to benzene as Mo/ZMS-5, but more stable towards deactivation with time on stream than the latter when tested under comparable experimental conditions.[313–316] This better performance of the MCM-22-based catalyst was attributed to its particular pore structure, more open than that of ZSM-5, which, besides favoring product diffusion, also improved the dispersion of the Mo species by facilitating their migration through the pores towards ion exchange positions.[317] Similar results were reported for Mo-loaded MCM-49, isostructural to MCM-22 [318]. Other medium pore zeolites described as catalysts for the MDA reaction have been ITQ-13, TNU-9 or IM-5.[155,319–321] In the case of ITQ-13, the low acidity of the zeolite described by Xu et al., could be the reason for its low activity.[319] However, TNU-9 and IM-5 both outperformed a reference ZSM-5 based catalysts in terms of activity and benzene selectivity.[155,320,321] All these studies evidence the importance of the zeolite framework topology, of the BAS density and their location on the activity and selectivity of zeolite based catalysts.

Regarding the transition metal (TM), Mo-based catalysts are the ones presenting the highest activity and selectivity to benzene (see Table 3).[322] Thus, the possible configurations of Mo active species have been the most studied and are the best understood, as we will show later, although their structure is still a matter of debate and the reason for its better performance as compared to other metals is another open question.[307] Co, Fe, Mn, Ni, Re or W are some of these TM, others than Mo, which have shown to be active for methane conversion to aromatics.[296,297,300,307]

Table 3. Comparison of different TMI supported on ZSM-5 as catalysts for MDA. Adapted from Ma et al.[296]

Active metals	Reaction conditions		CH_4 conversion (%)	Selectivity (%)	
	T (ºC)	Flow ($mL g_{cat}^{-1} h^{-1}$)		Bencene	Naphthalene
Mo	730	1500	16.7	60.4	8.1
Zn	700	1500	1.0	69.9	–
W	800	1500	13.3	52.0	–
Re	750	1440	9.3	52.0	0
Co-Ga	700	1500	12.8	66.5	7.2
Fe	750	800 ($GHSV/h^{-1}$)	4.1	73.4	16.1
Mn	800	1600	6.9	75.6	11.9
V	750	800 ($GHSV/h^{-1}$)	3.2	32.6	6.3
Cr	750	800 ($GHSV/h^{-1}$)	1.1	72.0	3.7

The combination of Mo with a second metal has also been described. Thus, small amounts of Fe, Co, Ni, Cu Z, Ga, Cr or Ag were seen to promote the catalytic behavior of Mo-loaded zeolites regarding methane conversion, benzene selectivity or stability towards deactivation. A more detailed analysis on the role of promoters can be found in more specific reviews.[296,323] More recent works also describe the addition of K, Fe and Rh to Mo,[324] the combination of Fe with Zr, Nb or Mo,[325] the use of bimetallic Mo-Co and Mo-Ni,[326] or noble metal promoted Fe[327] on HZSM-5-based MDA catalysts.

In the case of metal-loaded zeolite based catalysts, the metal incorporation method may have a significant effect on the final catalytic properties of the material. This is also true for MDA catalyst. Although in this case Mo/ZSM-5 is usually prepared by incipient wetness or slurry impregnation, employing ammonium heptamolybdate (AHM) as the

metal precursor,[328] molybdenum can also be incorporated by solid-state ion exchange[329–331] by physically mixing the zeolite with the Mo precursor, MoO_3. The absence of byproducts formed during calcination facilitated the study of the evolution of the Mo species during activation by means of different characterization techniques. This enabled the group of Iglesia to confirm the formation of MoO_3 crystallites on the external surface of the zeolite at temperatures of 623-773K, their migration into the zeolite pores at higher temperatures and their interaction with the zeolite BAS. The species proposed were $(Mo_2O_5)^{2+}$ dimers or mononuclear $[MoO_2^{2-}]$ interacting with one or two acid hydroxyls (see Scheme 6), depending on the Mo/Al ratio and the Al-disposition.[304] The presence of polynuclear Mo species on the zeolite surface and of mononuclear species inside of the zeolite channels, as well as the migration of Mo species during impregnation and further treatments, was evidenced by EPR spectroscopy combined with additional characterization by the group of Bao.[332,333] In later studies they identified $[Mo_5O_{12}^{6-}]$ species interacting with the zeolite BAS and reducing, in this way, the density of acid sites.[334] A thorough spectroscopic study on Mo/HZSM-5 with different Mo loadings and varying Si/Al ratios under operando conditions enabled Gao et al. to identify the active MoO_x nanostructures for methane conversion as those anchored to one or two framework Al atoms.[335] Direct evidences were given there for the formation of MoC_x or MoC_xO_y nanoparticles with an average size of 0.6 nm by exposure to the methane feed, and for the recovery of the isolated Mo oxide structures after an appropriate O_2 treatment.

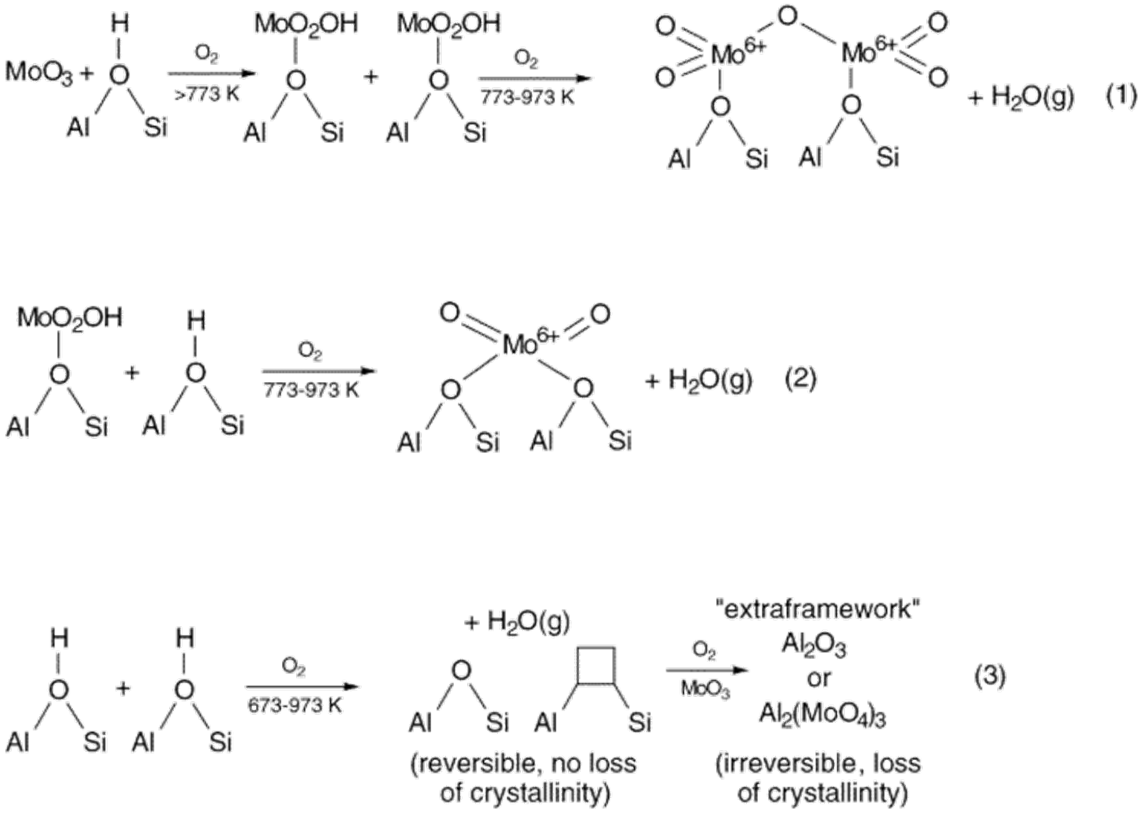

Scheme 6. Interaction between MoO_x species and Brønsted acid sites in H-ZSM-5. Adapted from ref.[336] *with permission from the American Chemical Society, Copyright 1999.*

Decreasing the Mo loading reduces the type of Mo species present in the parent sample and facilitates the identification of possible active site precursors. In this way, for Mo/H-ZSM-5 with Mo contents in the range of 1-2%, the metal is mainly in the zeolite micropores as cationic mono- and dinuclear Mo-oxo species, with increased oxidative stability as compared to catalysts with higher metal contents.[337] A thorough study on the influence of dispersion, acidity and textural properties of Mo/H-ZSM-5 on its performance on MDA was performed by Vollmer et al.[338] A set of 17 Mo/HZSM-5 catalysts was prepared using different procedures, varying Mo precursors and Mo loadings, and the samples obtained presented different proportion of cationic Mo species anchored to the zeolite framework and Mo clusters at the zeolite external

surface. Correlating the type of Mo species with the catalytic behavior of the samples, they showed that the cationic Mo complexes were responsible for the conversion of methane to benzene and naphthalene, whereas the selectivity to coke increased with the amount of Mo forming larger clusters of nanoparticles on the external surface of ZSM-5.

Regarding the active sites for methane activation, the application of ^{95}Mo NMR spectroscopy on a ultrahigh field NMR spectrometer to the study of fresh and working Mo/H-ZSM-5 MDA catalysts allowed the direct observation of the Mo-species involved and evidenced that those in ion exchange positions were the active sites responsible for the methane dehydrogenation reaction.[339] Earlier studies by Iglesia on the structure of Mo species in working Mo/H-ZSM-5 catalysts obtained by physical mixtures of MoO_3 and the acid zeolite revealed that under CH4 conversion conditions the $Mo_2O_5^{2+}$ dimers were reduced and carburized to small MoCx clusters (0.6-1.0 nm) restoring the original BAS of the zeolite.[340] More recent work based on operando microscopy and spectroscopy analysis of Mo/ZSM-5 samples concluded that the active Mo species were formed by partial reduction of single-atom Mo sites anchored to the framework, well dispersed inside the pores of the ZSM-5 structure.[156] The dynamic nature of the oxy-carbidic active sites under MDA reaction conditions was demonstrated by means of reactions performed using isotopically labeled methane.[341] According to the results obtained, the carbon that was forming the active Mo-oxo-carbide species was easily replaced by a carbon atom from methane, incorporating in this way the carbidic carbon into the hydrocarbon products.

Despite the advances and progress experienced by in-situ and operando spectroscopic techniques along the last two decades,[29,30] characterization of the metal-loaded zeolite MDA catalyst remains a challenge. As detailed in a recent review by Vollmer et al.,[300] the identification of the active species is hampered by different factors, such as the evolution of the Mo species during the MDA process, the high coke selectivity or the non-homogeneity of the Mo-species (see Figure 15), with part of them acting as "spectators" and not participating in the methane conversion reaction.

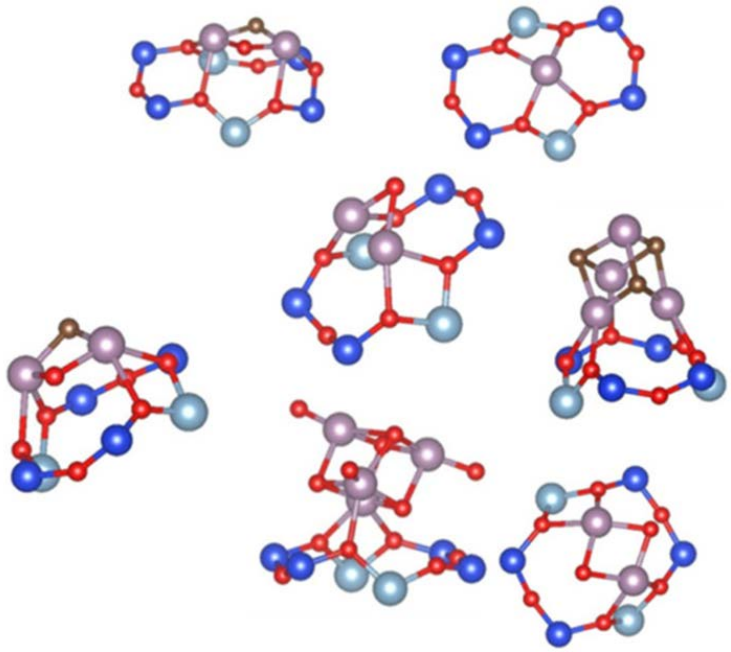

Figure 15. Various possible structures of (oxy-) carbidic Mo sites anchored on the HZSM-5 zeolite. Colors correspond to Mo (purple), Si (blue), Al (turquoise), O (red) and C (brown). Reproduced from ref.[300] *with permission from Wiley-VCH, copyright 2019.*

For most of the zeolite based MDA catalysts, it is generally accepted that the process follows a bi-functional mechanism, with the TM species being responsible for methane activation and formation of C_2 intermediates, which will oligomerize and cycle into the aromatic hydrocarbons on the BAS.[304,342,343] The observation of a maximum in the methane conversion reaction rate for catalysts with Mo/Al molar ratios in the range of

0.3-0.5 supports the need for both, the metal species and residual BAS to be present,[329] and the direct observation of the evolution of the proton signal by in situ 1H MAS NMR during MDA strongly supported the involvement of BAS in the aromatization reaction.[344] Moreover, the results obtained by different groups pointed out ethylene to be a primary product under MDA conditions.[345–347] More recent work by the group of Bahn,[348] based on the differentiation of kinetic and thermodynamic information, identified ethane as the sole primary product of methane dehydroaromatization, and ethylene and acetylene as secondary products formed by ethane dehydrogenation. Acetylene is proposed as a key intermediate, involved in rate and reversibility controlling elementary steps. In the same line, according to a paper by Vollmer et al.,[349] where ethylene aromatization is performed under MDA conditions, the different benzene and naphthalene selectivities as compared to those observed during methane conversion suggested that the main intermediate of the methane dehydroaromatization was probably not ethylene. The different nature of coke produced, less reactive in the case of ethylene than in the case of methane, supported this hypothesis. Further studies by this group of the early stages of the MDA reaction using advanced MAS solid-state NMR spectroscopy revealed the existence of, at least, two independent routes for methane C-H bond activation by Mo/H-ZSM-5 (see Scheme 7).[306] A first pathway (route (a) of Scheme 7), occurs on the Mo sites through Mo-methylidene species leading to acetylene intermediates and does not require the presence of BAS. A second bifunctional pathway (route (b) of Scheme 7), named as the carbonyl route, involves the formation of alkylated olefinic/(poli)aromatic species trapped within the zeolite structure, leading to a classical hydrocarbon pool type mechanism. Key intermediates participating in the two reaction mechanism such as surface-formate, -methoxy and acetals were

experimentally identified and support the co-existence of these two routes on Mo/H-ZSM-5 catalysts. These recent results confirm the alternative route proposed by Mériaudeau et al. twenty years ago.[350,351] There, acetylene formed on the Mo-sites was proposed as the main reaction intermediate, and the same Mo-sites were responsible for acetylene conversion into benzene. More recently, the bifunctional mechanism was also questioned by Hensen and his group.[117] Results obtained with Mo/Silicalite demonstrated that the molybdenum carbide species alone were capable of methane conversion into benzene at 700ºC and that the high benzene selectivity resulted from the shape-selectivity provided by the 10-ring channels. However, although according to these results BAS were not required for dehyroaromatization, they were seen to play an important role in promoting the dispersion of the metal-species into the zeolite microporous structure. In fact, DFT results confirmed that in the absence of Al the Mo-oxo species were not stabilized within the zeolite pores.[335] Mo carbide was identified as the only kinetically relevant site active for MDA in a recent work by Razdan et al.,[352] whereas BAS, besides enabling the dispersion of the Mo sites, were seen to contribute to the overall process by catalyzing equilibrated reaction steps, but were not involved in steps determining reaction rate or selectivity.

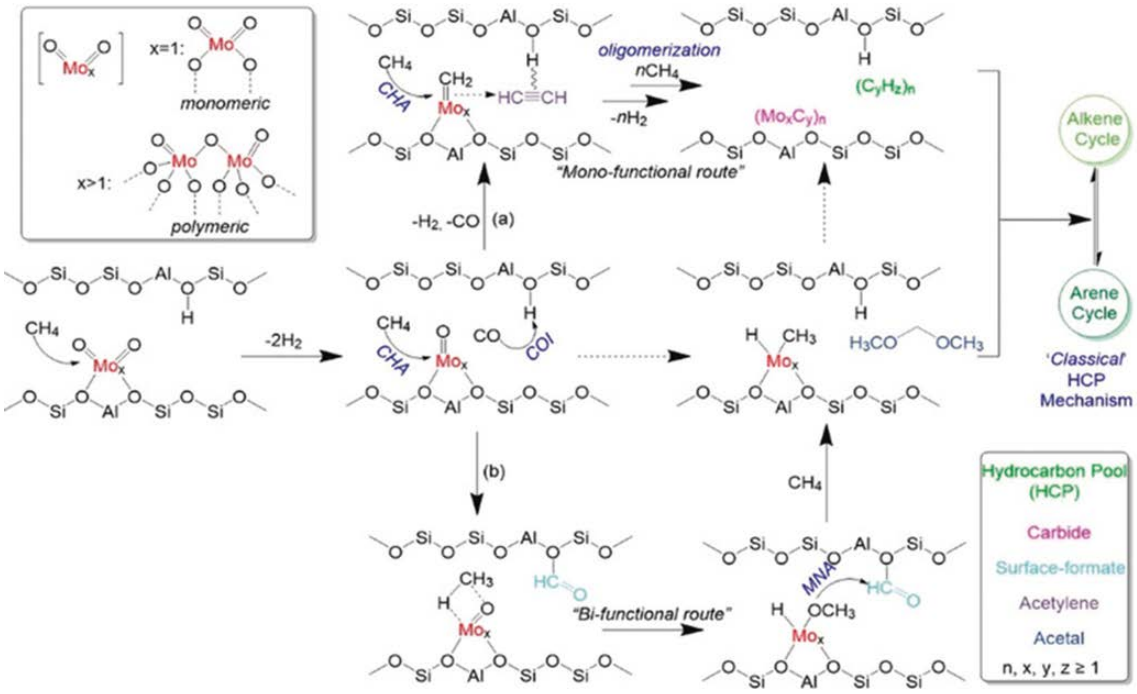

Scheme 7. Based on the experimental/spectroscopic evidences obtained in this work, the plausible reaction pathways during the MDA process evaluating the (a) mono- and (b) bi-functional features of the involved catalytic materials (CHA: C-H activation, COI: CO insertion, MNA: methoxy nucleophilic attack). Reproduced from ref.[306] *with permission from Wiley-VCH, copyright 2020.*

The contribution of a hydrocarbon pool mechanism to the MDA process, similar to the one proposed for the methanol-to-hydrocarbon (MTH) reactions (see Figure 16) was evidenced by means of a combination of methane isotope labelling and pulse reaction techniques.[156,353] In fact, it was observed that benzene formation occurred by secondary reactions of radical polyaromatic carbon species, confined within the zeolite micropores. The main difference of both mechanisms is that in the case of MDA the reactions involve radical intermediates, whereas in MTH they involve carbocations. The active role of internal coke in the MDA process, where its partial hydrogenation would contribute to the formation of ethylene and benzene, was already suggested by Liu et al., in 2002.[354] Recent spectroscopic and computational results also support the

hydrocarbon pool mechanism as the main route for methane dehydroaromatization.[355,356]

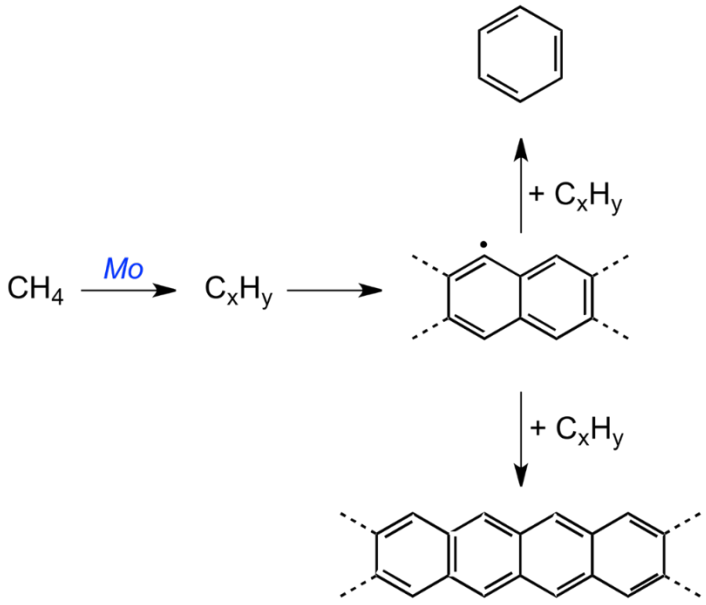

Figure 16. Scheme of the hydrocarbon pool MDA mechanism for Mo/ZSM-5. The formation of linear polyaromatic intermediates takes place during the induction stage. Once the hydrocarbon pool is established the formation of light aromatics occurs in parallel with the further growth of polyaromatic species, eventually blocking the zeolite pores. Adapted from ref.[353] with permission from the American Chemical Society, copyright 2018.

One of the main drawbacks of the Mo/Zeolite catalyzed MDA process is the fast deactivation of the catalyst by coking. These carbonaceous deposits may be located at the external surface of the zeolite blocking the access to the pores and, therefore, to the BAS, or within the microporous structure.[354,357] In order to overcome the catalyst deactivation problem, an important effort has been directed towards the incorporation of regeneration strategies aiming to increase benzene productivity. Portilla et al. showed how the combination of reaction-regeneration steps in a continuous cyclic mode on Mo/ZSM-5 (6 wt% Mo) led to threefold benzene yields over an 18 h TOS period (97 vs 33 $g_{BZ}{\cdot}Kg_{cat}^{-1}{\cdot}h^{-1}$) by limiting the reaction step to the first 1.5 h of maximum

benzene selectivity.[155] A detailed study of reaction-regeneration cycles by Han et al. concluded that oxidative regeneration at 450ºC enabled recovering the initial activity of the catalysts by selectively restoring the BAS close to the Mo sites and avoiding irreversible damage to the catalyst.[157] Reducing the Mo loadings on ZSM-5 to values in the range of 1-2 wt% was seen to avoid the formation of aluminum molybdate and preserved the zeolite framework at high temperatures, allowing the application of up to 100 reaction-regeneration cycles and leading to improved overall yield to aromatics as compared to 5 wt% Mo/ZSM-5.[337] Modifying the HZSM-5 support by steaming-dealuminization treatment led to catalysts with higher coking resistance and higher selectivity towards the desired aromatic products.[358]. Co-feeding CO, CO_2 or H_2 was also seen to increase catalyst stability with TOS.[359–361] The addition of small amounts of water to the methane feed when performing the dehydroaromatization at 998-1073K improved the catalytic performance of Mo/HZSM-5.[362] When the water content was kept below 2.6 %, its presence contributed to methane conversion by means of the steam reforming reaction yielding H_2 and CO and reducing the coke production, while preserving the crystalline structure of the zeolite. Combination of MDA with methane dry reforming in the presence of an integrated Mo/Al_2O_3 and Mo/MCM-49 catalyst was also seen to effectively improve the process regarding stability with TOS by reducing the rate of coke deposition on the surface of the MDA catalyst.[363]

In a different approach, Kosinov et al. proposed selective oxidation of coke to CO under dehydroaromatization conditions, simultaneously to the methane conversion to aromatics.[364] In another approach, coupling of MDA with methane CO_2 autothermal reforming under oxygen rich conditions was seen to decrease deactivation rate by removal of coke at the zeolite pore mouths.[365]

Recently, it has been proved that it is possible to increase catalyst lifetime and productivity to total hydrocarbon by performing the MDA reaction at pressures higher than atmospheric.[366] Thus, at 15 bar the coke selectivity of Mo/ZSM-5 catalysts is reduced, despite the higher amount of coke formation, because of the higher hydrogenation rate of surface carbonaceous species leading to higher aromatics' yield, and to the slower formation of coke deposits, of reversible nature.

In a completely different approach for improving the MDA process from the point of view of process intensification, e.g., benzene production and catalyst stability, intense research has been done on the design of reactors with specific configurations.[298,299,367,368] Cyclic CH_4-H_2 feed switch mode operation[369] and methane dehydroaromatization in a dual circulating fluidized bed reactor system[370] were two options proposed by the group of Zhang for improving catalyst life and product yields. The use of membrane reactors to overcome the thermodynamic constraints inherent to the dehydroaromatization process is another interesting alternative.[367] Thus, hydrogen-permeable membranes, such as metals or metal alloys, proton/electron conducting ceramics and zeolite-type materials have been proposed.[371–373] However, hydrogen removal leads to increased deactivation rate by coking.[371] An oxygen permeable membrane reactor was proposed by Cao et al.,[374] who showed that the controlled oxygen dosing through the membrane to the reaction media gave rise to higher methane conversion, higher selectivity to aromatics and increased catalyst life as compared to conventional fixed bed reactor operation. A new approach, combining the two former concepts, was described by Morejudo et al. (see Figure 17).[375] They presented the integration of the MDA reactor with an electrochemical $BaZrO_3$-based membrane that presented both, proton and oxide ion conductivity. Thus, the

simultaneous removal of hydrogen and controlled addition of oxide ions along the reactor length resulted in higher aromatic yields, reduced catalyst deactivation and improved carbon efficiencies.

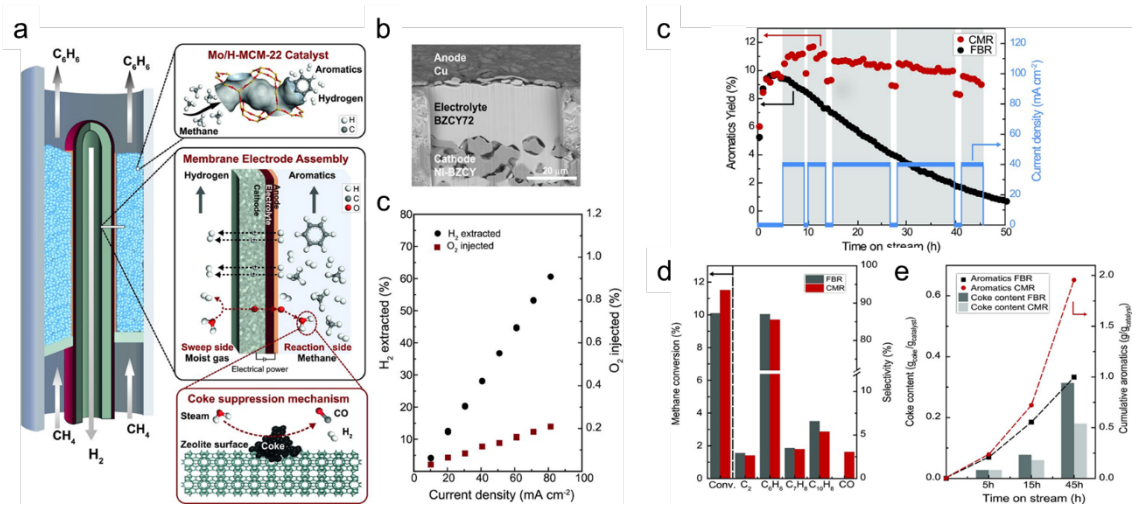

Figure 17. Current-controlled co-ionic membrane reactor. (a) CH_4 is converted to benzene and hydrogen via aMo/zeolite catalyst. H_2 is transported as protons to the sweep side. Oxide ions are transported to the reaction medium to react with H_2 and form steam as an intermediate before reacting with coke to form CO and H_2; (b) FBR and co-ionic CMR performance in MDA using a 6Mo/MCM-22 catalys;. (c) Aromatics yield versus time. Gray-shaded areas indicate when hydrogen is extracted; (d) CH_4 conversion and selectivity to main products after 5 hours (FBR) and 9 hours (CMR); (e) Coke deposition in 6Mo/MCM-22 and cumulative aromatics production in grams per gram of catalyst. Reaction conditions: 710°C, 1500ml g^{-1} $hour^{-1}$, 1 bar, and current density of 40 mA cm^{-2}. Reprinted from ref.[375] *with permission from the American Association for the Advancement of Science, copyright 2016.*

Net aromatization rates were also enhanced by combining MDA with absorptive H_2 removal in a single step.[376] Zr metal was used as absorbent and best results were obtained when it was added to the Mo/H-ZSM-5 catalyst as interpellet mixtures of as a separated down-flow bed.

Co-feeding methane with C_{2+} hydrocarbons should be beneficial from a thermodynamic perspective, enabling the process to take place at lower temperatures due to their higher reactivity and improving, therefore, the selectivity towards valuable products

such as aromatics. Choudhary et al. showed the conversion of methane at temperatures as low as 400ºC in the presence of higher alkenes or alkanes,[377] catalyzed by bifunctional H-GaAl-ZSM-5 zeolites. Methane was activated on the extra-framework Ga-oxide species, but cleavage of the C-H bond occurred by hydride transfer from the partially activated CH_4 to the carbenium or carbonium ion (see Scheme 8).

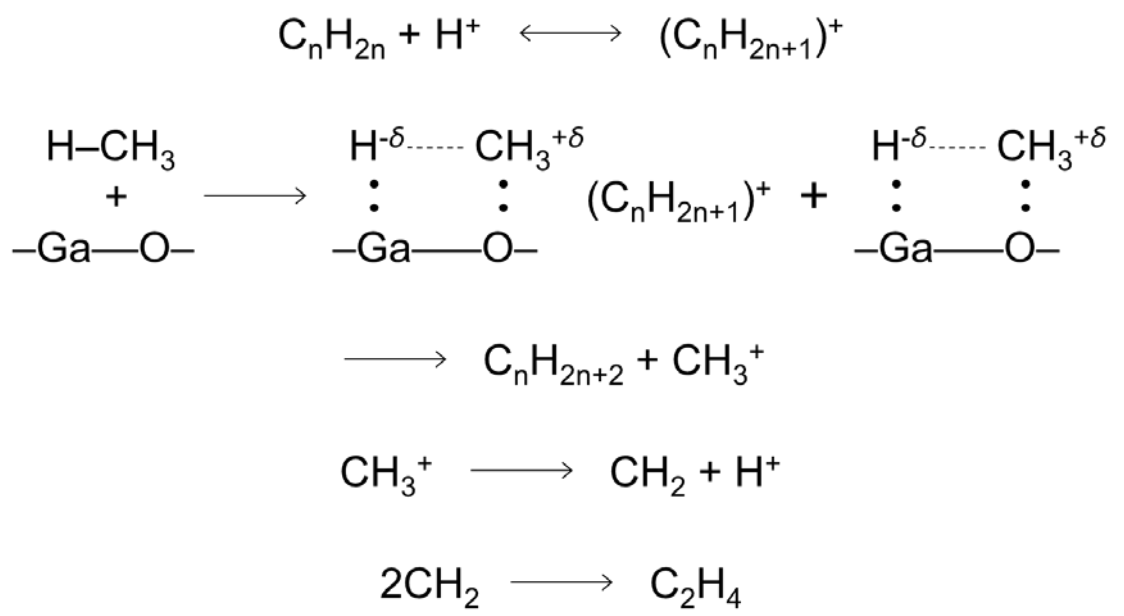

Scheme 8. Elementary steps in the low-temperature nonoxidative activation of methane over a bifunctional zeolite and overall reaction. Adapted from ref.[377] with permission from the American Association for the Advancement of Science, copyright 1997.

Zn and Ag-loaded zeolites have also been described as active for methane activation in the presence of higher hydrocarbons.[378,379] The involvement of methane in the aromatization process was demonstrated by Luzgin et al.[380] Indeed, they observed a high degree of transfer of isotopically ^{13}C-labeled atoms from methane into the aromatics produced by co-conversion of methane and propane on Zn-beta zeolites. A specific

review on co-aromatization of methane and propane is available for the interested reader.[381]

3.5. Methane carboxylation to acetic acid

Acetic acid production by simultaneous activation of methane and CO_2 is an ambitious and challenging approach, with a high atomic efficiency and interesting from an environmental perspective as it combines two of the main contributors to the greenhouse effect. Different non-zeolitic catalysts have been proposed for the direct carboxylation of methane, such as Pd/C, Pt/Al_2O_3, Pd-Rh supported on TiO_2 or SiO_2 or V_2O_5-$PdCl_2/Al_2O_3$, but the yields obtained were rather low in all cases.[168] On the other hand, bifunctional zeolite-based catalysts were seen to be highly selective in the production of acetic acid. For instance, Wu et al. evidenced by solid-state NMR spectroscopy that Zn/H-ZSM-5 was able to co-convert CH_4 and CO_2.[382] The role of Zn was to activate methane through the formation of Zn-CH_3 species, which react with CO_2 forming a surface carbonate, and the BAS contributed to the formation of acetic acid by proton transfer (see Scheme 9).

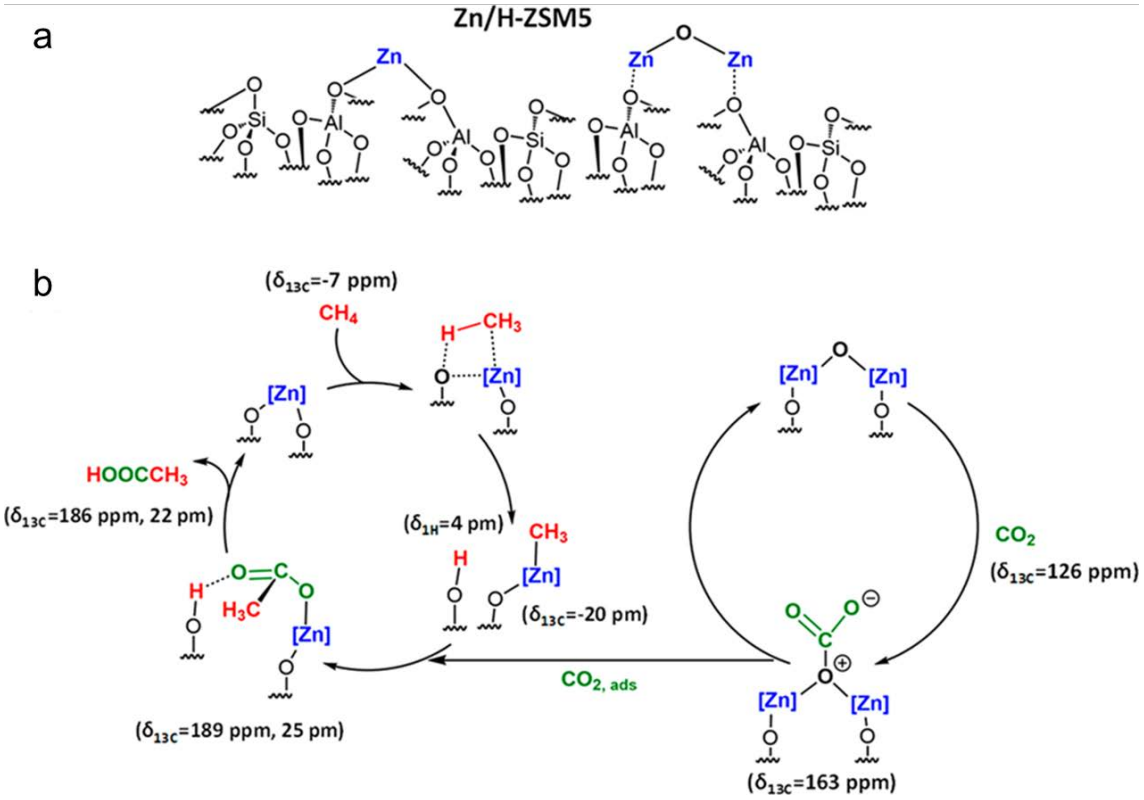

Scheme 9. (a) Proposed Structure for Zn/H-ZSM5 and (b) Proposed for the Co-conversion of CH_4 and CO_2 over Zn/HZSM5 to Acetic Acid Including SS NMR Signals. Reprinted from ref.[382] *with permission from the American Chemical Society, copyright 2013.*

Alkali- and alkaline-earth exchanged M^+-ZSM-5 loaded with Cu were also able to convert methane and CO_2 into acetic acid [383]. Here, methane activation and dissociation took place on the copper sites, forming Cu-CH_3 species, whereas the basic M^+ cations in the zeolite charge compensation sites activated the CO_2 forming the carbonate, which acted as a CO_2 reservoir and promoted the insertion of CO_2 into the Cu-C bond leading to a surface acetate intermediate. As no BAS were available in this case, acetic acid desorption after proton abstraction from methane was suggested. A recent DFT study compares different Cu-containing zeolites for the co-conversion of CH_4 and CO_2 into acetic acid, Cu-BEA, MFI, MOR and TON, and analyzes the influence of the copper species formed and the channel systems on the different steps of the catalytic process.

According to these theoretical calculations, the best performance corresponds to Cu-MOR, with copper present as tri-nuclear $[Cu_3(m\text{-}O)_3]^{2+}$ species.[384]

4. LIGHT ALKANE CONVERSION (C_2-C_4)

As mentioned previously, technological advances in the last decades such as hydrofracking or horizontal drilling has led to a huge increase of shale gas production.[385,386] This so called "shale gas revolution" has had an enormous impact in the Energy market,[387] lowering the price, not only of methane, the major component of natural gas, but also of light alkanes, which are usually present in different proportions depending on the location of the reserve, and may reach concentrations over 40 mol% (see Table 4).

Table 4. Composition of natural gas from various wells around the world. Adapted from.[120]

Composition (mol %)	**Field name**				
	Xifeng (China)	**Tengiz (Kazakhstan)**	**Ekofisk (Norway)**	**Salt Creek (USA)**	**Boscan (Venezuela)**
N_2	2	2	0	1	2
CO_2	2	4	3	1	6
C_1	49	69	79	81	84
C_2	13	10	10	9	4
C_3	19	3	4	4	2
C_{4+}	15	6	3	3	1
H_2S	0	15	1	0	1

According to the Annual Energy Outlook 2020,[388] the increase of these natural gas plant liquids (NGPL) is expected to reach 6.6 million b/d by 2028. NGPLs are presently removed from the main stream by natural gas processing plants and, besides ethane, propane, normal butane and isobutane, they may also include natural gasoline.

Thus, the large availability of low-cost natural gas will provide not only methane, but also important supplies of C_2-C_4 light alkanes, which may be used as alternative resources for production of chemicals and fuels in the next decades in addition to the more traditional cracking to olefins and reforming to syngas, provided that new efficient and cost-effective processes are developed.[2]

Light alkanes can be converted through non-oxidative catalyzed processes over pure acid or bifunctional metal-loaded zeolites. Light alkane cracking studies are mainly devoted to understand the cracking initiation mechanism, which provides the foundations for long alkanes cracking, which will be described in Section 5.1. Alkane dehydrogenation and aromatization are the main processes catalyzed by bifunctional metallozeolites. On the other hand, functionalization by oxydehydrogenation or selective oxidation are the main zeolite based alkane conversion reactions performed under oxidative conditions.

4.1. Light alkane conversion by C-C bond cleavage

Conversion of alkanes into smaller hydrocarbons by acid-catalyzed C-C bond cleavage is the basis for one of the main conversion processes in the oil refinery industry, the fluid catalytic cracking process (FCC), also the largest and oldest industrial application of zeolite based catalysts.[19,112] Traditionally the industrial unit processes heavy oil

fractions, such as vacuum gasoil, converting them mainly to liquid fuels and, more recently, to light olefins, mainly propene.[4] Depending on the demand of the final product and/or on the availability and type of feedstock, different zeolites and operation conditions can be selected. Regarding the catalytic cracking of alkanes, and of light alkanes belonging to the C_2-C_4 fraction in particular, the difficulty to break the C-C bond increases as the size of the alkane is reduced.[389] The larger reactivity of higher alkanes has been related to the entropy gains resulting from a larger amount of possible configurations of the adsorbed hydrocarbon and the transition state.[121] On the other hand, the final products obtained by cracking of ethane or propane, mostly methane, are of low industrial interest. Thus, ethane and the liquefied petroleum gas (LPG) fraction are usually converted to ethylene by steam cracking, a non-catalytic, pyrolysis based process, in which the feed is heated to its decomposition temperature within metallic tubular reactors in the presence of steam.[118,390] The main interest of the light alkane cracking is focused on the fundamental understanding of the alkane activation mechanism, and most of the studies performed are based on propane and butane. Nevertheless, some industrial relevant processes related to butanes cracking will also be highlighted at the end of this section.

As mentioned before, catalytic cracking takes place under non-oxidative conditions and in the presence of acid catalysts following a carbenium-type mechanism, and pioneer studies by Corma, Haag and Dessay and others published in the 1980's set the basis for the conceptual advances in the chemistry of catalytic cracking by acidic zeolites.[391–393] The mechanisms of alkane cracking by BAS are well established[394,395] and consists of the following three steps:

i. Initiation by alkane activation on the zeolite BAS to produce the penta-coordinated carbocation followed by the protolytic C-C or C-H bond cleavage leading to the formation of carbenium ions.

ii. Chain propagation by means of bimolecular hydride transfer from a reactant molecule to the adsorbed carbocation, and isomerization and beta-scission reactions involving the carbenium intermediates.

iii. Termination by desorption of the carbocation as an alkene and regeneration of the acid site of the zeolite.

As outlined in Section 2.3, it is widely accepted that the first activation step proceeds via a penta-coordinated carbonium ion followed by protolytic cracking or by dehydrogenation. The zeolite properties will determine the extension of these two initiation routes and the extension of the mono- and bimolecular mechanisms during the overall cracking process. Monomolecular cracking is favored for zeolites with reduced pore dimensions and high Si/Al ratios and, therefore, low BAS density. Regarding the influence of experimental conditions, high reaction temperature, low reactant partial pressure and low conversions, e.g., low alkenes concentration in the reaction media, also favors monomolecular cracking.[395] The bimolecular mechanism dominates at higher alkenes' concentration in the reaction pool or at milder temperatures and in the presence of zeolites with low Si/Al, with high acid site concentration and larger probability for presenting Al pairs.[396,397] The production of alkanes with higher carbon numbers occurs by consecutive oligomerization of the carbenium intermediates, charge rearrangement and beta-scission cracking, as shown in Scheme 10 for butane.

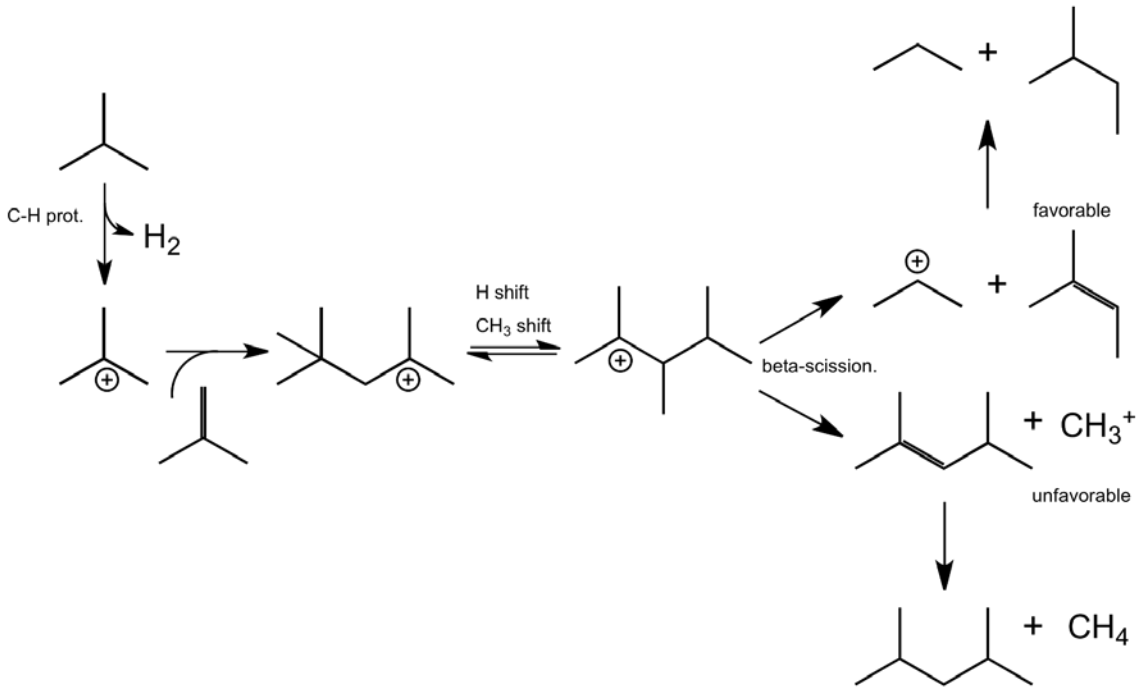

Scheme 10. Reaction mechanism for cracking of iso-butane by a bifunctional route.

Shape selective effects can also control the extent of the monomolecular or bimolecular mechanism, since the latter involve larger transition states.[15,94] Moreover, the size and shape of the zeolite micropores and cages are dominant factors in acid-catalyzed alkane cracking, because of their impact on the heats of adsorption of reactants and transition states, which in turn affect the reaction rates.[123,124] These aspects were recently reviewed by Van der Mysnbrugge et al.[398] Regarding the initiation step, the higher activation barriers reported for the dehydrogenation route with respect to protolytic cracking, were related to the lower stability of the carbocation intermediates formed by the former pathway as compared to those formed by the latter,[399,400] as previously shown in Section 2.3. Van Bokhoven and co-workers reported comparable intrinsic activation energies, directly related to the proton transfer ability from the BAS to the alkane, for zeolite structures with different pore sizes and structures suggesting that the active acid sites had similar strengths,[401,402] in good agreement with results obtained by

theoretical calculations. This led them to postulate that the activity of the BAS in zeolites observed for propane cracking and dehydrogenation was related to the rate-limiting step of the two reactions. Thus the alkane protonation, which is the rate-limiting step in the monomolecular cracking (Scheme 11a), is affected by the adsorption of the reactant on pores of different dimensions, being higher for the smaller pores. However, in the case of propane dehydrogenation, the rate limiting step is the desorption of the alkoxide species (Scheme 11b), whose stability depends on the local structure of the acid sites for the different zeolite structures and on the Al content.

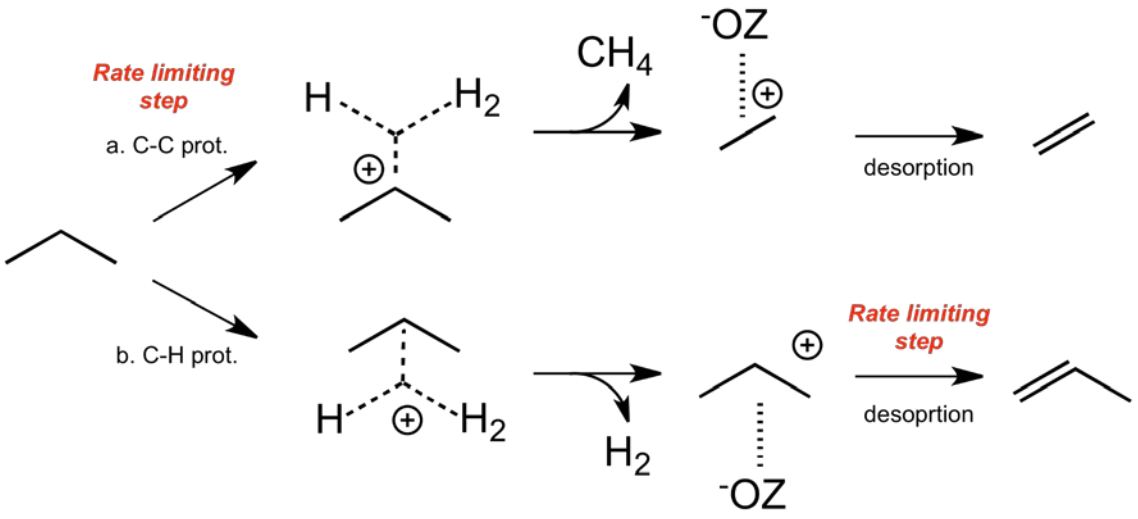

Scheme 11. Propane monomolecular cracking reactions by C-C or C-H protonation highlighting the rate determining step.

Other groups were critical regarding the pure shape selective implications for light alkane cracking, and considered the entropy variations derived from the confinement effects. Thus, Iglesia and co-workers also observed that the cracking rates of light alkanes within different void spaces in different zeolite frameworks with isolated BAS were only weakly affected by the zeolite acid strength, as evidenced by similar zeolite deprotonation enthalpies when considering isolated Al atoms in different frameworks.[97]

However, they were strongly influenced by the zeolite structure and degree of stabilization by the solvation environment of the transition state, which determined its entropy variation relative to the gas-phase alkane.[97,403,404] They demonstrated that the specific location of BAS in the 8-ring pockets of the mordenite structure favors the monomolecular cracking and dehydrogenation of propane and n-butane (see Figure 18a,b). The partial confinement of the transition state resulted in entropy gains that compensated its weaker binding and, therefore, the lower enthalpies and free energies of the transition state within the side pockets as compared to the 12-ring channels (see Figure 18c).

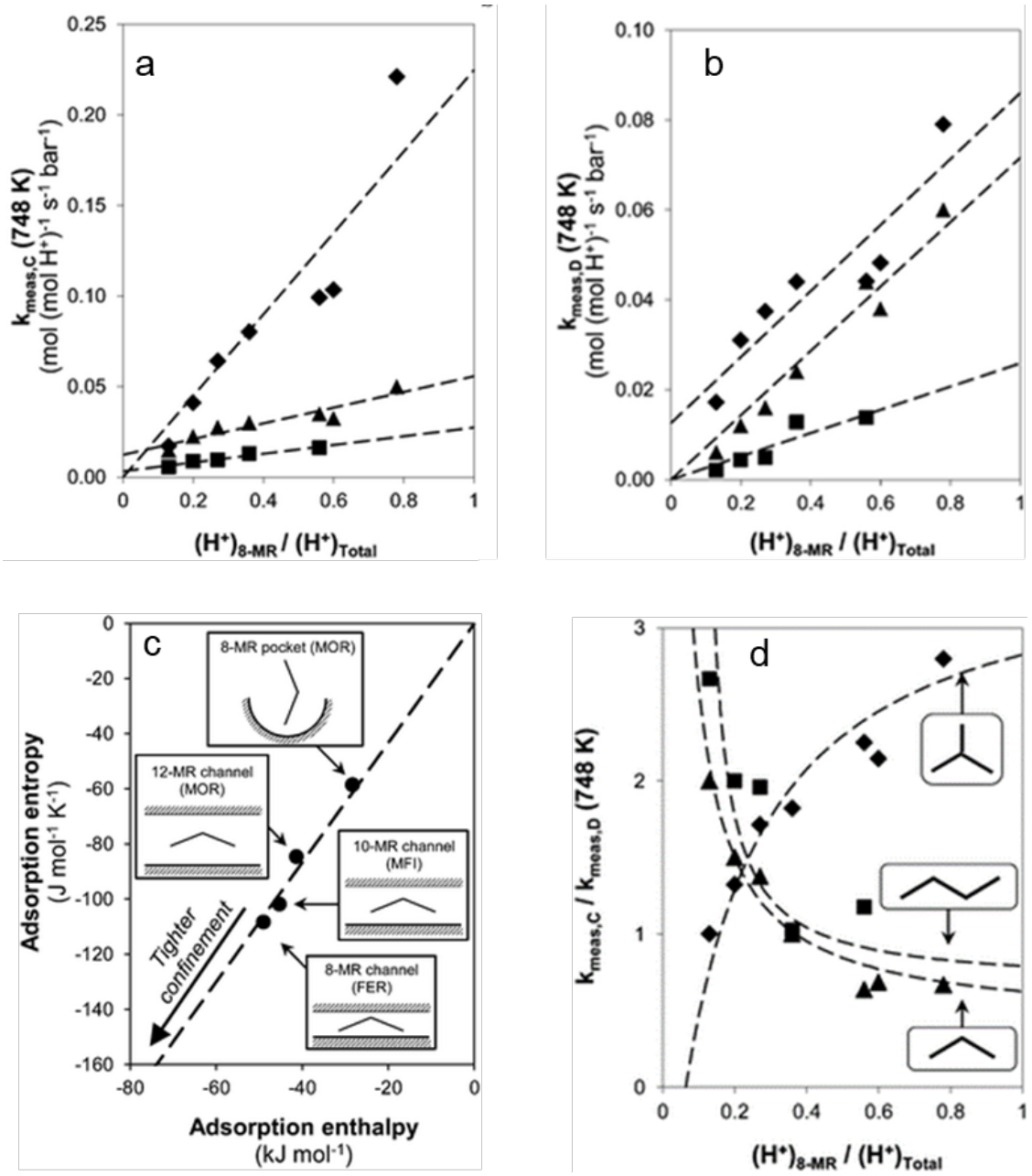

Figure 18. Monomolecular cracking (a), dehydrogenation (b) and monomolecular-to-dehydrogenation (d) rate constants for propane (▲), n-butane (■) and isobutane (◊) versus 8-MR H^+ fraction in Mordenite zeolite; (c) Adsorption entropy versus adsorption enthalpy for different confined spaces in zeolites. (a) and (b) Adapted from ref.[405] *with permission from Wiley-VCH, copyright 2010; (c) Adapted from ref.*[97] *with permission from the Royal Society of Chemistry, copyright 2013; (d) Adapted from ref.*[100] *with permission from the American Chemical Society, copyright 2012.*

The same arguments explained the selectivity variations related to the monomolecular cracking or dehydrogenation mechanisms of linear or branched alkanes (see Figure 18d).

In this line, Song et al. combined kinetics experiments and adsorption measurements with DFT calculations and found that the higher cracking turnover rates observed on Al pairs as compared to isolated BAS was mainly due to more positive intrinsic activation entropies.[406] This was also confirmed by measuring the coverage of acid sites by propane and n-butane alkanes on MFI, CHA, FER and TON zeolites under monomolecular cracking conditions by operando IR, combined with computational calculations, although the variations in activation entropies were less pronounced.[407,408]

The structure dependence of the kinetics and energetics of n-butane cracking mechanism was investigated by Monte Carlo simulations for eight zeolites with different channel topology and cages[409] and, when increasing confinement, central cracking was seen to be favored over terminal cracking and dehydrogenation. Janda and Bell showed higher dehydrogenation-to-cracking rates with increasing the Si/Al ratio of ZSM-5 and related that to a higher proportion of acid sites located in the channel intersections.[410] The stronger preference of dehydrogenation reactions, with a bulkier transition state, to occur at the channel intersections as compared to cracking, was ascribed, at least partly, to gains in intrinsic activation entropies that compensating increases in activation energies.

Louis et al. further showed that monomolecular cracking of light alkanes catalyzed by an acid ZSM-5 zeolite took place at temperatures as low as 150-200 ºC by using a zeolite with regular or deuterated acid sites.[411] This was demonstrated by the formation of H_2 and methane over H-zeolite or HD and CH_3D over D-zeolites, products that could not be obtained following the oligomerization and beta-scission mechanism,[412] which would lead to the formation of propane as the smallest alkane (see Scheme 10).

The presence of extra-framework Al (EFAl) species in ultra-stabilized Y (USY) zeolites, commonly used as the active component of commercial FCC catalysts, has been related to the generation of BAS of enhanced acid strength.[413] Van Bokhoven and co-workers also studied the influence of framework and EFAl on the catalytic activity of Y zeolite for cracking of propane. They observed that although the cracking rates per gram were higher for higher Si/Al ratios, neither the Si/Al ratio nor the presence of EFAl had an influence on the activation energies.[414] Additionally, confinement effects over the reaction transition states within the zeolite supercages were suggested to be promoted by the presence of EFAl species.[415] Lercher reported higher rates after mild steaming of ZSM-5 due to the presence of Al oxide clusters in the vicinity of BAS, which lead to increased activation entropies.[416] Longer steaming resulted in blocking of the BAS by bulky EFAl species deposited on the external zeolite surface.

La-exchanged Y and USY zeolites have also been widely employed as cracking catalysts.[393] Recent studies by Lercher et al. have been focused on the role of the nature, concentration, and location of cationic lanthanum species in FAU-type zeolites (zeolite X, Y and ultra-stabilized Y).[417,418] The structural properties and the location of the extraframework La species were determined by the chemical composition of the zeolite, and only the isolated La^{3+} cations stabilized at the ion-exchange sites within the FAU supercage were able to activate alkanes through the polarization of secondary and tertiary C-H bonds. This polarization was seen to be key for hydride transfer reactions to take place, contributing in this way to chain propagation by stable and repetitive generation of carbenium ions from di-branched alkanes at ambient conditions.

Among the acid zeolites described to catalytically crack light alkanes, ZSM-5 zeolite stands out because of its specific micropore structure and high activity, widely demonstrated for other hydrocarbon transformations. Most of the conversion processes of light hydrocarbons are directed to obtain propene and ethene starting from C_4 streams containing mixtures of olefins and paraffins.[419] In such cases, cracking of the alkane molecule following the protolytic mechanism to form methane and ethane is detrimental to the olefin selectivity.[420] Generally, the composition of the zeolite is modified in order to improve the cracking activity and catalyst stability by the addition of heteroatoms. Rahimi and Karimzadeh,[421] and more recently Blay et al.[110] extensively review this field by including alkaline-, transition metal-, rare earth- and phosphorous-modified ZSM-5 and other zeolite structures. Particularly, the addition of phosphorous has been reported to increase olefin selectivity and to reduce the butane conversion by protolytic cracking when feeding mixtures of butene and butane.[422,423] During steaming, the interaction of P eliminates strong acid sites and creates hydrothermally stable site environments that stabilize the intermediates formation in the pore structure of ZSM-5.[424] Regarding pure alkane conversion, Lu et al. showed that the addition of small amounts of Fe to the ZSM-5 zeolite enhanced the isobutane cracking activity and also the light olefin selectivity. This was ascribed to the possible modification of the zeolite acidity or to the enhancement of isobutane dehydrogenation to isobutene, which is easier to be cracked.[425] The addition of more Fe to the catalyst, however, decreased the selectivity to methane and to light olefins and increased the aromatic production, pointing to oligomerization and sequential aromatization reactions instead, in good agreement with early studies by Corma on CrHNaY zeolite for cracking of h-heptane [426,427] and with later results reported by Lu et al. when cracking isobutane over Cr-

modified ZSM-5.[428] Pereira and co-workers showed that the impregnation of Ni affected different structures differently. For ZSM-5 and Ferrierite, this resulted in increased isobutane cracking activity, which occured via the bifunctional mechanism by dehydrogenation on the metallic sites followed by acid-catalyzed cracking.[429,430] In the larger pores of Mordenite, Ni promoted hydrogen transfer reactions leading to coke formation and fast deactivation. Because of the increasing butenes formation, the competing bifunctional oligomerization-cracking reactions occurred to higher extent, leading to an increased ethene selectivity.

4.2. Light alkane isomerization

Even though hydroisomerization processes are mostly applied to convert linear alkanes with five or more carbons into valuable isomers, n-butane can also be converted by this route into iso-butane. The branched C_4 has industrial interest because of its use in different processes, such as dehydrogenation to isobutene or C_4 alkylation. It can also be employed, in certain countries, for the production of methyl- and ethyl-tert-butyl ether, added to gasoline as octane boosters.

As it was for light alkane cracking, determination of the reaction mechanism of n-butane hidroisomerization will serve as a basis for the fundamental understanding of long alkane hydroconversion reactions.

n-Butane hidroisomerization is catalyzed by bifunctional metal-loaded zeolites at temperatures of ca. 250-350 ºC. The first reaction step of the bifunctional mechanism is the dehydrogenation of the alkane into the corresponding olefin. As will be detailed in Section 4.3, pure dehydrogenation directed to the selective production of light olefins is

catalyzed, among others, by Pt on high or pure-silica supports, in order to avoid secondary reactions of the alkenes. In contrast, in the case of hydroisomerization, the n-butene formed has to diffuse to the protonic sites where it will be protonated and isomerized to iso-butene. The latter is finally hydrogenated to iso-butane on the metal sites.

Hydroisomerization of n-paraffins with five or more carbons is widely accepted to occur through a monomolecular pathway over noble metal loaded zeolites (Section 5.2). However, there is controversy in the literature on whether n-butane isomerization proceeds via a monomolecular or a bimolecular route, and different studies have provided evidences for one or the other mechanism. A recent study on n-butane conversion by H-mordenite and Pt/H-mordenite combining kinetic studies and isotopic labelling, confirmed the monomolecular route for the bifuncional catalyst.[431] In the case of the acid zeolite, the relative rates of reaction following the mono- or the bimolecular pathway were controlled by the concentration of butenes in the reaction media. Thus, n-butane conversion could also follow a monomolecular mechanism on H-mordenite at low butenes concentrations, below 20 ppm (see Scheme 12), consisting in isomerization of the n-C_4 intermediate by interacting with the zeolite support. The iso-carbenium can be either converted to the iso-butene and then hydrogenated on the Pt sites to iso-butane or converted by hydride transfer and desorb the acid sites as iso-butane. Higher olefin concentrations favored the bimolecular route, involving disproportionation reactions, and leading to the formation of propane and pentanes and reduced isobutane selectivity. In this case, the BAS of the zeolite support are not able to convert all the butenes to their branched isomers, and n-butene reacts with the C_4 carbenium to form a C_8 intermediate species, which is isomerized to the most stable configuration and

finally beta-cracked to propene, butenes and pentenes, which, in turn, are hydrogenated to the corresponding alkanes (see Scheme 12).[432,433]

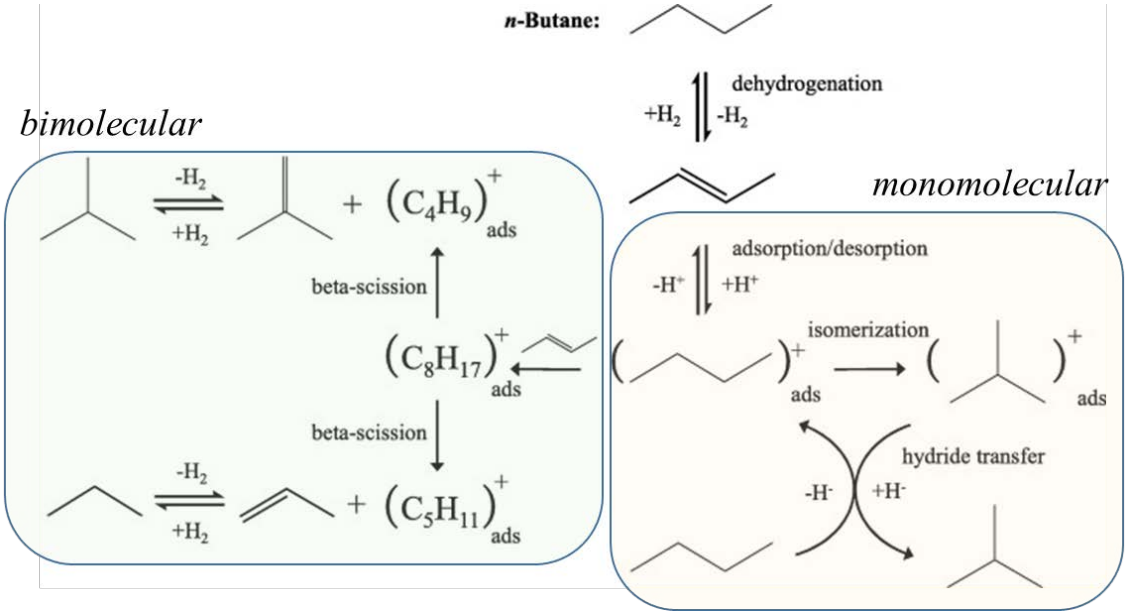

Scheme 12. Monomolecular and bimolecular routes for n-butane isomerization over bifunctional Pt/H-Mordenite catalyst. Adapted from ref.[431] *with permission from Elsevier, copyright 2015.*

Isomerization of n-butane has been approached, mainly, from a fundamental perspective, and has been studied in the presence of both, acid and bifunctional zeolite-based catalysts. Reaction temperature, zeolite Si/Al ratio and reactant partial pressure were seen to impact the process selectivity when converting n-butane over acid mordenite.[434] Recent studies by Bao and co-workers compare the influence of zeolite acidity on the relative conversion or light alkanes by monomolecular cracking or bimolecular isomerization on mono-functional acid zeolites.[397] They observed that the bimolecular pathway required the presence of two adjacent acid sites and, therefore, zeolites with lower Si/Al ratios. However, monomolecular cracking occurred on the isolated BAS and dominated under low n-butane partial pressure conditions, although it moved quickly towards the bimolecular route, which was tentatively ascribed to have a

lower apparent activation energy, when increasing n-butane concentration.[435] Some groups claimed that monomolecular skeletal isomerization hardly takes place, since it would involve the formation of primary carbocations after the opening of the cyclopropane ring and formation of the skeletal isomer, via the so-called protonated cyclopropane (PCP) route,[434,436] which is, indeed, operative for longer alkanes. Thus, zeolites with large cavities, such as MOR, which provide enough space for the formation and conversion of the bulky C_8 intermediates, will favor the bimolecular mechanism. Mordenite is the most studied zeolite for n-butane isomerization. A recent study describes the a new method for the preparation of mordenite nanoparticles starting from the natural zeolite, based on sequential ball-milling, recrystallization and dealumination.[437] This nano-sized mordenite was reported to be more selective to iso-butane and more stable towards catalyst decay. A recent study compared the n-butane isomerization performance of MFI and BETA zeolites and showed that the bimolecular route dominates in ZSM-5, whereas both monomolecular and bimolecular route simultaneously occur in the beta zeolite.[438] They found that the size of the intersection voids between the MFI channels favors the formation of the intermediates for the bimolecular pathway. Its narrow pore channels, however, affected the diffusion of the branched pentanes produced by the bimolecular route leading to re-cracking events to propane. On the other hand, the three dimensions of beta zeolite cause easier coke deposition.

From an applied perspective, pure acidic zeolites are significantly less active, stable and selective for n-butane isomerization as compared to bifunctional zeolite based catalysts, and Pt-loaded mordenite is the most employed bifunctional catalyst. Still, other zeolite structures have also been explored, and the diameter of the pores and the

dimensionality of the channel systems of different zeolites structures strongly affects the activity and selectivity of these catalysts. Thus, the influence of topology was studied by Pietese et al. for n-butane conversion on acid and Pt-loaded TON, FER and MOR.[439] The medium pore Pt-FER led to i-butane selectivities comparable to those obtained by Pt-MOR, but was less active due to lower acid site accessibility. On the other hand, the catalyst based on the monodimensional 10-ring TON zeolite, with significantly higher diffusional restrictions, was less selective and favored n-butane hydrogenolysis on the Pt sites.

The influence of the location of the noble metal species and the use of different zeolite structures has been also investigated.[440] Introducing the active metals by ion exchange can partially block the MOR channels. In order to avoid this, the acidic component can be physical mixt with the metal dispersed on a different support, such as montmorillite, leading to a hybrid catalysts. This approach was shown to promote catalyst activity and selectivity, together with attrition resistance. Pt or Pd supported on zeolites, such as MFI, BEA, TON and FER, have shown to catalyze n-butane isomerization but at higher temperatures. However, high temperatures cause a strong decrease of the thermodynamic concentration of iso-butane in the n-butane/iso-butane mixture, which makes the process non-economical feasible at the industrial scale.

Regarding additional microporous structures, Oliveira et al. converted n-butane over SAPO-5 supports modified with Cr or Fe prepared by adding the salt in the synthesis gel precursor.[441] The results showed that the added metals were preferrentally deposited as oxides at the outer surface of the SAPO crystals instead of entering the SAPO

structure. Both metals reduced the acidity of the support, and it was suggested that the metal oxides could behave as the hydrogenating/dehydrogenating active species.

n-Butane can also be converted to iso-butane by dehydroisomerization, combining n-butane dehydrogenation with isomerization in a one-pot two-step reaction, an interesting alternative to produce isobutene.[431]

4.3. Light alkane dehydrogenation

Traditionally, light olefins have been produced by steam cracking and as by-products of the FCC process. However, the high demand for light alkenes, especially for propene, has increased the interest in the development of on-purpose technologies for their production.[4,110] Dehydrogenation and oxydehydrogenation of light alkanes are two of these on-purpose processes. Despite the thermodynamic limitations imposed by the endothermic nature of this reaction, catalytic alkane dehydrogenation is performed commercially since the 1930's, and most processes are focused on the conversion of propane and isobutane to propene and isobutene, respectively. Industrially, supported Cr_2O_3 or noble metal Pt- or Pt/Sn-based catalysts are employed for direct alkane dehydrogenation,[442–445] and a comprehensive historical overview on the catalysts and the process evolution can be found in a review by Bashin et al.[446]

4.3.1. Direct dehydrogenation of light alkanes.

The main disadvantages of direct dehydrogenation are the high operation temperatures required to achieve high conversion due to thermodynamic limitations and, therefore, the high energy requirements, the possible occurrence of undesired reactions such as thermal cracking, and the need for catalyst regeneration because of its deactivation by

coke deposition.[447] According to theoretical equilibrium data for alkanes to alkenes, the shorter the hydrocarbon chain, the higher the temperature required for its dehydrogenation (see Figure 19). Still, direct dehydrogenation presents the advantages of H_2 by-production and a high selectivity to the alkene, although this selectivity decreases with temperature and chain length because of an enhancement of dehydrocyclization/aromatization, thermal cracking and coking.

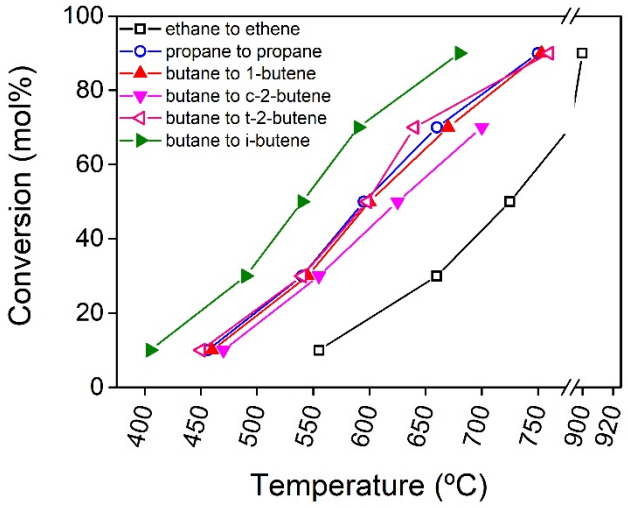

Figure 19. Dehydrogenation equilibria for several linear and branched alkanes. Data taken from.[442]

Although they are not yet commercially applied, the use of zeolite-related materials as alternatives to the conventional non-microporous supported dehydrogenation catalysts has been thoroughly described in the literature. Because of the higher strength of the C-H bond as compared to the C-C bond, around 363 and 246 kJ/mol, respectively, the use of zeolite-based catalysts in their acid form will favor cracking of the hydrocarbon instead of dehydrogenation. Still, in the case of propane, low alkane partial pressures and high temperatures enables its unimolecular dehydrogenation on the acid zeolite by

favoring the endothermic desorption step leading to propene.[443] The presence of an oxide or a metal facilitates the activation of the C-H bond,[448] and two main approaches have been described, the use of Zn, Co and Ga-containing ZSM-5 zeolites for activation of the alkane C-H bond, and the use of Pt-loaded zeolites.[443] The group of Iglesia studied the activation of alkanes on H-ZSM-5 and Zn-, Co and Ga-exchanged H-ZSM-5 under dehydrogenation conditions. According to their results, the rate determining step was not the C-H bond activation, but the desorption of the alkoxide species formed,[449] in agreement with previous results obtained by Meusinger and Corma for catalytic cracking of alkanes on acid zeolites.[450] Moreover, the stability of these alkoxide species was influenced by the local electronic and geometric structure of the BAS, i.e., by the zeolite topology and composition, as concluded by Van Bokhoven in a study of different acid zeolites in the catalytic monomolecular conversion of propane.[401] Regarding the role of the metal cations in zeolite exchange positions, it could be related to the electrophilic activation of the C-H bond, but they mainly contributed to the promotion of the re-combinative desorption of the H-adatom formed after the C-H cleavage.[449,451] Later experimental and theoretical studies by the group of Van Santen confirmed cationic Zn^{2+} and Ga^{+} as the active sites and evidenced that different activation mechanisms took place on Ga and Zn-zeolites (see Scheme 13).[452–455] Activation of propane on bifnctional Ga- and Zn-modified H-ZSM-5 zeolites was extensively studied by Derouane and Ivanova using ^{13}C and ^{1}H-MAS MMR in order to elucidate the initial stages of propane aromatization.[456,457] This will be revised in more detail in Section 4.4.

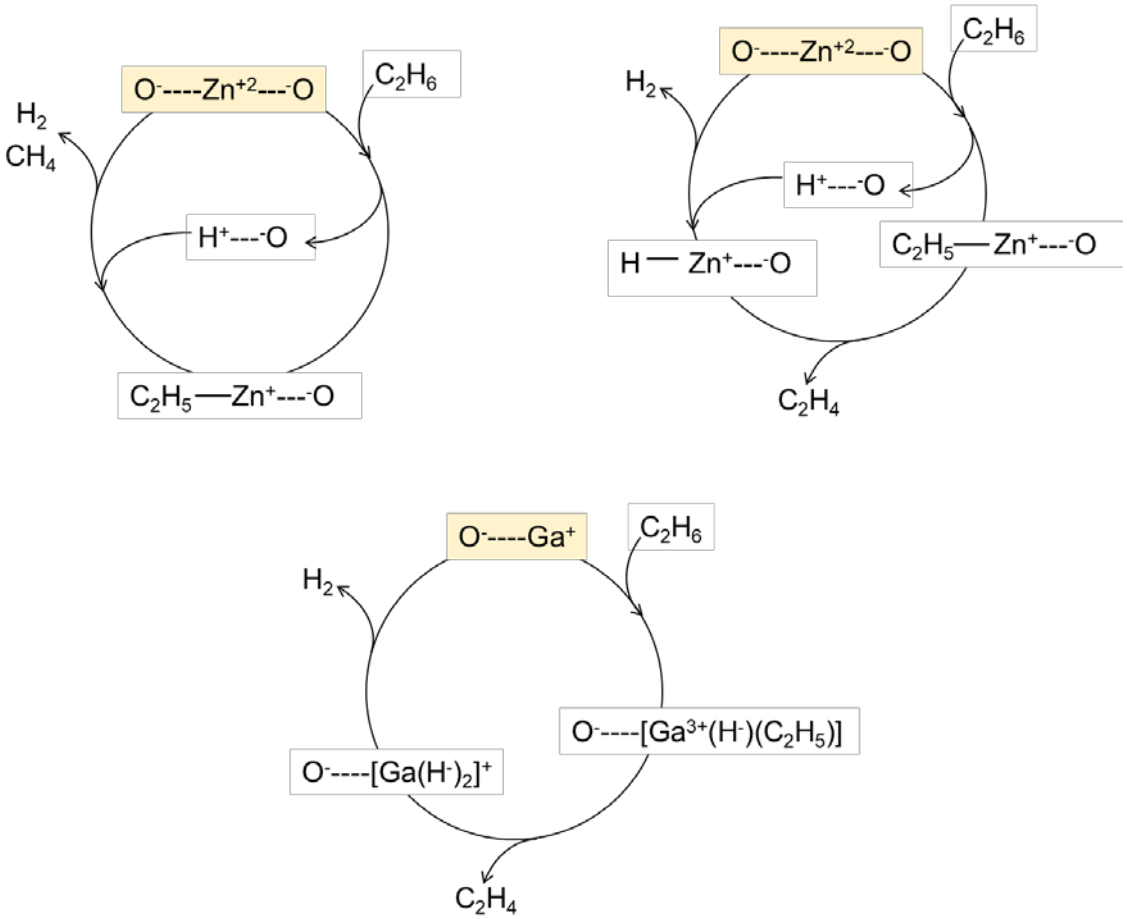

Scheme 13. Active sites and mechanisms of C-H activation on Zn and Ga exchanged H-ZSM-5. Adapted from ref.[452,454] *with permission from the American Chemical Society, copyright 2007, and from the Society of Chemistry, copyright 2005, respectively.*

High selectivity to the alkene can only be obtained in the absence of BAS, because the presence of BAS in zeolite supported dehydrogenation catalysts will lead to oligomerization and dehydrocyclation of the unsaturated products.[458] In fact, bifunctional Zn and Ga-containing zeolites are used for light alkanes aromatization as will be described in detail in Section 4.4.

Supported Pt catalysts are widely employed in industrial dehydrogenation processes, such as UOP's Oleflex or the STAR process from Phillips Petroleum, due to the high capacity of Pt for activation of C-H bonds combined with its low activity for C-C bond cleavage.[445,446,448] Main side reactions catalyzed by Pt are hydrogenolysis and coking,

and the addition of a second metal as promoter reduces the extension of both.[446] Among the different metals proposed, Sn is preferred.[445] Regarding the supports, materials with no or reduced acidity such as silica, alkali-metal doped alumina or basic calcined hydrotalcite-like carriers are used, in order to minimize undesired acid-catalyzed reactions, such as coking or isomerization.[445,448,459–461] Metal dispersion and size of the metal nanoparticles play a key role on the activity of the Pt-based catalysts, and an important drawback of these conventional Pt supported catalysts is deactivation due to sintering of the metal nanoparticles under the severe experimental conditions required for light alkane dehydrogenation.[462,463]

As we will see in Section 5.3 non-acidic K-exchanged Zeolite L, with a 1D 12-ring channel system, has been the preferred support for Pt-based catalysts used in C_6-C_8 alkanes dehydrocyclization.[464–467] Its high selectivity to the aromatic products was related to the particular size and morphology of its pores that favored the formation of small size Pt particles and inhibited bimolecular reactions leading to coke.[468] Pt-Sn supported on non-acidic L zeolite has also been claimed as isobutane dehydrogenation catalyst,[467,469–472] and, according to Mössbauer spectroscopic results on Pt-Sn/K-L reported by Dumesic and his group,[473] the structure of zeolite L promoted the dissociative adsorption of the alkane, increasing in this way the dehydrogenation rate. On the other hand, tin and potassium decreased the size of the Pt/Sn alloy particles inhibiting undesired reactions such as hydrogenolysis and isomerization and increasing the selective formation of isobutene.

Although zeolites possess the ability to stabilize metal nanoparticles within their cages or channels, when the metal is incorporated by conventional methods such as

impregnation or ion exchange, its location may be difficult to control. A different strategy, especially useful for small pore zeolites, where the small dimension of the channels prevents the access of the metal precursors to the intracrystalline spaces, is the metal incorporation during the hydrothermal zeolite synthesis, already described for Pt-containing Alpha zeolite in the early 1980's by researchers from Mobil.[474] The catalyst presented excellent shape-selectivity and high resistance towards poisoning as most of the Pt was located within the LTA structure. Later studies confirmed the higher sulfur tolerance of Ru and Pt clusters encapsulated within small pore zeolites.[475–479] In all those works, the metal forms nanoparticles with sizes in the range of 1-2 nm after reduction. Moliner et al. showed that chabazite encapsulated Pt species, prepared by direct synthesis of the zeolite using Pt-mercaptocomplexes as Pt-precursors, presented higher stability toward sintering of the metal as compared to Pt/SiO_2 at temperatures in the range of 650-750 º C.[128] In this work the controlled reversible interconversion of ~1 nm Pt nanoparticles into site-isolated single Pt atoms in reducing and oxidizing atmospheres was evidenced by X-ray absorption spectroscopy and aberration-corrected high-angle annular dark-field scanning transmission electron microscopy. Moreover, the chabazite structure was able to act as a metal trap of metals originally loaded on a second support such as SiO_2 or Al_2O_3 and evidences were given for this metal migration from one surface to the cavities of the small pore zeolite.[127]

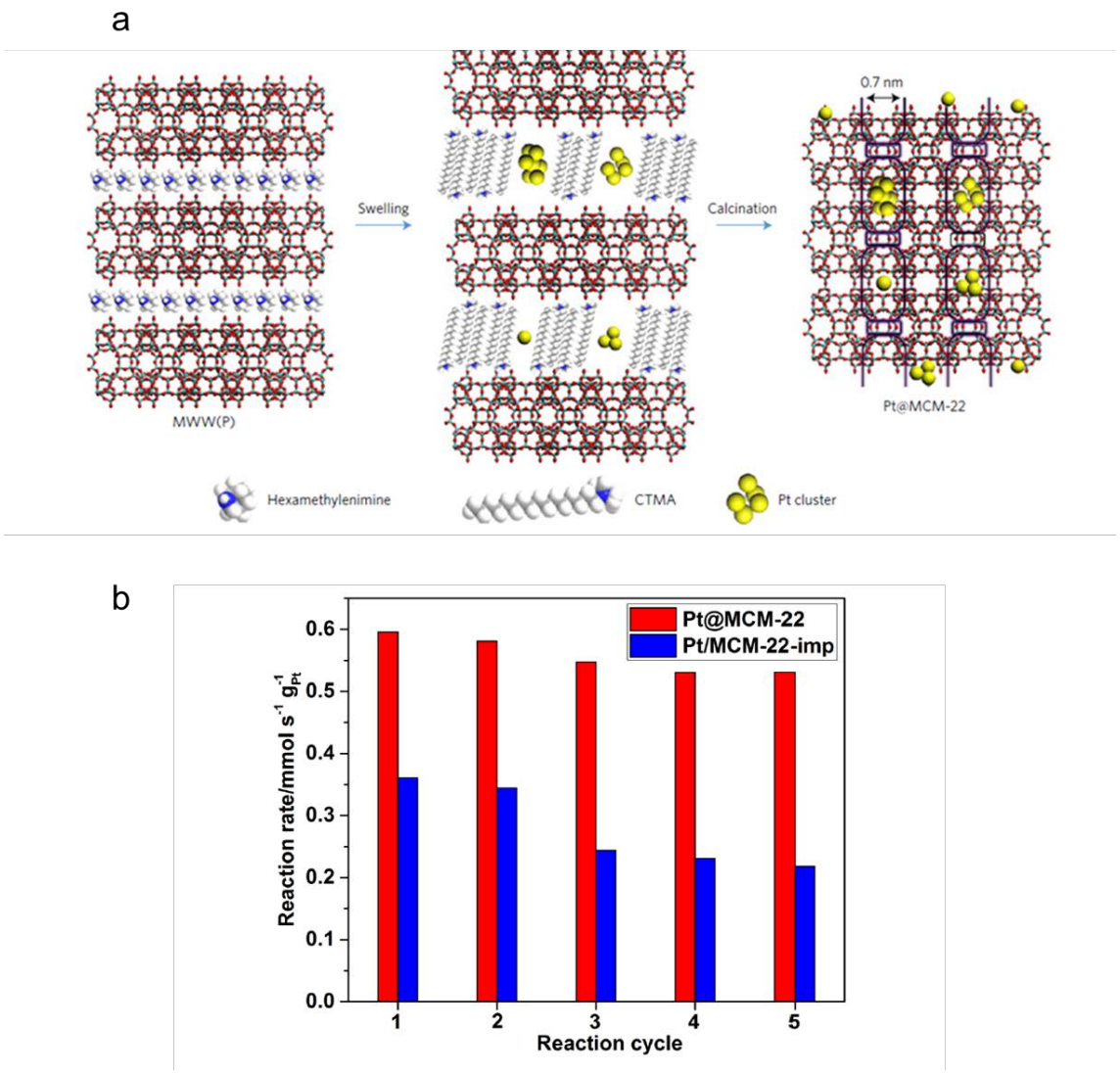

Figure 20. (a) Illustration of the preparation of Pt@MCM-22; (b) Activity and stability of Pt@MCM-22 and Pt/MCM-22 in consecutive cycles of propane dehydrogenation to propylene at 550ºC. Adapted from ref.[125] *with permission from Springer Nature, copyright 2017.*

The benefits of confining metal species within the zeolites structures for selective and stable dehydrogenation of light alkanes has been evidenced in several recent papers. Thus, highly stable subnanometric Pt species were stabilized within the cavities of pure silica MCM-22 following a new preparation method (see Figure 20a).[125] As compared to a conventional Pt impregnated MCM-22 with most of the Pt nanoparticles localized on the external surface area, the Pt@MCM-22 sample obtained by direct synthesis

presented a large proportion of the metal species within the 12-ring cavities. It was not only more active for propane dehydrogenation to propene at 550ºC, but it retained around 90% of its initial activity after five reaction-regeneration cycles vs less than 60% retained by Pt/MCM-22 (see Figure 20b).

Subnanometric PtSn clusters confined in the sinusoidal 10-ring channels of a K-PtSn@MFI catalyst (see Figure 21a) were highly active for propane dehydrogenation, and presented an exceptional improvement in stability towards deactivation as compared to a conventional K-PtSn/MFI prepared by incipient wetness impregnation.[126,480] Modulation of the subnanometric Pt clusters by adding partially reduced Sn species that interacted with platinum at the Pt/support interface, as evidenced by the combination of in situ extended X-ray absorption fine structure, high-angle annular dark-field scanning transmission electron microscopy and CO infrared data, decreased the deactivation rate in propane dehydrogenation by one-order of magnitude (see Figure 21b).[481] The outstanding catalytic behavior of K-PtSn@MFI, e.g., high propene selectivity and increased catalyst life, was confirmed under industrially relevant conditions, i.e., higher alkane partial pressures.

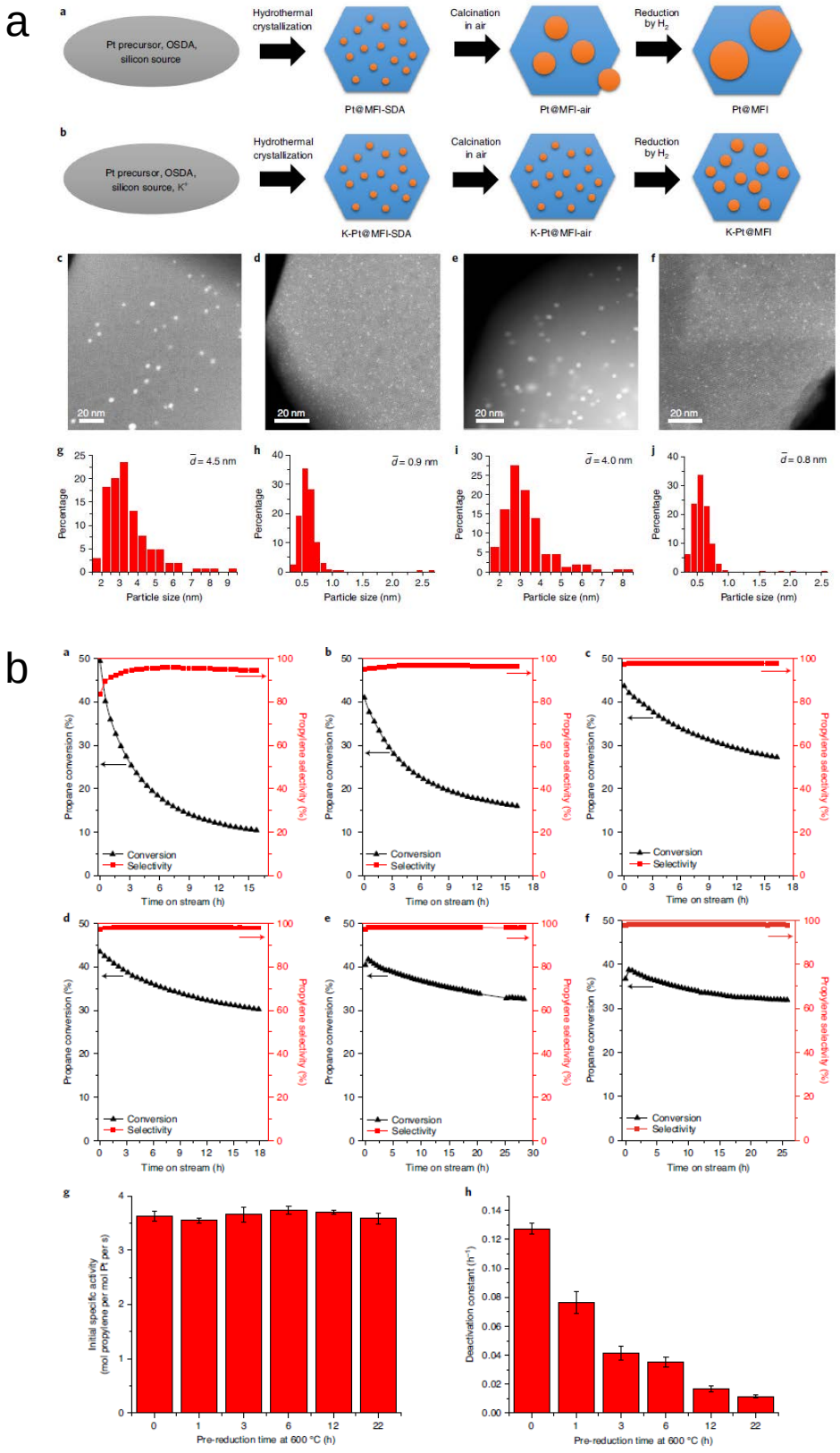

Figure 21. K-PtSn@MFI with regioselective location of subnanometric Pt or PtSn clusters within the sinusoidal 10-ring channels of a pure-silica ZSM-5. (a) Reproduced from ref.[126] *with permission from Springer Nature, copyright 2019; (b) reproduced from ref.*[481] *with permission from Springer Nature, copyright 2020.*

Highly dispersed subnanometric and even atomic bimetallic Pt–Zn species were encaged within a 10-ring silicalite-1 zeolite by Sun et al. following an energy efficient, easy ligand-protected direct hydrogen reduction method.[482] These catalysts were highly active for propane dehydrogenation to propene, and presented a stable behavior with time on stream.

Recent studies have described Fe-ZSM-5 based catalysts as active for light alkane dehydrogenation. Wang et al. prepared Fe/H-ZSM-5 zeolites by impregnation of a commercial ZSM-5 (Si/Al=25).[483] These catalysts outperformed ZSM-5 loaded with other metals, such as Pt, or Ga, Mo or Cr metal oxides, in activity, selectivity to propene and stability towards deactivation. They were also more active than Fe/Al_2O_3 catalysts, evidencing the positive role of the zeolite structure, which favored the formation of the active metallic and/or iron carbide species, according to XPS results. Lobo and co-workers described the use of Al-free Fe-silicate beta and ZSM-5 zeolites as catalysts for propane dehydrogenation.[484] According to their results, the main active sites were isolated framework Fe sites, although extra-framework species also presented some dehydrogenation activity. They suggested a redox catalytic cycle for the propane reaction on the framework active sites by formation of propane radical cations (see Scheme 14).

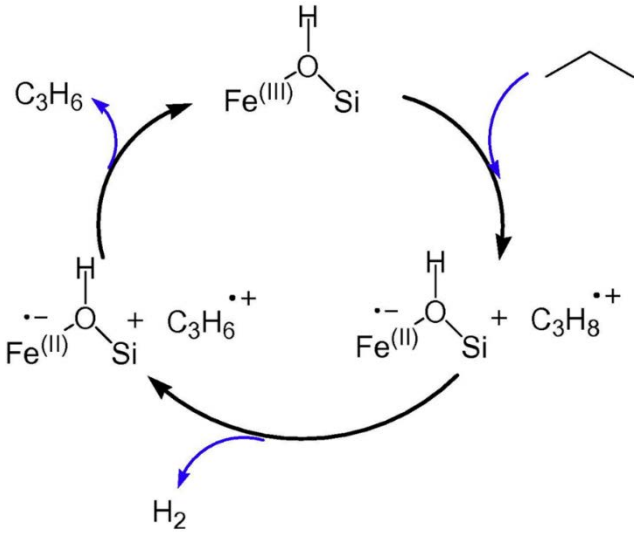

Scheme 14. Possible reaction mechanism for propane dehydrogentation in H-[Fe]ZSM-5. Adapted from ref.[484] with permission from Elsevier, copyright 2014.

Regarding the influence of the zeolite topology, different Pt-Zn containing medium and large pore zeolites in their Na-form were compared by De Cola et al. for propane non-oxidative dehydrogenation.[485] The 10-ring Na-ZSM-5 and Na-ZSM-11 favored consecutive aromatization reactions, whereas propene was the main product when the reaction was performed in the presence of large pore zeolites, Na-beta, Na-mordenite, K-L and Na-Y. Among those, 0.5Pt/2.6Zn-beta showed the best performance, with stable conversion, close to thermodynamic equilibrium under the experimental conditions employed, for at least 63 h on stream, and propene selectivity over 90%.

Tandem dehydrogenation-cracking of n-butane to light olefins on Pt-Sn/ZSM-5 based catalysts was described by Nawaz,[486] and high olefin selectivity (>90 wt%) and hydrothermal stability was achieved for Pt-Sn/ZSM-5 with Si/Al of 300.

4.3.2. Oxidative dehydrogenation of light alkanes.

Despite the interest aroused by direct dehydrogenation processes and the selectivity improvements described when catalysts based on microporous crystalline materials are used, they still exhibit conversion limitations due to thermodynamics and large energy costs related to the need for high temperature operation. Light alkanes dehydrogenation under oxidative conditions is an interesting alternative for the production of alkenes, as it can overcome thermodynamic equilibrium limitations and it can take place at significantly lower temperatures,[487] especially if the dehydrogenation of ethane is considered.[118,446,447,487] Different types of catalysts and different oxidants have been described for light alkane oxidative dehydrogenation (ODH) but, up to date, none of these catalytic systems has been commercially applied, as far as we know. The main drawbacks are safety concerns related to the formation of potentially flammable mixtures, especially when the reaction is carried out in the presence of oxygen, and the occurrence of over-oxidation reactions reducing the selectivity to the desired olefins and yielding carbon oxides, as described in Section 3.2 for the selective oxidation of methane to methanol. Moreover, the valuable H_2 by-product is also totally or partially consumed. Despite all these limitations, the use of molecular oxygen as the ODH oxidant has been largely studied, as it favors low temperature reactions and because of its availability and low cost. Alkane dehydrogenation in the presence of oxygen can be approached in two different ways. One posibility is to pursue the selective combustion of the H_2 produced during dehydrogenation, following an autothermal strategy. In this way, besides overcoming equilibrium limitations by conversion of H_2 to water, the heat generated by the exothermic combustion reaction will partly compensate the endothermicity of the

dehydrogenation.[443] Single Pt-based catalysts, capable of catalyzing the dehydrogenation and the combustion reaction, or multi-catalysts systems are employed in these cases.[488] The other option is the direct involvement of oxygen in the activation of the alkane, by means of homolytic or heterolytic C-H bond cleavage. Regarding the catalysts employed, both unsupported and supported catalysts have been described[489] and, unlike the case of direct dehydrogenation, when considering overall ODH the catalysts need to activate not only the alkane, but also the oxidant. Reducible oxides, typically vanadium oxides, can activate O_2 at lower temperatures, ranging from 300-400ºC, and non-reducible oxides, such as those employed for oxidative methane coupling, are able to do it at higher reaction temperatures (650-800ºC).[446] A significant number of reviews on oxygen mediated ODH have been published since the early 1990s, such as those by Cavani[490,491] and references included therein, and others where ODH is compared to direct dehydrogenation processes.[443,446,447] Most of the catalytic systems described in these reviews are non-zeolite based, and the interested reader can find there a thorough description of ODH catalysts based on groups V and VI transition metal oxides, on non-stoichiometric NiO_x or on Li-doped alkaline earth metal oxides.

Among all the catalysts described, those based on vanadium have attracted special interest.[487,492] The reducibility of the surface vanadium oxide species, directly related to their coordination number and aggregation state, and the presence of acid/base sites in their local environment were seen to have a significant effect on the catalytic behavior of supported vanadium oxides.[493] Similar trends were observed when vanadium was isomorphously incorporated into the framework of microporous crystalline materials, such as $AlPO_4$-5 or silicalite. López Nieto gave a complete overview of the synthesis, V oxidation states and catalytic behavior of V-containing microporous and mesoporous

materials, up to 2001.[494] Despite the incorporation of the vanadium precursors to the synthesis gel before the hydrothermal crystallization of the microporous material, it is generally accepted that only a small fraction of the metal is located in framework sites. In the case of microporous V-silicates, V^{5+} and V^{4+} may substitute Si^{4+} or they may bond to defects of the zeolite framework in tetrahedral or square pyramidal coordinations. In the case of V-containing crystalline aluminophosphates (AlPO-n zeotypes), different incorporation mechanisms have been suggested, such as the substitution of framework P^{5+} or Al^{3+} elements or its anchoring to the P of the AlPOs lattice. V-silicalite-1 and -2 obtained by direct synthesis were shown to be more selective to propene in the propane dehydrogenation reaction than the samples prepared by impregnation, suggesting a specific interaction between the V ions and the zeolite framework in the former case.[495] Incorporation of V to $AlPO_4$-5, a microporous aluminophosphate with a large-pore monodirectional channel system (AFI structure) led to a significant increase of the catalyst's activity for ethane and propane ODH, and olefin yields as high as 15-17% were obtained. The additional incorporation of divalent Mg^{2+} or Co^{2+} ions into framework positions of the $AlPO_4$-5 structure by substituting Al^{3+} resulted in the generation of BAS, which affected the catalytic behavior of the final materials in different degrees depending on the alkane. Whereas for propane ODH high selectivity to the olefin was obtained with non-acid materials (VAPO-5), the presence of acidity was beneficial in the case of ethane, and VMgAPO-5 and VCoAPO-5 were seen to further increase the selectivity to ethylene as compared to VAPO-5.[496,497]

The effect of the microporous structure of V- and/or Co-containing aluminophosphates on their catalytic behavior for ethane ODH was also described. Thus, the VAPO-18, CoAPO-18 and VCoAPO-18 catalysts based on $AlPO_4$-18, a zeotype with a three-

dimensional pore system with large cages accessible through 8-ring windows, were more selective to ethylene than the corresponding materials based on $AlPO_4$-5 (1D, 12-ring structure). Small pore SAPO-34 and La-containing SAPO-34, combining Brønsted and Lewis acidity, were also shown to be active and selective for ethane ODH. The high ethylene yields obtained, >60%, suggested that the reaction occurred within the chabazite cages and evidenced the potential of SAPO-34 based catalysts for ethane ODH.[498,499] The high ethene selectivity obtained with the small pore zeolites could be explained by the formation of hydrocarbon-pool-type intermediates within the large cages and the formation of ethene following the aromatic cycle mechanism, similar to what has been described for the methanol-to-olefin process.[500–502]

Recent publications have shown that boron-based catalysts are highly selective for alkanes ODH to the corresponding olefins. Thus, a layered borosilicate zeolite with MWW structure was described by Qui et al.,[503] and its activity for propane ODH was assigned to defective trigonal boron species, and not to boron in tetrahedral coordination. In a different study, Altvater et al. prepared, characterized and tested a B-MCM-22 for propane ODH.[504] This zeolite, with a tridimensional instead of a layered MWW structure, presented the boron mostly incorporated in framework positions as isolated B(OSi)3 units, and was not active for propane dehydrogenation. According to their study, in order to present ODH activity, the boron-based catalyst required at least some degree of boron aggregation.

The different effect on ethane and propane ODH of the presence of both redox and acid properties, was also observed for transition metal loaded zeolites. Thus, Poeppelmeier and Weitz compared Ni-, Cu- and Fe-loaded HY and KY and, for the same metal, they

observed higher ODH activity and ethene selectivity for the HY-based catalysts.[505] According to their results they suggest that the presence of BAS favors β-hydrogen abstraction of the metal ethoxide, formed when the alkane reacts with the surface oxide, leading to the formation of ethene (see Scheme 15).

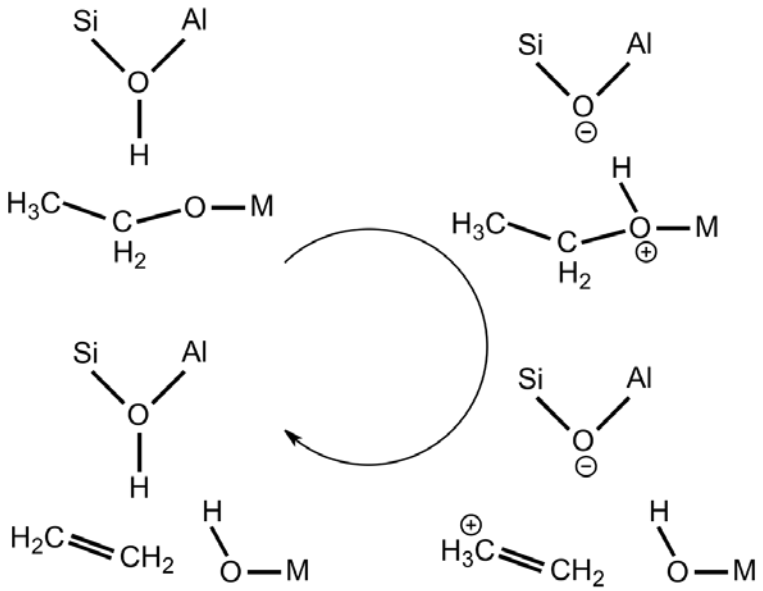

Scheme 15. β-Hydrogen abstraction reaction of metal ethoxide to form ethene catalyzed by the zeolitic BAS. Adapted from ref.[505] with permission from Elsevier, copyright 2009.

On the other hand, higher selectivity to propene was obtained for propane ODH catalyzed by [V,Al]-MCM-22 when the BAS density was reduced by ion-exchange with alkali ions, due to a decrease in cracking reactions.[506] In an interesting approach, the direct conversion of propane into aromatics was achieved on a bifunctional tandem catalyst combining VMgO and a ZSM-5 zeolite as ODH and cyclo-aromatization functions, respectively.[507] The addition of Ga to the H-ZSM-5 was detrimental, as Ga favored the combustion of hydrocarbons. When the two components were physically mixed in a single bed configuration, the (toluene+xylene)/benzene ratio was increased.

As mentioned at the beginning of this section, the use of oxygen as ODH oxidant has several drawbacks such as safety issues due to the explosive nature of O_2/hydrocarbon mixtures, costs related to downstream N_2 separation in case of using air, or heat management issues in case of using pure oxygen.[447] Moreover, the low olefins yields due to undesired over-oxidation reactions are far from those required for commercial implementation. Thus, an important effort has been directed towards the performance of ODH reactions in the presence of milder oxidants such as CO_2 or N_2O. In both cases, the process would present the additional benefit of valorization, not only of the alkane, but also of the oxidation agents.

The use of CO_2 is a sustainable and highly interesting option for several reasons. It will increase the selectivity to the olefin by avoiding overoxidation reactions to CO_x, it can contribute to coke removal during the process reducing in this way the catalyst deactivation rate, and it has the additional benefit of a lower environmental footprint by using and upgrading a greenhouse gas. A recent review on the CO_2-mediated ODH of propane (ODPC) was published by Atanga et al.[508] covering the main catalysts described for the process, including zeolite based catalysts, the advantages of using CO_2 as a soft oxidant, and future trends regarding catalysts design and reaction conditions.

When the alkane is dehydrogenated in the presence of CO_2, the latter will react with the H_2 formed in Eq. 7 by means of the reverse water gas shift (RWGS) reaction (Eq. 8) producing CO and H_2O and shifting in this way the dehydrogenation equilibrium towards the products. Still, the overall process that results from coupling these two reactions is endothermic (see Eq. 9). This is an important drawback of ODPC as it thermodynamically limits the reaction at low temperatures and high pressures. In fact, CO_2-mediated

ethane activation at temperatures below 500ºC is highly disfavored as compared to propane and butanes, as showed by Du et al.[509] On the other hand, the butenes formed by dehydrogenation of n-butane are more susceptible to undesired secondary cracking reactions than propene. Thus, among the light alkanes, propane dehydrogenation in the presence of CO_2 appears as the most attractive alternative, and most of the studies have been focused on this reaction.

$$C_3H_8 \leftrightarrow C_3H_6 + H_2 \qquad \Delta H_r^0(289\ K) = +124\ kJ\ mol^{-1} \qquad (7)$$

$$CO_2 + H_2 \leftrightarrow CO + H_2O \qquad \Delta H_r^0(289\ K) = +41\ kJ\ mol^{-1} \qquad (8)$$

$$C_3H_8 + CO_2 \leftrightarrow C_3H_6 + CO + H_2O \qquad \Delta H_r^0(289\ K) = +164\ kJ\ mol^{-1} \qquad (9)$$

Besides the direct participation of CO_2 in the dehydrogenation reaction (see Eq. 3), it can react with coke through the reverse Boudouard reaction (Eq. 10), stabilizing in this way the catalyst towards deactivation. However, at high temperatures, undesired reactions such as dry reforming of the alkane (Eq. 11) or cracking and hydrogenolysis (Eq. 12-15) can lead to reduced olefin selectivity.

$$CO_2 + C \leftrightarrow 2CO \qquad \Delta H_{298\ K}^0 = +172\ kJ\ mol^{-1} \qquad (10)$$

$$C_3H_8 + 3CO_2 \leftrightarrow 6CO + 4H_2 \qquad \Delta H_{298\ K} = +620\ kJ\ mol^{-1} \qquad (11)$$

$$2C_3H_8 + 2CO_2 \rightarrow 3C_2H_4 + 2CO + 2H_2O \qquad (12)$$

$$C_3H_8 \rightarrow C_2H_4 + 2CO + CH_4 \qquad (13)$$

$$C_3H_8 + H_2 \rightarrow C_2H_6 + CH_4 \qquad (14)$$

$$C_3H_8 + 2H_2 \rightarrow 3CH_4 \qquad (15)$$

An effective catalyst for the ODPC should be able, not only to dehyrogenate propane, but also to catalyze the RWGS reaction, and this involves the adsorption of both H_2 and CO_2. Thus, it has to combine basic sites able to adsorb the slightly acidic CO_2, and acid sites for adsorption of the alkane and H_2. The influence of performing the reaction in the presence of CO_2 and the contribution of CO_2 to the overall dehydrogenation process will be, therefore, highly dependent on the properties of the catalyst employed. Different types of catalysts have been explored for ODPC, such as zeolites, zeolite supported metal oxides and mixed metal oxides. Although most of the studies are based on metal oxides supported on mesoporous supports, such as MCM-41 or SBA-15, Cr-loaded zeolites have also been described as catalysts for the CO_2-mediated ethane and propane dehydrogenation. Regarding ethane, stable catalytic activity with time due to the coke removal capacity of CO_2 and high ethene selectivities were obtained when performing the experiments at high temperatures, in the range of 650-800ºC, and atmospheric pressure.[510,511] The zeolites were high silica ZSM-5 (SiO2/Al2O3>190), and high-oxidation-state Cr species (Cr^{6+}=O and Cr^{5+}=O) were identified as the active species for dehydrogenation. In the presence of ethane these species were reduced to Cr^{3+} but they could be reoxidized by treatment with CO_2. These results suggested that a Cr redox cycle occurred during ethane dehydrogenation in the presence of CO_2.[511] The results obtained by Zhu et al. on CO_2-mediated propane dehydrogenation catalyzed by a Cr-loaded MFI in its borosilicate form suggested that although Cr^{6+} monochromate was more active than Cr^{3+} polychromate, dispersed Cr^{3+} species, such as $[CrO]^+$, formed by steam treatment of the catalysts, were also able to catalyze the reaction.[512] The CO_2 promoting effect on propane dehydrogenation was also observed on Ga_2O_3 supported on high silica H-ZSM-5 and H-ZSM-48.[513] The 1D medium pore structure of ZSM-48 resulted in a higher

propene selectivity as compared to ZSM-5, but also in a lower stability towards deactivation.

A recent study by Al-Mamoori et al. describes a two-step process combining ethane ODH with an integrated CO_2 capture and utilization as a sustainable approach directed to the reduction of anthropogenic CO_2 emissions and upgrading of low value feedstocks to chemicals of industrial interest.[514] Cyclic adsorption-reaction operation was performed on a hybrid bed where a double salt K-Ca adsorbent and a Cr-impregnated H-ZSM-5 ODH catalyst were physically mixed. Adsorption was performed in a first step at 600 °C using 10 % CO_2/Ar mixture. In a second step the temperature is increased to 700ºC for conversion of a 5 % C_2H_6/Ar stream on the zeolite based catalyst, assisted by the CO_2 previously adsorbed and released in this second step. Although the proof of concept was demonstrated, the performance of both adsorbent and catalyst was worsened after four consecutive adsorption-reaction cycles due to sintering of the adsorbent particles and to reduction of the Cr^{6+} active sites (see Figure 22). Coke deposition was an additional possible cause of deactivation.

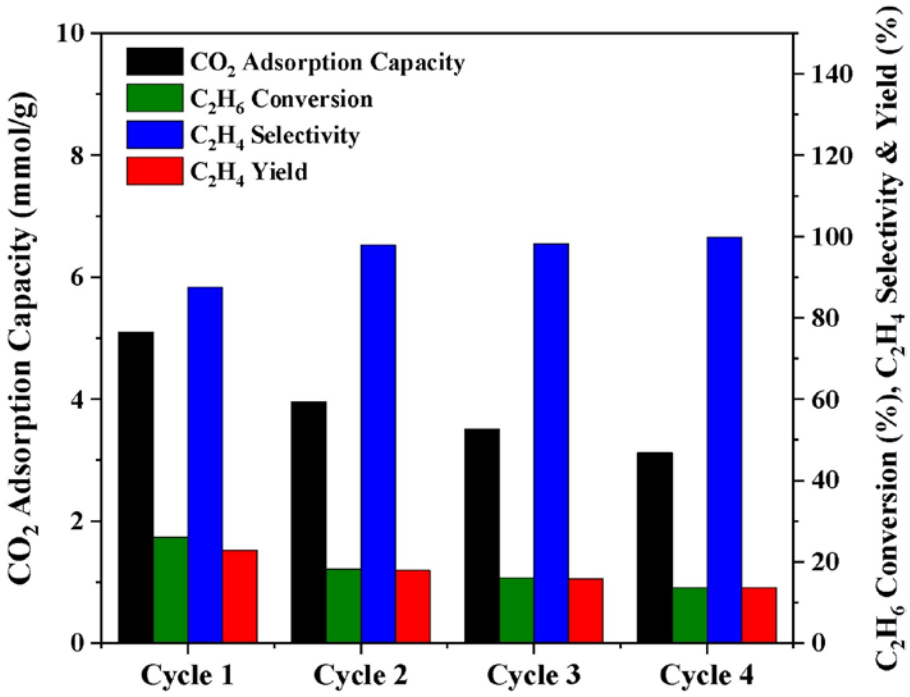

Figure 22. Cyclic adsorption results for (K-Ca)50/(Cr10/H-ZSM-5)50. Reprinted from ref.[514] *with permission from Elsevier, copyright 2020.*

The application of zeolite based catalysts and, in particular, the use of Fe-based medium pore zeolites, has received more attention in the field of N_2O mediated dehydrogenation of light alkanes. Panov evidenced how the ZSM-5 structure was able to stabilize iron complexes, which were reduced to divalent species, denominated α-sites, during the activation step (see Scheme 16).[515,516] These Fe^{2+} species were re-oxidized to Fe^{3+} by N_2O decomposition producing the so-called atomic α-oxygen species, which were seen to be exceptionally reactive and able to oxidize organic molecules even at room temperature. As shown in Section 3.2, these sites were even capable of methane activation.

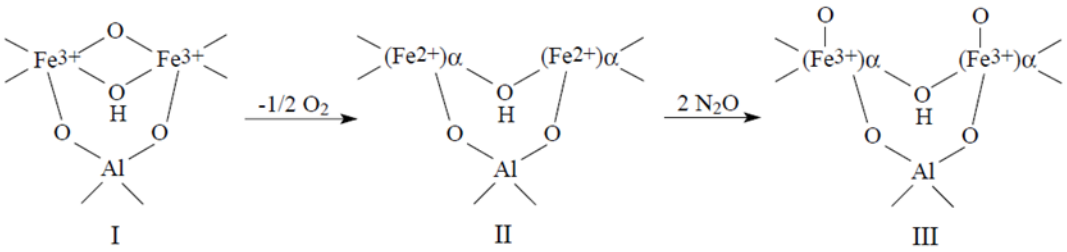

Scheme 16. Formation of a pair of a-sites in the form of a dinuclear iron complex. Adapted from ref.[516] with permission from Elsevier, copyright 2020.

Early studies in the 1990s had shown high selectivity of Fe-ZSM-5 catalysts towards light alkane dehydrogenation in the presence of N_2O, but at alkane conversions below 10%.[517] Some years later Pérez-Ramírez et al. reported the formation of propene and propionaldehyde with yields up to 24 and 6%, respectively, on steam-treated Fe-ZSM-5 at 525ºC.[518] This high production of functionalized hydrocarbons was obtained thanks to the combination of the high specificity of N_2O as monooxygen donor and the capability of certain extra-framework Fe species, stabilized by the medium pore zeolite, for coordinating the α-oxygen formed by N_2O decomposition as shown above. In fact, the tetrahedrally coordinated Fe, sited in framework positions, was unable to activate N_2O, and steam treatment of the catalyst was required in order to have an efficient dehydrogenation behavior.[519] The same group performed further studies to unravel the mechanism of N_2O and alkane conversion in the presence of steam-activated Fe-ZSM-5 zeolites,[520] and demonstrated that the atomic oxygen species in oligonuclear iron species formed during the hydrothermal treatment are more active, not only for the recombination of adsorbed oxygen atoms, but also for its transfer to a hydrocarbon molecule (Eq. 16-19).

$$N_2O + * \rightarrow N_2 + O* \quad (16)$$

$$N_2O + O* \rightarrow N_2 + O_2 + *$$ (17)

$$O* + O* \rightarrow O_2 + 2*$$ (18)

$$C_3H_8 + O* \rightarrow C_3H_6 + H_2O + *$$ (19)

The influence of the acidic properties of the zeolite support on the activity and selectivity of the Fe-ZSM-5 catalysts was only minor, and similar results were observed by Nowinska et al. in a study were ZSM-5 with different Al contents were ion exchanged with different transition metals (Fe^{3+}, Mn^{2+} and Co^{2+}).[521] Among the different metals, iron led to the most active catalysts, but only after high temperature treatments (calcination at 900ºC). Whereas carbon oxides were the main products when dehydrogenation was performed in the presence of O_2, high selectivity to propene was obtained when using N_2O as the oxidant.

Steamed Fe-ZSM-5 was also studied by Bulanek et al. for propane ODH in the presence of O_2, N_2O and O_2/N_2O mixtures.[522] The best results in terms of catalyst stability towards deactivation were obtained for mixtures of the two oxidants and in the absence of BAS. Under these conditions propane conversion and propene selectivity were 51.7% and 39.7%, respectively.

The positive confinement effect of the zeolite structure on the active iron species was clearly evidenced by Kumar et al. when Fe-silicalite was seen to be significantly more active than the mesoporous Fe-SBA-15 for propane ODH and other reactions.[523] As both catalysts presented comparable acidic properties and contained comparable amounts of iron, present mostly as isolated Fe^{3+} sites with similar structure, the better catalytic performance of the Fe-silicalite was related to the differences in the pore geometries of

the two catalysts. It was concluded that the microporous environment led to the stabilization of the active Fe species and favored the intimate contact of the molecules involved in the process with the active sites.

Waste N_2O has also been used as mild oxidant for oxydehydrogenation of ethane catalyzed by different zeolites ion-exchanged with Fe, in a temperature range of 350 to 450ºC.[524] The trends observed were similar as those described for propane dehydrogenation, and the catalysts, active in the presence of N_2O, presented a significantly lower activity when O_2 was used as the oxidant (see Figure 23a). Although the medium pore Fe-ZSM-5 was more active and more selective to ethene than the large pore zeolites Fe-Y an Fe-mordenite (see Figure 23b), the three zeolite-based catalysts were able to dehydrogenate ethane in the presence of N_2O. However, Fe-silicalite and Fe-loaded on non-microporous supports such as silica or silica-alumina were found to be inactive for ethane conversion under the conditions employed in this study.

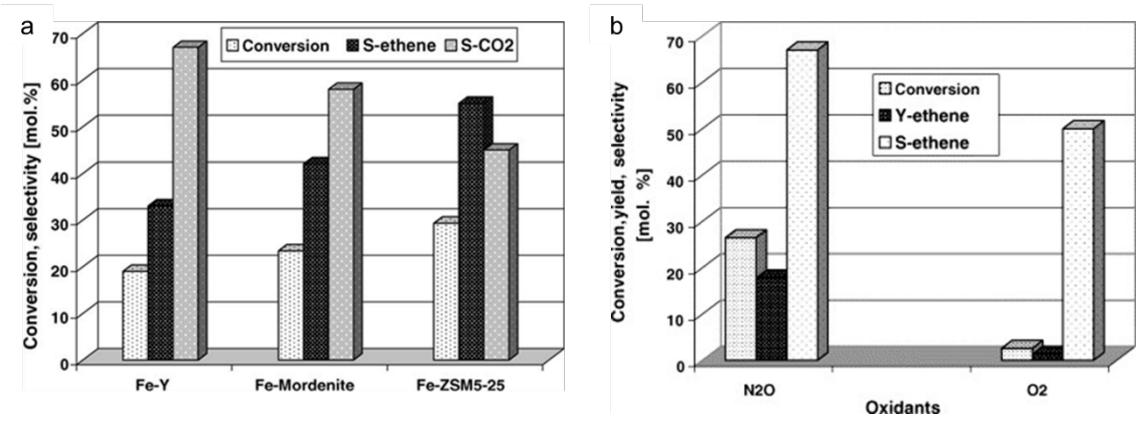

Figure 23. (a) Catalytic activity for ethane ODH reaction performed on Fe-Y, Fe-mordenite and Fe-ZSM-5 (b) Catalytic activity of Fe-ZSM-5-50 for ethane oxidation in the presence of different oxidants (N_2O or O_2). Adapted from ref.[524] with permission from Elsevier, copyright 2006.

4.4. Light alkane aromatization

Light alkane aromatization converts low value gaseous alkanes from natural gas, shale gas or LPG streams into valuable liquid aromatics, mainly benzene, toluene and xylenes (BTX streams), easier to be transported and key building blocks for the manufacture of plastics and fine chemicals.[19] Besides alleviating the high demand of aromatics, generally supported by naphtha processing,[525] and which will be revised in Section 5.3, light alkane aromatization presents the additional advantage of producing large amounts of hydrogen that can be further used in other hydrogen demanding processes.

Light alkanes are mainly converted to aromatics over bifunctional catalysts containing a metal component and an acidic zeolite support.[525,526] In fact, the Cyclar process, one of the commercial aromatization processes, employs a Ga/HZSM-5-based catalyst.[19,20] Unlike in dehydrogenation (Section 4.3), the metal function is unable to catalyze all the different steps occurring during the dehydroaromatization sequence, and the role of the zeolite acid sites is key. Indeed, the olefins formed in the first dehydrogenation step need to oligomerize (C-C bond formation) to intermediates with, at least, six carbon atoms able to cycle in a series of reactions that are catalyzed by the acid sites, and whereas olefins are the main products under low alkane conversions, BTX aromatics and hydrogen predominate at high conversions (see Figure 24). As we have stated in the former section, dehydrogenation is highly endothermic and thermodynamically favored at high temperatures and, under these conditions, other acid catalyzed reactions compete with the pure aromatization routes, such as cracking, over-oligomerization or hydrogen transfer, leading to undesired methane, ethane, propane or polyaromatics. Hydrodealkylation or disproportionation of the formed alkylaromatics can also take

place, although the latter could be considered if the objective is to maximize the selectivity to valuable products, such as p-xylene. The description of the reaction steps is not easy due to the complexity of the dehydroaromatization chemistry, and the mechanistic knowledge is often deduced from experimental product distributions or theoretical modelling approaches.[526]

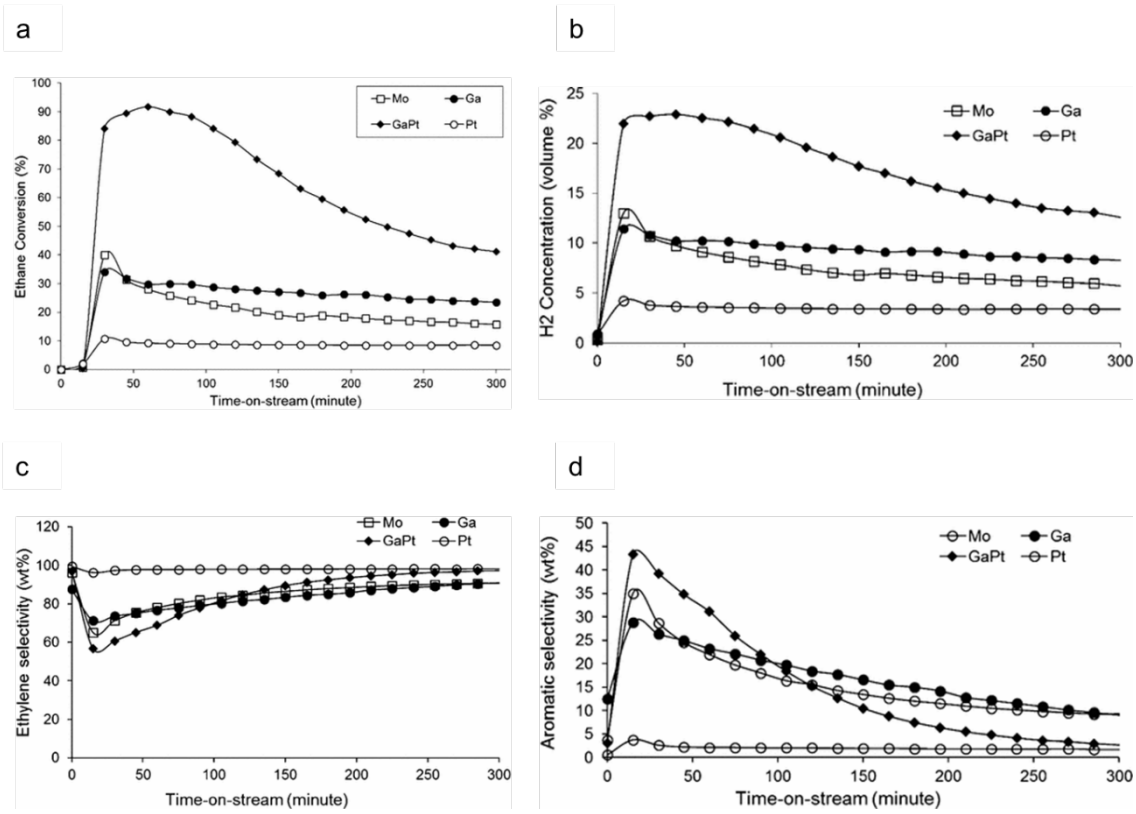

Figure 24. Evolution of ethane conversion (a), H_2 concentration (b), ethylene selectivity (c) and aromatics selectivity (d) with time-on-stream for ethane aromatization. High conversions correspond to short time-on-stream. Adapted from ref.[527] *with permission from Elsevier, copyright 2006.*

Bhan and Delgass extensively reviewed the mechanistic and modelling literature related to the elementary steps for propane aromatization over mono-functional acid H-ZSM-5 zeolites.[526] In these cases, the activity and selectivity to aromatics were rather low due to the production of significant quantities of methane and ethane by both protolytic

cracking and hydrogen transfer reactions. Moreover, the process required very high temperatures (>500 ºC) and was accompanied by rapid deactivation by coke. The addition of a metallic component, facilitating the alkane dehydrogenation steps (see steps 1, 5, 9 in Figure 25a) and the aromatization of the intermediates to BTX (step 10) would lead to higher activity and aromatics selectivity.[525,526] The acid catalyzed steps involve adsorption of the short olefins formed upon dehydrogenation and their further oligomerization to dimers and higher olefins (through oligomerization-cracking) and cyclization (steps 3 and 7 of Figure 25a, respectively).[528,529] Cyclization is supposed to involve an equilibrium between 5- and 6- ring species, and it is thought to occur via the attack of the C^+, formed upon protonation of a diene, to the remaining C-C double bond. This leads to an alkyl-cycloC_5 carbenium species, which will undergo ring expansion (see the detailed scheme for a C_6 intermediate in Figure 25b).[526] Several reviews have thoroughly described the role of the metal and the acid sites in relation to the reaction mechanisms for propane aromatization, mainly by metal modified ZSM-5 catalysts.[432,468,526]

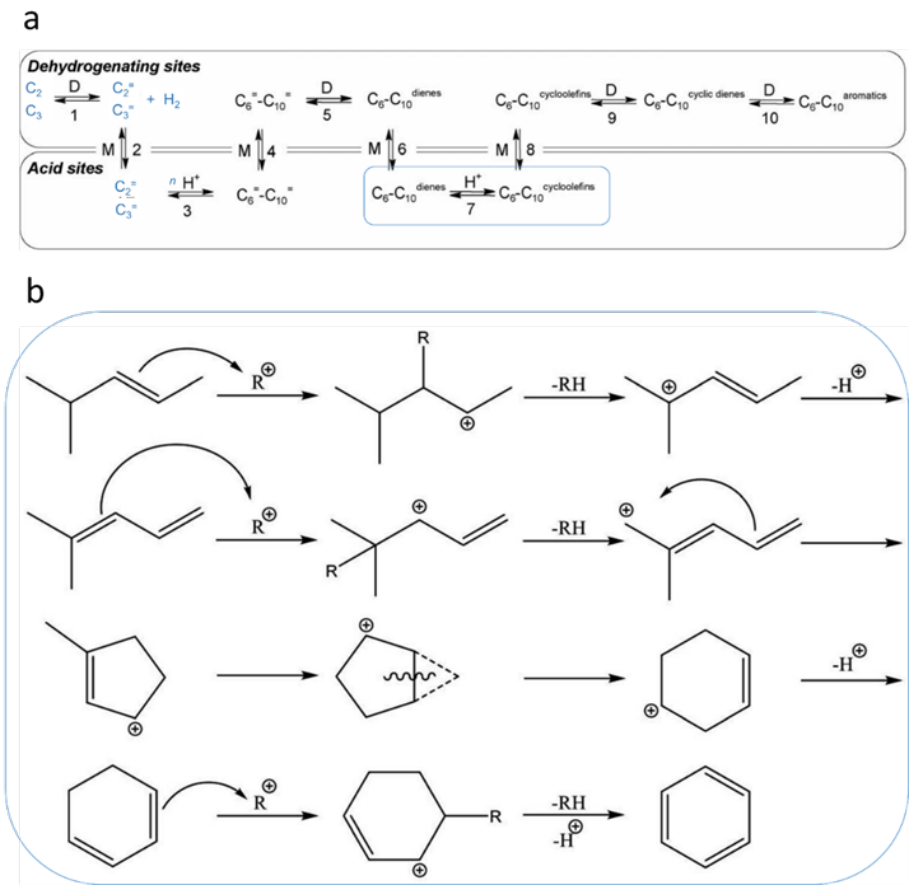

Figure 25. Propane aromatization over Ga/HMFI catalysts. Bifunctional reaction scheme. (H^+)-protonic sites, (D)-dehydrogenation sites and (M)-migration (diffusion) steps. (a), adapted from ref. [440] with permission from Elsevier, copyright 2006; and aromatization of oligomers over H-ZSM-5 (b), Adapted from ref.[525] with permission from the Royal Society of Chemistry, copyright 2020.

The aromatization of propane has been historically more investigated than that of ethane, a process that has not been commercially exploited yet. This is because higher activation temperatures are required for activating ethane as compared to propane, due to the easier cleavage of the C-H bond as we increase the length of the carbon chain. Thus, high temperatures are needed to reach appreciable conversions (Figure 26a) in a process that is spontaneous at temperatures above 700 ºC (Figure 26b). Moreover, the acid-catalyzed oligomerization of propene from a secondary carbenium is much faster than that of ethene, which involves the formation of energetically unfavorable primary

carbeniums. However, the emergence of shale gas has resulted in a shift to lighter alkane utilization,[530] which has exponentially increased the research interest on ethane aromatization in the last decades.[118,531]

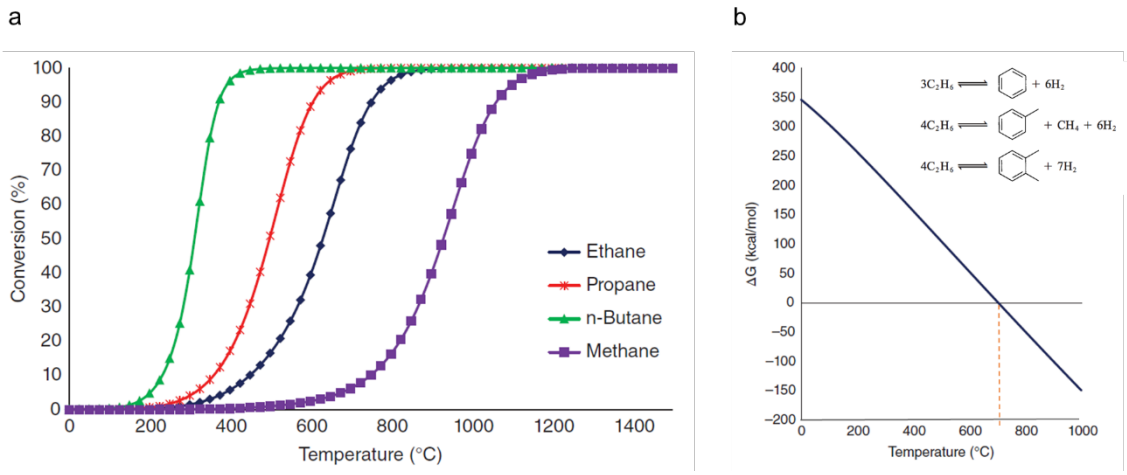

Figure 26. (a) Thermodynamics of light alkane aromatization; (b) Gibbs free energy plot for ethane aromatization reaction. Adapted from ref.[530] with permission from Wiley-VCH, copyright 2018.

Experimental conditions will affect not only the alkane conversion degree, but also the final product distribution of alkane dehydroaromatization. Thus, the BTX distribution was reported to change from a predominant formation of xylenes at temperatures below 723K to higher toluene and benzene selectivity at higher temperatures, approaching the equilibrium distribution.[532] Iglesia et al. reported a statistical distribution of the number of ^{13}C atoms in benzene and toluene for ^{13}C propane dehydroaromatization, indicating that the propane chain is randomly rearranged during the reaction, as a result of a rapid interconversion among olefins.[533] Partial pressure and contact time of the alkane have been also reported to influence the BTX selectivity.[534] Furthermore, the catalyst may suffer modifications during reduction steps under H_2 atmosphere or by pretreatment with lower hydrocarbons.[526]

The pore topology of the zeolite support strongly influences the aromatization reactivity.[525,530] Among all the structures explored, acid ZSM-5 zeolites modified with active metals are the best performing catalysts for light alkane aromatization.[432,525,526,530,535] Its 3-dimensional medium sized pore structure selectively converts light alkanes into monocyclic (BTX) aromatics, allowing their diffusion and restricting the formation of higher hydrocarbons leading to coke precursors and catalyst deactivation. Lower aromatization rates and selectivities are usually obtained when using other zeolite topologies. In general terms, zeolites with small pores require harsher conditions, while large pore zeolites produce heavy aromatics leading to easier coke formation. Indeed, Ga-beta was more selective to naphthalene and methylnaphthalenes than Ga-ZSM-5 and other undesired reactions, such as cracking and hydrogen transfer, were also favored by its larger pore dimensions.[536] As described in the previous sections, the zeolite structure may also affect the anchoring of the metal species in the zeolite channel, and thus the synergy between the metal and acid functions.

ZSM-5 also outperforms other 10-ring zeolites. Thus, Zn/ZMS-5 was more active and more selective to monocyclic aromatics, especially benzene, than Zn/ZSM-11, with a similar topology but straight intersecting pores of slightly larger dimensions than those of Zn/ZSM-5.[537,538] Zn-/ZSM-11 showed higher ethylene and lower aromatic selectivity, with a higher production of naphthalene and alkyl-naphtalenes, probably favored by its slightly larger pores, which will enable the more space demanding condensation reactions to take place (see Figure 27). ZSM-12 (MTW), with a large pore mono-dimensional structure, was significantly less active despite its higher BAS density. Moreover, it had low aromatization activity and high olefin selectivity, mainly ethylene

(see Figure 27) produced by cracking of oligomer intermediates. Moreover, the large pore structure promoted the formation of polyaromatics coke precursors.

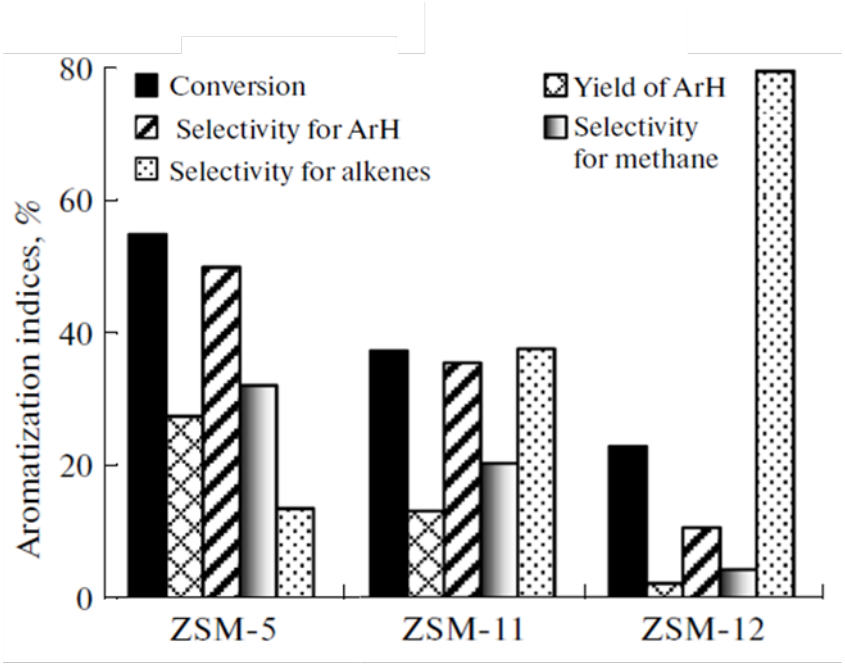

Figure 27. Catalytic variables for the aromatization of ethene over different Zn-modified zeolite structures. Adapted from ref.[537] with permission from Springer Nature Customer Service Centre GmbH: Springer Nature Petroleum Chemistry, copyright 2014.

In a different study, Zn loaded SSZ-13 (8-ring pores accessing cavities) and beta zeolites (12-ring tridimensional pore system) were compared as catalysts for ethane aromatization with Zn/ZSM-5[539], and both were less active than the latter under the same conditions. Since recent studies evidence that the intrinsic BAS strength is comparable for different structures,[96,540] the lower activity encountered for large pore structures as compared to ZSM-5 can be correctly attributed to the difference in their pore sizes, with larger pores leading to a weaker confinement and a lower activity.

Table 5. Ethane aromatization on Pt-Ga/HZSM-5 catalysts with different Si/Al ratios, at T=600 ºC, WHSV=450h^{-1}. Adapted from.[541]

Si/Al mol/mol	Ga (wt. %)	C_2H_6 conv. (%)	Aromatics yield (%)	Aromatics sel. (%)	CH_4 sel. (%)	C_2H_4 sel. (%)
15	0.5	47.1	30.3	64.3	19.5	7.0
28	0.5	39.9	24.0	60.2	23.3	6.5
45	0.5	27.2	14.8	54.5	11.1	19.5
15	2.0	47.6	30.1	63.2	20.1	7.8
28	2.0	24.7	12.7	51.4	7.7	21.5
45	2.0	17.0	4.2	24.8	3.5	53.9

Regarding the influence of the Si/Al ratio on ethane aromatization, generally lower conversions and selectivities to aromatics are observed with increasing Si/Al (see Table 5), because of enhanced alkane dehydrogenation to ethene vs further oligomerization-cycling-dehydroganation.[539,541,542] In fact, in the presence of BAS-free catalysts, alkane dehydrogenation is the main reaction on these type of catalysts, as described in Section 4.3. Also, higher Si/Al ratios imply lower amount of acid sites available for ion exchange with the metal cations. Ausavasukhi and Sookoi showed the influence of Si/Al on the dispersion of the metal species in the catalyst zeolite structure and, consequently, on the catalytic activity for the first dehydrogenation step.[543] Thus, an optimal Si/Al ratio is required for improved catalytic behavior, which was reported to be ≤ 30 for Pt-doped Ga/HZSM-5[541] or Zn/HZSM-5[539] catalysts.

Gallium and Zinc have been reported to be the most active metals for C_2-C_4 aromatization, the former being preferred for commercially exploited processes, mainly due to the high volatility of Zn caused by its lower melting point and higher vapor

pressure. The role of the metal sites on the dehydrocyclization mechanism has been reviewed by Hagen and Roessner and Ono et al. for ethane aromatization on Zn- and Ga-modified H-ZSM-5,[531,544] and by Bhan and Delgass for propane aromatization on Ga-modified H-ZSM-5.[526] Caeiro et al. also reviewed light alkane (C_2-C_4) activation over acid and bifunctional catalysts.[440] The interested reader is referred to these reviews for more information, and we will focus, instead, on the most recent advances on this topic.

The first step of the alkane aromatization process is the alkane activation under non-oxidative conditions, and its dehydrogenation, which has been extensively covered in Section 4.3. This step will determine the rate of olefins formation and, subsequently, the rate of aromatization. Thus, the metal species need to be well dispersed on the zeolite support to reach high ethane conversion rates,[530] and the alkane activation mechanism may be different over different metals, according to their oxidation state, Ga^{+} or Zn^{+2}.[545] However, Ga and Zn species will interact differently with the zeolitic acid supports, employed for aromatization, than with pure or high-silica supports used for dehydrogenation. Although still not fully understood, a synergism between metallic and acid species within the bifunctional catalyst has been proposed and, in any case, the introduction of metals in the zeolite structure will affect the concentration of both BAS and LAS. The metal function increases the olefin concentration in the gas phase and this affects the surface coverages and the extension of the unimolecular or bimolecular reactions catalyzed by the acid sites. In the same way, the interaction of the acid sites with the different species in the reaction media will affect associated kinetics of the reactions taking place on the metal sites.[526]

Bifunctional Ga/H-ZSM-5 can be prepared by post-synthesis incorporation or by direct synthesis of the galloaluminosilicates.[530] Ga activates alkane by hydrogen abstraction and formation of the corresponding alkene. In the dehydroaromatization catalyst, Ga may be present as Ga_2O_3 or in zeolite ion exchange positions[527] as GaO^+ species and, depending on the hydrogen pressure and the distance between Al atoms, Ga^+, GaH^+ and GaH_2^+ species may also be formed. The different chemical oxidation state of Ga species will influence the rate constants for C-C or C-H activation differently, and several mechanisms for alkane activation have been proposed involving the concerted action of protons and Ga sites.[454,455,546–548]

Early studies by Yakerson et al. based on extensive IR experiments and electron microscopy proposed Ga_2O_3 adsorbed on the zeolite external surface as the active species for ethane aromatization.[549] However, a recent work on ethane dehydroaromatization over Ga/ZSM-5 catalysts, showed a remarkable increase in the dehydrogenation activity after catalyst reduction under H_2, as well as a decrease in acidity attributed to the migration of the Ga^+ and GaH_2^+ reduced species into the channels of the zeolite support, and their replacement of H^+ in the charge compensating sites.[543] The activity of these species was ranked as $GaO^+ \approx Ga_2O_3 < Ga^+ < GaH_2$. Biscardi and Iglesia proposed an alternative dehydrogenation mechanism based on reactions with propane and deuterated propane mixtures over HZSM-5 and Ga-HZSM-5.[449] Ga cations were also thought to increase the rate of subsequent dehydrogenation steps for the propane conversion to aromatics, and to facilitate the desorption of propene from the zeolite.[550] Guisnet used catalysts prepared by physical mixing of Ga oxide with HZSM-5 to demonstrate the implication of successive reactions on both metal and acid sites of the bifunctional mechanism.[551] In Figure 28a, the ratio between the activity for

propane aromatization and acid activity (R) is plotted versus the dehydrogenation/acid activity ratio (D/A). Dehydrogenation would be the limiting step for low values of D/A, while for high values of D/A the acid reaction would be limiting with the bifunctional activity being proportional to the acid activity. Figure 28b shows that, in the low value range, R increases proportionally to D/A, demonstrating the existence of the bifunctional mechanism that is limited by dehydrogenation steps.

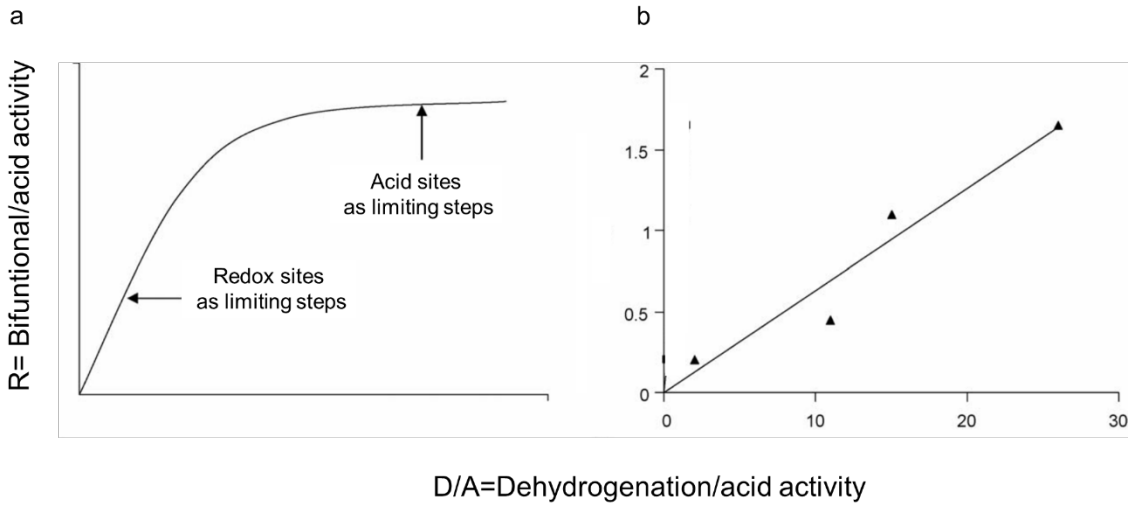

Figure 28. (a) Expected change of R the ratio between bifunctional/acid activities of classical bifunctional catalysts as a function of De/Ac, the ratio between their dehydrogenating and acid activities. (b) Aromatization/acid activity ratio (R) of mechanical mixtures of Ga_2O_3 and HMFI after pre-treatment under nitrogen at 600 ºC vs. De/Ac. Adapted from ref.[551] *with permission from Elsevier, copyright 1996.*

A very recent study[552] proposed that hydrocarbon species also contributed to the aromatization process, in a similar way as has been described for the hydrocarbon pool in the autocatalytic conversion of methanol to aromatics.[553]

Zn containing zeolites have also been widely studied as alkane dehydroaromatization catalysts. In this case, Zn is usually incorporated to the zeolite by means of post-synthesis procedures,[530,554,555] and the active Zn species can be classified into two main

groups, ion-exchange Zn species or ZnO species, with the latter being located as ZnO clusters within the zeolite structure or as nanoparticles on the external zeolite surface (see Figure 29a-c). Among the chemical states of Zn, Zn^{2+} bonding two adjacent Al atoms and ZnH^{+} at isolated Al sites have proven to be effective for dehydrogenation of light alkanes. Other divalent Zn species may exist, such as small ZnO clusters or species interacting with the lattice oxygen (O_L) of the zeolite, like $Zn(OH)^{+}$, stabilized by one framework Al Figure 29d presents the possible Zn-sites when interacting with a ZSM-5 zeolite. Under dehydrogenation conditions, these Zn species can be reduced to metallic Zn, which could be lost due to its high volatility. Dehydration may also lead to isolated Zn^{2+} ion-exchanging the nearest BAS. According to *in situ* Zn K-edge XANES spectroscopy, these species presented tetrahedral symmetry in the form of O_L-Zn^{+2}-O_L and were stabilized by two framework Al atoms, a clear example of stabilization by Al pairs.[556] Furthermore, X-Ray absorption and TPR revealed that Zn^{+2} species were not reduced to metallic Zn at 500 ºC, in opposition to ZnO, but they could be reduced to ZnH^{+} by H_2 desorption at Zn sites through back-spillover.[557–559] This supports the proposal of Biscardi and Iglesia,[560] which considered hydrogen desorption as the rate determining step in propane dehydrogenation over Zn/HZSM-5. Gao et al. performed XPS experiments at various temperatures and showed that ZnO clusters can be reduced to $Zn(OH)^{+}$ at 300 ºC, which can be converted to Zn^{+2} at 400 ºC.[558]

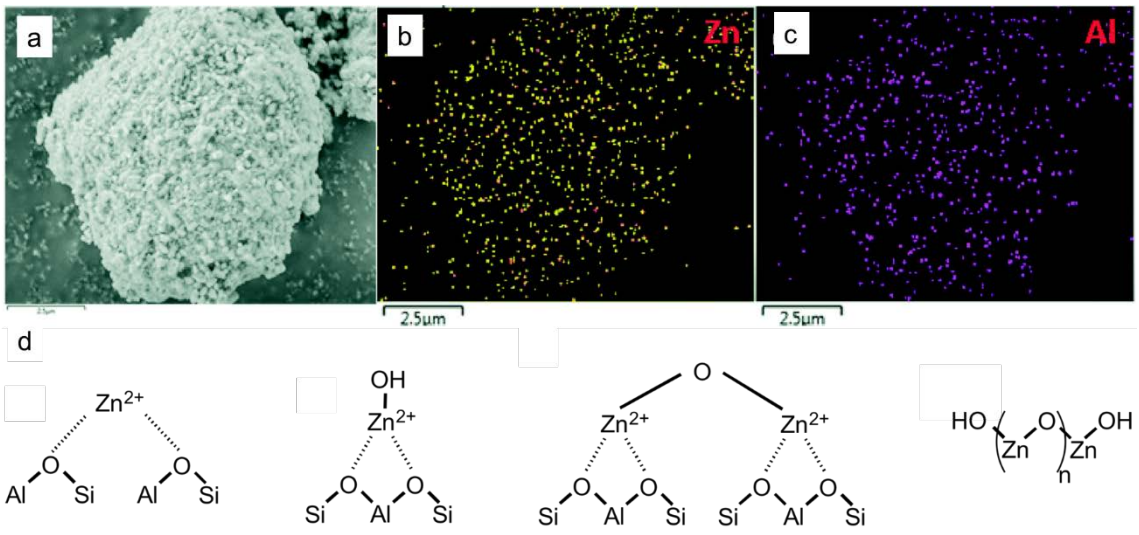

Figure 29. SEM image (a) and Zn (b) and Al (c) EDX mapping on Zn/ZSM-5 zeolite, Adapted from ref.[539] with permission from the Royal Society of Chemistry, copyright 2017. (d) Different Zn^{+2} sites in ZSM-5 zeolite.

Hensen and co-workers compared the Zn structures formed on HZSM-5 when incorporating the metal by impregnation, ion-exchange and chemical vapor deposition (CVD).[554] The latter allows a quasi-stoichiometric substitution of BAS with Zn^{+2} ions, resulting in the formation of isolated Zn^{+2} species, in contrast to the heterogeneous distribution of extra-framework Zn^{+2} species observed during ion exchange or incipient wet impregnation. However, the catalyst prepared by CVD was less active than the other two, which was ascribed to a lower abundance of active Zn^{+2} species and to the creation of multinuclear zinc oxide species, which blocked the zeolite pores. This was in good agreement with previous results reported by Pidko and van Santen, which indicated that binuclear Zn species were not favorable for ethane dehydrogenation and, therefore, little active for aromatization, because of the formation of stable intermediates on the binuclear sites.[561] DFT calculations suggested isolated Zn^{+2} as O_L-Zn^{+2}-O_L species to be more active for ethane dehydrogenation than ZnH^+ species under ethane dehydrogenation conditions.[562] On the other side, other groups recently claimed that

oxygen-bridged Zn dimers, such as O_L-Zn^{+2}-O-Zn^{+2}-O_L or (Zn-O_L-Zn)$^{+2}$$O_L$-$Zn^{+2}$-$O_L$ species (see Figure 29d) were the active species for ethane dehydrogenation and highly selective to aromatics when combined to BAS for light alkane dehydroaromatization.[539,554,563]

The aromatization activity is also influenced by the Zn/BAS ratio. The higher the Zn content, the higher the number of LAS and the lower the BAS site density of the metallozeolite. Optimal Zn loading were claimed to be between 3-5 wt%[530] or to give Zn/BAS ratios in the range of 3-4.[539]

Small amounts of Pd, Pb and Fe have been seen to promote the catalytic activity and aromatics selectivity of Ga- and Zn-containing zeolites, and to reduce Zn's volatility.[530,538,564–566] In Pt-promoted Ga-catalysts, multinuclear rather than mononuclear Ga clusters have been speculated as the active species.[566]

Platinum was also used as the metallic component in bifunctional light alkane aromatization catalysts, because of its high dehydrogenation activity. However, besides its higher cost, it is highly selective to olefins and promotes other undesired reactions such as hydrogenolysis, olefin re-hydrogenation and dealkylation, resulting in a lower aromatics selectivity due to the side-production of methane and ethane.[527,541] Different attempts have been reported in order to reduce the hydrogenolysis activity and to increase the overall aromatic selectivity, including size reduction of the metal particle in order to increase the dehydrogenation/hydrogenolysis ratio, or increasing reaction temperature.[468] An alternative approach is the dilution of the noble metal by addition of a second metal to form a bimetallic catalyst, which also reduces catalyst aging, as described for Pt-based alkane dehydrogenation catalysts (see Section 4.3). The synergistic effect of Pt and Ga for ethane aromatization over Pt modified Ga/HZSM-5

catalysts was reported by different authors,[541,564,566] and is clearly evidenced by the results enclosed in Table 6, Thus, combining specific proportions of the two metals, 2%wt Ga – 0.3wt% Pt, with an optimal Si/Al ratio of the ZSM-5 zeolite, the ethane conversion was significantly enhanced. Samanta et al. also observed high catalyst activity on bimetallic Ga-Pt nanoclusters and reduced deactivation rate due to coke removal by hydrogenolysis through H_2 spillover.[527]

Table 6. Influence of the Pt loadings in the Ga zeolites on the composition of the ethane conversion products at T=600°C and WHSV=500 h^{-1}. Adapted from.[564]

Pt wt. %	C_2H_6 conv. (%)	Aromatics yield (%)	Aromatics sel. (%)	CH_4 sel. (%)	C_2H_4 sel. (%)
0	25.0	16.0	64.1	18.4	6.5
0.05	46.9	26.5	56.5	25.5	5.6
0.1	51.6	31.3	60.7	22.0	5.4
0.2	58.8	37.9	64.4	19.5	4.6
0.3	63.1	43.6	69.1	14.8	3.9
0.5	49.5	30.3	61.1	21.3	5.8

Re-doped catalysts have also been explored for light alkane aromatization. Lacheen et al. proposed encapsulated Re clusters as active species for propane activation,[567] and Solymos and Tolmacsov suggested a promotion effect of Re on the C-H bond activation that resulted in increased ethane conversions and aromatics selectivity.[542] In a recent paper, Ma and Zou successfully prepared Re/HZSM-5 with encapsulated Re metal clusters by vapor-phase exchange and performed a kinetic study on the dehydroaromatization of ethane to bencene and toluene on these catalysts.[568] They

observed that the close proximity between the Re metal clusters and acid sites was critical to promote benzene formation. Moreover, their results indicated that the dehydrogenation of ethene to acetylene was the rate-determining step mediating the overall dehydroaromatization process. Other bifunctional catalysts proposed for light alkane aromatization have been Mo- and W promoted Mo/H-ZSM-5,[527,569–571] although with less success than the catalysts described so far.

Deactivation by coke formation is the main drawback associated to light alkane aromatization over metal-zeolite catalysts. Polyaromatic coke precursor species are formed through over-oligomerization of intermediate hydrocarbons and condensation of aromatics. Different approaches have been proposed for suppressing coke formation and increasing aromatics' selectivity on metal-modified HZSM-5, such as the addition of promoters to the Pt[445,446] or the preferential location and distribution of the BAS at the ZSM-5 channel intersections.[572]

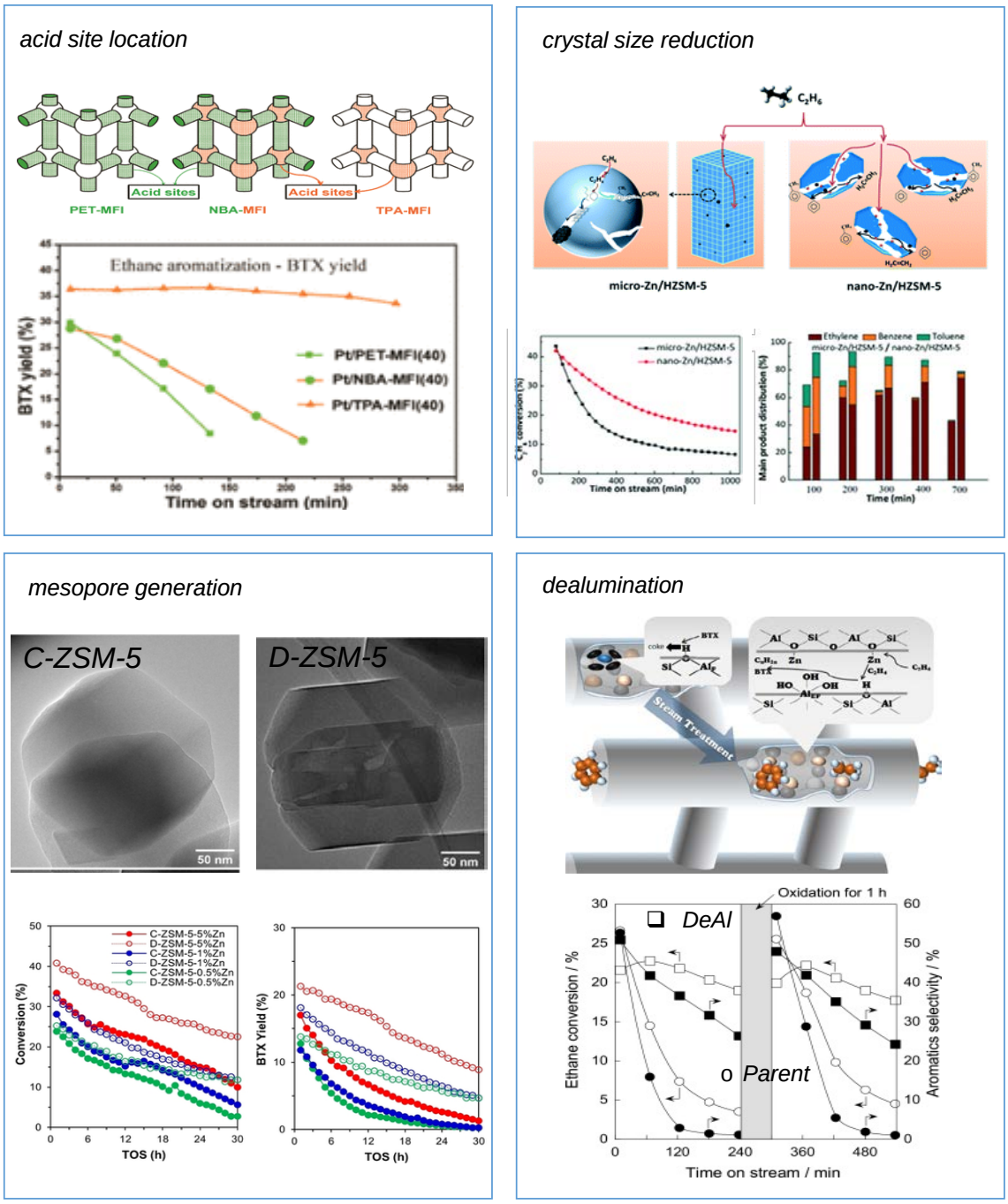

Figure 30. Different approaches proposed to reduce coke formation and to increase selectivity to desired aromatics on ZSM-5 bifunctional catalysts are: preferential siting of acid sites at channel intersections, reprinted from ref.[572] *with permission from the American Chemical Society, copyright 2019; reducing the crystallite size, reproduced from ref.*[563] *with permission from the Royal Society of Chemistry, copyright 2020; generating mesoporosity within the crystallites, reproduced from ref* [573] *with permission from Wiley-VCH, copyright 2020; or post-synthetic steam treatments, reprinted from ref.*[574] *with permission from Elsevier, Copyright 2018.*

Shortening of the diffusion paths by reducing the zeolite crystallite size,[563] by generation of intra-crystalline mesoporosity[573] or by synthesizing pillared ZSM-5 bifucntional catalysts[575] have proven to reduce catalyst deactivation rates. Saito et al were able to increase catalyst life by means of post-synthetic dealumination by steam treatments that led to a decrease of the number of Al forming BAS but not of the Al bonded to Zn species on ZSM-5.[574] The most interesting approaches related to catalyst life improvement are summarized in Figure 30.

In a recent work by Gomez et al. ethane aromatization has been combined with CO_2 reduction in a one-step tandem approach on P,Ga-modified ZSM-5.[576] The role of CO_2 is to assist the conversion of ethane into ethene by CO_2-assisted ODH, whereas the addition of low P loadings to the Ga/HZSM-5 catalyst increases its hydrothermal stability and decreases coke formation.

4.5. Selective oxidation

Oxygen functionalized hydrocarbons are important intermediates in the fabrication of base chemicals and building blocks for plastics and synthetic fibers, which can be obtained by selective partial oxidation of light alkanes by means of different type of catalysts. These may include bulk or supported complex multicomponent metal oxides, heteropolyacids or their salts, V on mesoporous supports such as MCM-41 or SBA-15, or metallozeolites and zeotypes. The interested reader is directed to specific reviews on selective oxidation of ethane,[577] propane,[578–581] or butane.[582] The purpose of this section is not to cover all possible partial oxidation processes of light alkanes, but to focus on those zeolite-catalyzed processes that have attracted more interest in the research community.

Development of heterogeneous zeolite-based catalysts for efficient direct oxidation of ethane to acetic acid is a subject of high interest as it would be a sustainable alternative to the homogeneous Ir-based commercial catalyst used nowadays.[583] ZSM-5-based catalysts have been described to be active for low temperature liquid phase oxidation of ethane to acetic acid. In 2013, Rahman et al. reported for the first time the direct conversion of ethane to acetic acid, with yield and selectivity of 19% and 49%, respectively.[584] The best results were obtained at 3.0 MPa and 393K when the reaction was catalyzed by low Si/Al H-ZSM5 in the presence of a PPh3 additive, and other products observed were formic acid and CO_2. Different routes were proposed for the formation of the acid, through acetaldehyde (Eqs. 20-23) or ethanol mediated (Eqs. 24-27). Although the reaction mechanism was not completely unraveled, the first pathway appeared to be dominating, and the results suggested that the OH radical was playing an important role.

$$H_2O_2 \rightarrow 2OH* \quad (20)$$

$$C_2H_6 + 4OH* \rightarrow CH_3CHO + 3H_2O \quad (21)$$

$$CH_3CHO + \frac{1}{2}O_2 \rightarrow CH_3COOH \quad (22)$$

$$CH_3CHO + \frac{3}{2}O_2 \rightarrow 2HCOOH \quad (23)$$

$$C_2H_6 + OH* \rightarrow C_2H_5OH \quad (24)$$

$$C_2H_5OH + O_2 \rightarrow CH_3COOH + H_2O \quad (25)$$

$$CH_3* + OH* \rightarrow CH_3OH \quad (26)$$

$$CH_3OH + O_2 \rightarrow HCOOH + H_2O \quad (27)$$

That same year, Hutchings and co-workers presented results on direct ethane oxidation with H_2O_2 under milder conditions than those used by Rahman and in the absence of the PPh3 additive.[585] The catalyst employed was Fe- and Fe-Cu/ZSM-5, which they had already shown to be efficient for selective oxidation of methane to methanol under similar conditions. The reaction mechanism proposed for ethane is more complex than the methane one (see Scheme 17) on similar zeolite-based catalysts, but the role of Cu and Fe in both cases was related. Thus, H-ZSM-5 and Fe/ZSM-5 were more selective to acetic acid than Cu/ZSM-5, whereas the latter was more selective to the primary ethene and ethanol by reducing the extension of secondary oxidations, as observed for methane.[586]

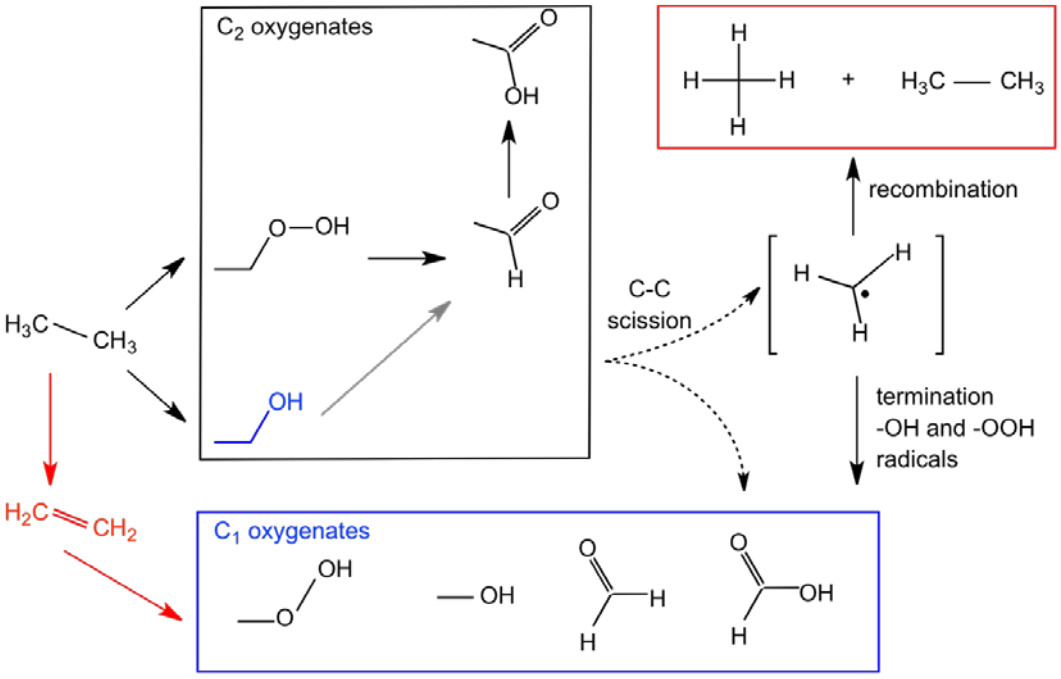

Scheme 17. Proposed reaction network for the oxidation of ethane using H_2O_2 over ZSM-5-based catalysts.

Extraframework iron species, including dimeric μ-oxo-hydroxo species, or iron species highly dispersed on the zeolite surface or located within the zeolite pores, were identified as the sites for activation of both, ethane and H_2O_2.[585] Further studies

suggested that surface Fe_xO_y may act as spectators and assigned the catalytic activity to the iron species located inside the zeolite channels.[587] Moreover, the selectivity to acids or alcohols on Fe/ZSM-5 could be controlled tuning the oxidation state and structure of the iron species by varying the pre-treatment conditions, with Fe^{II} leading to higher alcohol selectivity.[588]

Based on their experience on the capacity of metallo-zeolites for small alkane activation when used as catalysts for selective reduction of NO_x,[589] Armor and co-workers found that Co-exchanged beta zeolite was able to catalyze the direct ammoxidation of ethane to acetonitrile (see Eq. 28).[590] The acetonitrile formation rates observed were 1-2 orders of magnitude higher than those reported for metal oxide based catalysts in previous studies.

$$C_2H_6 + NH_3 + \frac{3}{2}O_2 \rightarrow CH_3CN + 3H_2O \qquad (28)$$

Regarding the influence of the zeolite structure, multidimensional medium and large pore zeolites such as ZSM-5, Nu-87 or beta, with proper ion-exchange capacity (Si/Al ratio) performed better than monodimensional structures such as mordenite or large pore topologies with cages such as that of Y zeolite.[591] Among different metals, cobalt was the most effective for ethane ammoxidation. In a further study, the same group proposed a reaction mechanism by which ethane was first converted to ethene by oxidative dehydrogenation and ethene would react with adsorbed NH_3 on isolated Co^{2+} sites, leading to adsorbed ethylamine (see Scheme 18). The nitrile would be obtained after a series of sequential dehydrogenation steps. The strength of the bond formed by the cation and the hydrocarbon species, ethylamine > acetonitrile > ammonia >> ethylene, was key for high activity and acetonitrile selectivity,[592] and the presence of

nanosized cobalt oxide particles was seen to favor the formation of CO_2.[593] Mhamdi et al. studied the influence of Co/ZSM-5 preparation conditions, of the Co/Al ratio and of cobalt precursors.[594,595] Co-MCM-49[596] and Mo-based catalysts[597] have also been described as active catalysts for the direct ammoxidation of ethane to acetonitrile.

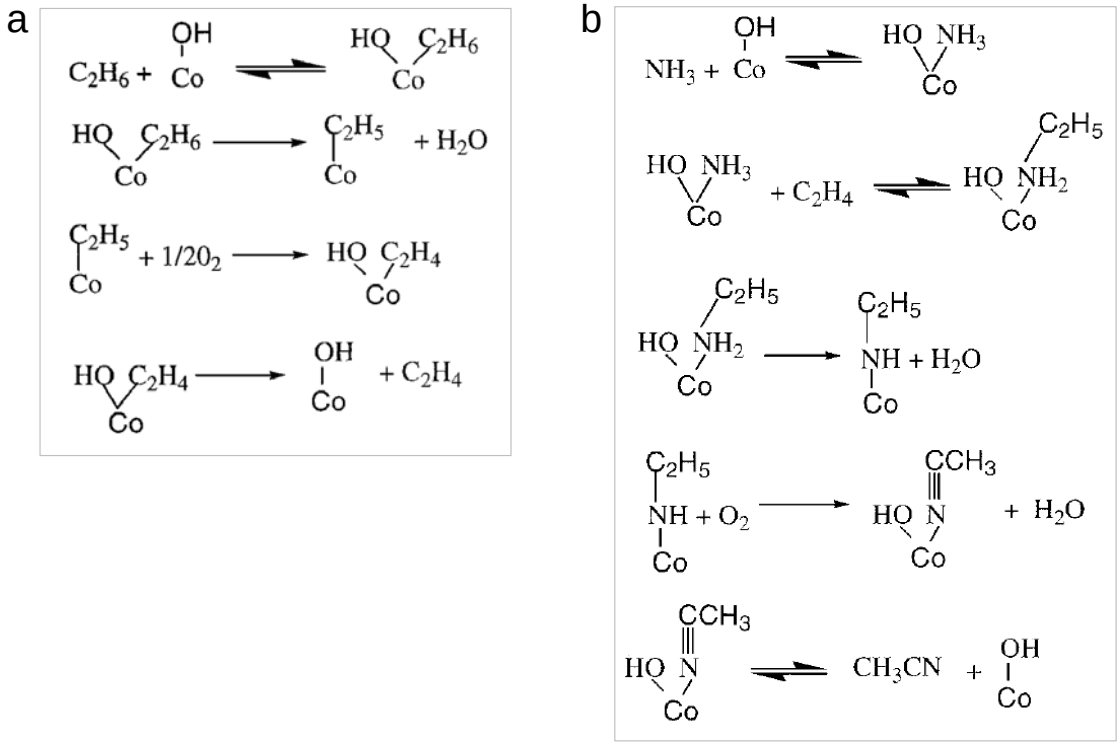

Scheme 18. Ethane activation (a) and acetonitrile formation pathway (b). Adapted from ref.[598] *with permission from Elsevier, copyright 1998.*

Wichterlova explored the activity of different Co-loaded zeolites for ethane and propane oxidative dehydrogenation and ammoxidation.[599] In good agreement with the results reported by Armor, cobalt exchanged beta and ZSM-5 were more active for alkane ammoxidation than mordenite or ferrierite. Ammoxidation of ethane produced ethylene, acetonitrile and CO_x. Acetonitrile was also formed when propane was reacted under ammoxidation conditions, due to the decomposition of acrylonitrile enhanced by the presence of NH3. Formation of propene was also observed.

Ga-modified ZSM-5 zeolites were studied by Derouane as catalysts for the ammoxidation of propane to acrylonitrile.[600] The results evidenced the synergy between the BAS and the Ga-species in these bifunctional catalysts, promoting the formation of C-N bonds when propane was converted in the presence of NH_3 and O_2. A new route was proposed for the activation of propane through the formation of a cyclic protonated pseudo-cyclopropane (PPCP) transition state (see Scheme 19). Ga/H-ZSM-5 was more selective than VSbyOx, a conventional mixed oxide catalyst, due to the reduced formation of carbon oxides on the former.[601]

In a different approach, Pérez-Ramírez et al. efficiently catalyzed the direct ammoxidation of propane by means of Fe-silicalite when combining N_2O and O_2 as oxidants. Under these conditions both, acetonitrile and acrylonitrile were obtained in yiels of 14% and 11%, respectively.[602]

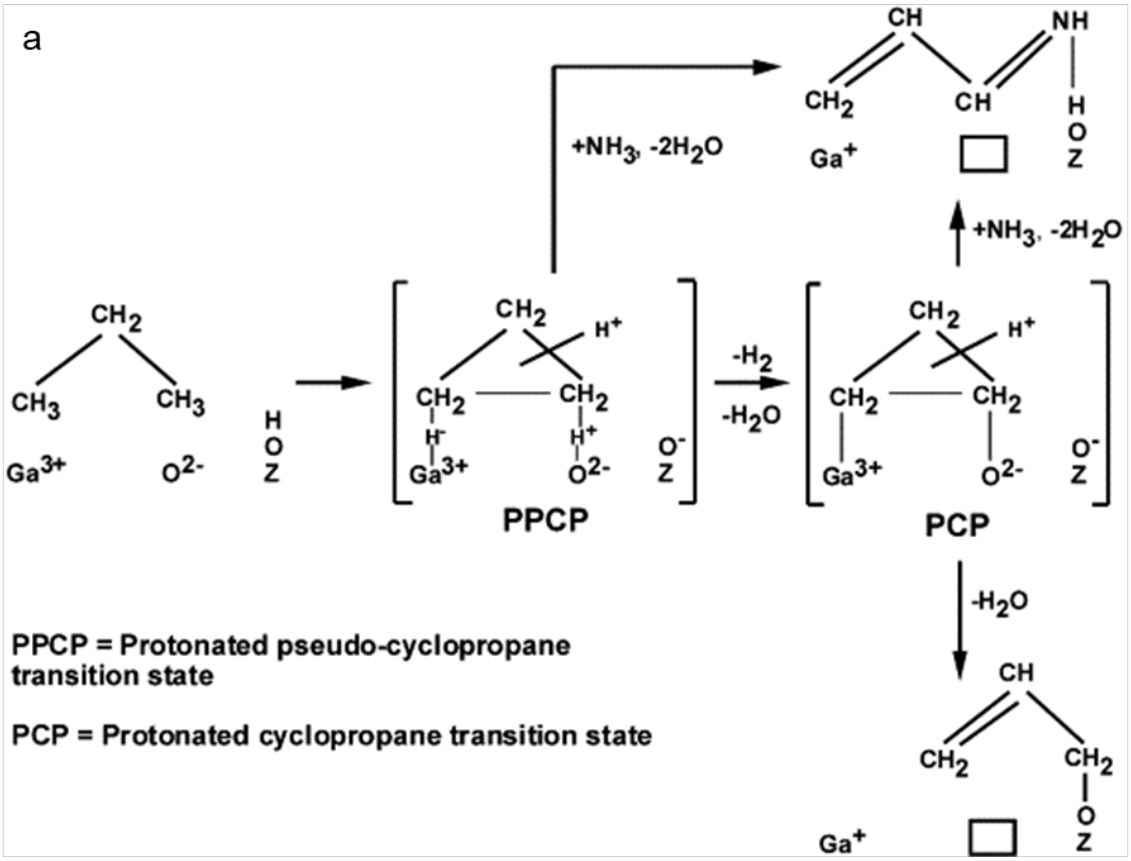

Scheme 19. Initial activation of propane in the presence of ammonia and oxygen (a) and overall mechanism for the propane ammoxidation (b) on Ga-modified H-ZSM-5 catalysts. Adapted from ref.[600] *with permission from Elsevier, copyright 2001.*

Bulanek et al. proposed extra-framework Fe ions generated by hydrolysis of framework Si-O-Fe bonds by means of hydrothermal treatments to be the active sites, and evidenced the detrimental effect of BAS on the final selectivity because of the capacity to decompose acrylonitrile.[603,604] The influence of Fe-silicalite pretreatment conditions was studied by the same group.[605,606]

Microporous crystalline materials have also been used for direct propane epoxidation with H_2 and O_2 in the presence of gold catalysts. Thus, a tandem process is performed in a dual-bed single reactor, where propane is first dehydrogenated to propene on an Au/TiO_2 catalyst located in the upper bed, and the olefin formed is selectively oxidized to the epoxide on an Au-loaded microporous Ti-silicalite, Au/Ti-S1, in the downstream lower bed.[607] The sequential propane dehydrogenation-propene epoxidation was made possible because Au/TiO_2 was found to be active for the alkane dehydrogenation at temperatures of 170 ºC that favor the epoxidation reaction. Propane conversion of 2% and selectivity to propylene oxide and propene of 8 and 57%, respectively, were reported, values that were maintained for 12 hours on stream.

5. C_{5+} ALKANE CONVERSION

In this review the higher alkanes are considered to be those with hydrocarbon chains containing at least five carbon atoms (C_{5+}). They can be found in oil distillate fractions, such as vacuum gas oil (VGO), light-cycle oil (LCO) and heavy or light-straight naphthas,[19,20] and are also present in processed streams, such as middle distillates and lube oils or Ficher-Tropsch derived waxes,[608,609] or alkane-rich fractions obtained by

processing of renewable sources,[93,610] such as bio-oils, vegetable oils,[610,611] or lignocellulose.[612,613]

This section focusses on the activation and conversion routes of C_{5+} alkanes into more valuable products by using microporous crystalline solid acid and bifunctional (metal + acid) catalysts. The reactions covered will be grouped in different sub-sections, e.g., alkane conversion by C-C bond cleavage, skeletal rearrangement, dehydrocyclization and selective oxidation. Nowadays, most of these reactions are the basis for well-known mature industrial technologies employing mono- or bifunctional zeolite-based catalysts. Regarding the zeolite structure, the zeolite pore openings, the cavity accessing windows and the channel intersections will play crucial shape selective effects,[95] and the reactivity and selectivity of the catalyst will be controlled by choosing an appropriate zeolite or zeotype pore topology. On the other hand, the accessibility to and from the active sites via the pore openings and internal channels of different sizes and shapes will be of special concern, since the alkanes considered in this section are longer and may suffer from transport limitations. Although the activation of C_{5+} paraffins will be similar to those described for shorter alkanes, they will be more reactive, and the knowledge of the chemistry behind the C-C or C-H bond activation as well as the kinetics and reactions mechanism involved in each process will be essential to design effective catalysts. Thus, as will be shown along the whole section, important efforts have been directed to improving the accessibility to the active sites of the zeolite based catalysts, and to improve selectivity by controlling the location of the active sites.

5.1. Monofunctional conversion of C_{5+} alkanes by C-C bond cleavage

5.1.1. Catalytic cracking

Long chain alkanes can be transformed into smaller hydrocarbons by C-C bond breaking (cracking), and zeolites are preferred as cracking catalyst because of their activity, shape selectivity and thermal and hydrothermal stability.[14] The main industrial use of zeolites as catalysts for the cracking of long-chain alkanes lies in the upgrading of low-value paraffinic refinery streams and of biomass-processed feedstocks. Heavy alkanes present in vacuum distillates and heavy atmospheric residual fractions are mainly converted by fluid catalytic cracking (FCC). Upgrading of refinery fractions such as straight-run distillates by direct cracking of complex paraffinic C_{5+} naphtha fractions is also carried out as an integrated process in the refinery. Depending on the demand of the final product and/or the availability and type of the feedstock, different zeolites are selected and operation conditions can be adapted. Thus, two main research lines will be described, the conversion of alkanes to maximize light olefins, to cover the increasing demand of propene, and transformation of heavy linear alkanes to smaller branched alkanes and aromatics, when the objective is to boost the octane number of the final blend product to be used as transportation fuel or to produce chemicals.[4,41,112]

During catalytic cracking of alkanes with zeolite catalysts, these can deactivate during use. The main cause of zeolite activity decay in cracking processes is the condensation of aromatic precursors into heavy carbonaceous species that block the access to the zeolite active sites located within the pores.[614] When processing industrial feedstocks, poisoning of the active sites resulting from the feed impurities (Ni, V, S) also adversely

affect catalyst activity and should be avoided. Moreover, the extreme conditions of the FCC process force the catalyst to have high physical and mechanical resistance. For this reason, the cracking catalyst combines different components in addition to the active zeolite, usually a stabilized form of Y zeolite within a matrix. Additives for specific functions may also be used such as, for instance, the medium pore ZSM-5 added as a propene boosting additive in the same or, preferentially, in different particles than those containing the faujasite.[15,19,20,112] Two excellent reviews on the catalytic cracking process and catalysts have been published recently by Vogt and Weckhuisen[112] and by Corma et al.[4]

In a commercial FCC unit, the temperature is high and the zeolite Y component is dealuminated to high Si/Al ratios, to increase hydrothermal stability and to favor cracking via the monomolecular protolytic mechanism. However, the process takes place at high conversions, which also involve hydride transfer and catalytic cracking following the bimolecular route[395,615], as described in Section 4.1, and confinement effects on the reactant alkanes or transition states within the different pores and cavities of the zeolite will affect the cracking selectivity by controlling the chain propagation steps.[395,616] Recent DFT calculations for the cracking of n-octane under industrial conditions related the larger contribution of monomolecular or bimolecular mechanisms in 10-ring ZSM-5 and 12-ring Y zeolites, respectively, with the better fitting of the corresponding transition states within their pore structure.[617]

The same routes as described for light alkanes (Section 4.1) are valid for the cracking mechanism of long chain alkanes over acid zeolites, and a number of elementary reactions will take place simultaneously as illustrated in Scheme 20a. The ease for

breaking the C-C bond is correlated with the length of the hydrocarbon chain,[393] and apparent cracking rates increase when increasing the alkane chain size, due to an increase of the adsorption enthalpy.[618,619] For light alkanes (C_3 to C_6) a compensating effect between high activation entropy and slightly decreasing adsorption enthalpy has been observed resulting in higher monomolecular cracking rates with increasing alkane chain number.[403] Moreover, different cracking mechanism depending on the number of C atoms of the alkane have been reported for 12-ring zeolites with different acid site density per unit cell.[620] Interestingly, it was found that when the cracking rate is calculated per bond susceptible to be cleaved, it increases with the carbon chain length for both, protolytic and beta-scission mechanisms.[621]. The kinetic findings led the authors to propose the cracking mechanism through a protonated cyclopropane (PCP) carbonium intermediate.

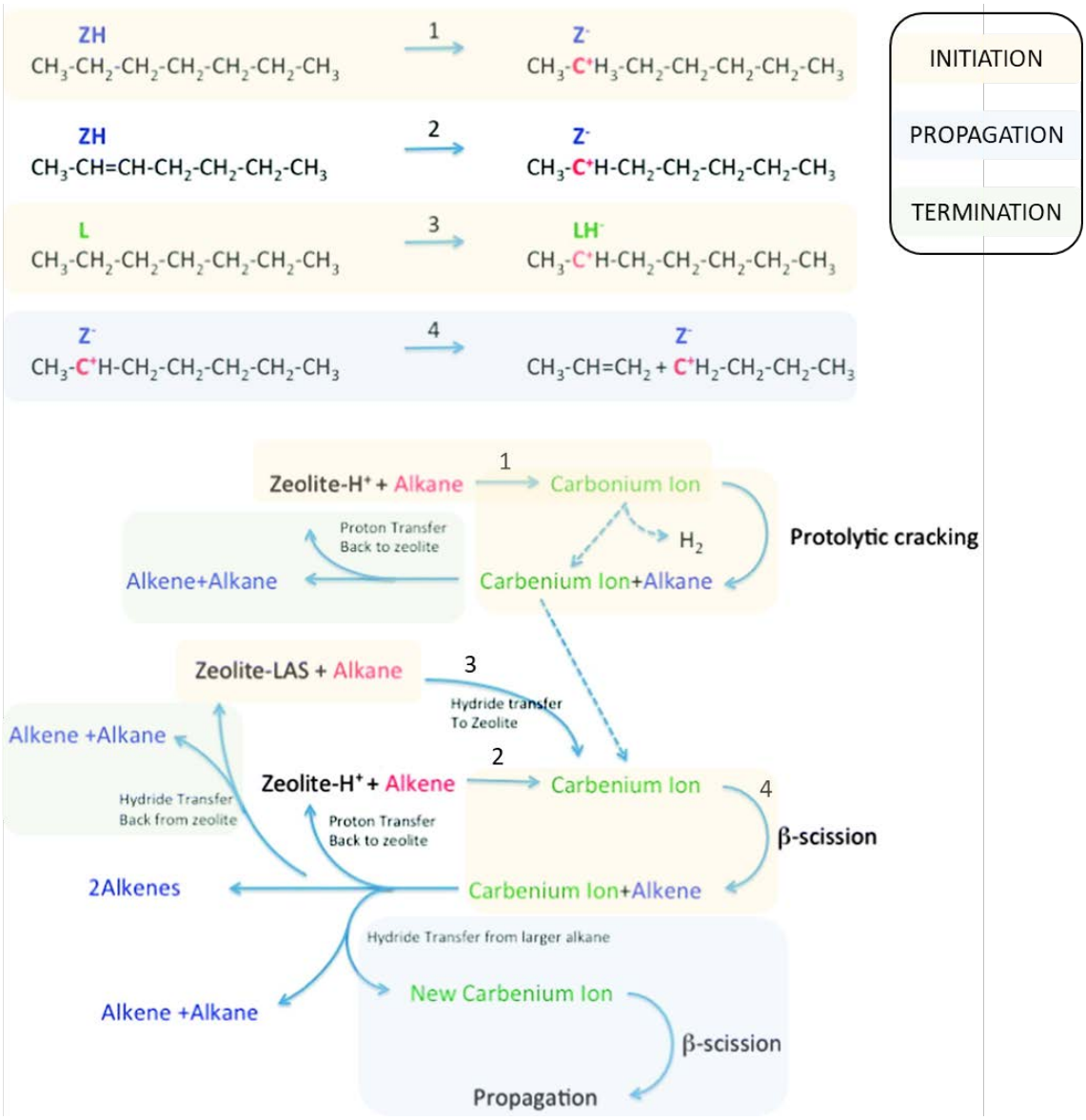

Scheme 20. Reaction network in zeolite catalyzed cracking of long-chain alkanes, including: (1) proton transfer from zeolite BAS to alkane to form a carbonium ion, (2) proton transfer from zeolite to alkene to form a carbenium ion, (3) hydride transfer from alkane to zeolite to form a carbenium ion and (4) beta-scission of a carbenium ion to form a new carbenium ion and alkene. Adapted from ref.[112] with permission from the Royal Society of Chemistry, copyright 2015.

Since its introduction as active FCC component in 1962,[622] zeolite Y in its dealuminated form, known as ultrastable Y-zeolite (USY), is mainly used as catalyst in the industrial FCC process. The 3-dimensional channel structure of this zeolite, with 12 Å cages

connected by openings up to 7-8 Å provides sufficient volume to efficiently catalyze the cracking of the long-chain alkanes present in the FCC pool and possible consecutive reactions. Zeolite Y with low acid site density (high Si/Al ratio) is preferred because of its higher hydrothermal stability and its reduced hydrogen transfer (HT) and coking activity, and is prepared by controlled dealumination by steaming alone or in combination of acid washing cycles. Steaming has an important effect in the alkane cracking reactivity, since it affects both the structure and the composition of the zeolite by creating mesoporosity and generating extra-framework aluminum species (EFAl), respectively.[623] EFAl may be present as condensed Al species or as dispersed low-weight type EFAl species, with stronger Lewis acidity and higher tendency to interact with BAS, leading to the generation of acid sites of enhanced strength or enhanced adsorption properties.[413,624–627] They may promote alkane hydride transfer to form carbeniums, or they can favor direct cracking due to interplay or efficient confinement when they are in close proximity to BAS.[404] The introduction of rare earth (RE) metals by ion exchange is another way to improve the stability of Y zeolites, as it reduces framework dealumination under severe hydrothermal conditions.[4,112] The reason for the enhanced stability lies on the RE migration, upon calcination, from crystallographic open positions in the supercages to sites ion-exchange sites within the soldadite cages and hexagonal prisms of the FAU framework,[622] where they bond with framework oxygen atoms and stabilize the zeolite structure. This will result in a catalyst with increased activity and hydrogen transfer capacity, leading to higher gasoline and lower light gases selectivity by reducing the extent of re-cracking events of the cracked intermediates.[628–630] Additionally, RE prevents deactivation by trapping V impurities. The declining availability and increased prices of RE has fostered the development of RE-free cracking catalyst

formulations.[4] They are, however, less active than RE-Y zeolite for alkane cracking and less resistant to poisons. Lercher and co-workers showed that the cooperative polarization of the alkane C-H bond by La^{+3} and the presence of LAS together with stable and strong BAS in La-exchanged USY zeolites results in an enhanced cracking rate of 2,2,4-trimethylpentane.[418] They proposed this was due to the presence of La^{+3} cations accessible to the reactant molecules in the Y zeolite supercages, as detected by solid state MAS NMR. The reaction mechanism for the iso-octane cracking is detailed in Scheme 21.

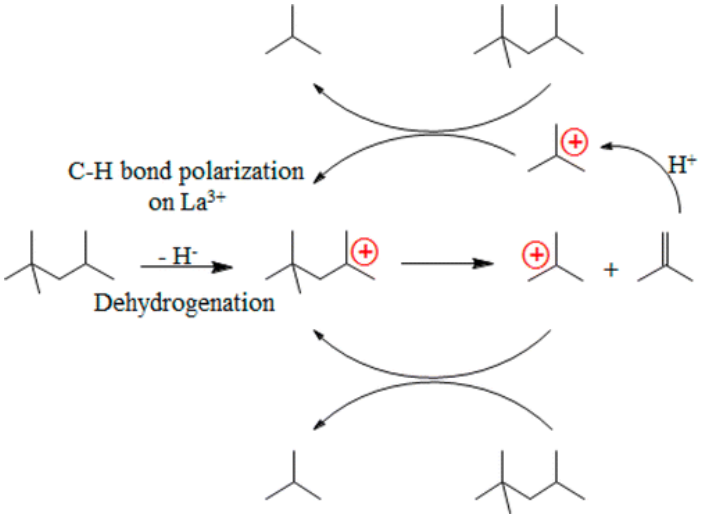

Scheme 21. Proposed reaction mechanism for the catalytic cracking of in-situ formed iso-octanes in the presence of accessible La^{+3} cations inside the Y zeolite supercages. Reprinted from ref.[418] with permission from the American Chemical Society, copyright 2014.

The medium pore ZSM-5 zeolite is added to the FCC catalyst to increase the final propene selectivity of the process.[4,15,19,20,112] Its structure, with smaller channel dimensions (5.1-5.6 Å) than the Y zeolite (7-8 Å) will limit the access to the pore system of large and/or branched alkanes with molecular diameters above 6 Å. Regarding the cracking mechanism, ZSM-5 contributes to increasing the protolytic to beta-scission

ratio. Rather than participating in the first alkane activation, the reactant confinement of lighter hydrocarbons fractions in the pores of ZSM-5 leads to preferential cracking of the gasoline-range olefins, formed from carbenium intermediates in the FCC pool, into smaller alkenes, mainly propene.[4] This is based on the higher cracking rates of olefins as compared to paraffins as detailed in Section 4.1.[631–633] Cracking of the gasoline range olefins also competes with paraffins' production via primary olefins hydrogenation and HT reactions on the main cracking catalyst, thus reducing the low-octane paraffinic content. However, bimolecular hydrogen transfer reactions with bulkier transition states are limited within the medium pore sized channel system in the ZSM-5 zeolite.

Modified ZSM-5 can also be used for the on-purpose selective production of light olefins (ethylene and propylene) by cracking of paraffinic C_6-C_8 naphtha or heavier feedstocks. This field has been thoroughly covered by several reviews in the last decade.[4,112,421] Incorporation of RE metals and increasing the Si/Al ratio of ZSM-5 decreases the yield to BTX aromatics and reduces the extent of consecutive reactions. The incorporation of phosphorous favors mono- versus bimolecular events, reducing hydride transfer capacity and enhancing propene selectivity,[96,424] and increases the hydrothermal stability of framework Al upon regerantion cycles. A recent study reported enhanced activity of BAS in MFI zeolites for pentane cracking and dehydrogenation caused by the presence of EFAL species, formed during steaming, in proximity to the BAS, which stabilized the transition state by increasing activation entropy.[634]

As mentioned, ZSM-5 is generally added to the FCC catalyst as a separate additive,[635] but the use of composite Y-ZSM-5 particles could be beneficial since it avoids the dilution effect of the additional binder. For instance, ZSM-5/Y zeolite composites obtained by

one-pot crystallization yielded more gasoline-range products than the mechanical mixture of the two zeolites when cracking heavy alkanes by favoring isomerization and aromatization reactions in the inter-crystalline space.[636] Taking into account that ZSM-5 will re-crack olefin intermediates formed in zeolite Y before being consumed in secondary reactions, such as oligomerization-cracking and HT to gasoline isoparaffins, that will also be favored in the large pore zeolite, the overall catalytic behavior may improve if both structures are intergrown together. Ghrib et al. showed that co-crystallized USY/ZSM-5 catalysts can be synthesized from kaolin and silica source through a two-step process. When used as catalyst for the cracking of VGO, the propylene yield and the quality of the gasoline fraction increased as compared to the catalyst prepared by physical mixtures of the two zeolites.[637]

Besides ZSM-5 and Y, other zeolite structures have been studied for catalytic cracking of high alkanes. The selection of the zeolite should be based, not only on its cracking activity, but also on its selectivity to specific products, including a low coke selectivity. In this line, the geometric disposition of the molecules within the zeolite pores and cavities and their interaction was seen to directly affect the adsorption and diffusion rates of reactants and targeted products,[638] greatly influencing the selectivity in cracking of long-chain alkanes, as predicted already in the 1980's by Chen and Garwood.[639] When comparing zeolites with different topologies for catalytic cracking of n-heptane,[640] the maximum propylene selectivity was obtained with three-directional 9- and 10-ring zeolites, whereas 11- and 12-ring catalysts yielded more branched gasoline-range products (Figure 31a). In particular, MCM-22 zeolite, composed of independent 12-ring supercages exposed as hemicages and accessible via 10-ring windows, showed lower

gasoline loss and higher light olefins selectivity than ZSM-5 at comparable Si/Al (15-30) when used as additives to USY VGO cracking catalyst.[641] This was ascribed to the reduced protolytic to beta-scission cracking ratio and to a higher contribution of the 10- versus 12-ring channels to the preferred mechanism due to a higher Al density in the former or because of preferential 12-ring cage dealumination.[642] The main drawback of MCM-22 was its high initial deactivation rate (see Figure 31b), induced by the coke (polyaromatics species) trapped in the MCM-22 supercages with 10-ring apertures.[643] In a different study, Ferrierite, was found to be active for the cracking of paraffinic naphtha fraction or heavy gasoil, but space demanding reactions such as hydrogen transfer and cyclizations were reduced as compared to ZSM-5, because of steric hindrance,[640,644] leading to lower propane and aromatics and higher olefin yields when tested alone for cracking n-hexane or mixed with ZSM-5 for cracking of gasoil.[645]

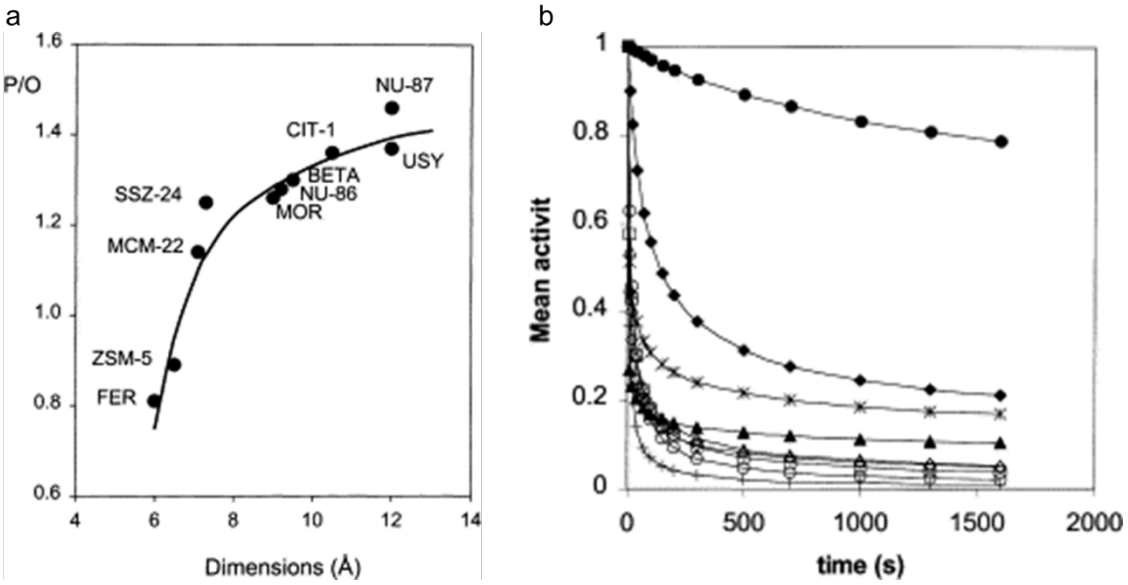

Figure 31. (a) Variation of the paraffin/olefin (P/O) ratio with void speace dimensions for 10 different zeolite structures; (b) Mean activity versus time on stream during n-heptane cracking for the different zeolites, coded: (+) Mordenite, (⧫) Beta, (◊) SSZ-24, (*) MCM-22, (□) CIT-1, (○) NU-87, (▵) NU-86, (•) ZSM-5, (▲) Ferrierite catalysts. Reprinted from ref.[640] with permission from Elsevier, copyright 1999.

A recent work comparing the n-hexane cracking performance on medium pore zeolites EU-1 zeolite, ZSM-5 and ZSM-48 illustrated the impact of side pockets in cracking selectivity.[646] In contrast to ZSM-5, with a 3D interconnected straight and sinusoidal 10-ring channel system, or to ZSM-48 with 1D 10-ring pores without cavities, the 1D 10 MR pores of EU-1 are periodically interrupted by wide 12-ring pockets (Figure 32a). Figure 32b shows that, at optimal Si/Al ratios of 150, the latter yields more propylene and lower BTX, as a result of the product shape selectivity induced by the confined channel system of the EU-1 topology, despite the creation of large intermediates or aromatic precursors in the large voids of the pockets, but this accumulation of aromatic coke precursors blocked the unidirectional pores and resulted in fast deactivation. The absence of extra void volumes in the 1D ZSM-48, in turn, results in transition shape selective properties preventing the formation of large hydrocarbons.

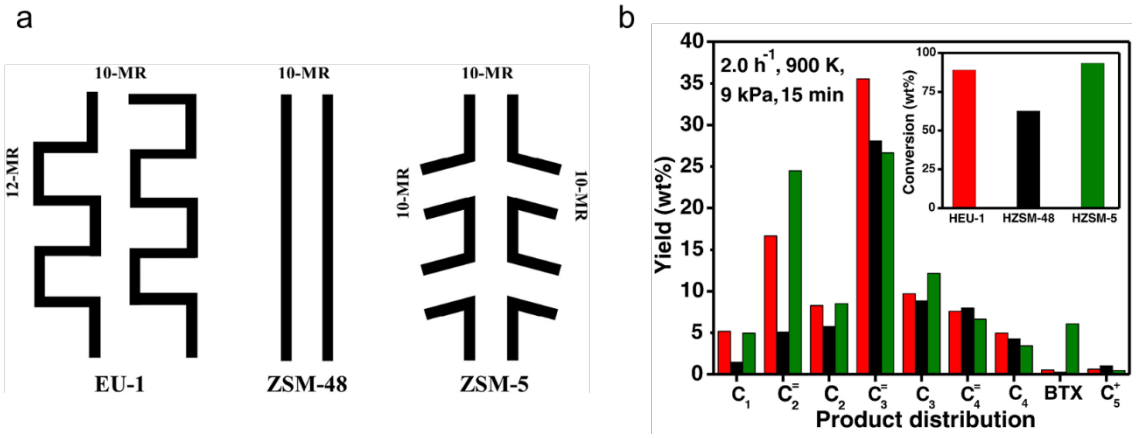

Figure 32. (a) Illustrations of the channel system and (b) Initial product yields and n-hexane conversion (inset) of EU-1, ZSM-48 and ZSM-5 medium pore zeolites. Reprinted from ref.[646] with permission from Elsevier, copyright 2016.

Other large pore zeolites have also been studied as cracking catalyst.[620,647] Among them, ITQ-21, with a 3D structure with linear 12-ring channels intersecting into large cavities comparable in size to the FAU supercages, but accessible through six 12-ring windows instead of four, showed higher cracking activity, more propene and lower gasoline olefinicity,[647] because of improved diffusion and accessibility to the active sites in the zeolite micropores. The same concept was applied to IM-5, a zeolite with medium-pore structure similar to ZSM-5 but with larger void spaces in the channel intersections.[648]

The large pore ITQ-7 zeolite, with a 3D channel system of 12-ring pores, less tortuous than those of the beta zeolite,[649] showed preference for the beta-scission versus protolytic cracking mechanism and limited HT activity when tested at high Si/Al ratios as additive for gasoil cracking, leading to high octane gasoline production with less aromatics and higher olefinity and branching as compared with beta zeolite.[650]

The combination of beta and mordenite with the medium pore ZSM-5 zeolite was seen to increase the conversion of a naphtha fraction to light products after P addition and hydrothermal treatment.[651]

Although the application of small pore zeolites is mostly restricted to gas separation and acid catalyzed processes, such as methanol-to-olefins or selective reduction of NOx[113], they have also been explored as possible cracking additives for selective production of light olefins. SSZ-33, with a small pore chabazite structure showed high hydrogen transfer activity and the product distribution was rich in aromatics and iso-paraffins with low propylene upgrade.[652] Moreover, the large internal cavities connected through narrow 8 MR apertures, limit the diffusion of bulky products out of the cages resulting in faster coking rates.

Finally, multipore zeolites presenting interconnected channels of different dimensions have also been proven as active catalyst for long alkane containing streams.[35] These structures may benefit from a special type of shape selectivity, known as molecular traffic control, which is observed when pores of different sizes favor the preferential diffusion of different reactant and/or products. Some of these multipore zeolites studied as cracking catalysts have been ITQ-39, with three-directional channel system with interconnected large 12-ring and medium 10-ring pores, which showed a good catalytic cracking behavior,[653] or MCM-68, with interconnected straight 12-ring and tortuous 10-ring channels and 18 x 12-ring supercages accessible only through the 10-ring pores,[654,655] which presented higher propylene selectivity than ZSM-5 with comparable Si/Al, aided by a selective propylene formation in the supercages, which showed limited access to bulky coke precursors. Another example of medium and large pore multiporous structure applied to cracking of chain alkanes is the aluminosilicate form of SSZ-57 synthesized by Zones et al,[656] less selective to cracking linear than branched alkanes as compared to ZSM-5.[657,658] In the case of ITQ-13, with a 3-directional structure composed of small 9- and medium 10-ring pores,[659] the small pores induced shape-selective properties providing high selectivity towards propene.

A very interesting case is that of ITQ-33, a germanosilicate with a structure formed by intersecting extra-large 18- and medium 10-ring pores.[46] The ITQ-33 structure maximized both diesel and propylene selectivity when combined with ZSM-5 as compared with USY/ZSM-5 catalyst (see Table 7), as the result of a preferential diffusion of diesel-range molecules through the 18-ring pores and cracking of the gasoline-range

hydrocarbons to light olefins in the medium 10-ring pores, shown in Figure 33a and Figure 33b, respectively.

Table 7. Catalytic cracking of Arabian light VGO at T=500 ºC and 60 s time on stream. Adapted from.[46]

Catalyst	Cat/oil	Conversion (%)	Yields (%)		
			Diesel	Gasoline	Propene
USY	0.62	92.5	15.7	40.4	4.7
USY	0.47	88.3	19.5	39.5	4.4
ITQ-33	0.70	89.2	22.6	34.5	4.2
Beta	0.70	84.0	14.1	32.3	7.5
USY + 20% ZSM-5	–	87.0	17.0	33.2	7.2
ITQ-33 + 20% ZSM-5	–	86.1	23.3	25.1	9.0

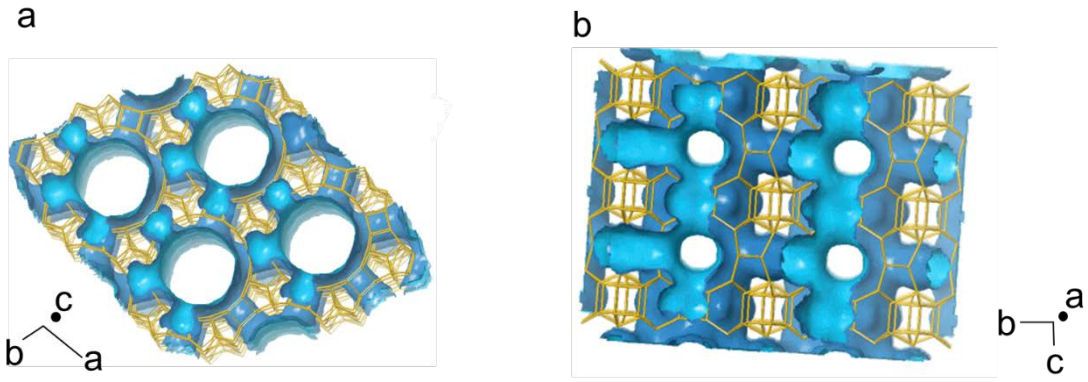

Figure 33. View of the ITQ-33 pore structure showing the 18-ring channel (a) and intersecting 10-ring channles (b) along [001] and [100], respectively. Structures taken from the IZA webpage.[37]

The different chemical composition of microporous silicoaluminophosphates (SAPOs) as compared to zeolites involves differences in their intrinsic acid properties that have implications in catalysis. Although the research of SAPOs-catalyzed cracking processes involving long-chain alkanes has been mainly directed to hydroconversion reactions, and will be revised in Section 5.2, SAPO-37, iso-structural to zeolite Y, was seen to be as active as a USY zeolite for gas oil cracking, but significantly less active in n-heptane cracking, as a consequence of the different acidities.[660] In these zeotypes, the Si distribution directly affects the acidity and cracking activity and, when used as catalyst for n-octane and n-decane cracking, an increased yield to light hydrocarbons was observed with increasing pretreatment temperature and Si content for SAPO-37, both factors leading to heterogeneous site distribution and formation of Si islands, as compared to samples containing isolated SiO_4 sites.[661,662]

Besides the zeolite structure and Si/Al ratio, the specific framework location of the Al atoms and, therefore, the location of the BAS in different geometrical environments may play an important role in the activity and the selectivity of zeolite-based cracking catalysts. Recent studies showed that according to DFT calculations[663], Al has no thermodynamic preference for a specific framework position in MFI. However, Al siting may be varied by means of the synthesis procedure employed. Tatsumi and co-workers observed selectivity differences for the cracking of 3-methylpentane among ZSM-5 zeolites synthesized with different organic structure directing agents (OSDA) and with or without Na ions.[664] The zeolite with higher proportion of Al atoms located in the channel intersections was more active and presented lower apparent activation energy and lower selectivity to monomolecular cracking products (methane + ethane +

hydrogen) because of the less restricted space for the transition state interaction with the active site. On the other hand, preferential location of Al within the straight and sinusoidal channels of ZSM-5 rather than at channel intersections resulted in lower coke selectivity for cracking of n-hexane.[665] The controlled location of Al in the 10-ring channels of a ZSM-5 zeolite was approached by Li et al. by synthesizing the zeolite as a boron-alumino-silicate.[663] Due to the preferential positioning of B at the channel intersections, the 10-ring pores were enriched in Al, and this had a direct effect on the product distribution observed for cracking of 1-hexene, with higher selectivity to propene, lower butenes/propene ratios, and on the catalyst lifetime when tested in the MTO reaction. The improved propene selectivity obtained for n-hexane cracking on MCM-68, a multipore zeolite with a 3D 12x10x10-ring structure, modified by dealumination, was suggested to be due to preferential dealumination of the 12-ring channels.[654]. In a similar way, the higher propene selectivity and lower coke formation observed on acid treated MCM-22,[666] was suggested to be related to the selective removal of Al sited within the MCM-22 supercages.

As mentioned in the introduction to this section, conversion of longer alkanes will involve increased diffusional problems within the micropores of the zeolites. Two main approaches have been proposed for increasing the accessibility of the zeolite active sites, reducing the zeolite crystal size or generation of mesoporosity by direct synthesis (bottom-up) or post-synthesis (top-down) procedures.[667] Early works by Corma and co-workers already evidenced the importance of crystal size and zeolite mesoporosity on the activity and selectivity of USY zeolite-based cracking catalysts. The improved USY zeolites were more active and selective to gasoline and diesel range products for the

cracking of heavy gasoil.[668,669] High activity and maximum selectivity to alkenes and i-butane were obtained when VGO cracking was catalyzed by nano-betas with average crystallite size of 400 nm.[670] Reducing the ZSM-5 crystallite size to the nanometer range also showed beneficial effects in terms of catalyst decay for cracking of VGO[671] and model alkanes.[672–675]

As mentioned earlier, the combination of hydrothermal treatment and acid leaching can be used for ultra-stabilization of Y zeolites and do generate some mesoporosity.[19] Combination of these treatments with basic desilication methods resulted in hierarchical USY zeolite catalysts with optimized BAS and reduced diffusion pathways in the zeolite crystals,[676] more selective to high quality diesel with low aromatic content, and olefin-enriched C3 and C4 gases, as compared to a conventional USY. Hierarchical zeolite crystals can also be created through synthesis by bottom-up approaches. In this line, mesostructured Y zeolite synthesized following a surfactant assisted procedure,[677] showed improved selectivity, yielding more fuels and less gases, bottoms and coke. ZSM-5 with intracrystalline mesoporosity, prepared following a similar approach presented higher overall cracking activity and higher LPG olefinicity. For further details on the advances in preparation and reactivity of hierarchical catalysts for catalytic cracking of heavy feedstocks we refer to a recent review.[678]

An alternative way to introduce mesopores within the microporous zeolite framework is the so-called pillaring process. Pillarization of the layered MCM 22 precursor led to the pillared structure MCM-36, presenting mesopores between the layers.[679,680] The accessibility benefit of such zeolite was demonstrated by its higher activity in the cracking of VGO as compared to the no-pillared MCM-22 counterpart.[101] Following a

similar preparation concept but working under milder conditions, Tsapatsis and co-workers succeed in preparing a MCM-36 zeolite with preserved crystallinity and higher BAS density, and more active and selective to the desired products when used for catalytic cracking of n-decane and VGO, as compared to a conventional MCM-36.[681]

An original approach proposed by the Corma group for increasing the accessibility of microporous crystalline materials is the preparation of zeolite single layers by post-synthesis delamination of layered zeolite precursors. In this way zeolites ITQ-2,[74,682] ITQ-6,[77,683] ITQ-18,[104] and ITQ-20[684] were prepared. The resultant zeolitic materials showed very high accessible surface areas and interesting catalytic properties for a large number of acid catalyzed reactions.[19] The benefits of ITQ-2 as compared to its microporous MCM-22 counterpart or to the pillared zeolite MCM-36, were also demonstrated for the catalytic cracking of a VGO,[101] with the delaminated zeolite being more selective to liquid products and formed less gases.

5.1.2. Steam assisted catalytic cracking

Alkane C-C bond breaking can also be achieved thermally through a radical cracking process. Thermal cracking should maximize olefins and has been used for the conversion of alkane containing naphtha fractions to propene and specially to ethene.[685] Based on that, steam catalytic cracking (SCC) has been developed to crack naphtha in the presence of steam in a dedicated small unit at higher temperatures and shorter contact times than FCC, but lower temperatures than thermal cracking. The higher reaction temperatures used in SCC as compared to FCC affects the propene-to-ethene ratio in the products, which is lower for SCC, although the total yield of propene and olefins is

larger than in conventional catalytic cracking. The extreme conditions for SCC require hydrothermally stable catalysts with strong acidity, since severe dealumination will cause rapid loss of catalytic activity. Corma and co-workers thoroughly studied the impact of the Si/Al ratio variation (15-40) in ZSM-5-based catalysts, its stabilization by P addition, and developed kinetic models to quantify the effects of steam on activity, selectivity and catalyst decay for the cracking of C_5-C_{12} alkanes at 700 ºC.[686,687] The presence of steam caused irreversible dealumination and reversible deactivation by interaction of water molecules with zeolite weak active sites, decreasing the apparent activation energy. It adversely affected the protolytic cracking activity when converting n-heptane, but also reduced re-cracking events, thus lowering the formation of hydrogen, methane and coke precursors. Severe dealumination resulted in similar final Si/Al ratios regardless of the initial zeolite composition and, therefore, in a negligible influence of the initial Si/Al ratio on activity and selectivity under SCC conditions. The rapid deactivation by dealumination was reduced by P incorporation and optimal cracking activity were found for P-containing zeolites, while maintaining high ethylene and propylene selectivity, thanks to to stabilization of the ZSM-5 framework while reducing its acidity.[424] They also observed lower iso-butane and aromatics but higher butene yields for the P-containing zeolites, indicators of a lower contribution of the bimolecular beta-scission and HT reactions. The isomorphic substitution of B in framework positions of ZSM-5 was recently shown to benefit the catalytic behavior of the zeolite for steam cracking of heavy naphtha (C_{12}) to a high octane gasoline blend, a fact that has been related to the creation of acidic silanol species.[688]

A comparative study of IM-5 and ZSM-5 zeolites with similar Si/Al ratios (ca. 15) in the SCC of n-heptane, a model compound representative of naphtha,[689] showed higher catalytic activity of IM5 (lower apparent activation energy and heat of adsorption) and comparable propene yields. The peculiar structure of IM-5, with smaller pore dimensions than ZSM-5, in combination with its strong acidity, favors re-cracking reactions and increases ethene selectivity. However, the large voids in the channel intersections favor hydrogen transfer reactions leading to more iso-alkanes and BTX products. The similar propene yields obtained for both zeolites and the lower i-butene/i-butane ratio for IM-5 indicate that dimerization-cyclization and HT reactions involved mainly butenes. As with ZSM-5, P addition to IM-5 largely improved its hydrothermal stability.

Large pore zeolites have also been studied as catalysts for SCC. Thus, Masuda and co-workers reported an increased stability of beta zeolites after triphenyl silane treatment, for the conversion of heavy oil to lighter hydrocarbons in the presence of steam at temperatures of 470 ºC and atmospheric pressure.[690,691] More recently, Shirvani and Ghashghaee demonstrated the benefits of steam addition for improving light olefins production in the catalytic conversion of fuel oil over USY zeolite.[692] The same group extended the studies to novel acid composite nanoporous catalysts with multiple active phases (MEL, MFI, CHA and AlPO) and supported their results with a kinetic model.[693]

5.2. Bifunctional conversion of C_{5+} alkanes by C-C bond rearrangement and cleavage

C_{5+} alkane containing streams can be converted by hydrogen-mediated processes over bifunctional metal loaded zeolites.[19,25,111] Operation in hydrogen atmosphere has direct implications on the activation process and the nature of the catalyst. As detailed in previous sections, the metallic function provides the hydrogenating/dehydrogenating activity to form the primary olefins and to desorb the final products whereas the zeolite catalyzes the C-C rearrangements and C-C cracking on the acid sites. The metal component for long alkane hydroconversion is usually Pt, Pd or their bimetallic combinations. Both noble metals belong to the same group and possess similar hydrogenating and redox properties. Combinations of Ni, Mo, W and Co are also interesting due to their high thio-resistance and lower cost, but show lower hydrogenating activity.

Regarding the reaction mechanism, the same reaction steps as those explained for light alkane hydroisomerization prevail for large paraffins conversion (see Section 4.2). Still, in the case of longer alkanes, the carbenium ions may be converted on the BAS by cracking and isomerization. In the case of feeding a linear alkane, the cracking would involve highly disfavored beta-scissions from a secondary to primary carbocation,[694] so n-alkanes would readily isomerize to a monobranched iso-alkylcarbenium. These monobranched isomers can undergo secondary isomerization to form di- and tri-branched alkyl-carbeniums, which can either desorb from the acid sites as branched alkenes or undergo C-C bond cleavage to shorter carbeniums on the acid sites and eventually desorb as shorter iso-alkenes. In a final step the olefins will diffuse to the

metal side where they will be hydrogenated to the corresponding iso-paraffins or lighter alkanes. If the distances between the acid and the metal site are too large, the intermediate alkenes formed may suffer undesired consecutive reactions leading to gas and to coke.

Choi and co-workers observed different selectivity to iso-dodecane when comparing two Pt/SAPO-11 catalysts with the BAS preferentially located either at the external surface of within the microporous channels.[695] The latter showed substantially higher selectivity to iso-dodecane, which was attributed to a promotion of consecutive cracking reactions on the external acid sites of the former.

The activity of the bifunctional catalyst is the highest when the acid-catalyzed steps of isomerization and beta-scission are rate controlling.[25,694,696] Two conditions are required for enabling this kinetic control, an optimum ratio between acid and metallic sites, such that the metal function is high enough for not limiting the steady-state concentration of intermediate alkenes in the micropores, [697] and a transport of reactants between the two sites faster than the chemical reaction.[698,699] Thus, in a first approximation, one may think that the hydroconversion of long chain alkanes will depend on the distance between the two functions,[111] as mentioned before. Regarding the influence of the composition of bifunctional hydroconversion catalyst, the effect of the hydrogenating (Pt)/acid(A) balance for n-decane conversion on Pt/Y catalyst, depicted in Figure 34, may serve as an explanatory example. Catalysts with a low degree of hydrogenation activity and a high degree of acidity (Figure 34a) are the best suited for maximizing hydrocracking versus hydroisomerization, since the high number of BAS pushes successive re-arrangements and further cracking of the alkene intermediates before

they are hydrogenated on the metal site. On the other hand, when the hydrogenation activity becomes higher (Figure 34b), the alkene intermediates will not be re-arranged in time, so cracking will be limited and isomerization will be favored. Regarding the distance between the two active sites, it is generally accepted that if they are in close proximity cracking activity is increased, whilst if the distance is too long the synergetic effects between the two acid sites is suppressed. This is the basis for the intimacy criterion proposed by Weisz, according to which when the distance between acid and metal sites exceeds a certain value, activity of the catalyst starts to decreases.[700] However, this criterion may not apply for all cases, as evidenced by Zecevic et al. when studying bifunctional catalysts for the conversion of large alkanes.[701] The catalysts were intimate mixtures of zeolite Y and an alumina binder, where the Pt metal was added either to the zeolite or to the binder. Characterization of the catalysts at the nanoscale and correlation with their activity and selectivity demonstrated that in the case of large hydrocarbons the best results were obtained when the metal was deposited on the binder, and not on the zeolite. When the large alkene molecules are formed on the Pt/binder, they will diffuse to the zeolite surface and react on the most accessible zeolite BAS, close to the pore mouths, following a "pore-mouth" type of catalysis, similar to the one described by Martens[702] for isomerization of long alkanes, and will diffuse back to the metal sites. In this way, the need for diffusing through the zeolite pores is avoided and the possibility of undesired acid-catalyzed reactions, such as recracking, is reduced. The concept was extended to lighter alkanes such as n-C_7 when converted on one-dimensional ZMS-22 (10-ring) and mordenite (12-ring) zeolites.[703] For more details on the effect of the metal-acid balance and the impact of the metal function on the n-alkane hydroconversion we refer to a recent thorough review.[111]

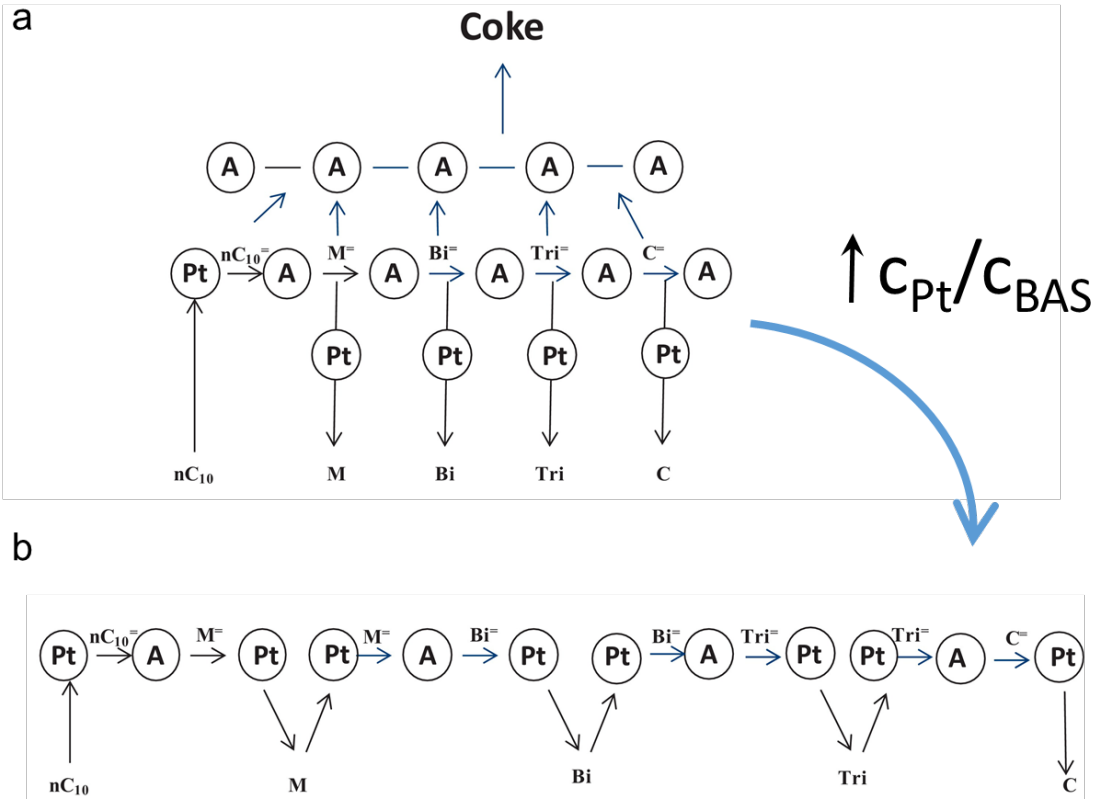

Figure 34. Hydroconversion of n-decane over a bifunctional catalyst with (a) low (< 0.03) and (b) high (> 0.17) value of the hydrogenating/acid balance, respectively. Adapted from ref.[696] *with permission from Elsevier, copyright 2013.*

Hydrocracking of long-chain n-alkanes is always consecutive to the skeletal isomerization.[704] This implies that at medium to high conversions, hydroisomerization is accompanied by hydrocracking limiting the production of isomers. Furthermore, the rate of isomerization of long-chain linear alkanes is thermodynamically controlled and decreases with increasing temperature. The isomerization via alkyl and hydride chain positional shifts has been reported to be much faster than isomerization via the formation of protonated cyclopropane (PCP),[705] so when alkanes are hydroconverted by bifunctional catalysts with no shape selectivity, positional isomers distribution obeys the thermodynamic equilibrium.

Cracking is faster for multi- than mono- or di-branched alkanes, and this allows controlling the hydrocracking/hydroisomerization ratio by suppressing the formation of multibranched isomers. The distribution of hydrocracked products can be controlled by using zeolites with confined pore structures that impose shape selective effects, as trimethyl carbeniums are usually rearranged in a way that the methyl groups are located at the center of the chain, yielding a narrow distribution of hydrocracked products with maximum selectivity at middle carbon numbers of the alkane feed. Steric considerations imply that as the pore size becomes smaller, the formation of bulky tribranched iso-carbeniums is reduced. Additionally, if one considers a feedstock of mixed iso and n-alkanes, linear alkanes will be selectively cracked in medium pore zeolites as compared to branched alkanes due to reactant shape selectivity. This concept was the bases for the development of the constraint index (CI).[657]

Maesen and co-workers carried out detailed kinetic studies and thermodynamic analysis by molecular simulation of the formation of different alkylcarbenium intermediates involved in long n-alkane hydroconversion within different zeolites and related this to shape selectivity effects.[95] The zeolites compared were a large pore 12-ring FAU structure and three medium pore 10-ring zeolites, i.e. the three-dimensional MFI and ZSM-11 MEL, with intersecting channels in zig-zag or linear disposition, and the uni-directional TON structure. Figure 35a shows the numbers for the Gibbs free-energy of formation of mono-, di- or tri-branched intermediates from n-decane. It is clear that the formation of bi- and specially tri-branched intermediates involve high energy penalty and is highly disfavored for medium pore zeolites, whereas little thermodynamic impediment is observed for the formation of any multi-branched iso-alkane in large pore

Y. Regarding the two 10-ring zeolites, the free-energy contributions of MFI and MEL are similar for most of branched alkanes, but they differ in some specific alkyl intermediates. Since specific cracking precursors are formed over each zeolite, different cracked products will be produced, caused by the distinct channel connectivity and shape (Figure 35b). The small and unidirectional pores of the TON structure prohibit the formation of di and tri-branched n-decane isomers, thus preventing the cracking activity. In fact, this confers 10-ring one-directional structures, such as ZSM-22 or SAPO-11, the ability to perform selective skeletal isomerization at the chain ends of the alkane feed. This concept, which is key for the production of diesel or lube oils with premium cold flow properties, has been extensively explored by researchers from Chevron[706,707] and the group of Martens and co-workers and will be described later in more detail. Before that, other relevant works dealing with the thermodynamic and diffusion implications on the hydroconversion performance of zeotypes with particular structures will be introduced.

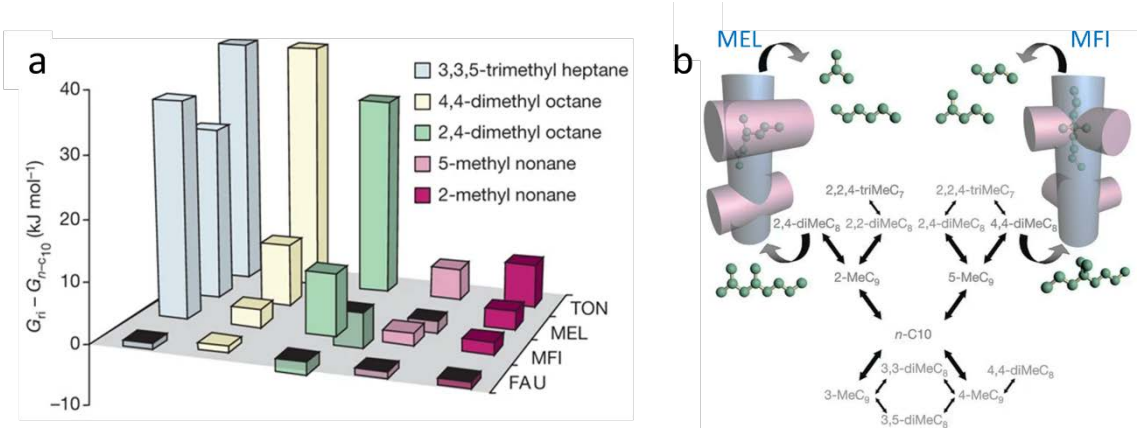

Figure 35. (a) Variation of the free energy of formation of five n-decane hydroconversion key intermediates relative to that of n-decane for FAU, MFI, MEL and TON zeolite structures; (b) Hydroconversion mechanism for n-decane within the different topology of MFI and MEL zeolite structures. Adapted from ref.[95] *with permission from Springer Nature Customer Service Centre GmbH: Springer Nature Nature, copyright 2008.*

Following a molecular perspective, Tsapatsis and co-workers[708] developed advanced theoretical simulations and computational screening on adsorption of linear and branched alkanes with 18 to 30 carbon atoms over a vast number of zeolite related structures, including those in the IZA-SC (International Zeolite Association Structure Commission database) and in PCOD (Predicted Crystallography Open Database). Adsorption results at the theoretical infinite dilution, i.e. at alkane partial pressures close to 0 MPa, showed that pore channels with smaller free diameter would be advantageous for isomerizing C_{18} alkanes because of the more favorable adsorption enthalpy, improved kinetic constants and stronger affinity. They also defined pore bumpiness (Δd) as the difference between the diameter of the largest sphere that can be included along the channel and the molecule free diameter, which can be considered an indirect measurement of confinement, and related it to the linear/branching selectivity ratio. The conclusion was that the lower the Δd of the support, the higher selectivity to branched alkanes. The calculation outcomes led the authors to conclude that one-dimensional channel structures were the ones that behave best for hydroisomerization. Interestingly, similar conclusions were lately obtained from experimental hydroisomerization results of a C_{10}-C_{13} n-alkane mixture over six Pt-containing bifunctional catalyst with 10-MR (MFI, TON, MTT) and 12-MR (BEA, MOR, MTW) one- and tri-directional pore zeolites by Zschiesche et al.[709]

Theoretical studies by Maesen et al. [710–713] focused on zeolite cage effects on the conversion of long-chain alkanes, correlated the simulated Gibbs free energy of adsorption of n-pentacosane (C_{25}) with the pore diameter of a number of zeolite structures.[710] Summarizing their results, Figure 36a shows that there is a switch of the

Van der Waals interactions from predominantly repulsive (leading to ΔG_{ads} n-C_{25} > 0 circles) to predominantly attractive (ΔG_{ads} n-C_{25} < 0 squares) for pore diameters around 0.48 nm, dimensions that are characteristic of MTT-type zeolites (1D 10-ring structure). Secondly, they showed that among the zeolites showing effective interactions with the fed n-alkane, those containing cages (ERI, AFX, FER) led to a particular type of reactant shape selectivity by which short-chain n-alkanes were preferentially hydroconverted versus longer alkanes. This arised from the restricted access of the larger molecules through the narrow window openings and the higher thermodynamic penalty (repulsive interactions that increase the Gibbs free energy of adsorption) imposed by alkanes with too long sizes to fit in a narrow cage. Adsorption molecular simulations on n-C_{13}, presented in Figure 36b, showed that, under a Henry kinetic regime, the ERI-type zeolites (3D 8-rings and 0.704 nm cages) requires n-alkane pressure higher than AFX (3D 8-rings and 0.776 nm cages) and significantly higher than FER zeolites (2D 10x8-rings and 0.631 nm cages) before they become saturated, indicating a strong resistance for the former zeolites to fit the long n-alkane inside the cages. Figure 36c schematically shows how the long n-alkanes (molecules depicted at the right) have to squeeze through the narrow ERI or AFX windows, whereas the FER pores (0.48 x 0.54 nm) are wide enough to well fit the n-alkanes and do not exert repulsive interactions. In addition to guest (long-chain alkane) – host (zeolite surface) interactions, the interplay among intermediates and products can affect the Gibbs free energy of adsorption.[711–713]

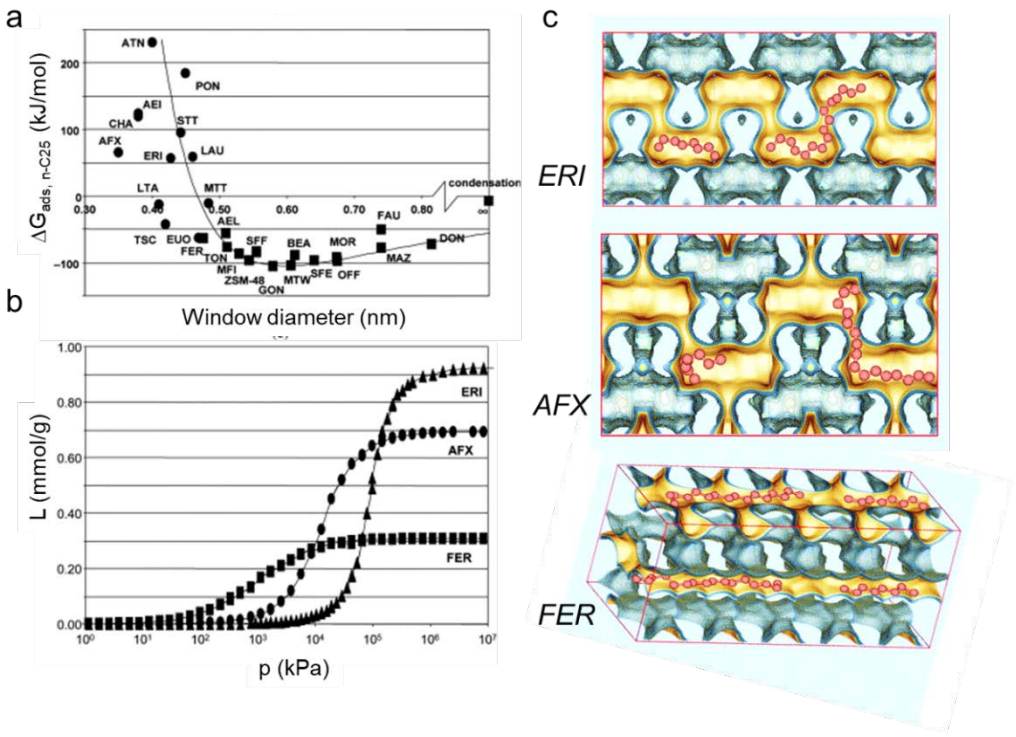

Figure 36. (a) Variation of the Gibbs free energy of adsorption of n-pentacosane at 605K as a function of the zeolite window size; (b) n-C_{13} adsorption isotherms at 670K and (c) selected n-alkanes adsorbed on ERI, AFX and FER structures. Adapted from ref.[710] *with permission from Elsevier, copyright 2006.*

Summarizing, in the hydroconversion of high alkanes, hydroisomerization reactions will never completely equilibrate since they compete with consecutive hydrocracking that will break down the isomers. The higher the competitive adsorption at the acid sites, the shorter the residence time of the alkene intermediates near the active sites, which will then be more likely to desorb as a branched isomer rather than to crack. The equilibrium between isomerization and cracking can be thermodynamically controlled by the pore structure (diffusion and shape selectivity) and composition (desorption and cracking ability) of the zeolite function. These later aspects can be tuned by direct synthesis or by post-synthesis modifications as will be described below for specific cases.

Finally, reactions conditions will also influence the hydrocracking/hydroisomerization ratio, since the former is endothermic and promoted at higher temperatures whilst the latter is thermodynamically controlled and favored at lower temperatures.[20]

After this revision of the main common features for alkane hydroconversion, such as their reaction mechanisms and the influence of the alkane length and the catalytic properties on the hydrocracking to hydroisomerization ratio, three main hydroconversion processes of alkanes will be described in the next sections, which are commercially employed for upgrading paraffinic streams. These are the isomerization of light straight run naphtha for octane increase, isodewaxing of long-chain alkane fractions (waxes) for improving cold properties of fuels and lube oils, and hydrocracking of heavy fractions to liquid fuels. We will focus on analyzing the correlation of zeolite structural and physico-chemical properties with their catalytic behavior in the different cases. For a deeper insight into the different technologies industrially available, the interested reader is referred to previous reviews.[19,20]

5.2.1. Isomerization of C_5-C_7 alkanes

Among the hydroconversion reactions of long n-alkanes over zeolite-based bifunctional catalysts, the most favored cracking of tri- or di-alkyl-carbenium intermediates require at least C_8 and C_7 n-alkanes, respectively.[25] The transformation of n-alkanes with 5 to 6 carbon numbers involve very slow or forbidden cracking modes, so they are much less susceptible to crack. This implies that they can be more selectively isomerized into iso-pentanes and mono- or di-branched hexanes, and this is the basis of the upgrading of the light straight run (LSR) gasoline, which is mainly composed by n-pentane and n-

hexane mixed with small proportions of n-heptane and naphthenes. The direct use of the LSR fraction as gasoline blend results in low average octane numbers (55-75), but when the linear alkanes are isomerized to the corresponding branched paraffins, particularly to di-methyl butanes, the octane number is greatly increased (>80),[714] as can be deduced from Figure 37a. The direct and selective isomerization of LSR alkanes through carbocation intermediates is challenging because of the low reactivity of the paraffins and the presence of competing reactions, such as cracking. The reaction is thermodynamically limited, and the rate of isomerization increases with decreasing temperature. Figure 37b shows how zeolite-based bifunctional catalysts benefits the process by pushing the equilibrium towards branched isomers after n-alkane activation when working at the lowest temperatures possible. Zeolites also show lower catalyst decay associated with presence of poisons such as sulphur and water in the mother stream and they are easy to regenerate. Considering integrated processes, the octane rate can be further increased by recycling the unconverted n-paraffins after separation of the branched products by means of a molecular sieve, such as zeolite LTA,[20] or by using ZSM-5 zeolite membranes.[715]

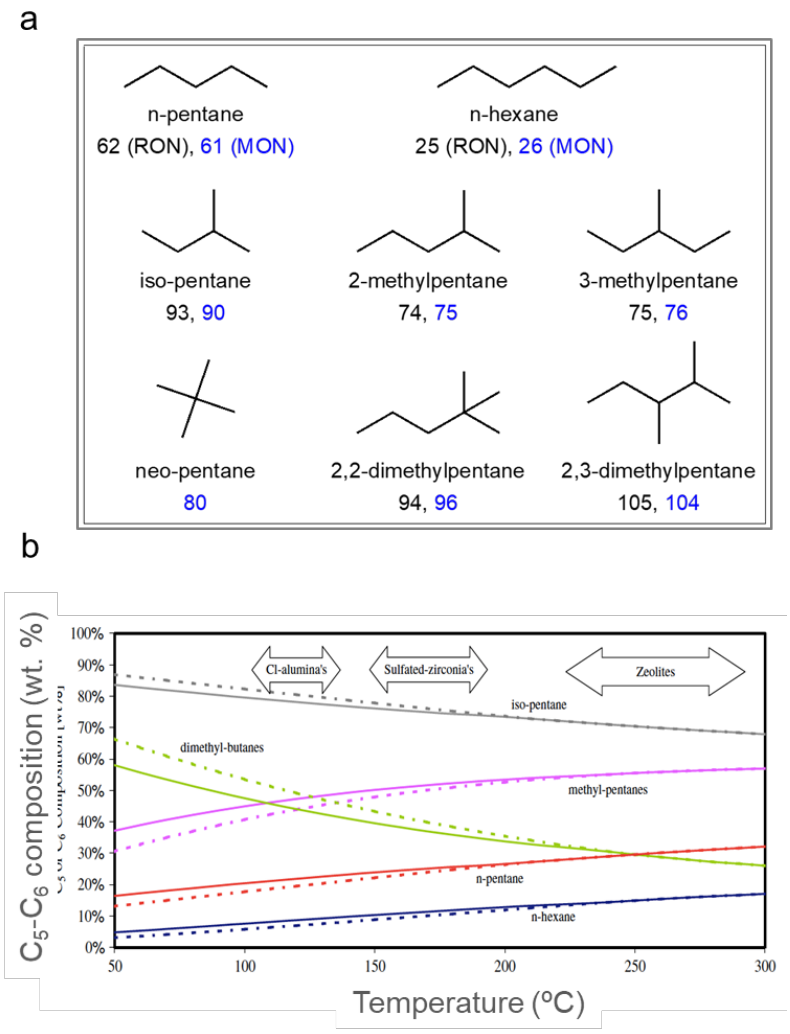

Figure 37. (a) Structure and research (RON) and motor (MON) octane numbers of the pentane and hexane skeletal isomers; (b) Thermodynamic equilibrium of pentanes and hexanes and temperature range of typical utilization of LSR isomerization catalysts including chlorinated, sulfated and mordenite-type zeolite. Solid and dashed lines represent liquid and gas phase equilibrium, respectively. Reprinted from ref.[20] with permission from Springer Nature Customer Service Centre GmbH: Springer Nature Topics in Catalysis, copyright 2009.

The zeolite-based catalyst of choice to perform n-C_5-C_6 hydroisomerization is the partly dealuminated large pore mordenite (MOR) containing Pt as the hydrogenating-dehydrogenating component.[19,20] The one-directional pores of the mordenite impose diffusion restrictions for the heavy alkane containing fractions, but selectively convert

the paraffinic light gasoline. [716] However, because of its lower acidity as compared with chlorinated or fluorinated alumina isomerization catalysts, mordenite based catalysts usually work at higher reaction temperatures (ca. 250ºC) (Figure 37b). An increased stabilization of the transition state for isomerization in the acid sites is then essential to isomerize LSR stream at lower temperatures. Thus, optimization of the composition, the distribution of active sites, the crystallite size and pore geometry of the microporous component would be necessary for improving the hydroisomerization activity.[703,717] This was the basis for a commercial light naphtha hydroisomerization process based on a Pt loaded modified mordenite catalyst, HYSOPAR®, and the CKS ISOM process, jointly developed by CEPSA, KBR and Süd-Chemie[718].

Besides the framework Si/Al ratio, EFAl species can influence the zeolite isomerization activity by means of a synergetic effect with the BAS, resulting in higher acid strength and increased isomerization activity.[624] On the other hand, Iglesia and co-workers investigated the consequences of acid strength, described by the deprotonation energy of microporous zeolites such as the tri-dimensional beta, on n-hexane isomerization, and showed that isomerization rate constants decreased exponentially with increasing deprotonation energies, which led them to conclude that acid strength primarily affects activation barriers.[719] By measuring energies for intermediates and transition states, they observed a higher (electrostatic) stabilization of the transition states for catalysts with weaker acid sites.

Regarding the isomerization mechanism, it is generally accepted that n-hexane isomerization proceeds via a protonated cyclopropyl (PCP) intermediate formation at the BAS, which will evolve into the most stable carbocation,[719,720] as illustrated in step 3

of the five reaction path mechanism presented in Figure 38a. The energy diagram (Figure 38b) shows that the transition state carbocation (B) from the skeletal rearrangement of the linear secondary carbenium ion (A) to the monobranched methyl-C_5 carbenium (C) consists of a PCP and the process occurs by C-C and C-H bond cleavage and formation.

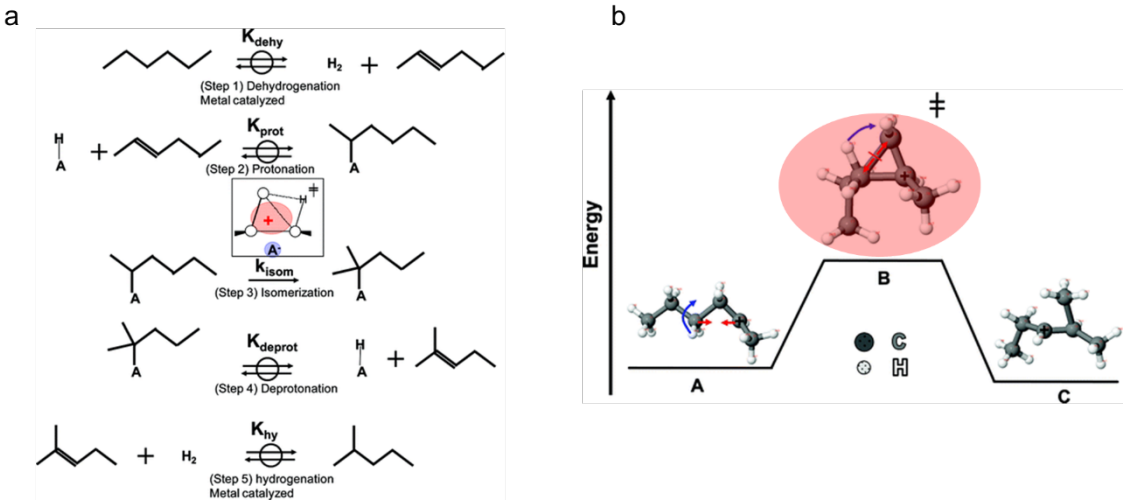

Figure 38. (a) Proposed mechanism for n-hexane isomerization on bifunctional metal-acid catalysts; (b) branching rearrangement of the linear secondary carbenium ion (2-hexenium, A) with the edge-protonated 1-ethyl-3-methyl-cyclopropane carbocation transition state (B) to the monobranchd 2-methyl-3-pentenium ion (C). Adapted from ref.[719] *with permission from the American Chemical Society, copyright 1999.*

The shape selective properties of n-hexane hydroisomerization have been correlated with the pore channel and structure of the zeolite component. An illustrative work by Chica et al.[721] explored the LSR hydroisomerization activity and selectivity of uni- and tri-directional 12-ring zeolites and multipore structures with 10x12 ring pores. They showed a good linear correlation between the hydroconversion activity and the number of acid sites (measured from FTIR with pyridine) regardless of the pore dimensions and zeolite composition (Figure 39). Feedstocks containing n-C_5-C_7 are selectively isomerized by

12MR tri-directional beta (BEA) zeolite, because of the faster diffusion rates of the reacting alkanes through the pores. Also, the large unidirectional pore SSZ-24 with AFI topology performed better than mordenite, the latter having slightly smaller pore diameter.

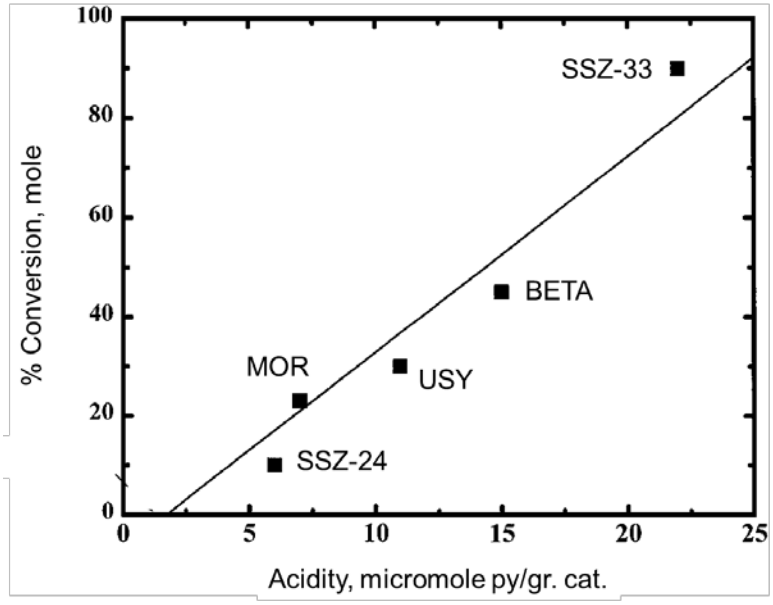

Figure 39. Variation of the hydroconversion activity with the number of acid sites present on the different catalyst, as measured by pyridine desorption at 400ºC. Adapted from ref[721] *with permission from Elsevier, copyright 1999.*

Davis and co-workers reported high iso-alkanes selectivity in n-hexane conversion on zeolite ITQ-27, with a two-dimensional 12ring microporous system, due to the particular topology of this zeolite that allowed a shorter contact time between the isoalkanes intermediates and the BAS, reducing in this way the undesired cracking reactions as compared to other zeolites (see Table 8).

Table 8. Isomers distribution in the hydroisomerization of n-hexane over selected zeolites at maximum isomer yields, p=1480 kPa, LHSV=1h^{-1}and 6:1 H_2/n-hexane. Equilibrium data at 277ºC. Adapted from.[722]

Zeolite	Max. isomer yield (mol%)	Distribution (mol %)			
		2,2-DMB	2,3-DMB	2-MP	3-MP
ITQ-27 (1)	75.5	17.8	10.9	43.0	28.3
ITQ-27 (2)	75.8	18.7	10.4	42.9	28.1
Y	79.5	21.9	10.0	41.1	27.0
Beta	81.5	21.4	11.3	41.2	26.1
Mordenite	78.6	21.5	10.8	40.7	27.0
ZSM-12	72.7	16.2	9.6	44.8	29.4
ZSM-5	74.4	0.2	3.0	59.6	37.2
At thermodynamic equilibrium	–	37.8	18.5	30.6	13.1

*DMB = dimethylbutane and TMP = trimethylpentane

Slawek et al. recently investigated the effect of the zeolite channel intersection geometry on the adsorption of the different hexane isomers by combining Monte Carlo simulations and temperature-programmed adsorption/desorption experiments to determine surface sites of adsorption for medium pore ZSM-5 and ZSM-11 zeolites (Figure 40a).[723] Both have 3D zeolites with intersecting 10-ring pores but with different channel intersection dimensions. According to the results obtained, hexane isomers were preferentially located in channel intersections for both structures. Furthermore, monobranched hexane isomers showed higher affinity for the longer but narrower

intersections of ZSM-11, whereas 2,3-dimethylbutane preferred to adsorb within the shorter but wider intersections of ZSM-5 (Figure 40b). These results agree with the adsorption and thermodynamic results exposed by Maesen and co-workers on n-decane hydroconversion.[95]. More recently, Noh and co-workers investigated the confinement effects on the n-heptane isomerization and the competing cracking reaction over a series of bifunctional Pt-containing catalysts with microporous zeolite structures of similar acid strength, including zeolites Y, beta and ZSM-5.[724] They showed higher isomerization rates for structures with small voids resembling the geometry of the transition state (ZSM-5 structure) because of the stabilization of the transition state by effective Van der Waals interactions. However, these voids also imposed diffusional impediments that influenced the degree of secondary interconversions of the alkene intermediates to a higher extent than the stabilization effects.

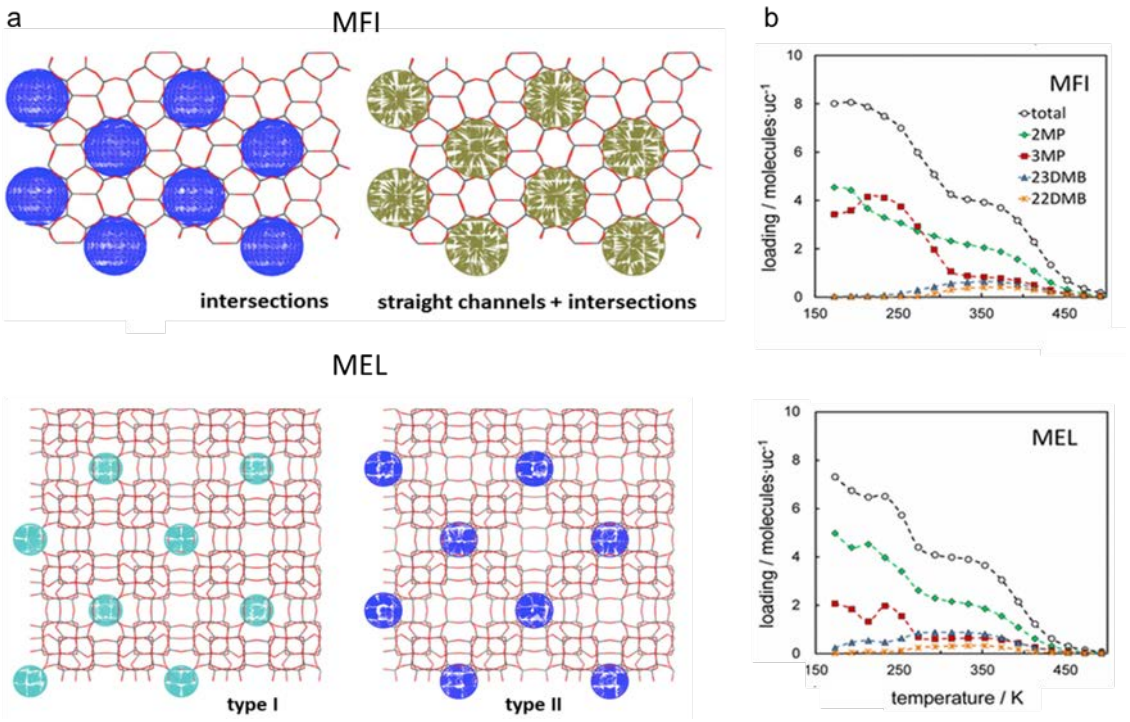

Figure 40. (a) 3D surfaces of adsorption sites defined in the (010) plane for (top) MFI with intersection (blue) and straight channel (green) sites and for (bottom) MEL with

type I (cyan) and type II sites (blue) ; (b) Calculated adsorption isobars (at 10 mbar) of an equimolar mixture of 2-methylpropane (2MP), 3-methylpropane (3MP), 2,3-dimethylbutane (23DMB) and 2,2-dimethylbutane (22DMB) in MFI (top) and MEL (bottom) zeolites. Adapted from ref.[723] *with permission from the American Chemical Society, copyright 2017.*

As mentioned in the introduction to this section, the distribution of the acid or dehydrogenating/hydrogenating function at the nanoscale within the bifunctional catalyst strongly affects the cracking/isomerization selectivity of C_{5+} alkanes. Very recently, the group of de Jong demonstrated this for the hydroisomerization of n-heptane in the presence of a bifunctional composite catalysts using the 1D 10-ring ZSM-22 or 1D 12-ring mordenite zeolites and a γ-alumina binder.[703] The Pt particles were selectively located, either inside the zeolite micropores or on the binder (see Figure 41a,c), thus varying the distance between the acid and metal sites. Catalyst Pt-Al2O3/H-ZSM-22, with both sites separated at the nanoscale, yielded more isomers than the catalyst with Pt inside the zeolite crystals, which offers closer proximity. This was also confirmed for the large crystal-sized mordenite. They claimed that the constrained space within the micropores impose diffusion limitations on the reaction intermediates leading to re-cracking events of the isomers and that this was more pronounced for zeolites with narrow pores or larger crystals. The dimensionality of the zeolite also affected the extent of the influence of the Pt distribution as observed by Samad et al[725] and Moussa et al.[717] Further studies by the group of de Jong showed that the location of the Pt particles did not affect the activity and showed very little impact on the selectivity for n-heptane hydroisomerization over 3D medium pore ZSM-5.[703] The only exceptions was the iso-butane/n-butane ratio, which was significantly lower for the

catalysts with Pt embedded in the micropores, suggesting that the energetically unfavorable secondary-to-secondary cracking reactions are promoted inside the ZSM-5 micropores. The results are in disagreement with previous work by Höchtl et al., also on n-heptane hydroconversion over Pd/SAPO-5 and SAPO-11, where it was reported that the distance between the two functions weakly influenced the isomerization selectivity as long as metal and zeolite are in direct contact.[726]

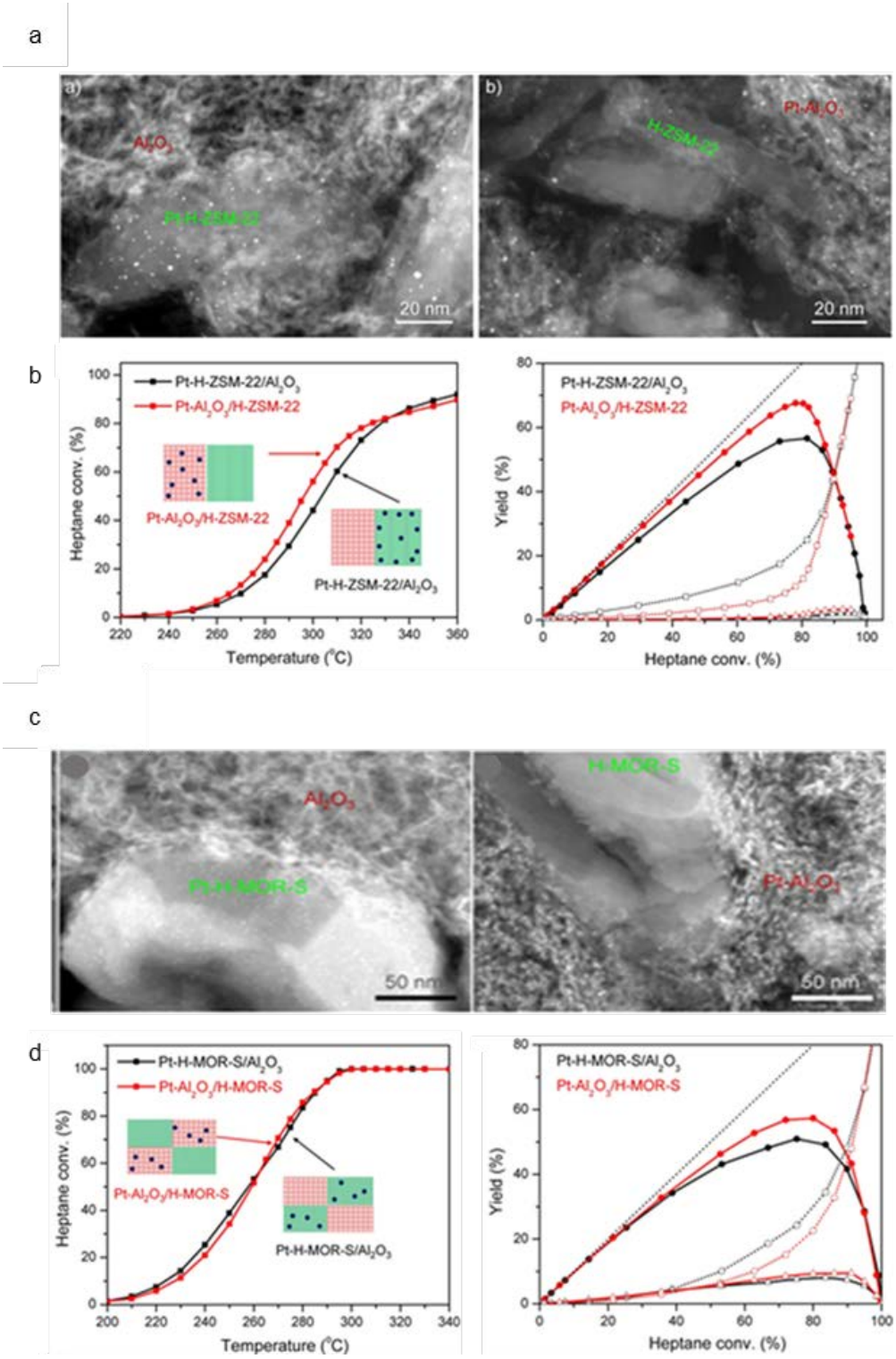

Figure 41. HAADF-STEM images with ultramicrotomy of Pt-H-ZSM-22/Al_2O_3 with Pt in and on the zeolite crystal (a, left), Pt-Al_2O_3/H-ZSM-22 with Pt on the alumina binder (a, right), Pt-H-MOR/Al_2O_3 in closest proximity (c, left) and Pt-Al_2O_3/H-MOR in nanoscale proximity (c, right). Impact of the Pt location on activities(b, d, left) and total (solid lines with circles), dibranched (solid lines with triangles) and cracking (dashed lines with squares) C_7 yields , (b, d, right) of n-heptane hydroconversion over these two catalysts. Reproduced from ref.[703] *with permission from Wiley-VCH, copyright 2020.*

The environmental constraints associated with the aromatic composition in the blend gasoline, particularly benzene, has driven the research to the possibility to selectively isomerize higher alkane chains (C_{7+}) previously directed to BTX formation by naphtha reforming. However, hydroconversion of these larger alkanes with high isomerization/cracking selectivity is a challenging issue, since these alkanes are easier to crack and this will force working at lower temperatures if formation of light gases is to be avoided.

The versatility of zeolites compositions and structures is, again, key to reach this goal, and crystalline materials with mild acidity and large pores, such as Y and SAPO-11 limit the undesired re-cracking of the branched octane isomers and favor the formation and diffusion of multibranched products.[706] Pt/ZSM-5 medium pore catalysts showed, however, lower selectivity to dimethylhexanes. A comparative study of different zeolites as catalysts for n-octane hydroisomerization, [727] showed that zeolite beta-based catalyst was the most selectivity to mono- and di-branched paraffins. This was explained by the fact that over this zeolite the rate of n-octane isomerization to the mono-branched products was faster than that of cracking of the active dibranched isomers, thus reaching the thermodynamic equilibrium under the given conditions. As the rate of mono- to dibranched isomerization was close to that of the dibranched isomers cracking, the selective formation of di- and specially tribranched C_8 isomers was difficult.

5.2.2. Isomerization of heavy C_{10+} alkanes

Precipitation of long chain n-alkanes at low temperatures leads to undesired cold properties of fuels and lube oils, such as their pour point, their freezing point or their cloud point. These properties can be improved by two main approaches: isomerization of the linear paraffins, or selective cracking of the n-alkanes to smaller branched products. Both processes, also known as dewaxing processes, are catalyzed by zeolites since the late 1960s and early 1970s. Pt-loaded mordenite (1D 12-ring) and ZSM-5 (3D 10-ring) were two of the first zeolite-base catalysts proposed.[19] In fact, the medium pore ZSM-5, in its acid form, was particularly active for dewaxing by selective cracking of the linear molecules by reactant shape selectivity. Another zeolite-related material proposed in these early years was SAPO-11. This zeotype, with a 1D medium pore channel system and a lower acidity, favored isomerization over cracking.[728] Besides Pt-based catalysts, zeolites containing less expensive transition metals, such as Ni or Mo, have also been reported to be active for catalytic dewaxing.[729]

Although dewaxing by hydrocracking or by combination of cracking and isomerization are effective routes for upgrading fuels and lube oils, the process is less suitable when the content of waxes in the feed is high, due to the large loss of product. In such cases, the selective conversion of long-chain n-alkanes by hydroisomerization on zeolite-based bifunctional catalyst is the preferred route. In the late 1980's, researchers from Chevron showed that zeolites with unidirectional medium pore structures, such as SAPO-11, were selectively converting long-chain alkanes into monobranched isomers,[706] and this was the basis for the isodewaxing process.[707]

ZSM-22, with a 1D 10-ring topology, has also been described as catalyst for the hydroisomerization of heavy n-paraffins. Thus, Martens and his group studied the adsorption of n-alkanes of different chain length and their hydroconversion over ZSM-22 acid zeolites.[730–735] According to their results they proposed the models of "pore-mouth" and "key-lock" catalysis,[702] as particular shape-selectivities, which consider that unidirectional medium pore acid structures will only catalyze specific alkane hydroisomerization reactions corresponding to specific physisorption modes.

The influence of the pore size was evidenced by comparison of diffusion constants and adsorption enthalpies and entropies obtained for a range of n-alkanes (C_5 to C_{24}) and different coverages over a set of large and medium pore zeolites.[734,736,737] Higher Van der Waals interaction of the n-alkane with the zeolite pores was observed with decreasing pore diameter and, as the zeolite pore size increased, a nonselective adsorption between n-alkanes and iso-alkanes inside the micropores or on the external surface was observed. ZSM-22 zeolite showed a selective adsorption of the n-alkanes through the pore mouths into the micropores and of the alkane isomers at the external surface only. This behavior led to the proposal of the "pore mouth" shape selectivity, according to which the longest possible linear backbone of the alkane will penetrate the zeolite pore, where its interaction with the zeolite is energetically favored, as illustrated for a C_{21} monomethyl isomer in Figure 42a. Additionally, a preferential selectivity to mono-branched iso-alkanes, with the methyl in the second carbon, was observed for conversion of n-alkanes up to C_{22} on ZSM-22 (Figure 42b). The model assumes that the hydroconversion does not involve net transport through the zeolite micropores due to the sterically hindrance. Therefore, the branching of the n-alkane is catalyzed by an acid

site located near the pore entrance, where the slightly wider space will allow free motion of the alkane methyl groups. The pore-mouth selectivity was also observed for ferrierite, with a 2D 8x10-ring pore structure.[738]

Martens and co-workers also defined the so-called "key-lock" mechanism for hydroisomerization on long-chain alkanes on ZSM-22.[698,699,730,731,733,735,736] This was not attributed to a shape selective effect, but to a selective hydroisomerization reaction on the external surface of ZSM-22, by which the monobranched alkane (key) anchored on an active site in one pore mouth, is stretched across the external zeolite surface and penetrates into one or more additional pore mouths (lock) (see Figure 42c).

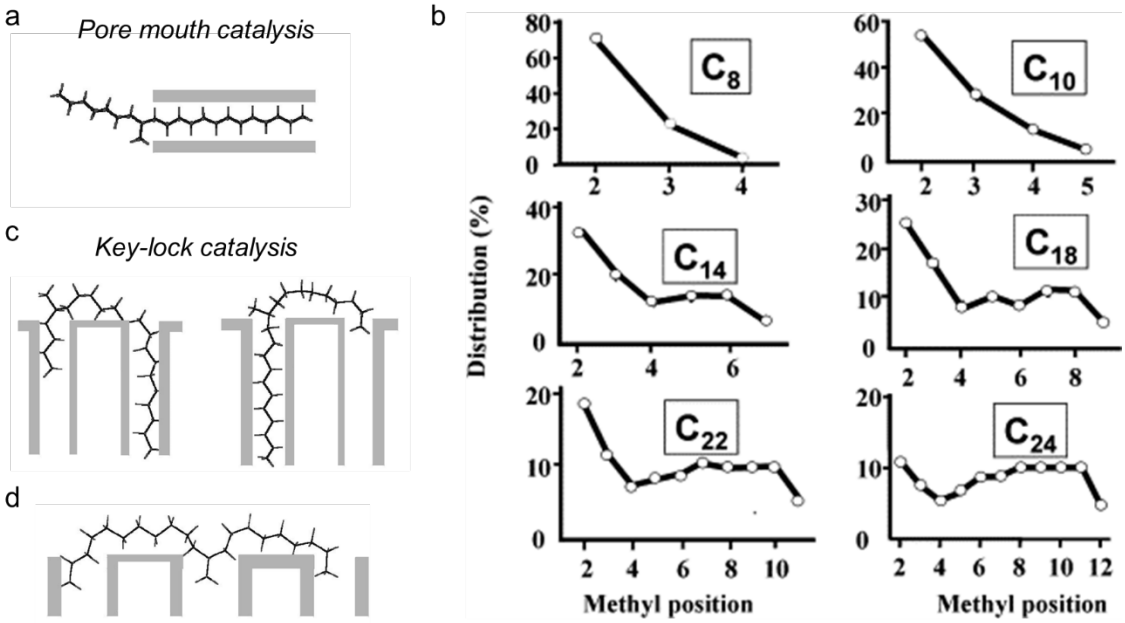

Figure 42. Schematic representation of favorable adsorption configurations of MC_{21} molecules on ZSM-22 structure simulating the pore mouth (a) and key-lock (c, d) catalysis; (b) Distribution (mol %) of methylalkane isomers obtained at 25-30% hydroisomerization conversion of n-alkanes on Pt/H-ZSM-22 catalyst at T=233 ºC and P_{H2}/P_{HC}=13.1. Adapted from ref.[702] *with permission from Elsevier, copyright 2001.*

Hydroisomerization of long n-alkanes on on Pt/ZSM-22 with the zeolite pores partially or fully filled with organic templates further confirmed the pour-mouth catalysis taking place on these mono-dimensional 10-ring zeolite structures.[739,740] Additional evidences for the "key-lock" mechanism have been recently reported for the hydroisomerization of n-hexadecane over a bifunctional ZSM-23-based catalysts, also with a 1D 10-ring structure.[741]

Although the aforementioned studies suggest that isomerization occurs at the pore mouths, close to the external zeolite surface, other groups demonstrated that the monobranching through PCP intermediates (Figure 43a) can occur on acid sites located inside the micropores of unidirectional 10-ring structures, such as ZSM-22 and Theta-1 (TON), ZSM-23 (MTT), ZSM-48 (MRE) and SAPO-41 (AFO).[713,742,743] Molecular dynamics and catalytic test results indicated that, for zeolites in which the external acid sites were depleted and the acid sites were located inside the micropores, terminal monobranched isomers can be formed and they react (to form dibranched isomers) in the micropore BAS more easily than bulkier isomers (Figure 43b, 3-4), because of the shape selective effect. These terminal monobranched alkanes can also diffuse out to the external zeolite surface and isomerise to dibranched alkanes when an acid center is located near the external surface, where there is no steric impediments for them or bulkier isomers (Figure 43b, 1-2). Another supporting finding was the minor variation of n-decane hydroconversion activity after a dramatic reduction in the density of external active sites of TON and MTT zeolites. Furthermore, adsorption thermodynamic studies showed that the adsorption entropy of n-alkanes was similar at the exterior and interior pore surfaces, [744] but stabilization by Van der Waals interactions increased when moving from

the external surface to the interior of the pore. For branched alkanes, the adsorption enthalpy was similar at the internal or external zeolite surfaces, but the entropy increased within the pores, resulting in higher interaction. In this case, the relative lack of mobility observed for the adsorbed methylalkanes at the external surface agrees with the assumptions of the “pore-mouth” and “key-lock” model.

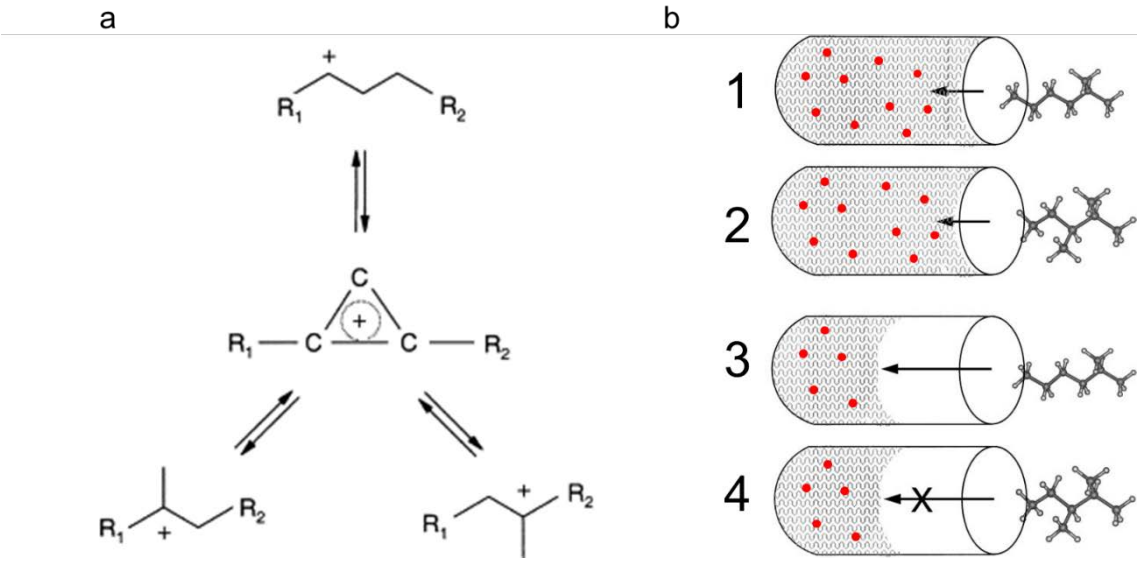

Figure 43. (a) Mechanims of n-alkane isomerization, adapted from ref.[745] *with permission from Elsevier, copyright 2005; (b) Isomerization of mono- and di-branched alkanes on acid sites located in the external surface of the micropore (1-2) or at the interior of the micropores (3-4), adapted from ref.*[743] *with permission from Elsevier, Copyright 2000.*

The long n-alkane hydroisomerization ability of unidirectional medium pore molecular sieves was successfully extended to 10-MR unidirectional silicoaluminophosphates, such as the cited SAPO-41 (AFO) or SAPO-11 (AEL) for hydroisomerition of heavy waxes.[424,742,746] A specific review on hydroisomerization of long-chain alkanes over SAPO-n molecular sieves is available for the interested reader.[747]

Several multi-stage processes based on bifunctional zeolite-metal catalysts have been reported for hydroconversion of more complex feedstocks containing long n-alkanes, which included a hydroisomerization step based on unidirectional medium pore zeolites. Thus, feedstocks containing n-alkanes but also a significant percentage of aromatics can be selectively converted by a two-isomerization steps, based, for instance, on a first beta zeolite bed to process aromatics and perform cracking and a second bed with ZSM-22 for hydroisomerization of the linear paraffins.[705] Dewaxing can also be combined with the overall gas-to-liquids Fischer-Tropsch process for upgrading the FT waxes by hydroisomerization alone or combined with hydrocracking.[608] A number of zeolites were studied for this purpose, namely ZSM-48, ZSM-30, EU-2 and EU-11. On the other hand, the presence of oxygenates in the FT streams can greatly alter the balance between the acidic and the metallic hydrogenation/dehydrogenation function and the middle distillates selectivity of the bifunctional catalysts.

In a recent publication, Weston and co-workers reported high activity and iso-decane selectivity obtained with a catalyst based on a new zeolite, EMM-17.[748] The good performance was related to the particular multipore structure of EMM-17, a 3D channel system with intersecting 11x10x10-ring pores that improved the accessibility of the feed alkane, leading to higher activity, and facilitated the transport of the isomerized intermediates out of the zeolite pores, thus improving iso-decane selectivity by avoiding re-cracking in the small pores.

5.2.3. Hydrocracking of heavy C_{10+} alkanes

Hydrocracking is a major conversion process in the refining industry aimed to convert complex heavy feedstocks such as gasoil from thermal cracking or VGO or paraffin-rich fractions, such as FT waxes or biomass derived fractions.[19,20,93] Unlike FCC, which preferentially yields gasoline or light olefins, hydrocracking is mainly directed to the production of middle-distillates, mainly diesel and kerosene, for their use as transportation fuel blendstocks. The process usually operates at lower temperatures than FCC (300-450 ºC) and high H_2 pressures (ca. 150 bar).[19,20] Lower temperatures favor aromatic hydrogenation and increase the cetane number of the middle distillates. The presence of hydrogen favors the saturation of the hydrogen-deficient compounds formed by cracking and minimizes coke formation. As it was for cracking, besides the alkane chain breaking, other elementary reactions occur during hydrocracking, such as isomerization to branched alkanes and hydrogenation/dehydrogenation of the C-C bond, together with ring closure to form aromatics and olefins. Regarding the severity of the process, the search for a poison resistant catalyst becomes more challenging when feeds contain high levels of impurities, such as N or S.

From the mechanism perspective, there are important differences when comparing the cracking and hydrocracking processes, first identified in the pioneering works of Coonradt and Garwood[749] and extensively confirmed by later studies.[25] On the one hand, the carbenium to be cleaved is formed from a penta-coordinated carbonium during cracking as described in previous sections, while it results from an unsaturated alkene in hydrocracking. On the other hand, the hydrogen co-fed in HDC saturates hydrocarbons from the reacting pool and minimizes the formation of carbonaceous

deposits, thus minimizing catalyst deactivation. Finally, the branching degree of the cracked products formed from the n-alkane can be controlled in hydrocracking, whereas it is extensive in FCC, leading to more re-cracking events. This is a consequence of the selective desorption mechanism of the primary cracked products from the acid sites before suffering a second C-C bond cleavage, leading to a homogeneous distribution of hydrocracked products. The yields to gasoline-range products or middle distillates can be adjusted by varying the severity of the process conditions or the properties of the zeolite component, such as the acid site density.[750] This illustrates the high product flexibility as compared to FCC. In addition, long alkanes with chains with more than 8 carbon numbers rapidly crack once they isomerize on monofunctional acidic zeolites, while bifunctional catalysts allow high isomer selectivities at moderate conversions.

The size of the feed alkanes and of the cracked products usually involve intra-crystalline diffusion constraints withing the zeolite micropores, so hydrocracking catalysts are usually based on large pore zeolites such as Y, mordenite or beta. In the case of ultra-heavy crudes processing, Mo nanoparticles dispersed on a FCC-type acid catalyst are useful.[19,20,751] As mentioned in former sections, the intrinsic reactivity of the zeolite generally increases with the length of the n-alkane. However, this is true if the reactions are kinetically but not diffusion limited as could be the case for large pore zeolites. In fact, the opposite trend was observed on a Pt-loaded ERI-type zeolite,with a 3-dimensional small pore structure with cages, where the particular topology leads to a monotonically decrease in reactivity with increasing the length of the n-alkane, in contrast to the behavior of the Y-based catalysts under the same reaction conditions (Figure 44). Thus, besides the kinetics and diffusion rates of the n-alkane,

thermodynamic implications, encompassed in the Gibbs free energy of adsorption, need to be considered when analyzing reactant shape selectivity, as mentioned in the introduction of this Section.

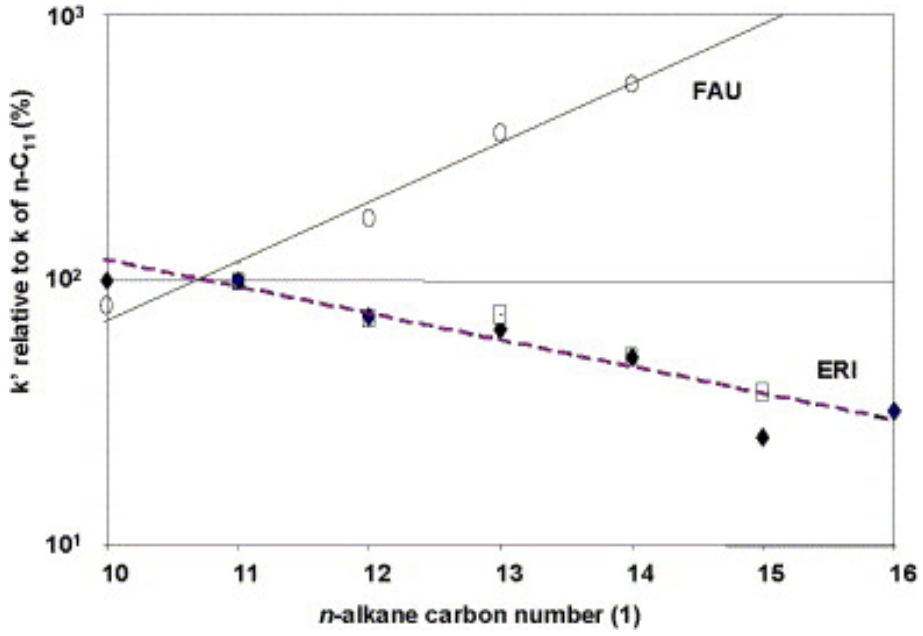

Figure 44. Variation in n-alkane hydroconversion activity (k´) with n-alkane chain length on Pt/ERI at 670-700K and Pt/FAU zeolites at 513K and similar hydrogen-to-hydrocarbon molar ratio and contact time. Reprinted from ref.[710] *with permission from Elsevier, copyright 2006.*

As it was for FCC, USY is the preferred acidic zeolite component of hydrocracking catalysts, because of its high activity, hydrothermal stability and resistance against deactivation by coking or poisoning. Moroever, USY provides reasonable product flexibility in n-alkane hydrocracking, since the Si/Al ratio can be adjusted by dealumination to direct the selectivity towards naphtha or middle distillates. Besides the framework BAS, the EFAl content and textural properties of the zeolite component drastically influence the product distribution,[19] underlining the importance of controlling the diffusional and compositional catalyst descriptors for hydrocracking.

Even for highly dealuminated USY zeolite, re-cracking of the middle distillates in the large micropores cannot be completely discarded. This can be tackled, for instance, by facilitating the diffusion of the middle distillates while keeping similar zeolite architecture. A prime example is the use of the large pore three-dimensional NiMo-ITQ-21 zeolite with enhanced void accessibility.[647] as hydrocracking component for a hydrotreated gasoil conversion.[752] As compared to zeolite Y- and beta-based catalysts, ITQ-21 maximized the selectivity to diesel-range products at high conversions under same reaction conditions, by facilitating the diffusion of primary products and minimizing re-cracking events.

As shown previously in this section, post-synthesis delamination of layered zeolite precursors is an interesting approach for increasing the accessibility of microporous crystalline materials. The benefits of these increased accessible surface areas were evidenced when ITQ-2, the delaminated counterpart of MCM-22, was compared to a Ni-USY zeolite for hydrocracking of a VGO,[753] and was shown to be more active and less selective towards light gases under similar experimental conditions. The advantages of ITQ-2 zeolite were also demonstrated for other stepwise hydrocracking related technologies, such as upgrading of heavy linear alkanes from primary Fischer-Tropsch synthesis fractions.[608,754]

Reducing the crystal size has also improved hydroconversion zeolite based catalysts. Camblor et al.[755] and later Arribas et al.[756] showed both cracking activity and selectivity benefits from the decrease of the beta zeolite crystal size as compared to the usual micrometer range crystallites. Additionally, bifunctional catalysts containing nano-beta zeolites were more selective to middle distillates and less to low weight gaseous alkanes,

formed by consecutive cracking steps, than the commonly used USY zeolite. Further studies supported these findings for n-hexadecane conversions over Pt-Pd-nanobeta bifunctional catalysts.[757] Relevant kinetic and diffusion studies by Marin and co-workers showed that the intracrystalline diffusion limitations suffered for the branched C_7 isomer after n-heptane hydroisomerization in the presence of ZSM-5, could be mitigated by decreasing the size of the ZSM-5 crystallites.[758,759]

The generation of mesopores within the crystals of zeolite Y and the benefits when using these improved zeolites as hydroprocessing catalyst were already studied in early works by Mao et al.,[760,761] and continued later by Sato et al.[762] Fajula and co-workers, following a post-synthetic approach that combined steaming, acid treatment and controlled desilication processes,[763] succeeded in the generation of well defined and interconnected intracrystalline mesopores with a trimodal distribution and improved diffusion properties. The resulting Y zeolites were reported to behave close to ideal hydrocracking catalyst with high selectivity to middle-range distillates from n-hexadecane and squalene (C_{30}).[25]

In a different approach, Brosius et al. highlighted the importance of the use of steam for ZSM-5 zeolite-based hexadecane hydrocracking, which was shown to be even more beneficial in terms of linear alkane selectivity than the generation of mesopores.[764] The presence of water suppressed re-cracking and isomerization of primary cracking products by competitive adsorption in the ZSM-5 micropores.

Alkaline desilication methods have been widely used to improve the performance of one-directional zeolite supports for long n-alkanes hydroconversion. By continuing their works on n-decane, n-dodecane and pristane (C_{19}) hydroisomerization, Martens et al.

demonstrated higher performance over mesoporous Pt/ZSM-22 catalysts obtained by alkaline treatment as compared to the pure microporous support.[765] This was also proven by Verboekend et al. for n-octane hydroisomerization over sequential base and acid treated ZSM-22.[766] The construction of hierarchical structures by combined alkaline-acid leaching treatments has been employed to increase the n-hexane isomerization selectivity for mordenite and beta based bifunctional catalysts.[767,768]

5.3. n-alkanes dehydrocyclization

Although other processes for production of aromatics (and H_2) are gaining interest, such as the dehydroaromatization of methane and light alkane described in the previous sections, dehydrocyclization of low value naphtha fractions, rich in linear and cycloalkanes, is still the main industrial route for producing BTX aromatics.[19] The main reactions involved in this alkane conversion process, also known as catalytic reforming, are cyclization and dehydrogenation.[19,769]

The process is strongly endothermic and thermodynamically unfavorable. The first activation step over the metallic sites, i.e. the alkane dehydrogenation, detailed for other processes in previous sections, is also valid here. However, the unsaturated intermediates formed in this case are long enough to directly cycle, so oligomerization of the formed alkenes is not required. Even though the C-H bond of longer alkanes is easier to activate due to the influence of the surrounding C atoms on the C-H dissociation energy, the efficiency to cycle and aromatize of the intermediate species is generally low,[716] and can be increased by using shape selective zeolites, such as zeolite L or ZSM-5, among others.

Noble-metals, such as Pt, have been extensively investigated for the n-alkane aromatization because of their high dehydrogenating activity.[468] Since the nonselective steps of cracking, isomerization or oligomerization of the intermediate alkenes should be minimized during aromatization, the acidic function of the zeolite is not a requirement and the catalyst efficiency will depend on a high hydrogenation/dehydrogenation activity provided by the metals. Thus, zeolites providing large surface area and no acid site density are used, with the main role of supporting the metal atoms and controlling the selectivity. The nature of the feed alkane also influences the selectivity, and the cycloalkane formed and the corresponding aromatic, i.e. benzene, toluene or xylenes, will depend on the number of carbons of the starting hydrocarbons.[770]

The mechanisms of n-hexane aromatization over Pt loaded zeolites have been studied for long.[468] Pt-loaded zeolite L, generally exchanged with elements providing a base character, such as K, Mg, Ba or Ce, and more specifically Pt/K-L, has been the preferred catalyst to convert linear C_6 paraffins into aromatics,[771] because of its nonacidic character and its 1D large pore structure (see Figure 45a). Both, the lower coke formation and the low metal sintering degree lead to a low deactivation rate. Whereas the metal, usually Pt, provides the adequate dehydrogenation activity, the aromatization mechanism is related to the zeolite pore shape effects, site accessibility, basicity and electronic descriptors derived from zeolite-metal interactions.[772,773] Dehydrocyclization is a complex process that involves multiple individual reactions of cyclization and dehydrogenation but also skeletal isomerization and hydrogenolysis (Figure 45b).[770]

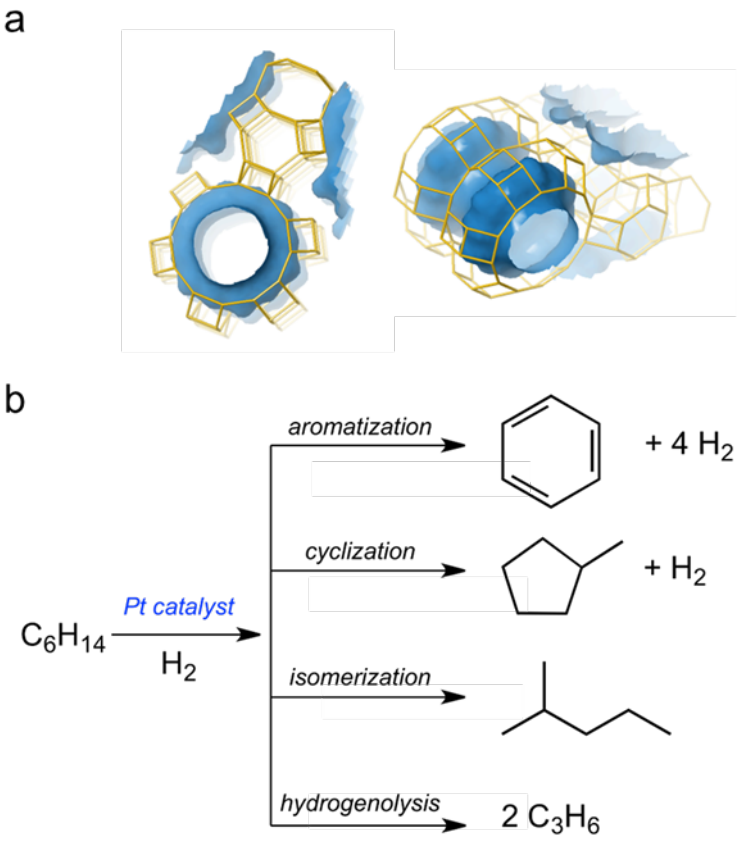

Figure 45. (a) Structure of the L zeolite highlighting the 12-ring internal channel. Structures taken from the IZA webpage.[37]; (b) Individual reactions that can be occurring during dehydrocyclization of n-hexane.

Early studies related to the possible reaction mechanisms over acid zeolites focused on the formation of the C_6 ring on Pt/K-L catalysts. [467,774] It was proposed that the K-L structure induced the orientation of the alkane molecule in the linear channels in such a way that it favored terminal carbon adsorption and C_1-C_6 ring closure on the Pt sites and not through 5-ring closure followed by ring expansion, because the latter can only occur following a carbocation pathway.[470] Furthermore, the cavities of the L-type zeolite might lead to alkane chain arrangement into an intermediate structure resembling that of the transition state for n-alkane cyclization and stabilized by confinement effects.[471] Later works payed more attention to the intermediates formation,[775–777] and partially dehydrogenated linear C_6 species were identified as intermediates in a reaction pathway

by which dehydrogenation steps were fast as compared to the C_1-C_6 ring closure, which was considered to be the rate-determining step.[770] n-Hexane conversion in the presence of a typical naphtha reforming bifunctional catalyst was suggested to proceed via successive dehydrogenation to hexa-1, 3, 5-triene, followed by C_1-C_6 ring closure to cyclohexadiene and finally dehydrogenation to benzene (Scheme 22a).[770] The dehydrocyclization mechanisms for the conversion of n-heptane to toluene over Pt/K-L follow similar reaction routes with heptatrienes and ethylcyclopentane being the intermediates involved in ring closure and isomer formation, respectively (see paths II and III-IV in Scheme 22b)[778] A parallel route involving first ring closure followed by progressive dehydrogenation can also take place (path I in Scheme 22b)[472] The detailed mechanisms proposed for the ring closure from heptatrienes or methyl-cyclohexane are showed in Scheme 23a and b, respectively. An exhaustive review on alkane dehydrocyclization mechanisms on different type of catalysts, including metal-loaded zeolites was published by Davis.[770]

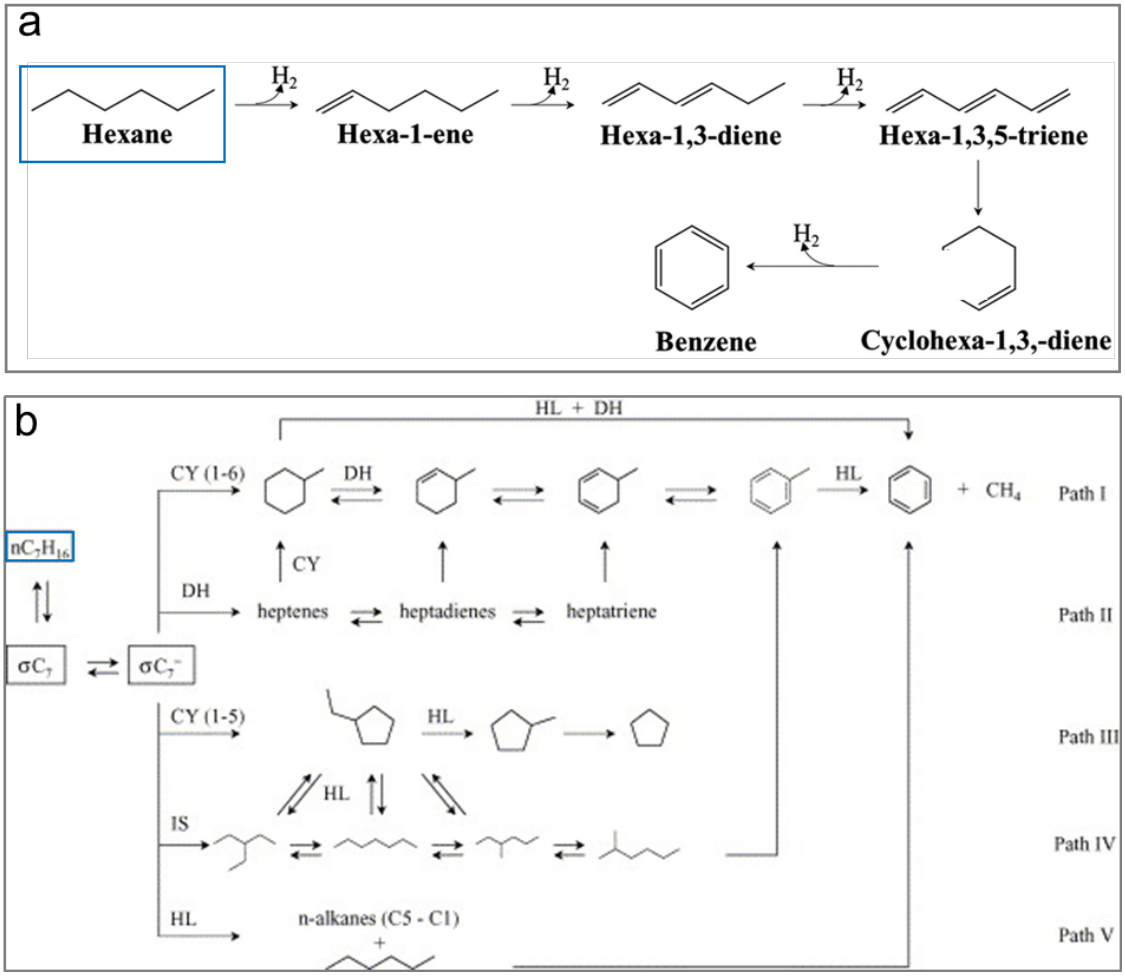

Scheme 22. (a) Possible routes for n-hexane aromatization through sequential dehydrogenation and ring C_1-C_6 ring closure, adapted from ref.[777] with permission from Elsevier, copyright 1994 and (b) proposed reaction mechanisms for the n-heptane dehydroclyclization to toluene (CY=cyclization, DH=dehydrogenation, HL=hydrogenolisis, IS=isomerization). Reprinted from ref.[472] with permission from Elsevier, Copyright 2005.

As Pt deactivation by coking was seen to take place mainly outside the zeolite pores, Jentoft et al. were able to significantly improve the catalyst performance by maximizing the proportion of Pt nanoparticles within the zeolite micropores where coke formation was inhibited.[779] Later studies confirmed the role of the zeolite structure in protecting the Pt clusters from carbon fouling.[780] Iglesia and Baumgartner related the n-heptane

dehydrocyclization activity to the clean Pt surface, regardless of the support.[781] They observed that a at atmospheric pressure, the 2-methyl-cyclopentane rings formed at the initial reaction stages, were involved in coking reactions and contributed to rapid catalyst deactivation and decreased aromatics production following a monofunctional route. However, when working at industrially relevant reforming conditions (high pressures), the C_5 rings could also undergo nonselective hydrogenolysis to acyclic alkanes that, in turn, might cycle to aromatics (see Scheme 23c).

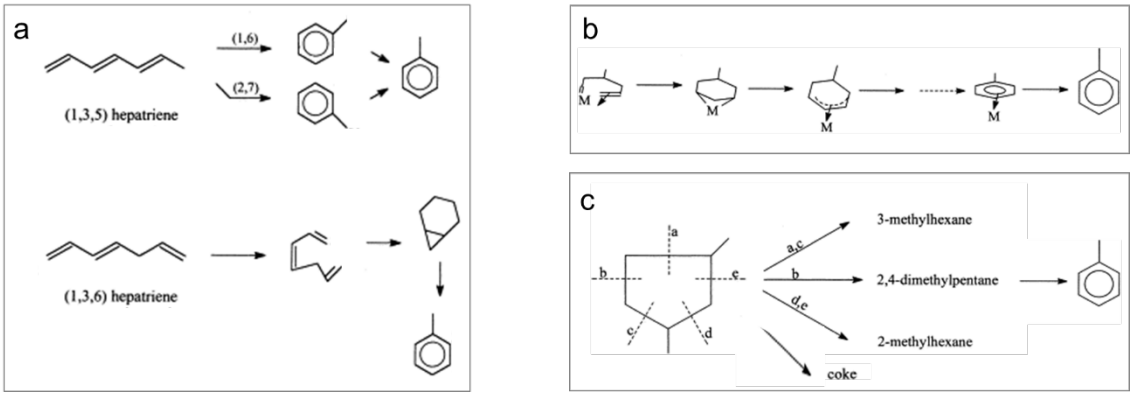

Scheme 23. Possible modes of C_7 ring closure from heptatrienes (a) by the formation of cyclic or bicyclic structure and subsequent rearrangement/hydrogenolisis of the cyclopropane ring or from methyl-cyclohexane (b); (c) Cyclopentane hydrogenolysis possible steps to isopentane products. Adapted from ref.[770] with permission from Elsevier, copyright 1999.

Zn- and Ga-containing ZSM-5, largely studied in light alkane aromatization, have also been reported as catalysts for naphtha dehydroaromatization. In an early work by Viswanadham, comparing H-ZSM-5 and Zn/H-ZSM5 catalysts for aromatization of pure n-heptane and a light naphtha stream,[782] an increase in the aromatic yield for the Zn/H-ZSM-5 was observed. Moreover, the increased toluene selectivity suggested that direct dehydrocyclization of the alkanes took place in the presence of Zn. As it was for L-type

zeolites, the conversion of C_6-C_8 olefinic intermediates to the corresponding aromatics was suggested to be favored by the suppression of consecutive acid catalyzed reactions such as oligomerization, cracking, hydrogen transfer and transalkylation.

The nature of the metal species and their interaction with the zeolite was investigated by Xin et al. and Thivasasith et al. for Ga/H-ZSM-5 dehydroaromatization catalysts.[783,784] Framework Ga species and dihydro gallium complexes, respectively, were identified as the active sites. More recently, Song and co-workers demonstrated that the use of ZSM-5 support containing an excess of K^+, beyond its ion exchange capacity, and well dispersed Pt in the micropores, catalyzes the aromatization of n-heptane and n-octane with high selectivity by 1,6-ring closure and reduces the deactivation usually encountered when aromatizing alkanes with more than six atoms.[785] K^+ was reported to play a double role, as inhibitor of strong acid sites and as an indirect Pt electron promoter.

The conversion of n-hexane to aromatics over metal-free zeolites following direct conversion route or by coupling with other conversion processes has also been approached. Generally, the presence of an oxidant is required in order to reduce the energy barrier for the alkane activation. Wei et al. studied the co-reaction of n-hexane with CO over acidic ZSM-5 and observed a significant increase in the aromatic selectivity upon addition of CO.[786] The identification of methyl-substituted cyclopentenones (CPOs) intermediates and CO_2 led the authors to propose a reaction mechanism (Scheme 24) based on the CO insertion into the carbonium ions formed by protonation of the alkane on the BAS. This generates an acyl group that will react with olefins formed by cracking of the alkane to form cyclopentenones (CPOs) by intramolecular cyclization or alkene

coupling by Friedel-Crafts acylation. The CPOs are finally converted to aromatics by expanding and eliminating one water molecule.

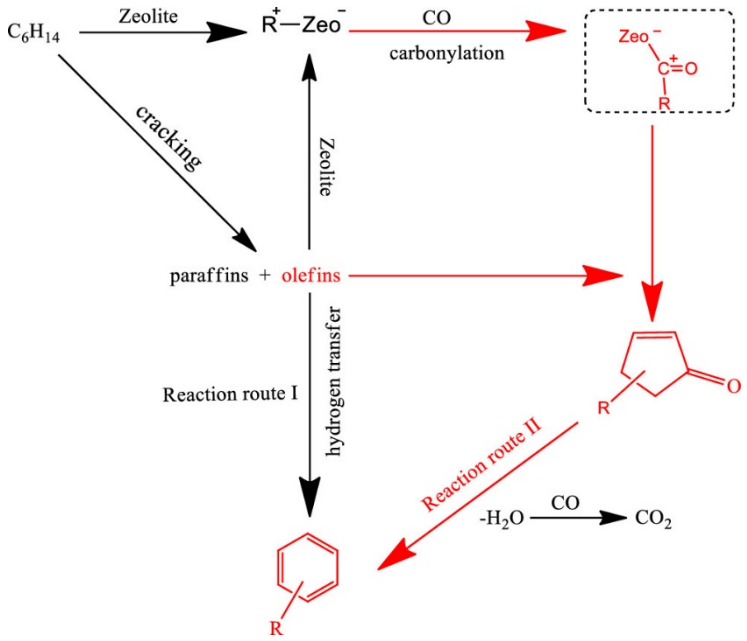

Scheme 24. Proposed mechanism for the coupling conversion of n-hexane and CO to aromatics over H-ZSM-5 catalyst. The new aromatic generation route and new detected intermediates are marked in red. Reprinted from ref.[786] with permission from the American Chemical Society, copyright 2020.

5.4. Selective oxidation of C_{5+} alkanes

The selective oxyfunctionalization of C_{5+} alkanes faces the same challenge that has been previously remarked for the partial oxidation of methane and light alkanes, the difficulty of performing the reaction with high selectivity to the target product, avoiding undesired overoxidation processes. The design of multi-functional catalysts with well defined, homogenously distributed active sites is, therefore, essential. In this section, we will cover the role of different modified zeolites and zeotypes as catalysts for

oxidation reactions of C_{5+} alkanes to different oxygenated hydrocarbons, such as alcohols, ketones and acids.

In the early eighties, researchers from ENI successfully prepared the TS-1 crystalline material by introducing Ti^{IV} in framework positions of silicalite, a pure silica ZSM-5 with MFI topology.[787,788] Shortly after, Jacobs and Tatsumi demonstrated that Ti containing silicalite with isolated Lewis acid sites was active for the shape-selective oxidation of alkanes into secondary alcohols and subsequent ketones in presence of H_2O_2, at moderate temperatures (20-150 ºC) and in an adequate solvent, following a mechanism that was thought to be ruled by radical species.[789,790] Ti-silicalite showed low regioselectivity for the formation of the alcohol but high selectivity to the formation of ketones. The oxidation rates of n-alkanes were seen to exceed those of branched alkanes and, among the linear hydrocarbons, the rates decreased with increasing carbon number. Thus, the medium pore structure of Ti-TS1 limited its application to the conversion of relatively small molecules, able to penetrate within the 10-ring pores of silicalite (< 0.6 nm), because of diffusional restrictions or reactant shape-selectivity.[790] Vayssilov thoroughly reviewed the studies directed to the identification of Ti states and coordination in Ti-silicalite.[791] The incorporation of titanium as Ti^{4+} in tetrahedrally coordinated framework sites was confirmed by different characterization techniques. When exposed to oxygen-containing molecules, such as H_2O_2, the Ti ions increased their coordination from 4 to 5 or 6, but at the time the exact geometry of the coordination complex formed was not fully understood. Still, three main modes were proposed, which are shown in Scheme 25. The formation of extraframework titania was also observed depending on the synthesis conditions, and negatively affected the catalytic

activity and selectivity. For more information about the synthesis strategies and Ti-sites interaction, the reader is referred to this review and the references therein.[791]

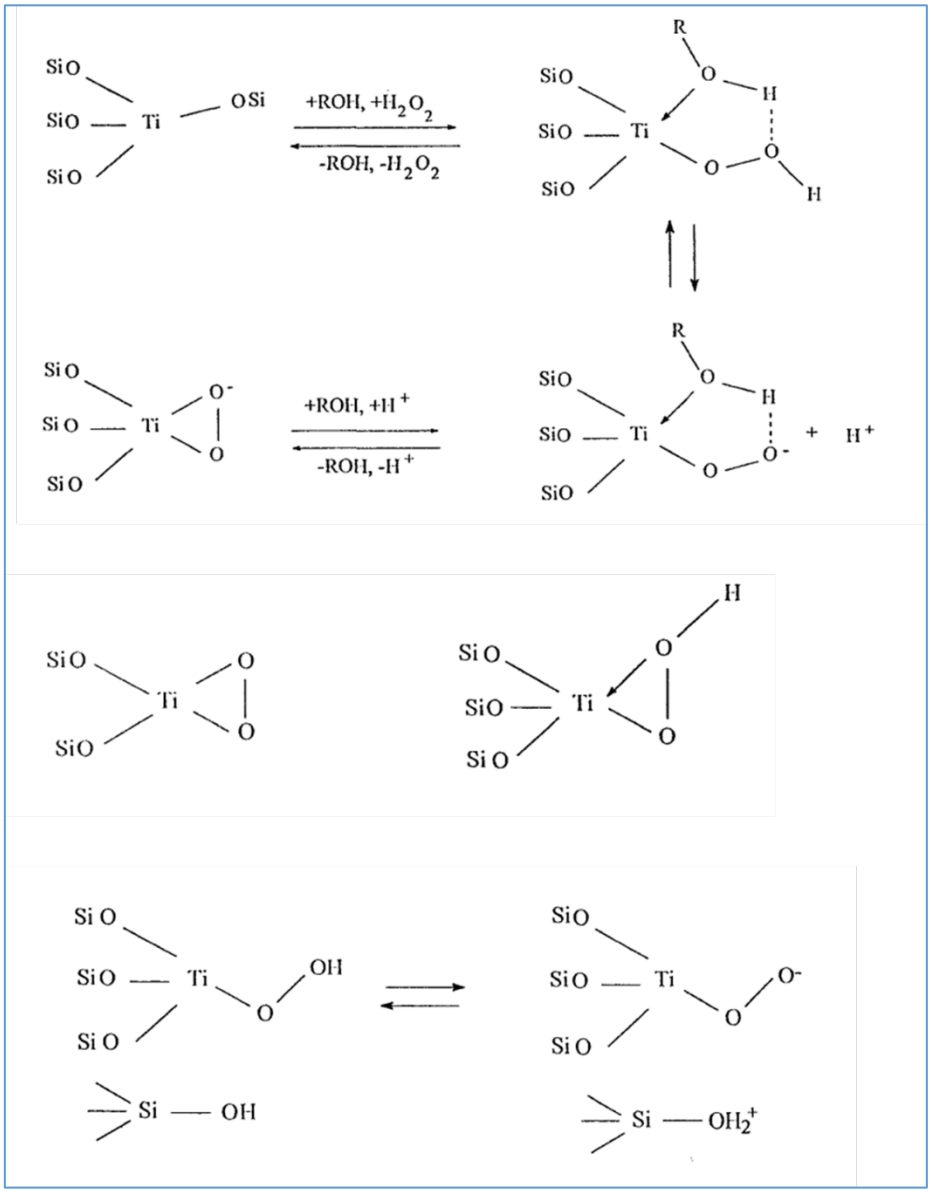

Scheme 25. Possible interactions of Ti-sites with oxygen containing molecules. Reprinted from ref.[791] with permission from Taylor & Francis Ltd, copyright 1997. http://www.tandonline.com

The nature of the surface intermediates and the reaction mechanism of n-hexane oxidation to hexanols and hexanones by H_2O_2 in the presence of Ti-silicalite for n-C_6 oxidation was also studied by Gallot.[792]

Two main approaches were proposed to overcome the limitations of TS-1 as catalyst for the oxidation of bulkier molecules, either improving the accessibility of TS-1 and shortening the diffusion paths by reducing particle size or tuning the morphology of the crystallite,[793] or synthesizing Ti-zeotypes with different, more accessible structures. In this line, Corma and co-workers synthesized for the first time a Ti-containing beta zeolite with both, Al and Ti in framework positions,[794] with the Ti-Si distances resembling those for Ti-silicalite, as evidenced by combination of common characterization with EXAFS and XANES spectroscopic techniques.[795] They also achieved the direct synthesis of pure silica Ti-beta zeolite in OH media[796] and in fluoride media,[797] the latter also free of connectivity defects. This improved the catalytic performance of Ti-beta as selective oxidation catalyst, and was particularly important for epoxidation reactions, where the BAS were seen to catalyze the epoxide ring opening, decreasing in this way the selectivity to the desired product.[798] Moreover, this discovery represented a step-forward in the use of zeolites as catalysts for oxyfunctionalization, and opened the pathway to the synthesis of other Lewis acidic materials, such as Sn- and Zr-beta, with complementary catalytic properties for very appealing oxidation reactions.[799–802] The 12MR channels of Ti-beta were accessible to larger reactants as compared to Ti-silicalite, thus expanding the possibility to catalyze the oxyfunctionalization of bulkier alkanes, among others.[796]

Recently, the preparation of Ti-beta zeolites with higher Ti loading than those prepared by conventional hydrothermal synthesis and with the majority of the Ti as isolated Ti^{IV} in framework positions was achieved by means of a two-step post-synthetic method.[803] The high Ti contents and the possibility of controlling the hydrophobicity/hydrophilicity of the final materials was expected to have a positive influence on their catalytic performance.

Regiospecific oxyfunctionalization of C_{5+} alkanes by oxidation of the hydrocarbon chain at the terminal or penultimate position, leading to linear terminal alcohols or acids, are reactions of high interest, because of the high value of these oxygenated products as intermediates in the chemical and pharmaceutical industry. In this line, Thomas and co-workers have thoroughly explored the direct selective terminal oxidation of n-alkanes over metal containing aluminophosphate (AlPO) microporous catalysts. Thus, AlPOs framework Al was partly substituted by small quantities of catalytically active transition metal ions, such as Co, Mn or Fe in high oxidation states and well-defined crystallographic sites. Co(II) and Mn(II) were incorporated to AlPO-18 and AlPO-34, two 8-ring small pore zeotypes with cages,[23,804] and it was during the calcination step required for removing the organic OSDAs, that the oxidation state of Co(II) and MN(II) increased to Co(III) and Mn(III). When used as alkane oxidation catalysts, the selectivity to the different oxygenates was determined by the Co/P ratio. At low ratios n-hexane was selectively converted to terminal alcohols (1-hexanol), whereas at high Co/P ratio the catalysts converted n-hexane to adipic acid. The pore diameter and cage configuration of AlPO-18,[804,805] and AlPO-34,[23] favored the shape-selective conversion at the terminal (C_1) methyl group of the n-alkane chain (see Figure 46a). In contrast,

when AlPO-36 (ATS) or AlPO-5 (AFI 1D 12-), with 1D 12-ring structures and much larger pores than AlPO-18 and AlPO-34, were used as catalysts, the shape selective effect disappeared, as well as the restriction for the n-alkane disposition into the framework, resulting in higher selectivities to products with high carbon numbers.[23] The process faces the difficulty associated with the activation of the C-H bond of primary carbon atoms, with a higher dissociation energy than secondary or tertiary carbons. From the molecular perspective and taking n-hexane as example, computer simulation experiments revealed that when the alkane adopted the state of the lowest energy[806] inside of the chabazite cavity of an AlPO-18 framework, the terminal methyl group tightly fitted into the catalyst pore and the extremes of its van der Waals radii were very close to those of the framework oxygen atoms, thus stabilizing the reactant-substrate pair.

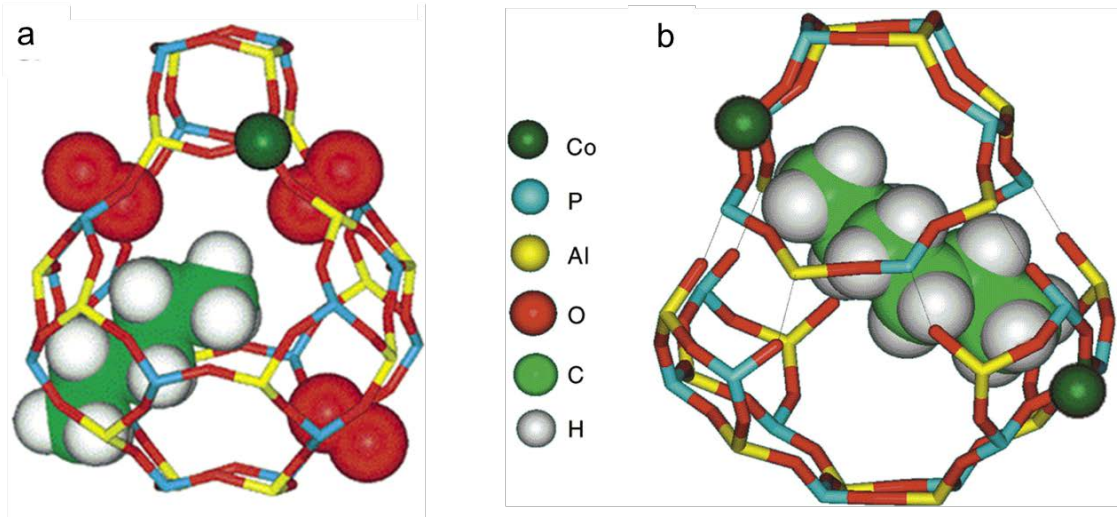

Figure 46. (a) View of a single chabazite cage with a single Co^{II} atom through which molecules of O_2 (red) permeate freely but alkanes (green chain) can enter the chabazite cage only by an end-on approach and (b) energy-minimized configuration of the n-hexane molecule and two separated Co^{II} ions in each cage of the AlPO-18 structure. Adapted from ref.[23] with permission from the American Chemical Society, copyright 2001.

The research conducted by the group of Thomas showed that following this theory not only n-hexane, but also n-octane, n-decane and n-dodecane exhibited high terminal selectivities by preferential oxidation at C_1 and C_2 chain positions, resulting in the production of the corresponding acids, aldehydes or alcohols. As anticipated, the fraction of the metal in the +3 oxidation state within the framework is crucial for the process. Particularly, the CoAlPO-18 catalyst with a Co/P ratio of 0.04 was highly selective to oxidize n-hexane to 1-hexanol.[23] The mechanism of the oxidation of the alkane with molecular oxygen (or air) by the Co and Mn ions in the MAlPO catalyst generally involved free-radicals and it was believed to be ruled by catalytic autoxidation.[804] Proofs of this were the easier oxidation after increasing the coordination number of the transition metal ions from M(II) in the as-prepared molecular sieve to M(III) in the active form, and the lack of oxidizing activity of catalyst containing divalent ions that could not be converted to higher oxidation states, such as Mg(II).[23] In addition, a strong poisoning effect for CoAlPO-18 catalysts was observed upon addition of acetonitrile, a molecule which easily coordinates Co (II) atoms,[807] supporting that the autoxidation proceeds via free radicals formed by interaction with the catalyst and not by free radicals produced in the gas phase.

The selective conversion of n-hexane to adipic acid involves the (oxy)functionalization of both methyl ends of the alkane. Therefore, the synthesis should allow the introduction of two Co(III) ions in each AlPO chabazite cage and preferably in sites opposite to each other. Computational estimations whereby framework Al atoms were spatially random substituted by Co(III) ions showed that this was possible by preparing

Co-AlPO catalysts with Co/P ratios higher than 0.08[806] (see the molecular energy-minimized configuration state in Figure 46b). The selectivity toward adipic acid for the n-hexane oxidation was demonstrated by using Co-AlPO-18 and Co-AlPO-34 molecular sieves as catalysts.[23] Detailed kinetic analysis clarified the reaction mechanism. First, 1-hexanol was predominantly formed, but it was subsequently converted to 1-hexanal and to hexanoic acid. Later, both methyl ends of the alkane chain were activated resulting in increasing selectivities to 1,6-hexanediol and 1,6-hexanedial. Finally, at longer reaction times, they oxidized to adipic acid and the concentration of the former gradually decreased. Interestingly, the hexanoic acid formation reached similar levels as that of adipic acid. Furthermore, the catalytic results indicated that the reaction was not affected by the n-hexane/Co mole ratio. The studies also showed that the Co-AlPO-18 catalysts with Co/P 0.1 was highly stable upon the action of moderate solvents.[808]

The regiospecific oxyfunctionalization of n-alkanes on the terminal position of the hydrocarbon chain by MeAPO type catalysts was questioned by later studies by Iglesia and co-workers for n-hexane oxidation on MnAPO-5 and MnAPO-18, with 1D, 12-ring and 3D, 8-ring + cages channel systems, respectively.[809] n-hexane was converted to different oxidation products included hydroperoxides, alcohols, ketones, aldehydes and acids, with limited terminal selectivity, below 10% (see Figure 47a). The oxidation mechanism proposed here involves the formation and decomposition of alkyl-hydroperoxide intermediates by means of bound radical-like intermediates (see Figure 47b). A similar mechanism was previously proposed for oxidation of cyclohexane on MnAPO-5.[810] The decomposition of hexyl-hydroperoxide on the Mn redox sites was identified as the kinetically-relevant step, and this rate was found to be the same for the

two MeAPOs, indicating that n-hexane easily diffused through the channels systems of both structures. However, the turnover rates observed for oxidation of cyclohehane were significantly lower for the small pore MnAPO-18, due to diffusional limitations.

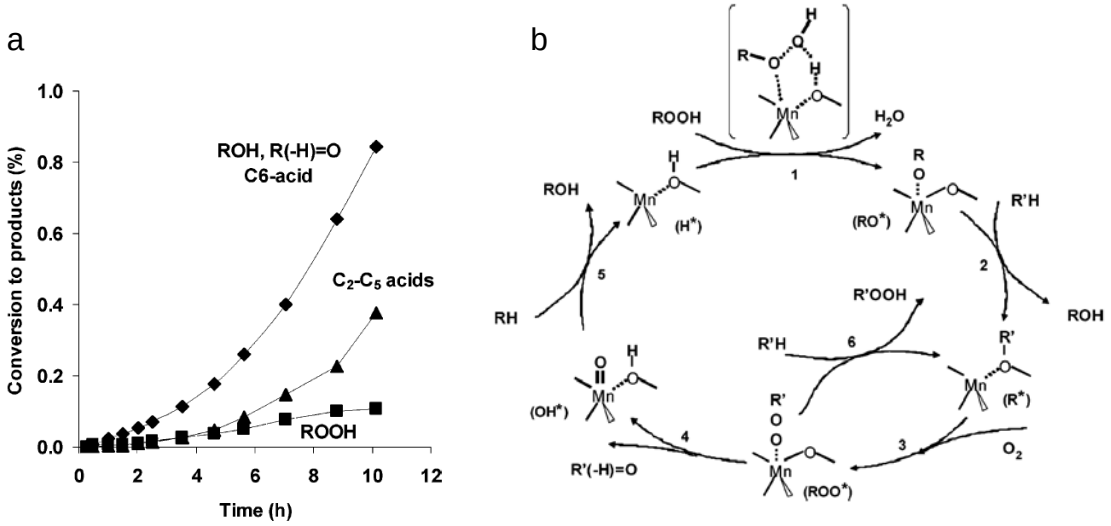

Figure 47. n-hexane conversion to products on MnAPO-18 (a); Cyclic scheme for alkane oxidation on MnAPO materials (b). Reprinted from ref.[809] *with permission from the American Chemical Society, copyright 2007.*

Additional studies of n-hexane oxidation on Mn-exchanged zeolites with different structures evidenced the reaction followed the same ROOH-mediated mechanism as in the case of the MnAPOs.[811] It was concluded that the regiospecific oxidation on terminal positions was strongly affected by the regeneration of the hydroperoxides, by the spatial constrains around the Mn cations, and by extension of non-catalytic, non-selective pathways.

6. OUTLOOK AND PERSPECTIVES

Along the different sections of this review, we have described the nature of the active sites and the role of pore confinement when using microporous zeolite-type materials as catalyst for the activation and conversion of alkanes. Their influence on the reaction mechanisms has been discussed and the challenge of selectively converting the alkanes with high yields has been evidenced, especially in the case of methane and light alkanes.

Activation of methane and its conversion into higher value chemicals and/or fuels following direct sustainable routes is, at present, one of the most attractive but also one of the most ambitious goals within the chemical industry. Much research is being done at the fundamental level, some of which has opened new possibilities for stablishing connections between the activation of methane by enzymes and by well defined active sites formed by two or three metal atoms, in where the cavities of the zeolite also act as a scaffold. However, despite the intense research effort performed in the last decades, upgrading methane to valuable chemicals by means of an efficient and sustainable, environmentally affordable route, has no yet been achieved, and remains a very exciting research subjet.

In the case of methane selective oxidation to methanol, high costs associated to oxidants other than oxygen are the main disadvantage when using Fe-exchanged zeolites. On the other hand, low activity and selectivity are the main drawbacks when using Cu-zeolites in the presence of O2. Now that the active sites and the activation mechanisms in metallozeolite-based catalysts are better understood, it is crucial to direct research efforts to increase the catalytic activity and process efficiency, together with the implementation of strategies for increasing methanol selectivity. Approaches based on

cascade-type reactions, such as the carbonylation of methanol produced by methane hydroxylation in a previous step, appears as an elegant solution that should be further explored.

Increasing catalyst life is the main objective when converting methane under non-oxidative conditions, as coke formation is thermodynamically favored at the high temperatures required for non-oxidative methane-coupling. Moreover, recent studies point to an active contribution of a hydrocarbon-pool-type mechanism to the methane aromatization process and, consequently, coking should be fully integrated as in the case of the methanol to hydrocarbon processes. Two main approaches can be considered. From the catalyst perspective, and despite the large number of zeolites and transition metals studied so far as bifunctional catalysts, there is still room for improvement by specific location of both, the metal species and the BAS. Not only the relative amount of the two catalytic functions but also their position within the zeolite structure may avoid the formation, by shape selectivity, of large aromatic-type coke precursors leading to catalyst deactivation, or may favor the stabilization of selective metal oxocarbide species. From the process perspective, optimization of reaction conditions, such as increasing pressure, or the design of specific reactor configurations, such as circulating fluidized bed systems, operation in cyclic CH_4-H_2 feed switch mode, or the use of membrane reactors are the most interesting approaches.

One step further in methane conversion, from the sustainability and carbon economy perspective, is the carboxylation of methane for direct synthesis of acetic acid. This direct conversion is feasible, as it occurs in marine sediments,[812] and has been achieved in the presence of metallozeolites, although with low conversion and selectivity.[383] The

coordination environment of the metal active species within the zeolite structure will be key in order to simultaneously active CO_2 and CH_4.[384]

Regarding methane's indirect conversion to chemicals via the production of syngas by dry reforming, although not commercially applied so far, could be an interesting alternative to steam reforming, as it involves conversion of both greenhouse gases, methane and CO_2. Stabilization of the active metal species by confinement within zeolite pores and/or cavities could be the answer to catalyst deactivation by metal sintering but a larger effort has to be directed to reducing deactivation by coking.

The processes involving the activation and conversion of light alkanes face similar drawbacks and challenges as those exposed for methane. Their high stability requires high temperatures for conversion under non-oxidative conditions, even in the presence of bi-functional catalysts, favoring coke formation and metal sintering. When working under oxidative conditions, avoiding over-oxidation of the primary products and achieving acceptable selectivities are two important milestones. Also in this case, an efficient alkane conversion will require highly specific catalysts, with the proper combination of structural and chemical features. Again, microporous zeolite-based materials appear as good candidates, as they are able to stabilize specific reaction intermediates or specific metal active sites, controlling in this way, not only the activation of the alkanes, but also their selective conversion to the desired products. In order to improve the design of catalysts based on zeolite-related materials, it is important to understand the catalytic process at the molecular level. The combination of advanced characterization techniques and theoretical modelling has demonstrated to be key for this purpose and is expected to be essential in the near future.[813]

Regarding the activation and upgrading of larger alkanes, most of the reactions described in this review are the basis for well-known mature industrial processes, many of which already employ zeolite-based catalysts. However, the appearance of alkane rich streams from sources alternative to oil, such as the Fischer-Tropsch synthesis or renewable sources such as bio-oils, vegetable oils or lignocellulose remains an incentive for improving and adapting existing technologies and for optimizing the catalysts employed. Again, the zeolite structure and the location of the active sites will play an important role in the final selectivity obtained. Nevertheless, in the case of these larger alkanes, with larger diffusion limitations, the accessibility of the active sites will be an issue of special concern. Thus, synthesizing nanocrystalline zeolites and optimizing hierarchical zeolite-type materials with inter- and/or intracrystalline mesoporosity on the one-hand, and controlling active site location within specific pores and/or cavities of the microporous structure on the other, will be key approaches for the design of efficient catalysts for C_{5+} alkanes conversion.

Besides the processes described in this review, new routes for alkane functionalization need to be explored, such as for instance, the selective halogenation of alkanes, the insertion of carbynes and nitrenes, regioselective catalysis by single metal atoms or aerobic oxidation in liquid phase. Alkane halogenation is an important reaction for the production of chemicals, pharmaceuticals and polymers, which proceeds through a radical mechanism, where controlling the product distribution becomes a difficult task. It would be highly interesting to study the reactivity of isolated Cu species in zeolites, as well as subnanometric Cu clusters for oxyhalogenation of alkanes in the zeolitic confined spaces.[814] Functionalization of alkanes by activation of C-H bonds and insertion of

carbine and nitrene is possible nowadays in the presence of molecular Rh-metal complexes,[815] but has never been achieved using solid catalysts. In a different approach, and taking into account that single metal atoms (Pt, Ir, Rh) can be stabilized within the zeolite structure, it would be worth exploring the combined effect of those active metal sites when interacting with the adequate framework atoms within a selected cavity or pore and their suitability for catalyzing regioselective reactions. Finally, the aerobic oxidation of alkanes in liquid phase usually follows a radical-type mechanism, in which the role of the metal catalyst is the production of oxygen radicals for sustaining the chain reaction. The use of metallozeolite-based catalysts in these type of processes may provide important benefits, as was already shown for the oxidation of cyclohexane to cyclohexanone, an intermediate for the production of caprolactame, efficiently performed in the presence of metal-containing zeolites.

AKNOWLEDGEMENTS

This work has been supported by EU through ERC-AdG-2014-671093 (SynCatMatch), by the Spanish Government-MICINN through “Severo Ochoa” (SEV-2016-0683) and RTI2018-101033-B-I00, and by Generalitat Valenciana (AICO/2019/060).

REFERENCES

1 P. Lanzafame, S. Abate, C. Ampelli, C. Genovese, R. Passalacqua, G. Centi and S. Perathoner, *ChemSusChem*, 2017, **10**, 4409–4419.

2 E. McFarland, *Science*, 2012, **338**, 340-342.

3 J. N. Armor, *J. Energy Chem.*, 2013, **22**, 21–26.

4 A. Corma, E. Corresa, Y. Mathieu, L. Sauvanaud, S. Al-Bogami, M. S. Al-Ghrami and A. Bourane, *Catal. Sci. Technol.*, 2017, **7**, 12–46.

5 M. Al Abdullah, A. Rodriguez Gomez, J. Vittenet, A. Bendjeriou-Sedjerari, W. Xu, I. A. Abba and J. Gascon, *ACS Catal.*, 2020, **10**, 8131-8140.

6 G. Centi, *ChemSusChem*, 2015, **8**, 212–216.

7 Q.-L. Zhou, *Angew. Chem., Int. Ed.*, 2016, **55**, 5352–5353.

8 B. Cornils and W. A. Herrmann, *J. Catal.*, 2003, **216**, 23–31.

9 D. J. Cole-Hamilton, *Science*, 2003, **299**, 1702-1706.

10 E. M. Gallego, M. T. Portilla, C. Paris, A. León-Escamilla, M. Boronat, M. Moliner and A. Corma, *Science*, 2017, **355**, 1051-1054.

11 P. Ferri, C. Li, C. Paris, A. Vidal-Moya, M. Moliner, M. Boronat and A. Corma, *ACS Catal.*, 2019, **9**, 11542–11551.

12 C. Li, C. Paris, J. Martinez-Triguero, M. Boronat, M. Moliner and A. Corma, *Nat. Catal.*, 2018, **1**, 547–554.

13 B. E. R. Snyder, M. L. Bols, R. A. Schoonheydt, B. F. Sels and E. I. Solomon, *Chem. Rev.*, 2018, **118**, 2718–2768.

14 A. Corma, *Chem. Rev.*, 1995, **95**, 559–614.

15 A. Corma, *Chem. Rev.*, 1997, **97**, 2373-2420.

16 M. E. Davis, *Chem. Mater.*, 2014, **26**, 239–245.

17 M. E. Potter, *ACS Catal.*, 2020, **10**, 9758–9789.

18 J. W. Harris, J. S. Bates, B. C. Bukowski, J. Greeley and R. Gounder, *ACS Catal.*, 2020, **10**, 9476–9495.

19 C. Martínez and A. Corma, *Coord. Chem. Rev.*, 2011, **255**, 1558–1580.

20 W. Vermeiren and J. P. Gilson, *Top. Catal.*, 2009, **52**, 1131–1161.

21 E. T. C. Vogt, G. T. Whiting, A. Dutta Chowdhury and B. M. Weckhuysen, in *Advances in Catalysis*, ed. F. C. B. T.-A. in C. Jentoft, Academic Press, 2015, vol. 58, pp. 143–314.

22 A. Corma, *J. Catal.*, 2003, **216**, 298–312.

23 J. M. Thomas, R. Raja, G. Sankar and R. G. Bell, *Acc. Chem. Res.*, 2001, **34**, 191–200.

24 R. van Santen, in *Catalysis*, Wiley-VCH Verlag GmbH & Co. KGaA, 2012, pp. 325–340.

25 J. Weitkamp, *ChemCatChem*, 2012, **4**, 292–306.

26 L. Liu and A. Corma, *Chem. Rev.*, 2018, **118**, 4981–5079.

27 V. Van Speybroeck, K. Hemelsoet, L. Joos, M. Waroquier, R. G. Bell and C. R. A. Catlow, *Chem. Soc. Rev.*, 2015, **44**, 7044–7111.

28 Z.-J. Zhao, C. Chiu and J. Gong, *Chem. Sci.*, 2015, **6**, 4403–4425.

29 W. Zhang, S. Xu, X. Han and X. Bao, *Chem. Soc. Rev.*, 2012, **41**, 192–210.

30 D. I. Sharapa, D. E. Doronkin, F. Studt, J.-D. Grunwaldt and S. Behrens, *Adv. Mater.*, 2019, **31**, 1807381.

31 L. B. McCusker, in *Compr. Supramol. Chem.*, Elsevier, 1996, vol. 7, pp. 393–423.

32 D. E. W. Vaughan, in *Compr. Supramol. Chem.*, Elsevier, 1996, vol. 7, pp. 379–391.

33 W. M. Meier and C. Baerlocher, *Mol. Sieves*, 1999, **2**, 141–161.

34 M. E. Davis and R. F. Lobo, *Chem. Mater.*, 1992, **4**, 756–768.

35 M. Moliner, C. Martínez and A. Corma, *Angew. Chem., Int. Ed.*, 2015, **54**, 3560–3579.

36 C. Colella and W. S. Wise, *Microporous Mesoporous Mater.*, 2014, **189**, 4–10.

37 International Zeolite Asociation, http://www.iza-online.org/, accessed November 2020.

38 P. Misaelides, *Microporous Mesoporous Mater.*, 2011, **144**, 15–18.

39 S. Wang and Y. Peng, *Chem. Eng. J.*, 2010, **156**, 11–24.

40 T. Maesen, in *Stud. Surf. Sci. Catal.*, 2007, **168**, 1–12.

41 J. Shi, Y. Wang, W. Yang, Y. Tang and Z. Xie, *Chem. Soc. Rev.*, 2015, **44**, 8877–8903.

42 C. S. Cundy and P. A. Cox, *Chem. Rev.*, 2003, **103**, 663-670 .

43 C. S. Cundy and P. A. Cox, *Microporous Mesoporous Mater.*, 2005, **82**, 1–78.

44 A. Corma and M. E. Davis, *ChemPhysChem*, 2004, **5**, 304–313.

45 J. Li, A. Corma and J. Yu, *Chem. Soc. Rev.*, 2015, **44**, 7112–7127.

46 A. Corma, M. J. Diaz-Cabanas, J. L. Jorda, C. Martinez and M. Moliner, *Nature*, 2006, **443**, 842–845.

47 A. Corma, M. J. Diaz-Cabanas, J. Jiang, M. Afeworki, D. L. Dorset, S. L. Soled and K. G. Strohmaier, *Proc. Natl. Acad. Sci.,* 2010, **107**, 13997-14002.

48 J. Jiang, J. L. Jorda, J. Yu, L. A. Baumes, E. Mugnaioli, M. J. Diaz-Cabanas, U. Kolb and A. Corma, *Science*, 2011, **333**, 1131–1134.

49 R. M. Barrer and P. J. Denny, *J. Chem. Soc.*, 1961, 971-982.

50 M. Moliner, F. Rey and A. Corma, *Angew. Chem., Int. Ed.*, 2013, **52**, 13880–13889.

51 M. Dusselier and M. E. Davis, *Chem. Rev.*, 2018, **118**, 5265–5329.

52 S. I. Zones, M. M. Olmstead and D. S. Santilli, *J. Am. Chem. Soc.*, 1992, **114**, 4195–4201.

53 S. I. Zones and S.-J. Hwang, *Chem. Mater.*, 2002, **14**, 313–320.

54 A. Jackowski, S. I. Zones, S.-J. Hwang and A. W. Burton, *J. Am. Chem. Soc.*, 2009, **131**, 1092–1100.

55 P. Wagner, Y. Nakagawa, G. S. Lee, M. E. Davis, S. Elomari, R. C. Medrud and S. I. Zones, *J. Am. Chem. Soc.*, 2000, **122**, 263–273.

56 D. L. Dorset, G. J. Kennedy, K. G. Strohmaier, M. J. Diaz-Cabanas, F. Rey and A. Corma, *J. Am. Chem. Soc.*, 2006, **128**, 8862–8867.

57 R. Simancas, D. Dari, N. Velamazán, M. T. Navarro, A. Cantín, J. L. Jordá, G. Sastre, A. Corma and F. Rey, *Science*, 2010, **330**, 1219-1222.

58 A. Corma, F. Rey, J. Rius, M. J. Sabater and S. Valencia, *Nat. (London, U. K.)*, 2004, **431**, 287–290.

59 R. Martinez-Franco, A. Cantin, A. Vidal-Moya, M. Moliner and A. Corma, *Chem. Mater.*, 2015, **27**, 2981–2989.

60 R. Martinez-Franco, M. Moliner, Y. Yun, J. Sun, W. Wan, X. Zou and A. Corma, *Proc. Natl. Acad. Sci. U. S. A.*, 2013, **110**, 3749–3754.

61 R. E. Morris, *Stud. Surf. Sci. Catal.*, 2008, **174A**, 33–42.

62 E. R. Parnham and R. E. Morris, *J. Am. Chem. Soc.*, 2006, **128**, 2204–2205.

63 V. J. Margarit, E. M. Gallego, C. Paris, M. Boronat, M. Moliner and A. Corma, *Green*

Chem., 2020, **22**, 5123-5131.

64 J. Wang, J. Song, C. Yin, Y. Ji, Y. Zou and F.-S. Xiao, *Microporous Mesoporous Mater.*, 2009, **117**, 561–569.

65 H. Lee, S. I. Zones and M. E. Davis, *Nature*, 2003, **425**, 385–388.

66 X. Meng, B. Xie and F.-S. Xiao, *Chinese J. Catal.*, 2009, **30**, 965–971.

67 B. Xie, J. Song, L. Ren, Y. Ji, J. Li and F.-S. Xiao, *Chem. Mater.*, 2008, **20**, 4533-4535.

68 K. Iyoki, Y. Kamimura, K. Itabashi, A. Shimojima and T. Okubo, *Chem. Lett.*, 2010, **39**, 730-731.

69 K. Itabashi, Y. Kamimura, K. Iyoki, A. Shimojima and T. Okubo, *J. Am. Chem. Soc.*, 2012, **134**, 11542–11549.

70 X. Meng and F.-S. Xiao, *Chem. Rev.*, 2014, **114**, 1521–1543.

71 J. Liu and J. Yu, in *Zeolites and Zeolite-like Materials*, eds. B. F. Sels and L. M. Kustov, Elsevier B.V., 2016, pp. 1–32.

72 L. Ren, Q. Wu, C. Yang, L. Zhu, C. Li, P. Zhang, H. Zhang, X. Meng and F.-S. Xiao, *J. Am. Chem. Soc.*, 2012, **134**, 15173–15176.

73 R. E. Morris and S. L. James, *Angew. Chem., Int. Ed.*, 2013, **52**, 2163–2165.

74 A. Corma, V. Fornes, S. B. Pergher, T. Maesen and J. G. Buglass, *Nature*, 1998, **396**, 353–356.

75 M. Choi, K. Na, J. Kim, Y. Sakamoto, O. Terasaki and R. Ryoo, *Nature*, 2009, **461**, 246–249.

76 H. Y. Luo, V. K. Michaelis, S. Hodges, R. G. Griffin and Y. Roman-Leshkov, *Chem. Sci.*, 2015, **6**, 6320-6324.

77 A. Corma, U. Diaz, M. E. Domine and V. Fornes, *Angew. Chem., Int. Ed.*, 2000, **39**, 1499–1501.

78 V. J. Margarit, M. E. Martínez-Armero, M. T. Navarro, C. Martínez and A. Corma, *Angew. Chem., Int. Ed.*, 2015, **54**, 13724–13728.

79 R. Martinez-Franco, C. Paris, M. E. Martinez-Armero, C. Martinez, M. Moliner and A. Corma, *Chem. Sci.*, 2016, **7**, 102–108.

80 S. Mintova, M. Jaber and V. Valtchev, *Chem. Soc. Rev.*, 2015, **44**, 7207–7233.

81 V. J. Margarit, M. R. Díaz-Rey, M. T. Navarro, C. Martínez and A. Corma, *Angew. Chem., Int. Ed.*, 2018, **57**, 3459–3463.

82 W. J. Roth, P. Nachtigall, R. E. Morris, P. S. Wheatley, V. R. Seymour, S. E. Ashbrook, P. Chlubná, L. Grajciar, M. Položij, A. Zukal, O. Shvets and J. Čejka, *Nat. Chem.*, 2013, **5**, 628–633.

83 Z. Huang, S. Seo, J. Shin, B. Wang, R. G. Bell, S. B. Hong and X. Zou, *Nat. Commun.*, 2020, **11**, 1-7.

84 J. B. Nagy, R. Aiello, G. Giordano, A. Katovic, F. Testa, Z. Konya and I. Kiricsi, *Mol. Sieves*, 2007, **5**, 365–478.

85 C. Li, M. Moliner and A. Corma, *Angew. Chem., Int. Ed.*, 2018, **57**, 15330–15353.

86 A. Corma, M. Moliner, F. Rey and A. Corma, 2013, **52**, 13880–13889.

87 J. Jiang, J. Yu and A. Corma, *Angew. Chem., Int. Ed.*, 2010, **49**, 3120–3145.

88 J. Yu and R. Xu, *Acc. Chem. Res.*, 2010, **43**, 1195–1204.

89 J. Přech, P. Pizarro, D. P. Serrano and J. Čejka, *Chem. Soc. Rev.*, 2018, **47**, 8263–8306.

90 P. Eliasova, M. Opanasenko, P. S. Wheatley, M. Shamzhy, M. Mazur, P. Nachtigall, W. J. Roth, R. E. Morris and J. Cejka, *Chem. Soc. Rev.*, 2015, **44**, 7177–7206.

91 M. Moliner, A. Corma and Y. Roman-Leshkov, *Acc. Chem. Res.*, 2019, **52**, 2971–2980.

92 Z. Jensen, E. Kim, S. Kwon, T. Z. H. Gani, Y. Roman-Leshkov, M. Moliner, A. Corma and E. Olivetti, *ACS Cent. Sci.*, 2019, **5**, 892–899.

93 G. W. Huber, S. Iborra and A. Corma, *Chem. Rev.*, 2006, **106**, 4044–4098.

94 T. F. Degnan Jr., *J. Catal.*, 2003, **216**, 32–46.

95 B. Smit and T. L. M. Maesen, *Nature*, 2008, **451**, 671–678.

96 M. Boronat and A. Corma, *ACS Catal.*, 2019, **9**, 1539–1548.

97 R. Gounder and E. Iglesia, *Chem. Commun.*, 2013, **49**, 3491-3509.

98 D. Lesthaeghe, V. Van Speybroeck and M. Waroquier, *Phys. Chem. Chem. Phys.*, 2009, **11**, 5222-5226.

99 H. Shi, S. Eckstein, A. Vjunov, D. M. Camaioni and J. A. Lercher, *Nat. Commun.*, 2017, **8**, 1-9.

100 R. Gounder and E. Iglesia, *Acc. Chem. Res.*, 2012, **45**, 229–238.

101 A. Corma, V. Forn, J. Mart, S. B. Pergher, V. Fornes, J. Martinez-Triguero and S. B. Pergher, *J. Catal.*, 1999, **186**, 57–63.

102 U. Diaz and A. Corma, *Dalt. Trans.*, 2014, **43**, 10292–10316.

103 A. Corma, U. Diaz, V. Fornes, J. M. Guil, J. Martinez-Triguero and E. J. Creyghton, *J. Catal.*, 2000, **191**, 218-224.

104 A. Corma, V. Fornes and U. Diaz, *Chem. Commun.*, 2001, **24**, 2642–2643.

105 D. Verboekend, N. Nuttens, R. Locus, J. Van Aelst, P. Verolme, J. C. Groen, J. Perez-Ramirez and B. F. Sels, *Chem. Soc. Rev.*, 2016, **45**, 3331–3352.

106 K. Li, J. Valla and J. Garcia-Martinez, *ChemCatChem*, 2014, **6**, 46–66.

107 K. Na, M. Choi and R. Ryoo, *Microporous Mesoporous Mater.*, 2013, **166**, 3–19.

108 M. Moliner, *ISRN Mater. Sci.*, 2012, **2012**, 1-24.

109 D. Verboekend and J. Perez-Ramirez, *Catal. Sci. Technol.*, 2011, **1**, 879–890.

110 V. Blay, B. Louis, R. Miravalles, T. Yokoi, K. A. Peccatiello, M. Clough and B. Yilmaz, *ACS Catal.*, 2017, **7**, 6542–6566.

111 W. Wang, C.-J. Liu and W. Wu, *Catal. Sci. Technol.*, 2019, **9**, 4162–4187.

112 E. T. C. Vogt and B. M. Weckhuysen, *Chem. Soc. Rev.*, 2015, **44**, 7342–7370.

113 M. Moliner, C. Martínez and A. Corma, *Chem. Mater.*, 2014, **26**, 246–258.

114 M. J. Climent, A. Corma and S. Iborra, *Chem. Rev.*, 2011, **111**, 1072-1133.

115 A. Corma, J. Planelles, J. Sanchez-Marin and F. Tomas, *J. Catal.*, 1985, **93**, 30–37.

116 W. O. Haag and R. M. Dessau, in *8th Int. Congress on Catalysis*, Berlin, 1984, vol. 2, p. 305.

117 N. Kosinov, F. J. A. G. Coumans, E. A. Uslamin, A. S. G. Wijpkema, B. Mezari and E. J. M. Hensen, *ACS Catal.*, 2017, **7**, 520–529.

118 H. Saito and Y. Sekine, *RSC Adv.*, 2020, **10**, 21427–21453.

119 A. Hagen and F. Roessner, *Catal. Rev. Sci. Eng.*, 2000, **42**, 403–437.

120 S. R. Kanitkar and J. J. Spivey, in *Natural Gas Processing from Midstream to Downstream*, eds. N. O. Elbashir, M. M. El-Halwagi, I. G. Economou and K. R. Hall, John Wiley & Sons Ltd., 1st edn., 2019, pp. 379–401.

121 A. Bhan, R. Gounder, J. Macht and E. Iglesia, *J. Catal.*, 2008, **253**, 221-224.

122 R. Gounder and E. Iglesia, *J. Am. Chem. Soc.*, 2009, **131**, 1958-1971.

123 F. Eder and J. A. Lercher, *Zeolites*, 1997, **18**, 75-81.

124 F. Eder, M. Stockenhuber and J. A. Lercher, *J. Phys. Chem. B*, 1997, **101**, 5414-5419.

125 L. Liu, U. Diaz, R. Arenal, G. Agostini, P. Concepcion and A. Corma, *Nat. Mater.*, 2017, **16**, 132–138.

126 L. Liu, M. Lopez-Haro, C. W. Lopes, C. Li, P. Concepcion, L. Simonelli, J. J. Calvino and A. Corma, *Nat. Mater.*, 2019, **18**, 866–873.

127 M. Moliner, J. Gabay, C. Kliewer, P. Serna and A. Corma, *ACS Catal.*, 2018, **8**, 9520–9528.

128 M. Moliner, J. E. Gabay, C. E. Kliewer, R. T. Carr, J. Guzman, G. L. Casty, P. Serna and A. Corma, *J. Am. Chem. Soc.*, 2016, **138**, 15743–15750.

129 L. Liu, M. Lopez-Haro, D. M. Meira, P. Concepcion, J. J. Calvino, and A.Corma, *Angew. Chem., Int. Ed.*, 2020, **59**, 15695-15702.

130 G. J. Hutchings and M. S. Scurrell, *Cattech*, 2003, **7**, 90–103.

131 W. Zhou, K. Cheng, J. Kang, C. Zhou, V. Subramanian, Q. Zhang and Y. Wang, *Chem. Soc. Rev.*, 2019, **48**, 3193–3228.

132 C. B. Roberts and N. O. Elbashir, *Fuel Process. Technol.*, 2003, **83**, 1–9.

133 S. Wang, I. Agirrezabal-Telleria, A. Bhan, D. Simonetti, K. Takanabe and E. Iglesia, *Faraday Discuss.*, 2017, **197**, 9–39.

134 L. Petrus and M. A. Noordermeer, *Green Chem.*, 2006, **8**, 861–867.

135 E. V Kondratenko, T. Peppel, D. Seeburg, V. A. Kondratenko, N. Kalevaru, A. Martin and S. Wohlrab, *Catal. Sci. Technol.*, 2017, **7**, 366–381.

136 P. Schwach, X. Pan and X. Bao, *Chem. Rev.*, 2017, **117**, 8497–8520.

137 S. Abate, G. Centi and S. Perathoner, CRC Press, 2015, pp. 3–49.

138 S. Perathoner, S. Gross, E. J. M. Hensen, H. Wessel, H. Chraye and G. Centi, *ChemCatChem*, 2017, **9**, 904–909.

139 L. Yang, X. Ge, C. Wan, F. Yu and Y. Li, *Renew. Sustain. Energy Rev.*, 2014, **40**, 1133–1152.

140 K. Kaygusuz, *J. Eng. Res. Appl. Sci.*, 2015, **4**, 317-327.

141 Energy Information Adminstration EIA, USA (2017) World natural gas consumption by region, Reference case, 2015–2050, accessed October 2020.

142 A. Caballero and P. J. Pérez, *Chem. Soc. Rev.*, 2013, **42**, 8809–8820.

143 K. Aasberg-Petersen, I. Dybkjær, C. V Ovesen, N. C. Schjødt, J. Sehested and S. G. Thomsen, *J. Nat. Gas Sci. Eng.*, 2011, **3**, 423–459.

144 R. C. Baliban, J. A. Elia and C. A. Floudas, *AIChE J.*, 2013, **59**, 505–531.

145 E. F. Sousa-Aguiar, F. B. Noronha and A. Faro Jr., *Catal. Sci. Technol.*, 2011, **1**, 22–37.

146 E. F. Sousa-Aguiar, L. Gorestin, C. Mota, L. G. Appel and C. Mota, *Catal. Today*, 2005, **101**, 3–7.

147 D. A. Wood, C. Nwaoha and B. F. Towler, *J. Nat. Gas Sci. Eng.*, 2012, **9**, 196–208.

148 A. Salvatore, C. Gabriele and P. Siglinda, in *Small-Scale Gas to Liquid Fuel Synthesis*, CRC Press, 2015, pp. 3–50.

149 M. Gharibi, F. T. Zangeneh, F. Yaripour and S. Sahebdelfar, *Appl. Catal. A.*, 2012, **443**–**444**, 8–26.

150 J. H. Lunsford, *Catal. Today*, 2000, **63**, 165–174.

151 A. Martínez, G. Prieto, A. García-trenco and E. Peris, in *Zeolites and Catalysis*, ed. S. Cejka, J., Corma A., Zones, Wiley-VCH, Weinhem, Germany, 2010, pp. 649–685.

152 K. T. Dinh, M. M. Sullivan, P. Serna, R. J. Meyer, M. Dincă and Y. Román-Leshkov, *ACS Catal.*, 2018, **8**, 8306–8313.

153 M. H. Mahyuddin, Y. Shiota, A. Staykov and K. Yoshizawa, *Acc. Chem. Res.*, 2018, **51**, 2382–2390.

154 H. Liu, L. Su, H. Wang, W. Shen, X. Bao and Y. Xu, *Appl. Catal. A.*, 2002, **236**, 263–280.

155 M. T. Portilla, F. J. Llopis and C. Martinez, *Catal. Sci. Technol.*, 2015, **5**, 3806–3821.

156 N. Kosinov, A. S. G. Wijpkema, E. Uslamin, R. Rohling, F. J. A. G. Coumans, B. Mezari, A. Parastaev, A. S. Poryvaev, M. V Fedin, E. A. Pidko and E. J. M. Hensen, *Angew. Chem., Int. Ed.*, 2018, **57**, 1016–1020.

157 S. J. Han, S. K. Kim, A. Hwang, S. Kim, D. Y. Hong, G. Kwak, K. W. Jun and Y. T. Kim, *Appl. Catal. B*, 2019, **241**, 305–318.

158 K. Skutil and M. Taniewski, *Fuel Process. Technol.*, 2007, **88**, 877–882.

159 Y. Li, L. Su, H. Wang, H. Liu, W. Shen, X. Bao and Y. Xu, *Catal. Letters*, 2003, **89**, 275–279.

160 K. Skutil and M. Taniewski, *Fuel Process. Technol.*, 2006, **87**, 511–521.

161 A. Machocki and A. Denis, *Chem. Eng. J.*, 2002, **90**, 165–172.

162 P. J. Byrne, E. J. Gohr, E. N. J. and R. T. Haslam, *Ind. Eng. Chem.*, 1932, **24**, 1129–1135.

163 J. P. Van Hook, *Catal. Rev. Sci. Eng.*, 1980, **21**, 1–51.

164 J. Rostrup-Nielsen, I. Dybkjaer and L. J. Christiansen, *NATO ASI Ser. E Appl. Sci.*, 1992, **225**, 249–281.

165 O. Machhammer, A. Bode and W. Hormuth, *Chem. Eng. Technol.*, 2016, **39**, 1185–1193.

166 W. Gac, T. Borowiecki and P. Kowalik, in *Nanotechnol. Catal.*, Wiley-VCH Verlag GmbH & Co. KGaA, 2017, vol. 2, pp. 401–420.

167 D. Pakhare and J. Spivey, *Chem. Soc. Rev.*, 2014, **43**, 7813–7837.

168 W. Taifan and J. Baltrusaitis, *Appl. Catal. B*, 2016, **198**, 525–547.

169 E. Meloni, M. Martino and V. Palma, *Catalysts*, 2020, **10**, 352-390.

170 H. Wu, V. La Parola, G. Pantaleo, F. Puleo, A. M. Venezia and L. F. Liotta, *Catalysts*, 2013, **3**, 563–583.

171 L. Chen, Z. Qi, S. Zhang, J. Su and G. A. Somorjai, *Catalysts*, 2020, **10**, 858-876.

172 M. Mosinska, M. I. Szynkowska and P. Mierczynski, *Catalysts*, 2020, **10**, 896-922.

173 A. Al-Ubaid and E. E. Wolf, *Appl. Catal.*, 1987, **34**, 119–134.

174 T. E. Solh, K. Jarosch and H. I. de Lasa, *Appl. Catal. A*, 2001, **210**, 315–324.

175 J. Zhang, T. Zhang, X. Zhang, W. Liu, H. Liu, J. Qiu and K. L. Yeung, *Catal. Today*, 2014, **236**, 34–40.

176 N. Wei, J. Zhang, H. Zhong, L. Pan, Y. Zhou and C. Cao, *J. Nanosci. Nanotechnol.*, 2019, **19**, 5831–5837.

177 U. Cimenler, B. Joseph and J. N. Kuhn, *Appl. Catal. A*, 2015, **505**, 494–500.

178 Z. Li, Z. Wang and S. Kawi, *ChemCatChem*, 2019, **11**, 202–224.

179 C. E. Figueira, P. F. Moreira, R. Giudici, R. M. B. Alves and M. Schmal, *Appl. Catal. A*, 2018, **550**, 297–307.

180 Z. Li, Z. Wang, B. Jiang and S. Kawi, *Catal. Sci. Technol.*, 2018, **8**, 3363–3371.

181 N. Wang, X. Yu, Y. Wang, W. Chu and M. Liu, *Catal. Today*, 2013, **212**, 98–107.

182 D. Liu, X. Y. Quek, W. N. E. Cheo, R. Lau, A. Borgna and Y. Yang, *J. Catal.*, 2009, **266**, 380–390.

183 H. Jiang, W. Hua, H. Li and Y. Dai, *Adv. Mater. Res.*, 2013, **650**, 85–91.

184 H. Drobna, M. Kout, A. Soltysek, V. M. Gonzalez-Delacruz, A. Caballero and L. Capek, *React. Kinet. Mech. Catal.*, 2017, **121**, 255–274.

185 A. Luengnaruemitchai and A. Kaengsilalai, *Chem. Eng. J.*, 2008, **144**, 96–102.

186 U. Cimenler, B. Joseph and J. N. Kuhn, *Energy & Fuels*, 2016, **30**, 5300–5308.

187 U. Cimenler, B. Joseph and J. N. Kuhn, *AIChE J.*, 2017, **63**, 200–207.

188 J. Zhang, X. Zhang, W. Liu, H. Liu, J. Qiu and K. L. Yeung, *J. Power Sources*, 2014, **246**, 74–83.

189 F. Dalena, A. Senatore, A. Marino, A. Gordano, M. Basile and A. Basile, in *Methanol Science and Engineering*, eds. A. Basile and F. B. T.-M. Dalena, Elsevier, 2018, pp. 3–28.

190 F. Dalena, A. Senatore, M. Basile, S. Knani, A. Basile and A. Iulianelli, *Membranes*, 2018, **8**, 98-125.

191 V. Arutyunov, in *Methanol Science and Engineering*, eds. A. Basile and F. B. T.-M. Dalena, Elsevier, 2018, pp. 129–172.

192 G. A. Olah, *Angew. Chem., Int. Ed.*, 2005, **44**, 2636–2639.

193 M. O. Ross and A. C. Rosenzweig, *JBIC, J. Biol. Inorg. Chem.*, 2017, **22**, 307-319.

194 M. Ravi, V. L. Sushkevich, A. J. Knorpp, M. A. Newton, D. Palagin, A. B. Pinar, M. Ranocchiari and J. A. van Bokhoven, *Nat. Catal.*, 2019, **2**, 485–494.

195 M. H. Mahyuddin, Y. Shiota and K. Yoshizawa, *Catal. Sci. Technol.*, 2019, **9**, 1744–1768.

196 H. S. Lacheen and E. Iglesia, *Phys. Chem. Chem. Phys.*, 2005, **7**, 538–547.

197 R. Sharma, H. Poelman, G. B. Marin and V. V Galvita, *Catalysts*, 2020, **10**, 194-220.

198 A. R. Kulkarni, Z.-J. Zhao, S. Siahrostami, J. K. Norskov and F. Studt, *Catal. Sci. Technol.*, 2018, **8**, 114-123.

199 G. J. Hutchings, *Top. Catal.*, 2016, **59**, 658-662.

200 P. Vanelderen, J. Vancauwenbergh, B. F. Sels and R. A. Schoonheydt, *Coord. Chem. Rev.*, 2013, **257**, 483–494.

201 P. Haack and C. Limberg, *Angew. Chem., Int. Ed.*, 2014, **53**, 4282–4293.

202 E. Borfecchia, P. Beato, S. Svelle, U. Olsbye, C. Lamberti and S. Bordiga, *Chem. Soc. Rev.*, 2018, **47**, 8097–8133.

203 M. A. Newton, A. J. Knorpp, V. L. Sushkevich, D. Palagin and J. A. van Bokhoven, *Chem. Soc. Rev.*, 2020, **49**, 1449–1486.

204 Z. R. Jovanovic, J.-P. Lange, M. Ravi, A. J. Knorpp, V. L. Sushkevich, M. A. Newton, D. Palagin and J. A. van Bokhoven, *J. Catal.*, 2020, **385**, 238–245.

205 M. Ravi, M. Ranocchiari and J. A. van Bokhoven, *Angew. Chem., Int. Ed.*, 2017, **56**, 16464-16483.

206 G. I. Pannov, V. I. Sobolev and A. S. Kharitonov, *J. Mol. Catal.*, 1990, **61**, 85–97.

207 V. I. Sobolev, G. I. Panov, A. S. Kharitonov, V. N. Romannikov, A. M. Volodin and K. G. Ione, *J. Catal.*, 1993, **139**, 435–443.

208 K. A. Dubkov, V. I. Sobolev, E. P. Talsi, M. A. Rodkin, N. H. Watkins, A. A. Shteinman and G. I. Panov, *J. Mol. Catal. A Chem.*, 1997, **123**, 155-161.

209 E. V Starokon, M. V Parfenov, L. V Pirutko, S. I. Abornev and G. I. Panov, *J. Phys. Chem. C*, 2011, **115**, 2155–2161.

210 E. V Starokon, M. V Parfenov, S. S. Arzumanov, L. V Pirutko, A. G. Stepanov and G. I. Panov, *J. Catal.*, 2013, **300**, 47-54.

211 M. V Parfenov, E. V Starokon, L. V Pirutko and G. I. Panov, *J. Catal.*, 2014, **318**, 14-21.

212 B. E. R. Snyder, L. H. Böttger, M. L. Bols, J. J. Yan, H. M. Rhoda, A. B. Jacobs, M. Y. Hu, J. Zhao, E. E. Alp, B. Hedman, K. O. Hodgson, R. A. Schoonheydt, B. F. Sels and E. I. Solomon, *Proc. Natl. Acad. Sci.*, 2018, **115**, 4565-4570.

213 B. E. R. Snyder, P. Vanelderen, M. L. Bols, S. D. Hallaert, L. H. Böttger, L. Ungur, K. Pierloot, R. A. Schoonheydt, B. F. Sels and E. I. Solomon, *Nature*, 2016, **536**, 317-321.

214 Y. K. Chow, N. F. Dummer, J. H. Carter, R. J. Meyer, R. D. Armstrong, C. Williams, G. Shaw, S. Yacob, M. M. Bhasin, D. J. Willock, S. H. Taylor and G. J. Hutchings, *ChemPhysChem*, 2018, **19**, 402–411.

215 Y. K. Chow, N. F. Dummer, J. H. Carter, C. Williams, G. Shaw, D. J. Willock, S. H. Taylor, S. Yacob, R. J. Meyer, M. M. Bhasin and G. J. Hutchings, *Catal. Sci. Technol.*, 2018, **8**, 154–163.

216 M. J. Wulfers, S. Teketel, B. Ipek and R. F. Lobo, *Chem. Commun.*, 2015, **51**, 4447–4450.

217 M. L. Bols, S. D. Hallaert, B. E. R. Snyder, J. Devos, D. Plessers, H. M. Rhoda, M. Dusselier, R. A. Schoonheydt, K. Pierloot, E. I. Solomon and B. F. Sels, *J. Am. Chem. Soc.*, 2018, **140**, 12021–12032.

218 J. Devos, M. L. Bols, D. Plessers, C. Van Goethem, J. W. Seo, S.-J. Hwang, B. F. Sels and M. Dusselier, *Chem. Mater.*, 2020, **32**, 273–285.

219 C. Hammond, M. M. Forde, M. H. Ab Rahim, A. Thetford, Q. He, R. L. Jenkins, N. Dimitratos, J. A. Lopez-Sanchez, N. F. Dummer, D. M. Murphy, A. F. Carley, S. H. Taylor, D. J. Willock, E. E. Stangland, J. Kang, H. Hagen, C. J. Kiely and G. J. Hutchings, *Angew. Chem., Int. Ed.*, 2012, **51**, 5129-5133.

220 C. Hammond, R. L. Jenkins, N. Dimitratos, J. A. Lopez-Sanchez, M. H. ab Rahim, M. M. Forde, A. Thetford, D. M. Murphy, H. Hagen, E. E. Stangland, J. M. Moulijn, S. H. Taylor, D. J. Willock and G. J. Hutchings, *Chem. Eur. J.*, 2012, **18**, 15735-15745.

221 C. Hammond, N. Dimitratos, R. L. Jenkins, J. A. Lopez-Sanchez, S. A. Kondrat, M. Hasbi ab Rahim, M. M. Forde, A. Thetford, S. H. Taylor, H. Hagen, E. E. Stangland, J. H. Kang, J. M. Moulijn, D. J. Willock and G. J. Hutchings, *ACS Catal.*, 2013, **3**, 689-699.

222 C. Hammond, N. Dimitratos, J. A. Lopez-Sanchez, R. L. Jenkins, G. Whiting, S. A. Kondrat, M. H. ab Rahim, M. M. Forde, A. Thetford, H. Hagen, E. E. Stangland, J. M. Moulijn, S. H. Taylor, D. J. Willock and G. J. Hutchings, *ACS Catal.*, 2013, **3**, 1835–1844.

223 R. J. Lewis, A. Bara-Estaun, N. Agarwal, S. J. Freakley, D. J. Morgan and G. J. Hutchings, *Catal. Letters*, 2019, **149**, 3066–3075.

224 E. M. Alayon, M. Nachtegaal, M. Ranocchiari and J. A. van Bokhoven, *Chem. Commun.*, 2012, **48**, 404–406.

225 P. Tomkins, A. Mansouri, S. E. Bozbag, F. Krumeich, M. B. Park, E. M. Alayon, M. Ranocchiari and J. A. van Bokhoven, *Angew. Chem., Int. Ed.*, 2016, **55**, 5467-5471.

226 A. J. Knorpp, M. A. Newton, S. C. M. Mizuno, J. Zhu, H. Mebrate, A. B. Pinar and J. A. van Bokhoven, *Chem. Commun.*, 2019, **55**, 11794–11797.

227 V. L. Sushkevich, D. Palagin, M. Ranocchiari and J. A. van Bokhoven, *Science*, 2017, **356**, 523-527.

228 A. Koishybay and D. F. Shantz, *J. Am. Chem. Soc.*, 2020, **142**, 11962–11966.

229 M. H. Groothaert, P. J. Smeets, B. F. Sels, P. A. Jacobs and R. A. Schoonheydt, *J. Am.*

Chem. Soc., 2005, **127**, 1394-1395.

230 J. S. Woertink, P. J. Smeets, M. H. Groothaert, M. A. Vance, B. F. Sels, R. A. Schoonheydt and E. I. Solomon, *Proc. Natl. Acad. Sci.*, 2009, **106**, 18908-18913.

231 P. J. Smeets, R. G. Hadt, J. S. Woertink, P. Vanelderen, R. A. Schoonheydt, B. F. Sels and E. I. Solomon, *J. Am. Chem. Soc.*, 2010, **132**, 14736–14738.

232 M.-L. Tsai, R. G. Hadt, P. Vanelderen, B. F. Sels, R. A. Schoonheydt and E. I. Solomon, *J. Am. Chem. Soc.*, 2014, **136**, 3522–3529.

233 P. Vanelderen, B. E. R. Snyder, M.-L. Tsai, R. G. Hadt, J. Vancauwenbergh, O. Coussens, R. A. Schoonheydt, B. F. Sels and E. I. Solomon, *J. Am. Chem. Soc.*, 2015, **137**, 6383–6392.

234 S. Grundner, M. A. Markovits, G. Li, M. Tromp, E. A. Pidko, E. J. Hensen, A. Jentys, M. Sanchez-Sanchez and J. A. Lercher, *Nat. Commun.*, 2015, **6**, 7546.

235 G. Li, P. Vassilev, M. Sanchez-Sanchez, J. A. Lercher, E. J. M. Hensen and E. A. Pidko, *J. Catal.*, 2016, **338**, 305–312.

236 D. K. Pappas, A. Martini, M. Dyballa, K. Kvande, S. Teketel, K. A. Lomachenko, R. Baran, P. Glatzel, B. Arstad, G. Berlier, C. Lamberti, S. Bordiga, U. Olsbye, S. Svelle, P. Beato and E. Borfecchia, *J. Am. Chem. Soc.*, 2018, **140**, 15270–15278.

237 D. Palagin, A. J. Knorpp, A. B. Pinar, M. Ranocchiari and J. A. van Bokhoven, in *Abstracts of Papers, 253rd ACS National Meeting & Exposition, San Francisco, CA, United States, April 2-6, 2017*, American Chemical Society, 2017, p. ENFL-10.

238 P. J. Smeets, M. H. Groothaert and R. A. Schoonheydt, *Catal. Today*, 2005, **110**, 303–309.

239 D. K. Pappas, E. Borfecchia, K. A. Lomachenko, A. Lazzarini, E. S. Gutteroed, M. Dyballa, A. Martini, G. Berlier, S. Bordiga, C. Lamberti, B. Arstad, U. Olsbye, P. Beato and S. Svelle, *Top. Catal.*, 2019, **62**, 712–723.

240 B. Ipek, M. J. Wulfers, H. Kim, F. Göltl, I. Hermans, J. P. Smith, K. S. Booksh, C. M. Brown and R. F. Lobo, *ACS Catal.*, 2017, **7**, 4291-4303.

241 A. R. Kulkarni, Z.-J. Zhao, S. Siahrostami, J. K. Nørskov and F. Studt, *ACS Catal.*, 2016, **6**, 6531-6536.

242 D. K. Pappas, E. Borfecchia, M. Dyballa, I. A. Pankin, K. A. Lomachenko, A. Martini, M. Signorile, S. Teketel, B. Arstad, G. Berlier, C. Lamberti, S. Bordiga, U. Olsbye, K. P.

Lillerud, S. Svelle and P. Beato, *J. Am. Chem. Soc.*, 2017, **139**, 14961-14975.

243 K. Kvande, D. K. Pappas, M. Dyballa, C. Buono, M. Signorile, E. Borfecchia, K. A. Lomachenko, B. Arstad, S. Bordiga, G. Berlier, U. Olsbye, P. Beato and S. Svelle, *Catalysts*, 2020, **10**, 191-208.

244 K. Narsimhan, K. Iyoki, K. Dinh and Y. Roman-Leshkov, *ACS Cent. Sci.*, 2016, **2**, 424-429.

245 E. M. C. Alayon, M. Nachtegaal, A. Bodi and J. A. van Bokhoven, *ACS Catal.*, 2014, **4**, 16–22.

246 V. L. Sushkevich and J. A. van Bokhoven, *Catal. Sci. Technol.*, 2018, **8**, 4141–4150.

247 M. Dyballa, K. Thorshaug, D. K. Pappas, E. Borfecchia, K. Kvande, S. Bordiga, G. Berlier, A. Lazzarini, U. Olsbye, P. Beato, S. Svelle and B. Arstad, *ChemCatChem*, 2019, **11**, 5022–5026.

248 M. Dyballa, D. K. Pappas, K. Kvande, E. Borfecchia, B. Arstad, P. Beato, U. Olsbye and S. Svelle, *ACS Catal.*, 2019, **9**, 365–375.

249 A. J. Knorpp, M. A. Newton, V. L. Sushkevich, P. P. Zimmermann, A. B. Pinar and J. A. van Bokhoven, *Catal. Sci. Technol.*, 2019, **9**, 2806–2811.

250 N. V Beznis, B. M. Weckhuysen and J. H. Bitter, *Catal. Letters*, 2010, **136**, 52–56.

251 N. V Beznis, A. N. C. van Laak, B. M. Weckhuysen and J. H. Bitter, *Microporous Mesoporous Mater.*, 2010, **138**, 176–183.

252 J. Shan, W. Huang, L. Nguyen, Y. Yu, S. Zhang, Y. Li, A. I. Frenkel and F. (Feng) Tao, *Langmuir*, 2014, **30**, 8558–8569.

253 W. Huang, S. Zhang, Y. Tang, Y. Li, L. Nguyen, Y. Li, J. Shan, D. Xiao, R. Gagne, A. I. Frenkel and F. (Feng) Tao, *Angew. Chem., Int. Ed.*, 2016, **55**, 13441–13445.

254 Z. Jin, L. Wang, E. Zuidema, K. Mondal, M. Zhang, J. Zhang, C. Wang, X. Meng, H. Yang, C. Mesters and F.-S. Xiao, *Science*, 2020, **367**, 193-197.

255 J. Shan, M. Li, L. F. Allard, S. Lee and M. Flytzani-Stephanopoulos, *Nature*, 2017, **551**, 605-608.

256 K. Narsimhan, V. K. Michaelis, G. Mathies, W. R. Gunther, R. G. Griffin and Y. Roman-Leshkov, *J. Am. Chem. Soc.*, 2015, **137**, 1825–1832.

257 G. Keller and M. Bhasin, *J. Catal.*, 1982, **73**, 9-19.

258 W. Hinsen and M. Baerns, *Chem. Zeitung*, 1983, **107**, 223-226.

259 T. Ito and J. H. Lunsford, *Nature*, 1985, **314**, 721–722.

260 J. H. Lunsford, *Angew. Chem., Int. Ed.*, 1995, **34**, 970–980.

261 B. L. Farrell, V. O. Igenegbai and S. Linic, *ACS Catal.*, 2016, **6**, 4340–4346.

262 A. Galadima and O. Muraza, *J. Ind. Eng. Chem.*, 2016, **37**, 1–13.

263 M. Makri, Y. Jiang, I. V Yentekakis and C. G. Vayenas, *Stud. Surf. Sci. Catal.*, 1996, **101**, 387–396.

264 J. H. Lunsford, E. M. Cordi, P. Qiu and M. P. Rosynek, *Stud. Surf. Sci. Catal.*, 1998, **119**, 227–234.

265 A. Machocki, A. Denis, J. Gryglicki and H. Mlynarska, *Stud. Surf. Sci. Catal.*, 2000, **130D**, 3831–3836.

266 Y. Li, T. Wu, W. Shen, X. Bao and Y. Xu, *Catal. Letters*, 2005, **105**, 77–82.

267 R. D. Samarth, S. Y. Chen and K. M. Dooley, *Appl. Catal. B*, 1994, **5**, 71–88.

268 S. Pak, T. Rades, M. P. Rosynek and J. H. Lunsford, *Catal. Letters*, 2000, **66**, 1–4.

269 P. O. Graf and L. Lefferts, *Chem. Eng. Sci.*, 2009, **64**, 2773–2780.

270 S. Arndt, T. Otremba, U. Simon, M. Yildiz, H. Schubert and R. Schomäcker, *Appl. Catal. A*, 2012, **425**–**426**, 53-61.

271 P. Wang, G. Zhao, Y. Wang and Y. Lu, *Sci. Adv.*, 2017, **3**, e1603180.

272 S. Ernst and J. Weitkamp, *Stud. Surf. Sci. Catal.*, 1991, **61**, 25–31.

273 N. Davidova, P. Kovacheva and A. H. Weiss, *Catal. Today*, 1992, **13**, 625–626.

274 P. Kovacheva, K. Arishtirova and N. Davidova, *Appl. Catal. A*, 1997, **163**, 255–260.

275 P. Kovacheva, K. Arishtirova and N. Davidova, *Appl. Catal. A*, 1997, **149**, 277–287.

276 P. Kovacheva, N. Davidova and A. H. Weiss, *Stud. Surf. Sci. Catal.*, 1994, **82**, 403–409.

277 P. Kovacheva, K. Arishtirova and N. Davidova, *Appl. Catal. A*, 1999, **178**, 111–115.

278 P. Kovacheva, A. Predoeva, K. Arishtirova and S. Vassilev, *Appl. Catal. A*, 2002, **223**, 121–128.

279 K. Arishtirova, P. Kovacheva and A. Predoeva, *Appl. Catal. A.*, 2003, **243**, 191–196.

280 S. J. X. He, M. A. Long, M. I. Attalla and M. A. Wilson, *Energy & Fuels*, 1992, **6**, 498–502.

281 S. J. X. He, M. A. Long, M. A. Wilson, M. L. Gorbaty and P. S. Maa, *Energy & Fuels*, 1995,

9, 616–619.

282 S. J. X. He, M. A. Long, M. I. Attalla and M. A. Wilson, *Energy & Fuels*, 1994, **8**, 286–287.

283 M. O. Adebajo, M. A. Long and R. L. Frost, *Catal. Commun.*, 2004, **5**, 125–130.

284 M. O. Adebajo, R. F. Howe and M. A. Long, *Catal. Letters*, 2001, **72**, 221–224.

285 E. M. Kennedy, F. Lonyi, T. H. Ballinger, M. P. Rosynek and J. H. Lunsford, *Energy & Fuels*, 1994, **8**, 846–850.

286 M. O. Adebajo, R. F. Howe and M. A. Long, *Energy & Fuels*, 2001, **15**, 671–674.

287 M. O. Adebajo, *Green Chem.*, 2007, **9**, 526–539.

288 M. Adebajo, M. A. Long and R. F. Howe, *Res. Chem. Intermed.*, 2000, **26**, 185–191.

289 X. Guo, G. Fang, G. Li, H. Ma, H. Fan, L. Yu, C. Ma, X. Wu, D. Deng and M. Wei, *Science*, 2014, **344**, 616-619.

290 Q. Zhang, J. Yu and A. Corma, *Adv. Mater.*, 2020, **32**, 2002927.

291 P. Tang, Q. Zhu, Z. Wu and D. Ma, *Energy Environ. Sci.*, 2014, **7**, 2580–2591.

292 H. Sheng, E. P. Schreiner, W. Zheng and R. F. Lobo, *ChemPhysChem*, 2018, **19**, 504–511.

293 Y. Xiao and A. Varma, *ACS Catal.*, 2018, **8**, 2735–2740.

294 T. V Choudhary, E. Aksoylu and D. W. Goodman, *Catal. Rev. - Sci. Eng.*, 2003, **45**, 151–203.

295 Z. R. Ismagilov, E. V Matus and L. T. Tsikoza, *Energy Environ. Sci.*, 2008, **1**, 526–541.

296 S. Ma, X. Guo, L. Zhao, S. Scott and X. Bao, *J. Energy Chem.*, 2013, **22**, 1–20.

297 J. J. Spivey and G. Hutchings, *Chem. Soc. Rev.*, 2014, **43**, 792–803.

298 N. Kosinov and E. J. M. Hensen, in *Nanotechnology in Catalysis: Applications in the Chemical Indsutry, Energy Development and Environment Protection.*, eds. B. F. Sels and M. Van de Voorde, Wiley-VCH Verlag GmbH & Co. KGaA, 1st Edit., 2017, pp. 469–482.

299 K. Sun, D. M. Ginosar, T. He, Y. Zhang, M. Fan and R. Chen, *Ind. Eng. Chem. Res.*, 2018, **57**, 1768–1789.

300 I. Vollmer, I. Yarulina, F. Kapteijn and J. Gascon, *ChemCatChem*, 2019, 11, 39–52.

301 A. Galadima and O. Muraza, *Catal. Surv. from Asia*, 2019, **23**, 149–170.

302 M. T. Portilla, H. L. T. Christiaan, M. Cristina and J. M. H. Emiel, in *Small-Scale Gas to*

Liquid Fuel Synthesis, CRC Press, 2015, pp. 263–292.

303 H. F. Abbas and W. M. A. Wan Daud, *Int. J. Hydrogen Energy*, 2010, **35**, 1160–1190.

304 Y. Kim, R. W. B. Iii and E. Iglesia, 2000, **36**, 495–509.

305 D. Ma, Y. Shu, M. Cheng, Y. Xu and X. Bao, *J. Catal.*, 2000, **194**, 105–114.

306 M. Çağlayan, A. Lucini Paioni, E. Abou-Hamad, G. Shterk, A. Pustovarenko, M. Baldus, A. D. Chowdhury and J. Gascon, *Angew. Chem., Int. Ed.*, 2020, **59**, 16741-16746.

307 N. Kosinov and E. J. M. Hensen, *Adv. Mater.*, 2020, **32**, 2002565-2002579.

308 C. L. Zhang, S. Li, Y. Yuan, W. X. Zhang, T. H. Wu and L. W. Lin, *Catal. Letters*, 1998, **56**, 207–213.

309 Y. Shu, D. Ma, L. Xu, X. Bao and Y. Xu, *Chinese J. Catal.*, 2002, **23**, 24–28.

310 C.T. Kresge, W.J. Roth, K.G. Simmons and J.C. Vartuli, *US Pat*., 5,229,341, 1993.

311 A. Martínez, E. Peris and G. Sastre, *Catal. Today*, 2005, **107**–**108**, 676–684.

312 P. Wu, Q. Kan, D. Wang, H. Xing, M. Jia and T. Wu, *Catal. Commun.*, 2005, **6**, 449–454.

313 Y. Shu, R. Ohnishi and M. Ichikawa, *Chem. Lett.*, 2002, **31**, 418–419.

314 Y. Shu, D. Ma, L. Xu, Y. Xu and X. Bao, *Catal. Letters*, 2000, **70**, 67–73.

315 D. Ma, Y. Shu, X. Han, X. Liu, Y. Xu and X. Bao, *J. Phys. Chem. B*, 2001, **105**, 1786–1793.

316 A. Smiešková, P. Hudec, N. Kumar, T. Salmi, D. Y. Murzin, V. Jorík and A. Smies, *Appl. Catal. A*, 2010, **377**, 83–91.

317 V. T. T. Ha, L. V Tiep, P. Meriaudeau and C. Naccache, *J. Mol. Catal. A Chem.*, 2002, **181**, 283–290.

318 D. Y. Wang, Q. B. Kan, N. Xu, P. Wu and T. H. Wu, *Catal. Today*, 2004, **93**–**95**, 75–80.

319 C. Xu, J. Guan, S. Wu, M. Jia, T. Wu and Q. Kan, *React. Kinet. Mech. Catal.*, 2010, **99**, 193–199.

320 H. Liu, S. Yang, S. Wu, F. Shang, X. Yu, C. Xu, J. Guan and Q. Kan, *Energy*, 2011, **36**, 1582–1589.

321 H. Liu, J. Hu, Z. Li, S. Wu, L. Liu, J. Guan and Q. Kan, *Kinet. Catal.*, 2013, **54**, 443–450.

322 B. M. Weckhuysen, D. Wang, M. P. Rosynek and J. H. Lunsford, *J Catal*., 1998, **175**, 338-343.

323 S. Majhi, P. Mohanty, H. Wang and K. K. Pant, *J. Energy Chem.*, 2013, **22**, 543–554.

324 V. Ramasubramanian, D. J. Lienhard, H. Ramsurn and G. L. Price, *Catal. Letters*, 2019, **149**, 950–964.

325 F. G. Denardin and O. W. Perez-Lopez, *Microporous Mesoporous Mater.*, 2020, **295**, 109961-109969.

326 A. Sridhar, M. Rahman, A. Infantes-Molina, B. J. Wylie, C. G. Borcik and S. J. Khatib, *Appl. Catal. A*, 2020, **589**, 117247.

327 J. P. Sim, B. J. Lee, G.-H. Han, D. H. Kim and K.-Y. Lee, *Fuel*, 2020, **274**, 117852.

328 Y. Xu, Y. Shu, S. Liu, J. Huang and X. Guo, *Catal. Letters*, 1995, **35**, 233–243.

329 R. W. Borry Iii, Y. H. Kim, A. Huffsmith, J. A. Reimer and E. Iglesia, *J. Phys. Chem. B*, 1999, **103**, 5787–5796.

330 Y. H. Kim, R. W. Borry Iii and E. Iglesia, *Microporous Mesoporous Mater.*, 2000, **35**–**36**, 495–509.

331 W. Li, G. D. Meitzner, R. W. Borry Iii and E. Iglesia, *J. Catal.*, 2000, **191**, 373–383.

332 D. Ma, Y. Shu, X. Bao and Y. Xu, *J. Catal.*, 2000, **189**, 314–325.

333 D. Ma, W. Zhang, Y. Shu, X. Liu, Y. Xu and X. Bao, *Catal. Letters*, 2000, **66**, 155–160.

334 B. Li, S. Li, N. Li, H. Chen, W. Zhang, X. Bao and B. Lin, *Microporous Mesoporous Mater.*, 2006, **88**, 244–253.

335 J. Gao, Y. Zheng, J. M. Jehng, Y. Tang, I. E. Wachs and S. G. Podkolzin, *Science (80-.).*, 2015, **348**, 686–690.

336 R. W. Borry, Y. H. Kim, A. Huffsmith, J. A. Reimer and E. Iglesia, *J Phys Chem B*, 1999, **103**, 5787-5796.

337 N. Kosinov, F. J. A. G. Coumans, G. Li, E. Uslamin, B. Mezari, A. S. G. Wijpkema, E. A. Pidko and E. J. M. Hensen, *J. Catal.*, 2017, **346**, 125–133.

338 I. Vollmer, A. Mondal, I. Yarulina, E. Abou-hamad, F. Kapteijn and J. Gascon, *Appl. Catal. A*, 2019, **574**, 144–150.

339 H. Zheng, D. Ma, X. Bao, Z. H. Jian, H. K. Ja, Y. Wang and C. H. F. Peden, *J. Am. Chem. Soc.*, 2008, **130**, 3722–3723.

340 W. Ding, S. Li, G. D. Meitzner and E. Iglesia, *J. Phys. Chem. B*, 2001, **105**, 506–513.

341 I. Vollmer, B. van der Linden, S. Ould-Chikh, A. Aguilar-Tapia, I. Yarulina, E. Abou-Hamad, Y. G. Sneider, A. I. Olivos Suarez, J.-L. Hazemann, F. Kapteijn and J. Gascon, *Chem. Sci.*, 2018, **9**, 4801–4807.

342 S. Liu, L. Wang, R. Ohnishi and M. Ichikawa, *J. Catal.*, 1999, **181**, 175–188.

343 L. Su, Y. Xu and X. Bao, *J. Nat. Gas Chem.*, 2002, **11**, 18–27.

344 D. Ma, Y. Shu, W. Zhang, X. Han, Y. Xu and X. Bao, *Angew. Chem., Int. Ed.*, 2000, **39**, 2928–2931.

345 L. Wang, L. Tao, M. Xie, G. Xu, J. Huang and Y. Xu, *Catal. Letters*, 1993, **21**, 35–41.

346 Y. Xu, S. Liu, X. Guo, L. Wang and M. Xie, *Catal. Letters*, 1995, **30**, 135–149.

347 D. Wang, J. H. Lunsford and M. P. Rosynek, *Top. Catal.*, 1996, **3**, 289–297.

348 N. K. Razdan, A. Kumar, B. L. Foley and A. Bhan, *J. Catal.*, 2020, **381**, 261–270.

349 I. Vollmer, E. Abou-hamad, J. Gascon and F. Kapteijn, *ChemCatChem*, 2020, **12**, 544–549.

350 P. Mériaudeau, L. V Tiep, V. T. T. Ha, C. Naccache and G. Szabo, *J. Mol. Catal. A Chem.*, 1999, **144**, 469–471.

351 P. Mériaudeau, V. T. T. Ha and L. Van Tiep, *Catal. Letters*, 2000, **64**, 49–51.

352 N. K. Razdan and A. Bhan, *J. Catal.*, 2020, **389**, 667–676.

353 N. Kosinov, E. A. Uslamin, F. J. A. G. Coumans, A. S. G. Wijpkema, R. Y. Rohling and E. J. M. Hensen, *ACS Catal.*, 2018, **8**, 8459–8467.

354 H. Liu, L. Su, H. Wang, W. Shen, X. Bao and Y. Xu, *Appl. Catal. A*, 2002, **236**, 263–280.

355 I. Vollmer, N. Kosinov, Á. Szécsényi, G. Li, I. Yarulina, E. Abou-hamad, A. Gurinov, S. Ould-chikh, A. Aguilar-tapia, J. Hazemann, E. Pidko, E. Hensen, F. Kapteijn and J. Gascon, *J. Catal.*, 2019, **370**, 321–331.

356 G. Li, I. Vollmer, C. Liu, J. Gascon and E. A. Pidko, *ACS Catal.*, 2019, **9**, 8731–8737.

357 C. H. L. Tempelman and E. J. M. Hensen, *Appl. Catal. B*, 2015, **176–177**, 731–739.

358 Y. Lu, D. Ma, Z. Xu, Z. Tian, X. Bao and L. Lin, *Chem. Commun*., 2001, 2048-2049.

359 R. Ohnishi, S. Liu, Q. Dong, L. Wang and M. Ichikawa, *J. Catal.*, 1999, **182**, 92–103.

360 Z. Liu, M. A. Nutt and E. Iglesia, *Catal. Letters*, 2002, **81**, 271–279.

361 M. Chen, Y. Song, B. Liu, X. Liu, Y. Xu and Z.-G. Zhang, *Fuel*, 2019, **262**, 116674.

362 S. Liu, R. Ohnishi and M. Ichikawa, *J. Catal.*, 2003, **220**, 57–65.

363 S. Yao, L. Gu, C. Sun, J. Li and W. Shen, *Ind. Eng. Chem. Res.*, 2009, **48**, 713–718.

364 N. Kosinov, F. J. A. G. Coumans, E. Uslamin, F. Kapteijn and E. J. M. Hensen, *Angew. Chem., Int. Ed.*, 2016, **55**, 15086–15090.

365 X. Chen, Y. Dong, S. Lin, H. Zhang, X. Yu, Z. Wang, Y. Liu, J. Liu and S. Yao, *Catal. Letters*, 2020, **150**, 2115–2131.

366 N. Kosinov, E. A. Uslamin, L. Meng, A. Parastaev, Y. Liu and E. J. M. Hensen, *Angew. Chem., Int. Ed.*, 2019, **58**, 7068–7072.

367 S. C. Oh, M. Sakbodin and D. Liu, *Catalysis*, 2019, **31**, 127–165.

368 Z.-G. Zhang, *Carbon Resour. Convers.*, 2019, **2**, 157–174.

369 Y. Song, Q. Zhang, Y. Xu, Y. Zhang, K. Matsuoka and Z.-G. Zhang, *Appl. Catal. A*, 2017, **530**, 12–20.

370 Y. Xu, Y. Song and Z.-G. Zhang, *Catal. Today*, 2017, **279**, 115–123.

371 M. C. Iliuta, F. Larachi, B. P. A. Grandjean, I. Iliuta and A. Sayari, *Ind. Eng. Chem. Res.*, 2002, **41**, 2371–2378.

372 A. K. Kinage, R. Ohnishi and M. Ichikawa, *Catal. Letters*, 2003, **88**, 199–202.

373 L. Li, R. W. Borry and E. Iglesia, *Chem. Eng. Sci.*, 2002, **57**, 4595–4604.

374 Z. Cao, H. Jiang, H. Luo, S. Baumann, W. A. Meulenberg, J. Assmann, L. Mleczko, Y. Liu and J. Caro, *Angew. Chem., Int. Ed.*, 2013, **52**, 13794–13797.

375 S. H. Morejudo, R. Zanon, S. Escolastico, I. Yuste-Tirados, H. Malerod-Fjeld, P. K. Vestre, W. G. Coors, A. Martinez, T. Norby, J. M. Serra and C. Kjolseth, *Science*, 2016, **353**, 563–566.

376 N. K. Razdan, A. Kumar and A. Bhan, *J. Catal.*, 2019, **372**, 370–381.

377 V. R. Choudhary, A. K. Kinage and T. V Choudhary, *Science*, 1997, **275**, 1286–1288.

378 A. A. Gabrienko, S. S. Arzumanov, I. B. Moroz, A. V Toktarev, W. Wang and A. G. Stepanov, *J. Phys. Chem. C*, 2013, **117**, 7690–7702.

379 A. A. Gabrienko, S. S. Arzumanov, A. V Toktarev, I. G. Danilova, I. P. Prosvirin, V. V Kriventsov, V. I. Zaikovskii, D. Freude and A. G. Stepanov, *ACS Catal.*, 2017, **7**, 1818–1830.

380 M. V Luzgin, V. A. Rogov, S. S. Arzumanov, A. V Toktarev, A. G. Stepanov and V. N. Parmon, *Angew. Chem., Int. Ed.*, 2008, **47**, 4559–4562.

381 J. Guo, H. Lou and X. Zheng, *J. Nat. Gas Chem.*, 2009, **18**, 260–272.

382 J.-F. Wu, S.-M. Yu, W. D. Wang, Y.-X. Fan, S. Bai, C.-W. Zhang, Q. Gao, J. Huang and W. Wang, *J. Am. Chem. Soc.*, 2013, **135**, 13567–13573.

383 A. M. Rabie, M. A. Betiha and S.-E. Park, *Appl. Catal. B*, 2017, **215**, 50–59.

384 S. Wang, S. Guo, Y. Luo, Z. Qin, Y. Chen, M. Dong, J. Li, W. Fan and J. Wang, *Catal. Sci. Technol.*, 2019, **9**, 6613–6626.

385 R. S. Middleton, R. Gupta, J. D. Hyman and H. S. Viswanathan, *Appl. Energy*, 2017, **199**, 88–95.

386 T. Boersma and C. Johnson, *Rev. Policy Res.*, 2012, **29**, 570–576.

387 BP Natural gas prices, http://www.bp.com/en/global/corporate/energy-economics/statistical-review-of-world-energy/natural-gas.html, accessed October 2020.

388 http://www.eia.gov/forecasts/aeo, Annual Energy Outlook 2020, accessed August 2020.

389 B. W. Wojciechowski and A. Corma, *Catalytic Cracking: Catalysis, Chemistry and Kinetics*, Marcel Dekker, Inc., New York, 1986.

390 L. D. Schmidt, J. Siddall and M. Bearden, *AIChE J.*, 2000, **46**, 1492–1495.

391 A. Corma and B. W. Wojciechowski, *Catal. Rev. Sci. Eng.*, 1985, **27**, 29–149.

392 J. Abbot and B. W. Wojciechowski, *J. Catal.*, 1987, **107**, 451–462.

393 A. Corma and B. W. Wojciechowski, *Catal. Rev. Sci. Eng*., 1982, **24**, 1-65.

394 P. V Shertukde, G. Marcelin, G. A. Sill and W. Keith Hall, *J. Catal.*, 1992, **136**, 446–462.

395 A. Corma and A. V Orchillés, *Microporous Mesoporous Mater.*, 2000, **35**–**36**, 21–30.

396 J. Dědeček, Z. Sobalík and B. Wichterlová, *Catal. Rev. Sci. Eng.*, 2012, **54**, 135–223.

397 P. Wang, S. Wang, Y. Yue, T. Wang and X. Bao, *Microporous Mesoporous Mater.*, 2020, **292**, 109748.

398 J. Van der Mynsbrugge, A. Janda, L. Lin, V. Van Speybroeck, M. Head-Gordon and A. T. Bell, *ChemPhysChem*, 2018, **19**, 341–358.

399 P. M. Esteves, C. J. A. Mota, A. Ramírez-Solís and R. Hernández-Lamoneda, *J. Am. Chem. Soc.*, 1998, **120**, 3213–3219.

400 P. M. Esteves, G. G. P. Alberto, A. Ramírez-Solís and C. J. A. Mota, *J. Phys. Chem. A*, 2000, **104**, 6233–6240.

401 B. Xu, C. Sievers, S. B. Hong, R. Prins and J. A. van Bokhoven, *J. Catal.*, 2006, **244**, 163–168.

402 J. A. Van Bokhoven, B. A. Williams, W. Ji, D. C. Koningsberger, H. H. Kung and J. T. Miller, *J. Catal.*, 2004, **224**, 50–59.

403 A. Bhan, R. Gounder, J. Macht and E. Iglesia, *J. Catal.*, 2008, **253**, 221–224.

404 R. Gounder and E. Iglesia, *J. Am. Chem. Soc.*, 2009, **131**, 1958–1971.

405 R. Gounder and E. Iglesia, *Angew. Chem., Int. Ed.*, 2010, **49**, 808–811.

406 C. Song, Y. Chu, M. Wang, H. Shi, L. Zhao, X. Guo, W. Yang, J. Shen, N. Xue and L. Peng, *J. Catal.*, 2017, **349**, 163–174.

407 H. Li, S. A. Kadam, A. Vimont, R. F. Wormsbecher and A. Travert, *ACS Catal.*, 2016, **6**, 4536–4548.

408 S. A. Kadam, H. Li, R. F. Wormsbecher and A. Travert, *Chem. Eur. J.*, 2018, **24**, 5489–5492.

409 A. Janda, B. Vlaisavljevich, L.-C. Lin, B. Smit and A. T. Bell, *J. Am. Chem. Soc.*, 2016, **138**, 4739–4756.

410 A. Janda and A. T. Bell, *J. Am. Chem. Soc.*, 2013, **135**, 19193–19207.

411 B. Louis, M. M. Pereira, F. M. Santos, P. M. Esteves and J. Sommer, *Chem. Eur. J.*, 2010, **16**, 573–576.

412 M. Boronat and A. Corma, *Appl. Catal. A*, 2008, **336**, 2–10.

413 G. Garralón, A. Corma and V. Fornés, *Zeolites*, 1989, **9**, 84–86.

414 B. Xu, S. Bordiga, R. Prins and J. A. van Bokhoven, *Appl. Catal. A*, 2007, **333**, 245–253.

415 R. Gounder, A. J. Jones, R. T. Carr and E. Iglesia, *J. Catal.*, 2012, **286**, 214–223.

416 N. Xue, A. Vjunov, S. Schallmoser, J. L. Fulton, M. Sanchez-Sanchez, J. Z. Hu, D. Mei and J. A. Lercher, *J. Catal.*, 2018, **365**, 359–366.

417 F. Schüßler, E. A. Pidko, R. Kolvenbach, C. Sievers, E. J. M. Hensen, R. A. van Santen and

J. A. Lercher, *J. Phys. Chem. C*, 2011, **115**, 21763–21776.

418 F. Schüßler, S. Schallmoser, H. Shi, G. L. Haller, E. Ember and J. A. Lercher, *ACS Catal.*, 2014, **4**, 1743–1752.

419 S. M. Sadrameli, *Fuel*, 2016, **173**, 285–297.

420 P. del Campo, M. T. Navarro, S. K. Shaikh, M. D. Khokhar, F. Aljumah, C. Martínez and A. Corma, *ACS Catal.*, 2020, 11878–11891.

421 N. Rahimi and R. Karimzadeh, *Appl. Catal. A*, 2011, **398**, 1–17.

422 N. Xue, X. Chen, L. Nie, X. Guo, W. Ding, Y. Chen, M. Gu and Z. Xie, *J. Catal.*, 2007, **248**, 20.

423 G. Zhao, J. Teng, Z. Xie, W. Jin, W. Yang, Q. Chen and Y. Tang, *J. Catal.*, 2007, **248**, 29–37.

424 T. Blasco, A. Corma and J. Martínez-Triguero, *J. Catal.*, 2006, **237**, 267–277.

425 J. Lu, Z. Zhao, C. Xu, P. Zhang and A. Duan, *Catal Commun*, 2006, **7**, 199-203.

426 A. Corma, A. L. Agudo, I. Nebot and F. Tomás, *J. Catal.*, 1982, **77**, 159–168.

427 A. L. Agudo, A. Asensio and A. Corma, *Can. J. Chem. Eng.*, 1982, **60**, 50–54.

428 J. Lu, Z. Zhao, C. Xu, A. Duan and P. Zhang, *Catal. Letters*, 2006, **109**, 65–70.

429 A. J. Maia, B. G. Oliveira, P. M. Esteves, B. Louis, Y. L. Lam and M. M. Pereira, *Appl. Catal. A*, 2011, **403**, 58–64.

430 A. D. F. Ferreira, A. J. Maia, B. Guatiguaba, M. H. Herbst, P. T. L. Rocha, M. M. Pereira and B. Louis, *Catal. Today*, 2014, **226**, 67–72.

431 M. J. Wulfers and F. C. Jentoft, *J. Catal.*, 2015, **330**, 507–519.

432 Y. Ono, *Catal. Today*, 2003, **81**, 3–16.

433 R. A. Asuquo, G. Eder-Mirth, K. Seshan, J. A. Z. Pieterse and J. A. Lercher, *J. Catal.*, 1997, **168**, 292–300.

434 R. A. Asuquo, G. Edermirth and J. A. Lercher, *J. Catal.*, 1995, **155**, 376–382.

435 P. Wang, W. Zhang, H. Zhu, P. Yuan, C. Yang, C. Li and X. Bao, *Appl. Catal. A*, 2019, **584**, 117135.

436 M. Guisnet and N. S. Gnep, *Appl. Catal. A*, 1996, **146**, 33–64.

437 T. Kurniawan, O. Muraza, A. S. Hakeem, I. A. Bakare, T. Nishitoba, T. Yokoi, Z. H. Yamani

and A. M. Al Amer, *Energy & Fuels*, 2017, **31**, 12691–12700.

438 W. Zhang, P. Wang, C. Yang and C. Li, *Catal. Letters*, 2019, **149**, 1017–1025.

439 J. A. Z. Pieterse, K. Seshan and J. A. Lercher, *J. Catal.*, 2000, **195**, 326–335.

440 G. Caeiro, R. H. Carvalho, X. Wang, M. A. N. D. Lemos, F. Lemos, M. Guisnet and F. R. Ribeiro, *J. Mol. Catal. A Chem.*, 2006, **255**, 131–158.

441 A. C. Oliveira, N. Essayem, A. Tuel, J.-M. Clacens and Y. Ben Taarit, *Catal. Today*, 2008, **133**, 56–62.

442 B. M. Weckhuysen and R. A. Schoonheydt, *Catal. Today*, 1999, **51**, 223–232.

443 O. O. James, S. Mandal, N. Alele, B. Chowdhury and S. Maity, *Fuel Process. Technol.*, 2016, **149**, 239–255.

444 Z. Nawaz, *Rev. Chem. Eng.*, 2015, **31**, 413–436.

445 J. J. H. B. Sattler, J. Ruiz-Martinez, E. Santillan-Jimenez and B. M. Weckhuysen, *Chem. Rev.*, 2014, **114**, 10613–10653.

446 M. M. Bhasin, J. H. McCain, B. V Vora, T. Imai and P. R. Pujadó, *Appl. Catal. A*, 2001, **221**, 397–419.

447 J. Valente, R. Solórzano and H. Armendáriz, *Catalyst Rev.*, 2018, **31**, 6-13.

448 D. E. Resasco, *Dehydrogenation – Heterogeneous. In Encyclopedia of Catalysis*, I. Horváth (Ed.), John Wiley & Sons, 2002.

449 J. A. Biscardi and E. Iglesia, *Catal. Today*, 1996, **31**, 207–231.

450 J. Meusinger and A. Corma, *J. Catal.*, 1995, **152**, 189–197.

451 G. D. Meitzner, E. Iglesia, J. E. Baumgartner and E. S. Huang, *J. Catal.*, 1993, **140**, 209–225.

452 E. A. Pidko and R. A. van Santen, *J. Phys. Chem. C*, 2007, **111**, 2643–2655.

453 M. V Frash and R. A. van Santen, *Phys. Chem. Chem. Phys.*, 2000, **2**, 1085–1089.

454 V. B. Kazansky, I. R. Subbotina, N. Rane, R. A. van Santen and E. J. M. Hensen, *Phys. Chem. Chem. Phys.*, 2005, **7**, 3088–3092.

455 E. A. Pidko, V. B. Kazansky, E. J. M. Hensen and R. A. van Santen, *J. Catal.*, 2006, **240**, 73–84.

456 S. B. A. Hamid, E. G. Derouane, G. Demortier, J. Riga and M. A. Yarmo, *Appl. Catal. A*,

1994, **108**, 85–96.

457 A. G. Stepanov, S. S. Arzumanov, V. N. Parmon, Y. G. Kolyagin, I. I. Ivanova and D. Freude, *Catal. Letters*, 2007, **114**, 85–90.

458 J. A. Biscardi and E. Iglesia, *Phys. Chem. Chem. Phys.*, 1999, **1**, 5753–5759.

459 B. V Vora, *Top. Catal.*, 2012, **55**, 1297–1308.

460 D. Akporiaye, S. F. Jensen, U. Olsbye, F. Rohr, E. Rytter, M. Rønnekleiv and A. I. Spjelkavik, *Ind. Eng. Chem. Res.*, 2001, **40**, 4741–4748.

461 G. Siddiqi, P. Sun, V. Galvita and A. T. Bell, *J. Catal.*, 2010, **274**, 200–206.

462 S. B. Simonsen, I. Chorkendorff, S. Dahl, M. Skoglundh, J. Sehested and S. Helveg, *J. Am. Chem. Soc.*, 2010, **132**, 7968–7975.

463 J. Im and M. Choi, *ACS Catal.*, 2016, **6**, 2819–2826.

464 W. C Buss and T.R. Hughes, *US Pat.*, 4,435,283 A, 1984.

465 J. P. Gilson, R. W. Johnson, S. L. Lambert and R. J. Lawson, *US Pat.*, 4,614,834 A, 1985.

466 J. R. Bernard, J. Nury, *US Pat.*, 4,104,320 A, 1978.

467 C. Besoukhanova, D. Barthomeuf, M. Breysse and J. R. Bernard, *Stud. Surf. Sci. Catal.*, 1981, **7**, 1410–1411.

468 P. Meriaudeau and C. Naccache, *Catal. Rev. Sci. Eng.*, 1997, **39**, 5–48.

469 S. J. Miller, *US Pat.*, 4,727,216 A, 1988.

470 S. J. Tauster and J. J. Steger, *J. Catal.*, 1990, **125**, 387–389.

471 E. G. Derouane and D. J. Vanderveken, *Appl. Catal.*, 1988, **45**, L15–L22.

472 A. Arcoya, X. L. Seoane and J. M. Grau, *Appl. Catal. A*, 2005, **284**, 85–95.

473 R. D. Cortright and J. A. Dumesic, *Appl. Catal. A*, 1995, **129**, 101–115.

474 G. H. Kuehl, *US Pat.*, 4,299,686 A, 1981.

475 H. Yang, H. Chen, J. Chen, O. Omotoso and Z. Ring, *J. Catal.*, 2006, **243**, 36–42.

476 B.-Z. Zhan and E. Iglesia, *Angew. Chem., Int. Ed.*, 2007, **46**, 3697–3700.

477 M. Choi, Z. Wu and E. Iglesia, *J. Am. Chem. Soc.*, 2010, **132**, 9129–9137.

478 S. Goel, S. I. Zones and E. Iglesia, *J. Am. Chem. Soc.*, 2014, **136**, 15280–15290.

479 H. Yang, H. Chen, H. Du, R. Hawkins, F. Craig, Z. Ring, O. Omotoso, V. Munoz and R.

Mikula, *Microporous Mesoporous Mater.*, 2009, **117**, 33–40.

480 L. Liu, P. Concepcion and A. Corma, *J. Catal.*, 2019, **369**, 312–323.

481 L. Liu, M. Lopez-Haro, C. W. Lopes, S. Rojas-Buzo, P. Concepcion, R. Manzorro, L. Simonelli, A. Sattler, P. Serna, J. J. Calvino and A. Corma, *Nat. Catal.*, 2020, **3**, 628–638.

482 Q. Sun, N. Wang, Q. Fan, L. Zeng, A. Mayoral, S. Miao, R. Yang, Z. Jiang, W. Zhou, J. Zhang, T. Zhang, J. Xu, P. Zhang, J. Cheng, D.-C. Yang, R. Jia, L. Li, Q. Zhang, Y. Wang, O. Terasaki and J. Yu, *Angew. Chem., Int. Ed.*, 2020, **59**, 19450-19459.

483 L.-C. Wang, Y. Zhang, J. Xu, W. Diao, S. Karakalos, B. Liu, X. Song, W. Wu, T. He and D. Ding, *Appl. Catal. B*, 2019, **256**, 117816.

484 J. H. Yun and R. F. Lobo, *J. Catal.*, 2014, **312**, 263–270.

485 P. L. De Cola, R. Glaeser and J. Weitkamp, *Appl. Catal. A*, 2006, **306**, 85–97.

486 Z. Nawaz, S. Qing, G. Jixian, X. Tang and F. Wei, *J. Ind. Eng. Chem.*, 2010, **16**, 57–62.

487 L. M. Madeira and M. F. Portela, *Catal. Rev.*, 2002, **44**, 247–286.

488 R. K. Grasselli, D. L. Stern and J. G. Tsikoyiannis, *Appl. Catal. A Gen.*, 1999, **189**, 1–8.

489 L. M. Madeira, M. F. Portela, C. Mazzocchia, A. Kaddouri and R. Anouchinsky, *Catal. Today*, 1998, **40**, 229-243.

490 F. Cavani, N. Ballarini and A. Cericola, *Catal. Today*, 2007, **127**, 113–131.

491 S. Albonetti, F. Cavani and F. Trifirò, *Catal. Rev.*, 1996, **38**, 413–438.

492 M. K. Samantaray, V. D'Elia, E. Pump, L. Falivene, M. Harb, S. Ould Chikh, L. Cavallo and J.-M. Basset, *Chem. Rev.*, 2020, **120**, 734–813.

493 T. Blasco and J. M. L. Nieto, *Appl. Catal. A*, 1997, **157**, 117–142.

494 J. M. López Nieto, *Top. Catal.*, 2001, **15**, 189–194.

495 G. Centi and F. Trifiro, *Appl. Catal. A*, 1996, **143**, 3–16.

496 P. Concepción, J. M. López Nieto, A. Mifsud and J. Pérez-Pariente, *Appl. Catal. A*, 1997, **151**, 373–392.

497 P. Concepción, A. Corma, J. M. López Nieto and J. Pérez-Pariente, *Appl. Catal. A*, 1996, **143**, 17–28.

498 L. Lisi, L. Marchese, H. O. Pastore, A. Frache, G. Ruoppolo and G. Russo, *Top. Catal.*, 2003, **22**, 95–99.

499 L. Marchese, A. Frache, G. Gatti, S. Coluccia, L. Lisi, G. Ruoppolo, G. Russo and H. O. Pastore, *J. Catal.*, 2002, **208**, 479–484.

500 M. Stöcker, *Microporous Mesoporous Mater.*, 1999, **29**, 3–48.

501 Z. Li, M. T. Navarro, J. Martínez-Triguero, J. Yu and A. Corma, *Catal. Sci. Technol.*, 2016, **6**, 5856–5863.

502 E. M. Gallego, C. Li, C. Paris, N. Martín, J. Martínez-Triguero, M. Boronat, M. Moliner and A. Corma, *Chem. A Eur. J.*, 2018, **24**, 14631–14635.

503 B. Qiu, F. Jiang, W.-D. Lu, B. Yan, W.-C. Li, Z.-C. Zhao and A.-H. Lu, *J. Catal.*, 2020, **385**, 176–182.

504 N. R. Altvater, R. W. Dorn, M. C. Cendejas, W. P. McDermott, B. Thomas, A. J. Rossini and I. Hermans, *Angew. Chem., Int. Ed.*, 2020, **59**, 6546-6550.

505 X. Lin, C. A. Hoel, W. M. H. Sachtler, K. R. Poeppelmeier and E. Weitz, *J. Catal.*, 2009, **265**, 54–62.

506 A. A. Teixeira-Neto, L. Marchese, G. Landi, L. Lisi and H. O. Pastore, *Catal. Today*, 2008, **133**–**135**, 1–6.

507 A. Corma, J. M. Lopez Nieto and N. Paredes, *J. Mol. Catal. A Chem.*, 1997, **123**, 75–84.

508 M. A. Atanga, F. Rezaei, A. Jawad, M. Fitch and A. A. Rownaghi, *Appl. Catal. B*, 2018, **220**, 429–445.

509 X. Du, B. Yao, S. Gonzalez-Cortes, V. L. Kuznetsov, H. AlMegren, T. Xiao and P. P. Edwards, *Faraday Discuss.*, 2015, **183**, 161–176.

510 N. Mimura, I. Takahara, M. Inaba, M. Okamoto and K. Murata, *Catal. Commun.*, 2002, **3**, 257–262.

511 N. Mimura, M. Okamoto, H. Yamashita, S. T. Oyama and K. Murata, *J. Phys. Chem. B*, 2006, **110**, 21764–21770.

512 Q. Zhu, M. Takiguchi, T. Setoyama, T. Yokoi, J. N. Kondo and T. Tatsumi, *Catal. Letters*, 2011, **141**, 670–677.

513 Y. Ren, J. Wang, W. Hua, Y. Yue and Z. Gao, *J. Ind. Eng. Chem.*, 2012, **18**, 731–736.

514 A. Al-Mamoori, S. Lawson, A. A. Rownaghi and F. Rezaei, *Appl. Catal. B*, 2020, **278**, 119329.

515 G. I. Panov, A. S. Kharitonov and V. I. Sobolev, *Appl. Catal. A.*, 1993, **98**, 1–20.

516 K. A. Dubkov, N. S. Ovanesyan, A. A. Shteinman, E. V Starokon and G. I. Panov, *J. Catal.*, 2002, **207**, 341–352.

517 S. N. Vereshchagin, N. P. Kirik, N. N. Shishkina and A. G. Anshits, *Catal. Letters*, 1998, **56**, 145–148.

518 J. Perez-Ramirez and E. V Kondratenko, *Chem. Commun.*, 2003, **17**, 2152–2153.

519 J. Perez-Ramirez, F. Kapteijn, J. C. Groen, A. Domenech, G. Mul and J. A. Moulijn, *J. Catal.*, 2003, **214**, 33–45.

520 E. V Kondratenko and J. Perez-Ramirez, *Appl. Catal. A*, 2004, **267**, 181–189.

521 K. Nowińska, A. Wącław and A. Izbińska, *Appl. Catal. A*, 2003, **243**, 225–236.

522 R. Bulánek, B. Wichterlová, K. Novoveská and V. Kreibich, *Appl. Catal. A*, 2004, **264**, 13–22.

523 M. S. Kumar, J. Pérez-Ramírez, M. N. Debbagh, B. Smarsly, U. Bentrup and A. Brückner, *Appl. Catal. B*, 2006, **62**, 244–254.

524 A. Held, J. Kowalska and K. Nowinska, *Appl. Catal. B*, 2006, **64**, 201–208.

525 H. Saito and Y. Sekine, *RSC Adv.*, 2020, **10**, 21427–21453.

526 A. Bhan and W. Nicholas Delgass, *Catal. Rev.*, 2008, **50**, 19–151.

527 A. Samanta, X. Bai, B. Robinson, H. Chen and J. Hu, *Ind. Eng. Chem. Res.*, 2017, **56**, 11006–11012.

528 T. Koyama, Y. Hayashi, H. Horie, S. Kawauchi, A. Matsumoto, Y. Iwase, Y. Sakamoto, A. Miyaji, K. Motokura and T. Baba, *Phys. Chem. Chem. Phys.*, 2010, **12**, 2541–2554.

529 Y. Iwase, Y. Sakamoto, A. Shiga, A. Miyaji, K. Motokura, T. -r. Koyama and T. Baba, *J. Phys. Chem. C*, 2012, **116**, 5182-5196.

530 S. R. Kanitkar and J. J. Spivey, *Nat. Gas Process. from Midstream to Downstr.*, 2018, 379–401.

531 A. Hagen and F. Roessner, *Catal. Rev. Sci. Eng.*, 2000, **42**, 403–437.

532 K.-H. Steinberg, U. Mroczek and F. Roessner, *Appl. Catal.*, 1990, **66**, 37–44.

533 E. Iglesia, J. E. Baumgartner and G. L. Price, *J Catal*, 1992, **134**, 549-571.

534 T. Liang, H. Toghiani and Y. Xiang, *Ind. Eng. Chem. Res.*, 2018, **57**, 15301–15309.

535 M. Guisnet, N. S. Gnep and F. Alario, *Appl. Catal. A*, 1992, **89**, 1–30.

536 A. Corma, C. Goberna, J. M. Lopez Nieto, N. Paredes and M. Perez, *Stud. Surf. Sci. Catal.*, 1991, **69**, 409–416.

537 L. N. Vosmerikova, Y. E. Barbashin and A. V Vosmerikov, *Pet. Chem.*, 2014, **54**, 420–425.

538 O. A. Anunziata, G. A. Eimer and L. B. Pierella, *Catal. Letters*, 2001, **75**, 93–97.

539 A. Mehdad and R. F. Lobo, *Catal. Sci. Technol.*, 2017, **7**, 3562–3572.

540 A. J. Jones and E. Iglesia, *ACS Catal.*, 2015, **5**, 5741-5755.

541 A. L. Lapidus, A. A. Dergachev, V. A. Kostina and A. A. Silakova, *Pet. Chem.*, 2008, **48**, 83–86.

542 F. Solymosi and P. Tolmacsov, *Catal. Letters*, 2004, **93**, 7–11.

543 A. Ausavasukhi and T. Sooknoi, *Catal. Commun.*, 2014, **45**, 63–68.

544 Y. Ono, *Eng*, 1992, **34**, 179-226.

545 V. B. Kazansky, I. R. Subbotina, N. Rane, R. A. Van Santen and E. J. M. Hensen, *Phys. Chem. Chem. Phys.*, 2005, **7**, 3088–3092.

546 G. Buckles and G. J. Hutchings, *Catal. Letters*, 1994, **27**, 361–367.

547 E. G. Derouane, S. B. Abdul Hamid, A. Pasau-Claerbout and M. Seivert, *Stud. Surf. Sci. Catal.*, 1995, **92**, 123-123.

548 M. V Frash and R. A. Van Santen, *J. Phys. Chem. A*, 2000, **104**, 2468–2475.

549 V. I. Yakerson, T. V Vasina, L. I. Lafer, V. P. Sytnyk, G. L. Dykh, A. V Mokhov, O. V Bragin and K. M. Minachev, *Catal. Letters*, 1989, **3**, 339–345.

550 P. Meriaudeau and C. Naccache, *J. Mol. Catal.*, 1990, **59**, L31–L36.

551 M. Guisnet and N. S. Gnep, *Catal. Today*, 1996, **31**, 275–292.

552 E. A. Uslamin, H. Saito, N. Kosinov, E. Pidko, Y. Sekine and E. J. M. Hensen, *Catal. Sci. Technol.*, 2020, **10**, 2774–2785.

553 U. Olsbye, S. Svelle, M. Bjørgen, P. Beato, T. V. W. Janssens, F. Joensen, S. Bordiga and K. P. Lillerud, *Angew. Chem. Int. Ed.*, 2012, **51**, 5810–5831.

554 S. M. T. Almutairi, B. Mezari, P. C. M. M. Magusin, E. A. Pidko and E. J. M. Hensen, *ACS Catal.*, 2012, **2**, 71–83.

555 N. Katada, *Mol. Catal.*, 2018, **458**, 116–126.

556 J. A. Biscardi, G. D. Meitzner and E. Iglesia, *J. Catal.*, 1998, **179**, 192–202.

557 S. Tamiyakul, T. Sooknoi, L. L. Lobban and S. Jongpatiwut, *Appl. Catal. A*, 2016, **525**, 190–196.

558 J. Gao, C. Wei, M. Dong, G. Wang, Z. Li, Z. Qin, J. Wang and W. Fan, *ChemCatChem*, 2019, **11**, 3892–3902.

559 V. B. Kazansky and A. I. Serykh, *Phys. Chem. Chem. Phys.*, 2004, **6**, 3760–3764.

560 J. A. Biscardi and E. Iglesia, *J Catal*, 1999, **182**, 117-128.

561 E. A. Pidko and R. A. Van Santen, *J. Phys. Chem. C*, 2007, **111**, 2643–2655.

562 H. A. Aleksandrov and G. N. Vayssilov, *Catal. Today*, 2010, **152**, 78–87.

563 Y. Zhang, S. Wu, X. Xu and H. Jiang, *Catal. Sci. Technol.*, 2020, **10**, 835–843.

564 V. I. Zaikovskii, L. N. Vosmerikova and A. V Vosmerikov, *Kinet. Catal.*, 2012, **53**, 731–736.

565 U. Mroczek, W. Reschetilowski, K. Pietzsch and K. H. Steinberg, *React. Kinet. Catal. Lett.*, 1991, **43**, 539–544.

566 M. N. Mikhailov, I. V Mishin, L. M. Kustov and A. L. Lapidus, *Microporous Mesoporous Mater.*, 2007, **104**, 145–150.

567 H. S. Lacheen, P. J. Cordeiro and E. Iglesia, *Chem. A Eur. J.*, 2007, **13**, 3048–3057.

568 L. Ma and X. Zou, *Appl. Catal. B*, 2019, **243**, 703–710.

569 S.-T. Wong, Y. Xu, L. Wang, S. Liu, G. Li, M. Xie and X. Guo, *Catal. Letters*, 1996, **38**, 39–43.

570 F. Solymosi and A. Szo, *Appl. Catal. A*, 1998, **166**, 225–235.

571 E. A. Uslamin, H. Saito, Y. Sekine, E. J. M. Hensen and N. Kosinov, *Catal. Today*., 2021, **369**, 184-192.

572 H. Liu, H. Wang, A.-H. Xing and J.-H. Cheng, *J. Phys. Chem. C*, 2019, **123**, 15637–15647.

573 F. Goodarzi, R. P. Thumbayil, K. Enemark-Rasmussen, J. Mielby, T. T. M. Nguyen, P. Beato, F. Joensen and S. Kegnæs, *ChemCatChem*., 2020, **12**, 1519-1526.

574 H. Saito, S. Inagaki, K. Kojima, Q. Han, T. Yabe, S. Ogo, Y. Kubota and Y. Sekine, *Appl. Catal. A*, 2018, **549**, 76–81.

575 J. Ye, L. Bai, B. Liu, H. Tian, J. Hu, F. Polo-Garzon, R. T. Mayes, Z. Wu and Y. Fang, *Ind. Eng. Chem. Res.*, 2019, **58**, 7094–7106.

576 E. Gomez, X. Nie, J. H. Lee, Z. Xie and J. G. Chen, *J. Am. Chem. Soc.*, 2019, **141**, 17771–17782.

577 R. D. Armstrong, G. J. Hutchings and S. H. Taylor, *Catalysts*, 2016, **6**, 71.

578 G. Mazloom and S. M. Alavi, *Part. Sci. Technol.*, 2018, **36**, 61–71.

579 A. Trunschke, *RSC Nanosci. Nanotechnol.*, 2011, **19**, 56–95.

580 J. C. Vedrine, E. K. Novakova and E. G. Derouane, *Catal. Today*, 2003, **81**, 247–262.

581 M. M. Lin, *Appl. Catal. A*, 2001, **207**, 1–16.

582 G. J. Hutchings, *Appl. Catal.*, 1991, **72**, 1–32.

583 J. H. Jones, *Platin. Met. Rev.*, 2000, **44**, 94–105.

584 A. K. M. L. Rahman, R. Indo, H. Hagiwara and T. Ishihara, *Appl. Catal. A*, 2013, **456**, 82–87.

585 M. M. Forde, R. D. Armstrong, C. Hammond, Q. He, R. L. Jenkins, S. A. Kondrat, N. Dimitratos, J. A. Lopez-Sanchez, S. H. Taylor, D. Willock, C. J. Kiely and G. J. Hutchings, *J. Am. Chem. Soc.*, 2013, **135**, 11087–11099.

586 R. D. Armstrong, V. Peneau, N. Ritterskamp, C. J. Kiely, S. H. Taylor and G. J. Hutchings, *ChemPhysChem*, 2018, **19**, 469–478.

587 R. D. Armstrong, S. J. Freakley, M. M. Forde, V. Peneau, R. L. Jenkins, S. H. Taylor, J. A. Moulijn, D. J. Morgan and G. J. Hutchings, *J. Catal.*, 2015, **330**, 84–92.

588 M. M. Forde, R. D. Armstrong, R. McVicker, P. P. Wells, N. Dimitratos, Q. He, L. Lu, R. L. Jenkins, C. Hammond, J. A. Lopez-Sanchez, C. J. Kiely and G. J. Hutchings, *Chem. Sci.*, 2014, **5**, 3603–3616.

589 Y. Li and J. N. Armor, *Appl. Catal. B*, 1993, **2**, 239–256.

590 Y. Li and J. N. Armor, *Chem. Commun.*, 1997, 2013–2014.

591 Y. Li and J. N. Armor, *J.Catal.*, 1998, **173**, 511–518.

592 Z. Sobalik, A. A. Belhekar, Z. Tvaruzkova and B. Wichterlova, *Appl. Catal. A*, 1999, **188**, 175–186.

593 X. Liu, T. Liang, R. Barbosa, G. Chen, H. Toghiani and Y. Xiang, *ACS Omega*, 2020, **5**, 1669–1678.

594 M. Mhamdi, S. Khaddar-Zine and A. Ghorbel, *Appl. Catal. A*, 2009, **357**, 42–50.

595 M. Mhamdi, S. Khaddar-Zine and A. Ghorbel, *Appl. Catal. A*, 2008, **337**, 39–47.

596 W. Pan, M. Jia, H. Lian, Y. Shang, T. Wu and W. Zhang, *React. Kinet. Catal. Lett.*, 2005, **86**, 67–73.

597 E. Mannei, F. Ayari, C. Petitto, E. Asedegbega-Nieto, A. R. Guerrero-Ruiz, G. Delahay, M. Mhamdi and A. Ghorbel, *Microporous Mesoporous Mater.*, 2017, **241**, 246–257.

598 Y. Li and J. N. Armor, *J. Catal.*, 1998, **176**, 495–502.

599 R. Bulanek, K. Novoveska and B. Wichterlova, *Appl. Catal. A*, 2002, **235**, 181–191.

600 S. B. D.-A. Hamid, P. Pal, H. He and E. G. Derouane, *Catal. Today*, 2001, **64**, 129–138.

601 S. B. D.-A. Hamid, G. Centi, P. Pal and E. G. Derouane, *Top. Catal.*, 2001, **15**, 161–168.

602 J. Perez-Ramirez, N. Blangenois and P. Ruiz, *Catal. Lett.*, 2005, **104**, 163–167.

603 R. Bulanek and F. Castek, *Top. Catal.*, 2007, **45**, 233–237.

604 R. Bulanek, K. Raabova, G. Kosova-Kucerova and L. Capek, *Stud. Surf. Sci. Catal.*, 2008, **174B**, 1151–1154.

605 R. Bulanek, K. Raabova and E. Badurova, *Catal. Today*, 2012, **179**, 73–77.

606 K. Raabova, R. Bulanek and E. Badurova, *Catal. Today*, 2013, **204**, 54–59.

607 J. J. Bravo-Suárez, K. K. Bando, J. Lu, T. Fujitani and S. T. Oyama, *J. Catal.*, 2008, **255**, 114–126.

608 C. Bouchy, G. Hastoy, E. Guillon and J. A. Martens, *Oil Gas Sci. Technol. l'IFP*, 2009, **64**, 91–112.

609 T. J. Remans and G. Jenzer, Handbook of Hetergeneous Catalysis: Online, Wiley-VCH Verlag GmbH & Co. KGaA, 2008.

610 G. W. Huber and A. Corma, *Angew. Chem., Int. Ed.*, 2007, **46**, 7184–7201.

611 G. W. Huber, P. O'Connor and A. Corma, *Appl. Catal. A*, 2007, **329**, 120–129.

612 Y. Mathieu, L. Sauvanaud, L. Humphreys, W. Rowlands, T. Maschmeyer and A. Corma, *ChemCatChem*, 2017, **9**, 1574–1578.

613 Y. Mathieu, L. Sauvanaud, L. Humphreys, W. Rowlands, T. Maschmeyer and A. Corma, *Faraday Discuss.*, 2017, **197**, 389–401.

614 M. Guisnet, L. Costa and F. R. Ribeiro, *J. Mol. Catal. A Chem.*, 2009, **305**, 69–83.

615 A. Corma, P. J. Miguel and A. V Orchilles, *Ind. Eng. Chem. Res.*, 1997, **36**, 3400–3415.

616 G. Sastre and A. Corma, *J. Mol. Catal. A Chem.*, 2009, **305**, 3–7.

617 J. Fu, X. Feng, Y. Liu, H. Shan and C. Yang, *J. Phys. Chem. C*, 2018, **122**, 12222–12230.

618 T. F. Narbeshuber, H. Vinek and J. A. Lercher, *J. Catal.*, 1995, **157**, 388–395.

619 M. Boronat, P. Viruela and A. Corma, *Phys. Chem. Chem. Phys.*, 2000, **2**, 3327–3333.

620 M.-T. Tran, N. S. Gnep, G. Szabo and M. Guisnet, *Appl. Catal. A*, 1998, **170**, 49–58.

621 A. Corma, P. J. Miguel and A. V Orchilles, *Appl. Catal. A*, 1994, **117**, 29–40.

622 E. F. Sousa-Aguiar, in *Zeolites Zeolite-Like Mater.*, Elsevier B.V., 2017, pp. 265–282.

623 M.-C. Silaghi, C. Chizallet, J. Sauer and P. Raybaud, *J. Catal.*, 2016, **339**, 242–255.

624 C. Mirodatos and D. Barthomeuf, *J. Chem. Soc. Chem. Commun.*, 1981, **2**, 39–40.

625 G. Garralon, V. Fornes and A. Corma, *Zeolites*, 1988, **8**, 262–268.

626 A. Corma, V. Fornes, A. Martinez, F. Melo and O. Pallota, in *Innovation in Zeolite Materials Science*, eds. P. J. Grobet, W. J. Mortier, E. F. Vansant and G. B. T.-S. in S. S. and C. Schulz-Ekloff, Elsevier, 1988, vol. 37, pp. 495–503.

627 A. Corma, F. Melo, L. Sauvanaud and F. J. Ortega, *Appl. Catal. A*, 2004, **265**, 195–206.

628 P. O'Connor, A. Hakuli and P. Imhof, *Studi. Surf. Sci. Catal.*, 2004, **149**, 305–321.

629 F. Lemos, F. R. Ribeiro, M. Kern, G. Giannetto and M. Guisnet, *Appl. Catal.*, 1988, **39**, 227–237.

630 E. F. Sousa-Aguiar, V. L. D. Camorim, F. M. Z. Zotin and R. L. C. dos Santos, *Microporous Mesoporous Mater.*, 1998, **25**, 25–34.

631 J. S. Buchanan, J. G. Santiesteban and W. O. Haag, *J. Catal.*, 1996, **158**, 279–287.

632 S. Kotrel, H. Knözinger and B. C. Gates, *Microporous Mesoporous Mater.*, 2000, **35**, 11–20.

633 B. A. de Moor, M. F. Reyniers, O. C. Gobin, J. A. Lercher and G. B. Marin, *J. Phys. Chem. C*, 2011, **115**, 1204-1219.

634 Y. Zhang, R. Zhao, M. Sanchez-Sanchez, G. L. Haller, J. Hu, R. Bermejo-Deval, Y. Liu and J. A. Lercher, *J. Catal.*, 2019, **370**, 424–433.

635 T. F. Degnan, G. K. Chitnis and P. H. Schipper, *Microporous Mesoporous Mater.*, 2000, **35**, 245–252.

636 H. Chen, B. Shen and H. Pan, *Chem. Lett.*, 2003, **32**, 726–727.

637 Y. Ghrib, N. Frini-Srasra, E. Srasra, J. Martínez-Triguero and A. Corma, *Catal. Sci. Technol.*, 2018, **8**, 716–725.

638 E. G. Derouane, J. M. Andre and A. A. Lucas, *J. Catal.*, 1988, **110**, 58-73.

639 N. Y. Chen and W. E. Garwood, *J. Catal.*, **52**, 453-458.

640 A. Corma, V. Gonzalez-Alfaro and A. V Orchilles, *Appl. Catal. A*, 1999, **187**, 245–254.

641 A. Corma and J. Martinez-Triguero, *J. Catal.*, 1997, **165**, 102–120.

642 D. Meloni, D. Martin and M. Guisnet, *Appl. Catal. A*, 2001, **215**, 67–79.

643 Y. Wang, T. Yokoi, S. Namba, J. N. Kondo and T. Tatsumi, *Appl. Catal. A*, 2015, **504**, 192–202.

644 B. G. Anderson, R. R. Schumacher, R. Van Duren, A. P. Singh and R. A. Van Santen, *J. Mol. Catal. A Chem.*, 2002, **181**, 291–301.

645 R. Bastiani, Y. L. Lam, C. A. Henriques and V. T. da Silva, *Fuel*, 2013, **107**, 680–687.

646 Y.-F. Zhang, X.-L. Liu, L.-Y. Sun, Q.-H. Xu, X.-J. Wang and Y.-J. Gong, *Fuel Process. Technol.*, 2016, **153**, 163–172.

647 A. Corma, M. J. Diaz-Cabanas, J. Martinez-Triguero, F. Rey and J. Rius, *Nature*, 2002, **418**, 514–517.

648 A. Corma, J. Martinez-Triguero, S. Valencia, E. Benazzi and S. Lacombe, *J. Catal.*, 2002, **206**, 125–133.

649 A. Corma, M. J. Diaz-Cabanas and V. Fornes, *Angew. Chem., Int. Ed.*, 2000, **39**, 2346–2349.

650 A. Corma, J. Martinez-Triguero and C. Martinez, *J. Catal.*, 2001, **197**, 151–159.

651 A. F. Costa, H. S. Cerqueira, J. M. M. Ferreira, N. M. S. Ruiz and S. M. C. Menezes, *Appl. Catal. A*, 2007, **319**, 137–143.

652 M. A. B. Siddiqui, A. M. Aitani, M. R. Saeed, N. Al-Yassir and S. Al-Khattaf, *Fuel*, 2011, **90**, 459–466.

653 M. Moliner, J. Gonzalez, M. T. Portilla, T. Willhammar, F. Rey, F. J. Llopis, X. Zou and A. Corma, *J. Am. Chem. Soc.*, 2011, **133**, 9497–9505.

654 S. Inagaki, K. Takechi and Y. Kubota, *Chem. Commun.*, 2010, **46**, 2662–2664.

655 Y. Kubota, S. Inagaki and K. Takechi, *Catal. Today*, 2014, **226**, 109–116.

656 C. Baerlocher, T. Weber, L. B. McCusker, L. Palatinus and S. I. Zones, *Science*, 2011, **333**, 1134–1137.

657 V. J. Frillette, W. O. Haag and R. M. Lago, *J Catal*, 1981, **67**, 218–222.

658 S. I. Zones, J. Ruan, S. Elomari, O. Terasaki, C. Y. Chen and A. Corma, *Solid State Sci.*, 2011, **13**, 706–713.

659 R. Castaneda, A. Corma, V. Fornes, J. Martinez-Triguero and S. Valencia, *J. Catal.*, 2006, **238**, 79–87.

660 A. Corma, V. Fornes, M. J. Franco, F. A. Mocholi and J. Perez-Pariente, *ACS Symp. Ser.*, 1991, **452**, 79–95.

661 M. Briend, M. Derewinski, A. Lamy and D. Barthomeuf, in *Stud. Surf. Sci. Catal.*, 1993, **75**, 409–420.

662 D. Barthomeuf, *Appl. Catal. A*, 1995, **126**, 187–194.

663 C. Li, A. Vidal-Moya, P. J. Miguel, J. Dedecek, M. Boronat and A. Corma, *ACS Catal.*, 2018, **8**, 7688–7697.

664 T. Yokoi, H. Mochizuki, S. Namba, J. N. Kondo and T. Tatsumi, *J. Phys. Chem. C*, 2015, **119**, 15303–15315.

665 T. Yokoi, H. Mochizuki, T. Biligetu, Y. Wang and T. Tatsumi, *Chem. Lett.*, 2017, **46**, 798–800.

666 Y. Wang, T. Yokoi, S. Namba, J. N. Kondo and T. Tatsumi, *J. Catal.*, 2016, **333**, 17–28.

667 J. Pérez-Ramírez, C. H. Christensen, K. Egeblad, C. H. Christensen and J. C. Groen, *Chem. Soc. Rev.*, 2008, **37**, 2530–2542.

668 A. Corma, V. Fornés, A. Martínez and A. V Orchillés, in *Perspectives in Molecular Sieve Science*, American Chemical Society, 1988, vol. 368, pp. 35–542.

669 M. A. Camblor, A. Corma, A. Martinez, F. A. Mocholi and P. J. Perez, *Appl. Catal.*, 1989, **55**, 65–74.

670 L. Bonetto, M. A. Camblor, A. Corma and J. Perez-Pariente, *Appl. Catal. A*, 1992, **82**, 37–50.

671 X. Gao, Z. Tang, H. Zhang, D. Ji, G. Lu, Z. Wang and Z. Tan, *J. Mol. Catal. A Chem.*, 2010, **325**, 36–39.

672 J. K. Reddy, K. Motokura, T. Koyama, A. Miyaji and T. Baba, *J. Catal.*, 2012, **289**, 53–61.

673 Y. Nakasaka, T. Okamura, H. Konno, T. Tago and T. Masuda, *Microporous Mesoporous Mater.*, 2013, **182**, 244–249.

674 H. Mochizuki, T. Yokoi, H. Imai, R. Watanabe, S. Namba, J. N. Kondo and T. Tatsumi, *Microporous Mesoporous Mater.*, 2011, **145**, 165–171.

675 H. Konno, T. Tago, Y. Nakasaka, R. Ohnaka, J. Nishimura and T. Masuda, *Microporous Mesoporous Mater.*, 2013, **175**, 25–33.

676 C. Martínez, D. Verboekend, J. Pérez-Ramírez and A. Corma, *Catal. Sci. Technol.*, 2013, **3**, 972–981.

677 J. García-Martínez, M. Johnson, J. Valla, K. Li and J. Y. Ying, *Catal. Sci. Technol.*, 2012, **2**, 987–994.

678 A. Ishihara, *Fuel Process. Technol.*, 2019, **194**, 106116.

679 C. T. Kresge, W. J. Roth, K. G. Simmons, J. C. Vartuli, *US Pat.*, 5,229,341 A, 1993.

680 S. Laforge, P. Ayrault, D. Martin and M. Guisnet, *Appl. Catal. A*, 2005, **279**, 79–88.

681 S. Maheshwari, C. Martinez, P. M. Teresa, F. J. Llopis, A. Corma and M. Tsapatsis, *J. Catal.*, 2010, **272**, 298–308.

682 A. Corma, V. Fornes, J. M. Guil, S. Pergher, T. L. M. Maesen and J. G. Buglass, *Microporous Mesoporous Mater.*, 2000, **38**, 301–309.

683 A. Corma, U. Diaz, M. E. Domine and V. Fornes, *J. Am. Chem. Soc.*, 2000, **122**, 2804–2809.

684 A. Corma Canos, U. Diaz Morales and V. Fornes Segui, *US Pat.*, 7,008,611 B2, 2006.

685 P. M. Eletskii, O. O. Mironenko, R. G. Kukushkin, G. A. Sosnin and V. A. Yakovlev, *Catal. Ind.*, 2018, **10**, 185–201.

686 A. Corma, J. Mengual and P. J. Miguel, *Appl. Catal. A*, 2012, **417**, 220–235.

687 A. Corma, J. Mengual and P. J. Miguel, *Appl. Catal. A*, 2012, **421**, 121–134.

688 M. A. Sanhoob, O. Muraza, E. N. Shafei, T. Yokoi and K.-H. Choi, *Appl. Catal. B*, 2017, **210**, 432–443.

689 A. Corma, J. Mengual and P. J. Miguel, *Appl. Catal. A*, 2013, **460**, 106–115.

690 U. Khalil, O. Muraza, H. Kondoh, G. Watanabe, Y. Nakasaka, A. Al-Amer and T. Masuda, *Energy & Fuels*, 2016, **30**, 1304–1309.

691 U. Khalil, O. Muraza, H. Kondoh, G. Watanabe, Y. Nakasaka, A. Al-Amer and T. Masuda, *Fuel*, 2016, **168**, 61–67.

692 S. Shirvani and M. Ghashghaee, *Pet. Sci. Technol.*, 2018, **36**, 750–755.

693 M. Ghashghaee, S. Shirvani and S. Kegnæs, *J. Anal. Appl. Pyrolysis*, 2019, **138**, 281–293.

694 J. W. Thybaut, I. R. Choudhury, J. F. Denayer, G. V Baron, P. A. Jacobs, J. A. Martens and G. B. Marin, *Top. Catal.*, 2009, **52**, 1251–1260.

695 M. Y. Kim, K. Lee and M. Choi, *J. Catal.*, 2014, **319**, 232–238.

696 M. Guisnet, *Catal. Today*, 2013, **218**–**219**, 123–134.

697 L. Meng, G. Vanbutsele, R. Pestman, A. Godin, D. E. Romero, A. J. F. van Hoof, L. Gao, T. F. Kimpel, J. Chai and J. A. Martens, *J. Catal.*, 2020, **389**, 544–555.

698 J. A. M. Arroyo, G. G. Martens, G. F. Froment, G. B. Marin, P. A. Jacobs and J. A. Martens, *Appl. Catal. A*, 2000, **192**, 9–22.

699 R. Parton, L. Uytterhoeven, J. A. Martens, P. A. Jacobs and G. F. Froment, *Appl. Catal.*, 1991, **76**, 131–142.

700 P. B. Weisz, eds. D. D. Eley, P. W. Selwood, P. B. Weisz, A. A. Balandin, J. H. De Boer, P. J. Debye, P. H. Emmett, J. Horiuti, W. Jost, G. Natta, E. K. Rideal and H. S. B. T.-A. in C. Taylor, Academic Press, 1962, vol. 13, pp. 137–190.

701 J. Zecevic, G. Vanbutsele, K. P. De Jong and J. A. Martens, *Nature*, 2015, **528**, 245–248.

702 J. A. Martens, G. Vanbutsele, P. A. Jacobs, J. Denayer, R. Ocakoglu, G. Baron, J. A. M. Arroyo, J. Thybaut and G. B. Marin, *Catal. Today*, 2001, **65**, 111–116.

703 K. Cheng, L. I. van der Wal, H. Yoshida, J. Oenema, J. Harmel, Z. Zhang, G. Sunley, J. Zečević and K. P. de Jong, *Angew. Chem., Int. Ed.*, 2020, **59**, 3592–3600.

704 J. Weitkamp, *Ind. Eng. Chem. Prod. Res. Dev.*, 1982, **21**, 550–558.

705 C. Perego and A. Carati, in *Zeolites: From Model Materials to Industrial Catalysts*, ed. J. P.-P. J. Cejka and W.J. Roth, 2008, pp. 357–389.

706 S. J. Miller, *Microporous Mater.*, 1994, **2**, 439–449.

707 S. J. Miller, *US Pat.*, 4,859,311 A, 1989.

708 P. Bai, M. Y. Jeon, L. Ren, C. Knight, M. W. Deem, M. Tsapatsis and J. I. Siepmann, *Nat. Commun.*, 2015, **6**, 1–9.

709 C. Zschiesche, D. Himsl, R. Rakoczy, A. Reitzmann, J. Freiding, N. Wilde and R. Gläser, *Chem. Eng. Technol.*, 2018, **41**, 199–204.

710 T. L. M. Maesen, E. Beerdsen, S. Calero, D. Dubbeldam and B. Smit, *J. Catal.*, 2006, **237**, 278–290.

711 T. L. M. Maesen, S. Calero, M. Schenk and B. Smit, *J. Catal.*, 2004, **221**, 241–251.

712 M. Schenk, S. Calero, T. L. M. Maesen, L. L. Van Benthem, M. G. Verbeek and B. Smit, *Angew. Chem., Int. Ed.*, 2002, **41**, 2499-2502.

713 M. Schenk, S. Calero, T. L. M. Maesen, T. J. H. Vlugt, L. L. van Benthem, M. G. Verbeek, B. Schnell and B. Smit, *J. Catal.*, 2003, **214**, 88–99.

714 A. Corma and A. Martinez, *NATO ASI Ser. Ser. 3 High Technol.*, 1998, **44**, 35–74.

715 A. Baudot and L. Bournay, *Oil Gas Sci. Technol. l'IFP*, 2009, **64**, 759–771.

716 A. Corma, *Catal. Lett.*, 1993, **22**, 33–52.

717 O. Ben Moussa, L. Tinat, X. Jin, W. Baaziz, O. Durupthy, C. Sayag and J. Blanchard, *ACS Catal.*, 2018, **8**, 6071–6078.

718 J. J. Lazaro Munoz, A. Corma Canos and J. M. Frontela Delgado, *US Pat.*, 5,057,471 A, 1991.

719 J. Macht, R. T. Carr and E. Iglesia, *J. Am. Chem. Soc.*, 2009, **131**, 6554–6565.

720 M. Boronat, P. Viruela and A. Corma, *J. Phys. Chem.*, 1996, **100**, 16514–16521.

721 A. Chica and A. Corma, *J. Catal.*, 1999, **187**, 167–176.

722 J. E. Schmidt, C. Chen, S. K. Brand, S. I. Zones and M. E. Davis, *Chem. Eur. J.*, 2016, **22**, 4022–4029.

723 A. Sławek, J. M. Vicent-Luna, B. Marszałek, W. Makowski and S. Calero, *J. Phys. Chem. C*, 2017, **121**, 19226–19238.

724 G. Noh, Z. Shi, S. I. Zones and E. Iglesia, *J. Catal.*, 2018, **368**, 389–410.

725 J. E. Samad, J. Blanchard, C. Sayag, C. Louis and J. R. Regalbuto, *J. Catal.*, 2016, **342**, 203–212.

726 M. Höchtl, A. Jentys and H. Vinek, *J. Catal.*, 2000, **190**, 419–432.

727 A. Chica and A. Corma, *Chem. Ing. Tech.*, 2007, **79**, 857–870.

728 N. Y. Chen, in *Shape-Selective Catalysis*, American Chemical Society, 1999, vol. 738, pp.

3–39.

729 M. F. Menoufy, A. E. Nadia and H. S. Ahmed, *Pet. Sci. Technol.*, 2009, **27**, 568–574.

730 W. Souverijns, J. A. Martens, G. F. Froment and P. A. Jacobs, *J. Catal.*, 1998, **174**, 177–184.

731 M. C. Claude, G. Vanbutsele and J. A. Martens, *J. Catal.*, 2001, **203**, 213–231.

732 C. S. L. Narasimhan, J. W. Thybaut, G. B. Marin, P. A. Jacobs, J. A. Martens, J. F. Denayer and G. V Baron, *J. Catal.*, 2003, **220**, 399–413.

733 M. C. Claude and J. A. Martens, *J. Catal.*, 2000, **190**, 39–48.

734 J. F. Denayer, G. V Baron, J. A. Martens and P. A. Jacobs, *J. Phys. Chem. B*, 1998, **102**, 3077–3081.

735 J. A. Martens, W. Souverijns, W. Verrelst, R. Parton, G. F. Froment and P. A. Jacobs, *Angew. Chem., Int. Ed.*, 1995, **34**, 2528–2530.

736 C. S. L. Narasimhan, J. W. Thybaut, G. B. Marin, J. A. Martens, J. F. Denayer and G. V Baron, *J. Catal.*, 2003, **218**, 135–147.

737 J. F. Denayer, W. Souverijns, P. A. Jacobs, J. A. Martens and G. V Baron, *J. Phys. Chem. B*, 1998, **102**, 4588–4597.

738 J. A. Z. Pieterse, S. Veefkind-Reyes, K. Seshan and J. A. Lercher, *J. Phys. Chem. B*, 2000, **104**, 5715–5723.

739 G. Lv, C. Wang, P. Wang, L. Sun, H. Liu, W. Qu, D. Wang, H. Ma and Z. Tian, *ChemCatChem*, 2019, **11**, 1431–1436.

740 P. Niu, P. Liu, H. Xi, J. Ren, M. Lin, Q. Wang, X. Chen, L. Jia, B. Hou and D. Li, *Appl. Catal. A*, 2018, **562**, 310–320.

741 Y. Chen, C. Li, X. Chen, Y. Liu, C.-W. Tsang and C. Liang, *Ind. Eng. Chem. Res.*, 2018, **57**, 13721–13730.

742 P. Mériaudeau, V. A. Tuan, F. Lefebvre, V. T. Nghiem and C. Naccache, *Microporous Mesoporous Mater.*, 1998, **26**, 161–173.

743 G. Sastre, A. Chica and A. Corma, *J. Catal.*, 2000, **195**, 227–236.

744 T. L. M. Maesen, R. Krishna, J. M. van Baten, B. Smit, S. Calero and J. M. C. Sanchez, *J. Catal.*, 2008, **256**, 95–107.

745 M. Stöcker, *Microporous Mesoporous Mater.*, 2005, **82**, 257–292.

746 S. J. Miller, H. S. Lacheen and C.-Y. Chen, *Ind. Eng. Chem. Res.*, 2016, **55**, 6760–6767.

747 R. Yadav and A. Sakthivel, *Appl. Catal. A*, 2014, **481**, 143–160.

748 S. C. Weston, B. K. Peterson, J. E. Gatt, W. W. Lonergan, H. B. Vroman, M. Afeworki, G. J. Kennedy, D. L. Dorset, M. D. Shannon and K. G. Strohmaier, *J. Am. Chem. Soc.*, 2019, **141**, 15910–15920.

749 H. L. Coonradt and W. E. Garwood, *Ind. Eng. Chem. Process Des. Dev.*, 1964, **3**, 38–45.

750 R. Bezman, *Catal. Today*, 1992, **13**, 143–156.

751 C. Manrique, A. Guzmán, J. Pérez-Pariente, C. Márquez-Álvarez and A. Echavarría, *Microporous Mesoporous Mater.*, 2016, **234**, 347–360.

752 A. Corma, M. J. Diaz-Cabanas, C. Lopez and A. Martinez, *Stud. Surf. Sci. Catal.*, 2004, **154C**, 2380–2386.

753 A. Corma, A. Martinez and V. Martinez-Soria, *J. Catal.*, 2001, **200**, 259–269.

754 A. Martínez, S. Valencia, R. Murciano, H. S. Cerqueira, A. F. Costa and E. F. S.- Aguiar, *Appl. Catal. A*, 2008, **346**, 117–125.

755 M. A. Camblor, A. Corma, A. Martinez, V. Martinez-Soria and S. Valencia, *J. Catal.*, 1998, **179**, 537–547.

756 M. A. Arribas, F. Márquez and A. Martı&nez, *J. Catal.*, 2000, **190**, 309–319.

757 F. Bauer, K. Ficht, M. Bertmer, W.-D. Einicke, T. Kuchling and R. Gläser, *Catal. Sci. Technol.*, 2014, **4**, 4045–4054.

758 B. D. Vandegehuchte, I. R. Choudhury, J. W. Thybaut, J. A. Martens and G. B. Marin, *J. Phys. Chem. C*, 2014, **118**, 22053–22068.

759 B. D. Vandegehuchte, J. W. Thybaut and G. B. Marin, *Ind. Eng. Chem. Res.*, 2014, **53**, 15333–15347.

760 R. Van Mao, *J. Mater. Chem.*, 1994, **4**, 605–610.

761 R. Van Mao, *J. Mater. Chem.*, 1995, **5**, 533–535.

762 K. Sato, Y. Nishimura, K. Honna, N. Matsubayashi and H. Shimada, *J. Catal.*, 2001, **200**, 288–297.

763 K. P. de Jong, J. Zečević, H. Friedrich, P. E. de Jongh, M. Bulut, S. van Donk, R. Kenmogne, A. Finiels, V. Hulea and F. Fajula, *Angew.Chem., Int. Ed.*, 2010, **49**, 10074-10078.

764 R. Brosius, P. J. Kooyman and J. C. Q. Fletcher, *ACS Catal.*, 2016, **6**, 7710–7715.

765 J. A. Martens, D. Verboekend, K. Thomas, G. Vanbutsele, J. Gilson and J. Pérez-Ramírez, *ChemSusChem*, 2013, **6**, 421–425.

766 D. Verboekend, K. Thomas, M. Milina, S. Mitchell, J. Perez-Ramirez and J.-P. Gilson, *Catal. Sci. Technol.*, 2011, **1**, 1331–1335.

767 J. Pastvova, D. Kaucky, J. Moravkova, J. Rathousky, S. Sklenak, M. Vorokhta, L. Brabec, R. Pilar, I. Jakubec and E. Tabor, *ACS Catal.*, 2017, **7**, 5781–5795.

768 M. Tromp, J. A. van Bokhoven, M. T. G. Oostenbrink, J. H. Bitter, K. P. De Jong and D. C. Koningsberger, *J. Catal.*, 2000, **190**, 209–214.

769 G. J. Antos and A. M. Aitani, *Catalytic Naphtha Reforming, Revised and Expanded*, CRC Press, Marcel Dekker, Inc. New York - Basel, 2004.

770 B. H. Davis, *Catal. Today*, 1999, **53**, 443–516.

771 G. A. Olah and Á. Molnár, *Hydrocarbon Chemistry*, John Wiley & Sons Inc., Hoboke, New Jersey, 2003.

772 E. Mielczarski, S. B. Hong, R. J. Davis and M. E. Davis, *J. Catal.*, 1992, **134**, 359–369.

773 N. D. Triantafillou, J. T. Miller and B. C. Gates, *J. Catal.*, 1995, **155**, 131–140.

774 P. V Menacherry and G. L. Haller, *J. Catal.*, 1998, **177**, 175–188.

775 G. S. Lane, F. S. Modica and J. T. Miller, *J. Catal.*, 1991, **129**, 145–158.

776 J. T. Miller, N. G. B. Agrawal, G. S. Lane and F. S. Modica, *J. Catal.*, 1996, **163**, 106–116.

777 D. S. Lafyatis, G. F. Froment, A. Pasauclaerbout and E. G. Derouane, *J. Catal.*, 1994, **147**, 552–566.

778 E. Iglesia, J. Baumgartner, G. L. Price, K. D. Rose and J. L. Robbins, *J. Catal.*, 1990, **125**, 95–111.

779 R. E. Jentoft, M. Tsapatsis, M. E. Davis and B. C. Gates, *J. Catal.*, 1998, **179**, 565–580.

780 K. G. Azzam, G. Jacobs, W. D. Shafer and B. H. Davis, *J. Catal.*, 2010, **270**, 242–248.

781 E. Iglesia and J. E. Baumgartner, *Stud. Surf. Sci. Catal.*, 1993, **75**, 993–1006.

782 N. Viswanadham, A. R. Pradhan, N. Ray, S. C. Vishnoi, U. Shanker and T. S. R. Prasada Rao, *Appl. Catal. A*, 1996, **137**, 225–233.

783 M. Xin, E. Xing, X. Gao, Y. Wang, Y. Ouyang, G. Xu, Y. Luo and X. Shu, *Ind. Eng. Chem.*

Res., 2019, **58**, 6970–6981.

784 A. Thivasasith, T. Maihom, S. Pengpanich, J. Limtrakul and C. Wattanakit, *Phys. Chem. Chem. Phys.*, 2019, **21**, 5359–5367.

785 J. S. Jarvis, J. H. Harrhy, A. Wang, T. Bere, D. J. Morgan, J. H. Carter, A. G. R. Howe, Q. He, G. J. Hutchings and H. Song, *ACS Catal.*, 2020, **10**, 8428–8443.

786 C. Wei, Q. Yu, J. Li and Z. Liu, *ACS Catal.*, 2020, **10**, 4171–4180.

787 M. Taramasso, G. Perego and B. Notari, *US Pat.*, 4,410,501 A, 1983.

788 G. Peregot, G. Bellussi, C. Corno, M. Taramasso, F. Buonomot and A. Esposito, in *Stud. Surf. Sci. Catal.*, 1986, **28**, 129–136.

789 D. R. C. Huybrechts, L. De Bruycker and P. A. Jacobs, *Nature*, 1990, **345**, 240-242.

790 T. Tatsumi, M. Nakamura, S. Negishi and H. Tominaga, *J. Chem. Soc. Chem. Commun.*, 1990, **6**, 476–477.

791 G. N. Vayssilov, *Catal. Rev.*, 1997, **39**, 209–251.

792 J. E. Gallot and S. Kaliaguine, *Can. J. Chem. Eng.*, 1998, **76**, 833–852.

793 J. Přech, *Catal. Rev.*, 2018, **60**, 71–131.

794 M. A. Camblor, A. Corma, A. Martínez and J. Pérez-Pariente, *J. Chem. Soc. Chem. Commun.*, 1992, **8**, 589–590.

795 T. Blasco, M. A. Camblor, A. Corma and J. Perez-Pariente, *J. Am. Chem. Soc.*, 1993, **115**, 11806–11813.

796 A. Corma, M. A. Camblor, P. Esteve, A. Martinez and J. Perez-Pariente, *J. Catal.*, 1994, **145**, 151–158.

797 T. Blasco, M. A. Camblor, A. Corma, P. Esteve, A. Martinez, C. Prieto and S. Valencia, *Chem. Commun.*, 1996, **20**, 2367–2368.

798 M. A. Camblor, M. Costantini, A. Corma, L. Gilbert, P. Esteve, A. Martinez and S. Valencia, *Chem. Commun.*, 1996, **11**, 1339–1340.

799 M. Boronat, A. Corma, M. Renz and P. M. Viruela, *Chem.Eur. J.*, 2006, **12**, 7067–7077.

800 A. Corma, L. T. Nemeth, M. Renz and S. Valencia, *Nature*, 2001, **412**, 423–425.

801 A. Corma and M. Renz, *Angew. Chem., Int. Ed.*, 2007, **46**, 298–300.

802 M. S. Holm, S. Saravanamurugan and E. Taarning, *Science*, 2010, **328**, 602–605.

803 N. Hoeven, G. Mali, M. Mertens and P. Cool, *Microporous Mesoporous Mater.*, 2019, **288**, 109588.

804 J. M. Thomas, R. Raja, G. Sankar and R. G. Bell, *Nature*, 1999, **398**, 227–230.

805 R. Raja and J. M. Thomas, *Chem. Commun.*, 1998, **17**, 1841–1842.

806 C. M. Freeman, C. R. A. Catlow, J. M. Thomas and S. Brode, *Chem. Phys. Lett.*, 1991, **186**, 137–142.

807 P. A. Barrett, G. Sankar, R. H. Jones, C. R. A. Catlow and J. M. Thomas, *J. Phys. Chem. B*, 1997, **101**, 9555–9562.

808 R. Raja, G. Sankar and J. M. Thomas, *Angew. Chem., Int. Ed.*, 2000, **39**, 2313–2316.

809 B. Modén, B.-Z. Zhan, J. Dakka, J. G. Santiesteban and E. Iglesia, *J. Phys. Chem. C*, 2007, **111**, 1402–1411.

810 B. Modén, B.-Z. Zhan, J. Dakka, J. G. Santiesteban and E. Iglesia, *J. Catal.*, 2006, **239**, 390–401.

811 B.-Z. Zhan, B. Modén, J. Dakka, J. G. Santiesteban and E. Iglesia, *J. Catal.*, 2007, **245**, 316–325.

812 T. M. Hoehler, M. J. Alperin, D. B. Albert and C. S. Martens, *Global Biogeochem. Cycles*, 1994, **8**, 451–463.

813 A. Corma, *Angew. Chem., Int. Ed.*, 2016, **55**, 6112–6113.

814 V. Paunović, G. Zichittella, M. Moser, A. P. Amrute and J. Pérez-Ramírez, *Nat. Chem.*, 2016, **8**, 803–809.

815 A. Demonceau, A. F. Noels and A. J. Hubert, *J. Mol. Catal.*, 1989, **57**, 149–152.